CPSK TRANSMISSION THROUGH NONLINEAR CHANNELS

PERFORMANCE ANALYSIS OF CPSK TRANSMISSION THROUGH NONLINEAR CHANNELS

By

PRITI HETRAKUL, B.E., M.E.

A thesis

Submitted to the School of Graduate Studies

in Partial Fulfilment of the Requirements

for the Degree

Doctor of Philosophy

McMaster University

March, 1976

DOCTOR OF PHILOSOPHY (1976) McMASTER UNIVERSITY
(Electrical Engineering) Hamilton, Ontario

TITLE: Performance Analysis of CPSK Transmission through Nonlinear Channels.

AUTHOR: Priti Hetrakul
B.E. (University of New South Wales, 1971)
M.E. (University of Newcastle, 1972)

SUPERVISOR: Dr. D.P. Taylor

NUMBER OF PAGES: xvii, 210.

ABSTRACT

Virtually all satellite repeaters use a traveling-wave tube (TWT) as their main power amplifier. Because on-board power is a limited commodity, it is highly desirable that the TWT be operated as efficiently as possible, namely in or near saturation where it is highly nonlinear. These nonlinear effects manifest themselves as an amplitude compression (AM/AM conversion) effect and an amplitude dependent phase modulation (AM/PM conversion) effect. In this thesis a number of investigations have been made in relation to the TWT nonlinearities and their effect on the performance of communication systems.

A novel quadrature model of the TWT has been developed. This model is most useful in that it is analytic and requires the choice of only four parameters to obtain an excellent fit to the TWT characteristics.

An optimal bandpass nonlinear transfer characteristic that maximizes its output signal to interference power ratio has also been derived. By making use of this optimal transfer characteristic and the quadrature model of the tube, a computer-aided design procedure has been described for obtaining a predistortion compensation network for the TWT. This network consists of a simple arrangement of attenuators and power-law devices and has been shown, by computer simulation, to yield about 1 dB improvement in system performance for the case when only a single carrier is present in the TWT.

In the case when a single sample detection and majority logic decision circuit is assumed at the receiver, it has been possible to derive analytical expressions for the probability of error for M-ary CPSK signals transmitted through a piecewise-linear envelope limiting repeater. An infinite series expression for the bit error rate of binary CPSK transmission through an actual TWT channel has also been derived.

A performance analysis of a correlation receiver with a linear integrate and dump circuit has been carried out for the case of binary CPSK transmission through a bandpass nonlinearity exhibiting AM/PM conversion.

For the case of purely amplitude-limiting channels, an optimal (maximum-likelihood) receiver structure and its approximate performance has also been investigated.

ACKNOWLEDGEMENTS

The author gratefully acknowledges the help and guidance given to him by his supervisor, Dr. Desmond P. Taylor throughout the preparation of the thesis. Special thanks are due to Dr. S. S. Haykin for his suggestion of the problem and many valuable discussions and to Dr. M. A. Stephens for serving on the supervisory committee.

The author would like to thank Dr. H.C. Chan for his permission to include figures 4-3 to 4-8 in the thesis and his many enjoyable and helpful discussions. Thanks are also due to the research personnel of the Communications Research Laboratory at McMaster University for participating in many lively discussions, and to Ms. Bernice Johnson for her assistance in the typing.

Finally, the author is grateful for the financial support from McMaster University through the award of a Benefactor Scholarship.

TABLE OF CONTENTS

Tables of Contents (Continued)

LIST OF ILLUSTRATIONS

List of Illustrations (Continued)

List of Illustrations, (Continued)

LIST OF TABLES

LIST OF PRINCIPAL SYMBOLS

Symbol	Representation
A	Single carrier signal amplitude
A'	Equivalent signal amplitude at the output of the nonlinear device
A_k	kth coefficient of $N_p(\cdot)$
a_k	kth coefficient of $G_p(\cdot)$
AM/AM	Amplitude modulation to amplitude modulation
AM/PM	Amplitude modulation to phase modulation
APK	Amplitude phase shift keying
B_k	kth coefficient of $N_q(\cdot)$
b_k	kth coefficient of $G_q(\cdot)$
BMT	Butler matrix transponder
C/I	Carrier to interference power ratio
CNR	Carrier to noise power ratio
$C_n(\cdot)$	Characteristic function of random variable n
CPSK	Coherent phase shift keying
$(CNR)_d$	Down-link CNR
$(CNR)_u$	Up-link CNR
DC	Direct current
dB	Decibel
dBm	Decibel relative to 1 milliwatt power
dBW	Decibel relative to 1 watt power

List of Principal Symbols (Continued)

Symbol	Representation
E_b/N_0	Bit energy to noise power spectral density ratio
$E_R[\cdot]$	Expectation with respect to the probability distribution function of random variable R
$E_{R,\varepsilon}[\cdot]$	Expectation with respect to the joint probability distribution function of R and ε
erf(·)	Error function
erfc(·)	Complementary error function
${}_1F_1[a, b; x]$	Confluent hypergeometric function
FDM	Frequency division multiplexing
FDMA	Frequency division multiple access
FM	Frequency modulation
f(R)	Piecewise-linear envelope limiting nonlinearity
G_{ss1}	Small signal gain of TWT_1
$G_p(\cdot)$	In-phase envelope nonlinearity of the compensator
$G_q(\cdot)$	Quadrature envelope nonlinearity of the compensator
$H_k(\cdot)$	Hermite polynomial of degree k
I	Countable index set
I'	Countable index set excluding zero
Im(x)	Imaginary part of the complex number x
IMP	Intermodulation products

List of Principal Symbols (Continued)

Symbol	Representation
$I_n(\cdot)$	Modified Bessel function of the first kind of order n
J	Unconstrained objective function
$k!$	Factorial of integer k
$\begin{pmatrix} k \\ m \end{pmatrix}$	$= \frac{k!}{m!\ (k-m)!}$
LPF	Low pass filter
$\ell(\cdot)$	Log-likelihood ratio functional
$\ln(\cdot)$	Natural logarithm
MHz	Megacycles per second
ML	Maximum likelihood
m_k	kth central moment
N	Noise power
N_0	Noise power spectral density
$N[\mu,\sigma^2]$	Normal density function with mean μ, and variance σ^2
N_d	Down-link noise power
$N_p[\cdot]$	In-phase instantaneous voltage nonlinearity of the compensator
$N_q[\cdot]$	Quadrature instantaneous voltage nonlinearity of the compensator
N_u	Up-link noise power
N'_u	Effective in-phase noise power at the output of the nonlinear device

List of Principal Symbols (Continued)

Symbol	Representation
$n'(t)$	Effective noise component at the output of the nonlinear device
$n_1'(t)$	Equivalent in-phase noise component at the output of the nonlinear device
$n_2'(t)$	Equivalent quadrature noise component at the output of the nonlinear device
PCM	Pulse code modulation
PDF	Probability distribution function
pdf	Probability density function
$P_b(M)$	Bit error probability for M-ary CPSK
$P_e(M)$	Symbol error probability for M-ary CPSK
PSK	Phase shift keying
QPSK	Quaternary phase shift keying
R	Envelope of signal plus narrowband noise
Re(x)	Real part of the complex number x
RF	Radio frequency
S	Signal power
S^*	Optimal signal power
SSMA	Spread spectrum multiple access
$s'(t)$	Effective signal component at the output of the nonlinear device
sgn(x)	Sign of real number x

List of Principal Symbols (Continued)

Symbol	Representation
sup	Supremum
T	Symbol duration
$T_m(\cdot)$	Chebyshev polynomial of order m
TWT	Traveling wave tube
W	System bandwidth
$\|x\|$	Modulus of real or complex number x
$\langle x \rangle$	Integer part of real number x
$Z_p(\cdot)$	In-phase envelope nonlinearity
$Z_p^*(\cdot)$	Optimal in-phase envelope nonlinearity
$Z_q(\cdot)$	Quadrature envelope nonlinearity
$Z_q^*(\cdot)$	Optimal quadrature envelope nonlinearity
$Z^*(\cdot)$	Optimal overall envelope transfer characteristic
β	Effective phase shift at the output of the nonlinear device
ε	Random phase of signal plus narrowband noise
ξ_1, ξ_2	In-phase and quadrature components of down-link Gaussian noise
γ_u	Up-link carrier to noise power ratio
γ_d	Down-link carrier to noise power ratio
λ	Limiter softness factor
λ^*	Normalized limiter softness factor
$\hat{\lambda}$	Lagrange multiplier

List of Principal Symbols (Continued)

Symbol	Representation
π	= 3.1415926.....
$\phi(x)$	= N[0, 1]
$\Phi(x)$	= $\frac{1}{2}\,\mathrm{erfc}[-x/\sqrt{2}]$
ρ	Effective receiver carrier to noise power ratio
$\theta_n, \theta_n(i)$	Transmitted phase during the nth symbol interval
μ_k	kth cumulant
ω_θ	Carrier frequency (in radians per second)
$\underline{\Delta}$	Defined as
$\approx$	Approximately equal to

CHAPTER 1

INTRODUCTION AND BACKGROUND

1.1) INTRODUCTION

Since the launch of the first, successful geo-stationary satellite, SYNCOM II, in July 1963, satellite communications have expanded at a phenomenal rate. Within the last decade, communications traffic has been growing at an approximate rate of 15 to 25 per cent per year. This growth is expected to continue for the next 10 to 20 years [62].

At an orbital altitude of 34,863 km above the equator, i.e. about six times the earth's radius, economical means can be provided to keep a satellite stationary with respect to the rotating earth. This is known as synchronous orbit. The angle subtended by the earth from the satellite is about 18° and the resulting earth coverage for communication purposes is approximately four-tenths of the earth's surface. Hence only three such satellites are sufficient in principle to provide communication between any two points on the earth's surface [26].

Early satellites were sharply power-limited but had more than sufficient bandwidth for the small number of

available users (ground station accesses). In order to trade off bandwidth for signalling power, wideband frequency modulation (FM) techniques were used in conjunction with frequency division multiplexing (FDM) in order to accommodate a large number of simultaneous messages from each user. An additional factor influencing this choice was that the FM/FDM technology was highly developed and widely used in terrestrial microwave systems.

In today's systems it is desirable that a large number of earth terminals (each with a different volume of message traffic) simultaneously access or use a given satellite channel. This is known as multiple access communications and there are several methods of achieving it [65]. Of main concern to us in the subsequent analysis are the following multiple access methods:

(1) frequency division multiple access (FDMA)

(2) time division multiple access (TDMA)

(3) spread spectrum multiple access (SSMA)

Commercially, the most widely used methods are frequency division multiple access (FDMA) and time-division multiple access (TDMA). In frequency-division multiple access, the repeater bandwidth is divided into a number of nonoverlapping frequency bands which constitute access channels. The transmitting stations are then assigned to each of these access channels. Either frequency-division multiplexing (FDM) or time division multiplexing may be employed in order to assemble the individual baseband

channels prior to the transmission. This multiplexed baseband is then modulated onto the main radio frequency (RF) carrier either by analog means, such as, wideband frequency modulation (FM) or phase modulation (PM), or by digital methods, such as, phase shift keying (PSK). When each user is transmitting an analog modulated FM/FDM signal, the only viable multiple access method is FDMA with pre-assigned channels. In such systems, several simultaneously transmitted signals with different carrier frequencies are passed through the traveling wave tube (TWT) amplifier transponder on board the satellite (see section 1.2). As a result of the TWT nonlinearity, these multicarrier signals interact with each other to cause intermodulation products (intermodulation noise) to appear at the output of the satellite repeater. This intermodulation effect increases with the number of simultaneous users. It may result in out-of-band noise which is subtracted from the output power available to the desired signal or it may be within the frequency band of a desired signal causing severe signal distortion. This undesirable effect may be mitigated to some extent by properly spacing the frequency bands of the various transmitted signals so that most of the intermodulation noise falls outside the bands of the desired signals. However, this causes a significant portion of the satellite bandwidth to be unused and unusable and hence a significant

decrease in available transmission capacity and efficiency of utilization of the satellite [74].

Another major problem of the FM/FDM/FDMA system is the need for complicated and stringent up-link power control among the transmitting stations. In general, the ratio of powers of any two component signals at the output of the TWT will differ from the power ratio of the same two components at the input, the change favoring the stronger signal at the expense of the weaker one (weak signal suppression effect). This situation may require extra margin in the power requirement for each weak-signal transmitting earth station and, in the absence of power control, reduce the total number of stations able to use the repeater simultaneously.

An alternative multiple access communications method is time-division multiple access (TDMA) in which earth stations or users communicate with each other by using short non-overlapping bursts of signal. In the case of PCM/PSK/TDMA used for voice transmission each user first converts the analog signals (e.g. voice) into digital signals via pulse code modulation (PCM) encoding. These digital signals are converted into burst signals by using compression buffers. These burst signals are then used to digitally modulate the assigned carrier by means of phase shift keying (PSK) and these are transmitted over

the satellite link[60]. Because only one signal is passing through the satellite at any instant, intermodulation noise problems and accurate power control requirements are eliminated. Thus, a substantial improvement in useful channel capacity may be obtained. Fig. 1-1 (reproduced from [69]) illustrates the transmission capacity of an Intelsat IV transponder as a function of the number of active earth stations (those simultaneously accessing the satellite transponder) in a network using the different multiple access systems. It is readily evident from the plots in Fig. 1-1 that when only a small number of earth stations is accessing the channel in either its assigned frequency or time partition, then the available transponder capacity is high and efficient use is made of the satellite transponder in both the TDMA and FDMA modes. However, as the number of simultaneous accesses increases, the transponder capacity drops sharply for the FDMA mode while that of TDMA decreases much more slowly. Table 1-1 compares the general capabilities and requirements of TDMA and FDMA satellite systems (extracted and modified from [58]).

Either FDMA or TDMA is well suited for a high capacity system with few traffic fluctuations with TDMA having an advantage as the number of accesses increases. However, if there exists a large number of users (in the order of several hundreds), each with small but changing communications traffic requirements, other forms of multiple

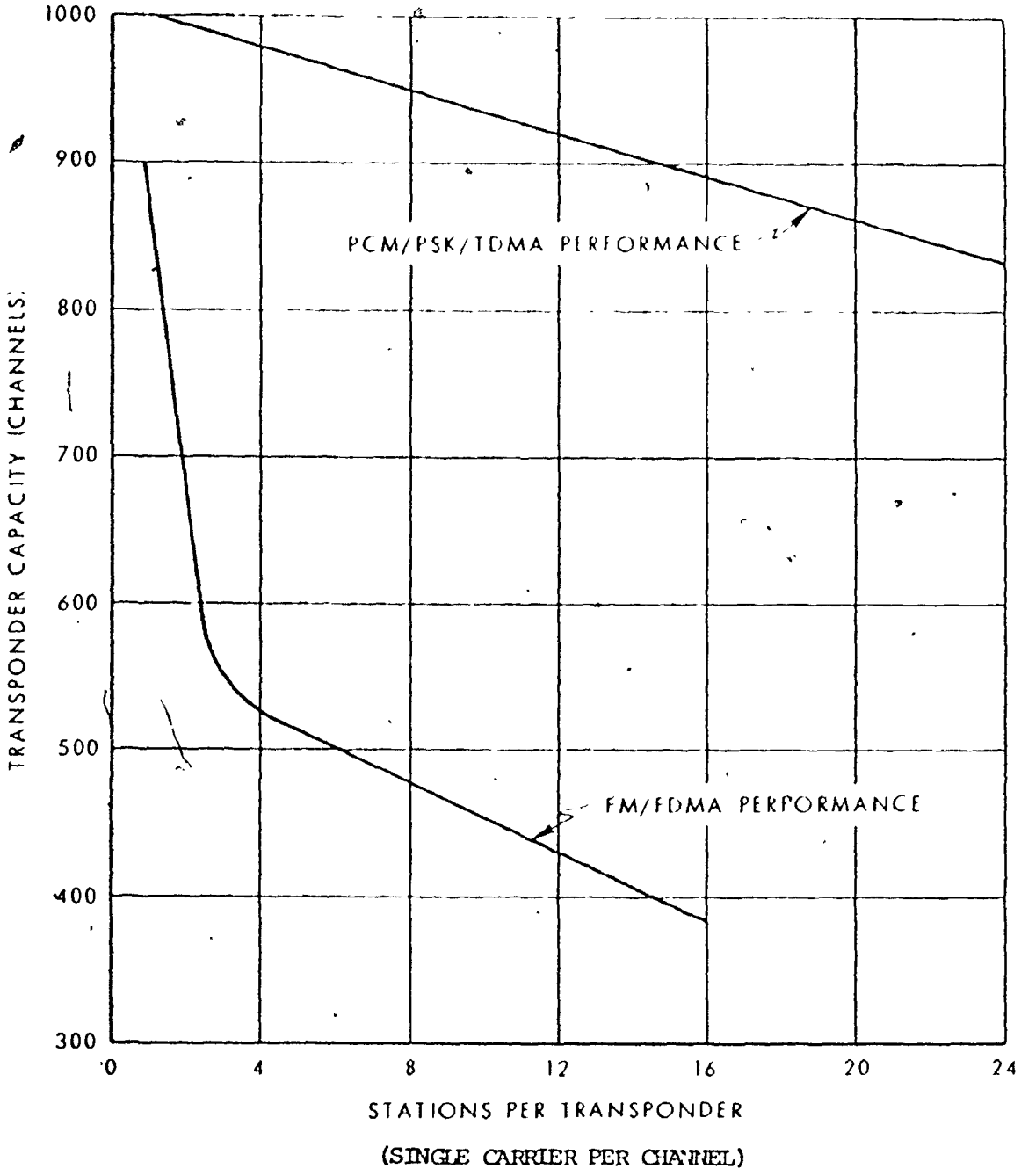

Fig. 1-1. Capacity comparison.

Table 1-1

COMPARISON OF TDMA AND FDMA FOR SATELLITE COMMUNICATIONS

	TDMA	FDMA
Total system capacity	Drops slowly with number of accesses	Undergoes a rapid drop from one to four accesses
Effective peak transmit power requirement at earth station	Each station may saturate satellite transponder	Power requirement is proportional to traffic density
Message modulation	Digital	Analog or digital
Up-link power control	Not critical	May be critical if high capacity is required
Frequency stability	Short-term frequency stability may be critical to carrier recovery circuit	Long-term frequency control is critical for small channel bandwidths
Interference to adjacent RF channels	A band-limiting filter following the satellite TWT may be required to reduce the effect of energy spreading	Out of band intermodulation products do not generally limit system design

(continued)

Table 1-1 (continued)

	TDMA	FDMA
Modems	Identical wideband burst modems for all stations	Operating bandwidth of modem varies with station's traffic requirement
Timing and control	Burst synchronization with modem control interface is required at each station for time multiplexing at the satellite repeater	Not required
Data buffers	Required	Not required
Frequency planning for earth station	Simple because of the same, single transmit and receive carrier frequency for all earth stations	* Complex frequency multiplexing equipment is required

(continued)

* Only applies to FM/FDM/FDMA case.

Table 1-1 (continued)

	TDMA	FDMA
Power bandwidth efficiency	Bandwidth utilization efficiency can be increased by using higher order modulation. In power-limited case forward-acting error correcting codes can be applied to improve the performance of the overall system.	* Bandwidth is intentionally traded off for power.
Cost of present technology (up to 1975).	Expensive time multiplexing equipment is required.	* Can use the existing terrestrial microwave equipment to reduce the overall cost.

*Only applies to FM/FDM/FDMA case.

access, e.g. spread spectrum multiple access (SSMA), may be more appropriate.

In SSMA, the carriers from each earth station are frequency or phase modulated in such a way that their transmitted spectra occupy the whole of the available transmission bandwidth. The message modulation bandwidth in such a system (SSMA) is normally small relative to the system bandwidth. The message modulation can take the form of an analog frequency or phase modulated signal or it can take a digital form such as phase or frequency shift keying. The usual method of generating a spread-spectrum signal, known as the direct-sequence method, is to assign to each user a distinct pseudonoise (PN) sequence*. This is known as pseudonoise carrier. The clock rate of this PN sequence (equal to half the transmitted signal bandwidth) is normally several orders of magnitude (≈1000) larger than the message bandwidth. Each active user then modulates his message onto this pseudonoise (PN) sequence and transmits the resulting PN carrier through the satellite repeater to the receiving terminals. Both the spectrum spreading and the function of addressing the transmitting station are achieved by this PN carrier. Upon receiving this spread-spectrum signal, each earth station employs a phase coherent

*A sequence of 2^n-1 binary numbers (zeros and ones) that is generated from a linear feedback shift register of length n.

correlator capable of locking onto any one of the transmitted signals while rejecting the others. Once the receiving station is locked onto one of the PN carriers, the message can then be recovered by correlation detection.

The PN sequence used to spread the spectrum of the multiple-access carrier also serves to address the transmitted carrier to the desired receiver automatically. In general, owing to the length of the PN sequence normally used, an extremely large number of distinctly different addresses are available, many more than the number of active links a satellite repeater can support. However, this multiple access method is not widely used commercially at present because it requires fast symbol synchronization to the transmitted PN sequence, and because it usually can handle only slow to medium speed messages. Furthermore, it requires more complex terminal equipment, more accurate power control at the transmitter (in order to avoid the incidence of weak signal suppression), and most important of all it yields very poor transponder bandwidth utilization.

1.2) THE TRAVELING WAVE TUBE (TWT)

Most satellite transponders to date and in the near future will employ traveling wave tube (TWT) amplifiers in the high power amplifier stage of the transmitting section of the satellite repeater. This choice has been dictated

by the needs for broad bandwidth, high gain, relatively light weight, long life, high reliability and high direct-current (DC) to radio frequency (RF) power conversion efficiency all of which are supplied by the TWT.

In order to facilitate an understanding of its behaviour, a brief and elementary physical description of the traveling wave tube is now given. The discussion in this section essentially follows that in [57], and can be found in most texts on electromagnetic devices [64].

The basic elements of a traveling wave tube are an electron beam and, surrounding the beam, an RF slow wave structure [64] which supports the propagation of a traveling electromagnetic wave. The RF structure, an electron gun (cathode, anode), electron focusing structure and a collector comprise the components of the TWT as shown in Fig. 1-2.

In the TWT an electron beam generated by the electron gun traverses the cylindrical axis of an evacuated glass tube about 30 cm. long and about 25 mm. wide. The beam, which travels through the centre of the tube, is enclosed by a spiral wire coil (the helix). The coil and the electron collector are both given a positive bias. In order to keep the beam focused, the tube is surrounded by an axial magnetic field. This focusing field, which is produced by an external magnetic coil, is also known

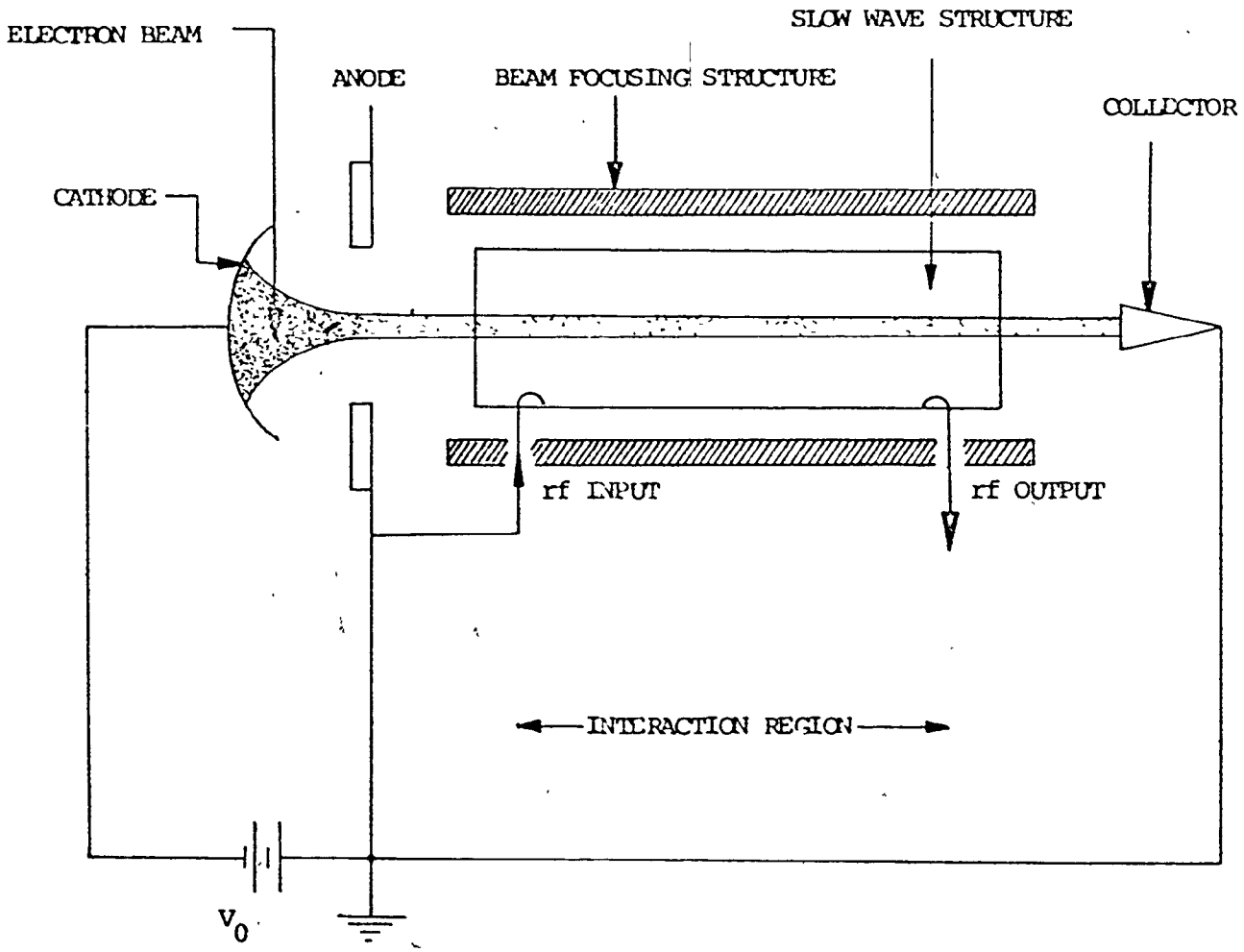

Fig. 1-2. Traveling wave tube.

as the beam directing field.

The high frequency signal(RF input) that is to be amplified is fed in at the beginning of the helix. It becomes increasingly amplified in its passage along the helix and is then uncoupled at the end (RF output). The continuous and progressive interaction of the fields of the electron beam and the signal leads to a bunching of the beam electrons. These bunched electrons form electric fields and consequently induce electric fields on the helix. These induced fields are 90° out of phase with the initially present field. The resultant field present on the helix appears greater in comparison to the original field, and thus exhibits an amplification effect. Essentially there is a transfer of energy from the electrons to the signal field. Under correct operating conditions, the total energy of the electrons decreases along the beam and the total energy of the high frequency signal increases along the helix.

At low RF drive levels a faithful reproduction of the input signal is found at the cutput of the TWT, except that there has been a considerable increase in power due to beam-wave interaction as explained earlier. The TWT in this case is a linear device, where the output signal grows in direct proportion to the applied input signal. Above a certain power level, however, an increase in RF

input power will no longer result in a corresponding increase in output power. The TWT's amplification process is then said to be in saturation. This relationship between input and output power of the TWT is generally known as the amplitude modulation to amplitude modulation (AM/AM) conversion effect.

Apart from this AM/AM effect, the input drive power level also effects the velocity distribution of the electron bunches and therefore results in an amplitude-dependent phase change at the output of TWT. This phase shift as a result of input drive level is known as amplitude modulation to phase modulation (AM/PM) conversion effect. At small input signal level this relative phase shift is small but it increases as the saturation level is approached. This is to be expected, since a large velocity change of the electron bunches occurs when the input is high which in turn results in a large phase shift at the output of the TWT. The plots of phase shift and output power versus input power level for a typical TWT (Hughes 261-H tube) is as shown in Fig. 1-3.

In general, both AM/PM and AM/AM conversion effects cause nonlinear signal distortion at the output of the TWT. When a single carrier is present at the input, unwanted harmonic signals, which are frequency multiples of the fundamental signal at the input, are generated at

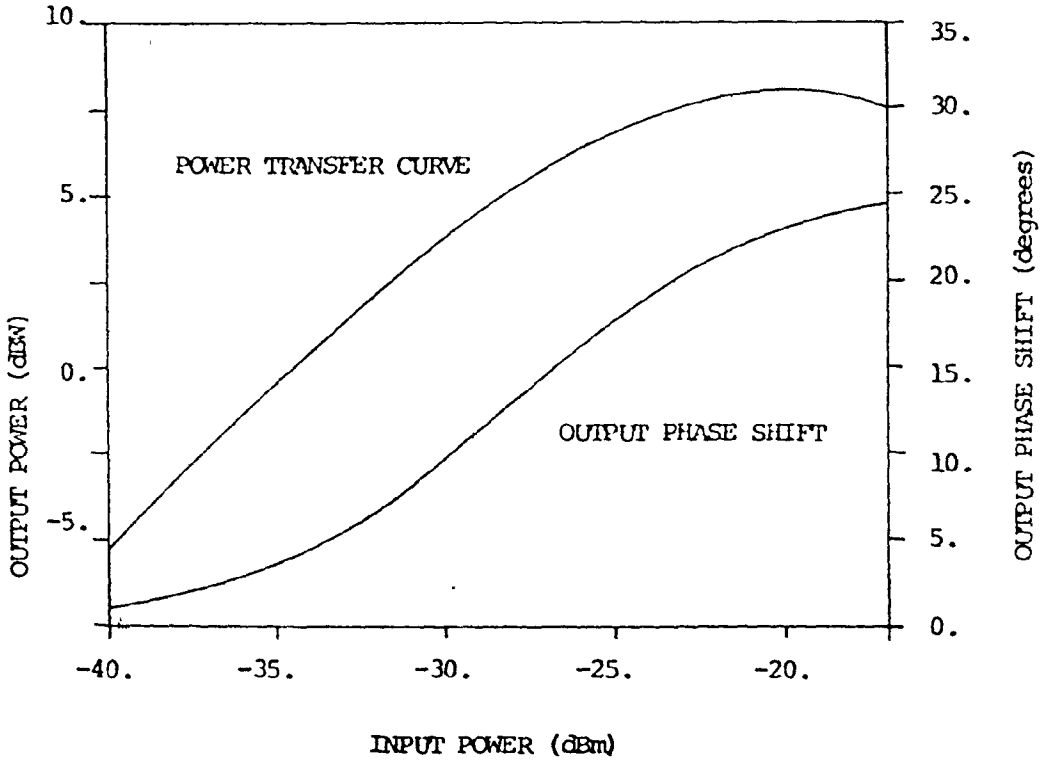

Fig. 1-3. The single-carrier characteristic of an Intelsat IV TWT, Hughes 261-H.

the output. In the case of multicarrier input signals, the output signal usually contains the intermodulation products that are displaced in frequency on the high and low side of the original carriers. Both these harmonic signals and intermodulation products can severely distort the output signal especially when the TWT is operating near its saturation point.

1.3) SCOPE OF THE THESIS

The analysis of the effect of TWT nonlinearity on the performance of coherent phase shift keying (CPSK) is examined in some detail in the thesis. Other impairments caused by multipath propagation, amplitude fading, carrier recovery, bit timing recovery and frequency translation in the satellite will not be considered, however, as each of these defects does create a number of new problems. In most cases, provided the nonlinear distortion effects are properly accounted for these other problems can be handled by well known means [9, 22, 36, 53, 55-56].

The satellite repeater is assumed to be nonregenerative and its main function is to amplify the signal, transmitted from an earth station, prior to retransmitting it to another receiving earth station. Therefore in this thesis, the satellite communications channel will be modelled simply by:

(1) additive Gaussian noise sources on the up-link and the down-link paths.

(2) a wideband TWT exhibiting a nonlinear and frequency independent gain and phase shift characteristics.

This proposed communications model approximates the PSK/TDMA case with wideband transmitting and receiving filters. Furthermore it also represents the PSK/SSMA case where the channels, other than the one being monitored, can be regarded as independent equal power white noise processes [4].

A review of the analysis of coherent phase shift keying (CPSK) systems through the linear additive noise channel is given in Chapter 2. This analysis, though not directly applicable to the system of interest here yields a bound on the attainable performance that can be used to compare with that of the nonlinear channel. In the latter part of Chapter 2, different existing models of wideband TWT's are described and compared concurrently with the development of a new and simple quadrature model. This novel model is most useful in that it is well behaved for all input drive levels and requires the choice of only four parameters to obtain a good fit to the actual TWT characteristics.

In Chapter 3 the optimum bandpass nonlinearity that maximizes its output signal to noise ratio for a certain

class of input signals is derived, and different methods of compensating the TWT to approximate this optimum bandpass nonlinearity are investigated.

The performance of CPSK systems through nonlinear channels is examined in Chapter 4 for both the bandwidth-limited and the power-limited channel. For the latter case a single sample detection and majority logic decision receiver is assumed, and the bit error rate is determined as a function of up-link and down-link bit energy to noise spectral density ratio.

In Chapter 5 the performance of a binary CPSK signal transmitted through a purely amplitude - limiting channel is considered for two other types of receiver. These are:

(1) the linear integrate and dump correlation receiver

(2) the nonlinear maximum - likelihood receiver.

Finally, Chapter 6 presents conclusions and suggestions for further research.

CHAPTER 2

PRELIMINARY DISCUSSION AND CHANNEL MODELLING

In this chapter we first, briefly review the performance obtainable when M-ary coherent phase shift keying (CPSK) signals are transmitted through a linear channel. This performance will be used, in the subsequent chapters, as the basis of comparison for the performance of a similar CPSK system transmitting signals through a nonlinear channel. In the latter part of this chapter a novel quadrature model of the TWT is developed and compared to other existing TWT models.

2.1. PERFORMANCE OF COHERENT PHASE SHIFT KEYING (CPSK)

At high transmission rates, coherent phase shift keying (CPSK) techniques are the most widely used of all digital modulation methods. This occurs because they are efficient from the point of view of

(1) conservation of bandwidth

(2) the possibilities of using very simple techniques for transmission and reception.

The performance of a CPSK system in an additive thermal noise channel is well known and can be found in most texts on digital communication [20, 53, 76, 79].

Nevertheless, we shall include the review here for the sake of completeness.

In the case of an additive noise channel, the transmitted signal in the time interval $0 \leq t \leq T$, where T is the symbol interval, can be written as

$$s_i(t) = \begin{cases} \sqrt{\frac{2E}{T}}\, g(t) \cos(\omega_o t + \theta_i) & 0 \leq t \leq T \\ 0 \quad \text{elsewhere} \end{cases}$$

$$i = 1, 2, 3, \ldots, M. \qquad (2.1)$$

where 1) E is the transmitted signal energy per symbol

2) g(t) is a unit energy pulse shape, which in the additive noise case may be conveniently taken to be rectangular

3) ω_o is the angular carrier frequency which is assumed to be a fixed integer multiple of $\frac{2\pi}{T}$ where T^{-1} is the symbol rate or $\omega_o >> \frac{2\pi}{T}$

4) θ_i is the transmitted phase and assumes one of the values $\frac{2\pi i}{M}$, $i = 1,2,\ldots,M$ in each symbol interval.

Assuming that the ith symbol has been transmitted, the received signal may be written as

$$x(t) = s_i(t) + n(t) \qquad 0 \leq t \leq T. \qquad (2.2)$$

where n(t) is narrowband white Gaussian noise which may be written as

$$n(t) = n_1(t) \cos \omega_o t - n_2(t) \sin \omega_o t \qquad (2.3)$$

where $n_1(t)$ and $n_2(t)$ are both zero mean, statistically independent white Gaussian noises, with single sided power spectral density N_o watts/Hz.

Within one symbol duration the received signal may be written as

$$x(t) = \sqrt{\frac{2E}{T}} \cos [\omega_o t + \theta_i] + n_1(t) \cos \omega_o t - n_2(t) \sin \omega_o t \qquad 0 \leq t \leq T . \tag{2.4}$$

Assuming that θ_i is equally likely to have any one of the M possible values, demodulation is readily accomplished by forming the quantities

$$X = \sqrt{\frac{2}{T}} \int_0^T x(t) \cos \omega_o t \, dt \tag{2.5}$$

and

$$Y = \sqrt{\frac{2}{T}} \int_0^T x(t) \sin \omega_o t \, dt \tag{2.6}$$

which are then sampled and passed, at time T, to a decision device which makes a decision on the value of the transmitted θ_i. A block diagram of this receiver is shown in Figure 2-1.

Conditioned on the knowledge of θ_i, the variables X and Y are statistically independent Gaussian random variables with means $\sqrt{E} \cos \theta_i$ and $\sqrt{E} \sin \theta_i$ and common variance $\frac{N_o}{2}$ watts. The conditional joint probability density function (pdf) of X and Y given θ_i may be written as

$$p(X,Y|\theta_i) = \frac{1}{\pi N_o} \exp \left[-\frac{(X - \sqrt{E} \cos \theta_i)^2}{N_o} - \frac{(Y - \sqrt{E} \sin \theta_i)^2}{N_o} \right] \tag{2.7}$$

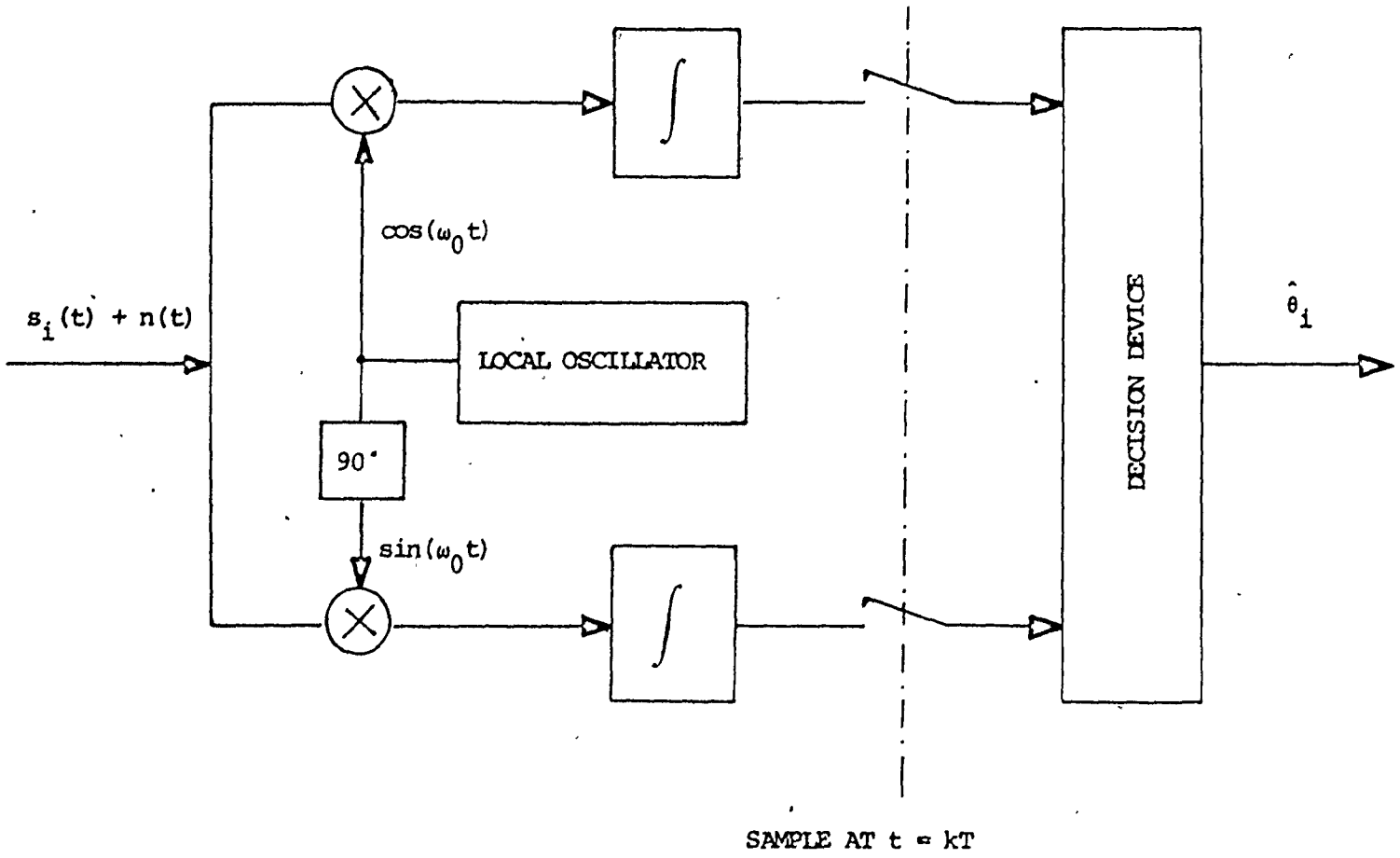

Fig. 2-1. Block diagram of a correlation receiver for CPSK systems.

Now define the new random variables R and ε as

$$X = R N_o \cos \varepsilon$$

$$Y = R N_o \sin \varepsilon \qquad (2.8)$$

In terms of R and ε equation (2.7) then becomes

$$p(R,\varepsilon|\theta_i) = \frac{R}{\pi} \exp\{-[R^2 - 2R\rho \cos(\varepsilon + \theta_i) + \rho^2]\} \qquad (2.9)$$

where $\rho = \frac{E}{N_o}$ is the symbol energy to noise power spectral density ratio.

Since the values of the transmitted phase θ_i are equally probable, we can take θ_i to be zero without loss of generality and the symbol probability of error is given by the probability that $|\varepsilon| > \frac{\pi}{M}$ which can be written as

$$P_e(M) = 1 - \int_{-\frac{\pi}{M}}^{\frac{\pi}{M}} \int_0^\infty p(R,\varepsilon|\theta_i=0)\, dR\, d\varepsilon \qquad (2.10)$$

Substitution of equation (2.9) into (2.10) yields after some manipulation

$$P_e(M) = 1 - \frac{2}{\pi} \int_0^\infty \exp[-(u-\rho)^2] \left(\int_0^{u\tan(\frac{\pi}{M})} \exp[-v^2]\, dv \right) du \qquad (2.11)$$

It was shown by Lindsey [54] that equation (2.11) can be reduced to a readily computable expression as

$$P_e(M) = \frac{M-1}{M} - \frac{1}{2}\operatorname{erf}[\rho \sin \tfrac{\pi}{M}] -$$

$$\frac{1}{\sqrt{\pi}} \int_0^{\rho \sin(\pi/M)} \exp[-y^2] \operatorname{erf}[y \cot \tfrac{\pi}{M}]\, dy \qquad (2.12)$$

where erf (x) = $\frac{2}{\sqrt{\pi}} \int_0^x e^{-t^2} dt$ is the well known error function.

In the case of binary phase shift keying (M=2), equation (2.12) reduces to the well known result

$$P_e(2) = \frac{1}{2} \text{erfc } [\rho] \tag{2.13}$$

where erfc (x) = 1 - erf (x)

It is also possible to evaluate equation (2.12) in closed form for 4-phase CPSK (M=4). The result is given by [53].

$$P_e(4) = \text{erfc } [\frac{\rho}{\sqrt{2}}] - \frac{1}{4} \text{erfc}^2 [\frac{\rho}{\sqrt{2}}] \tag{2.14}$$

In the region where $\rho >> 1$, equation (2.14) can be approximated by

$$P_e(4) \approx \text{erfc } [\frac{\rho}{\sqrt{2}}] \tag{2.15}$$

In the M-ary case, if we encode the equiprobable, source symbols using a Gray code [56], which has the property that only one binary bit is changed in going from one symbol to an adjacent symbol, then the average bit error probability $P_b(M)$ is related to the average symbol error probability, $P_e(M)$ by [77]

$$P_b(M) \approx \frac{P_e(M)}{\log_2 M} \tag{2.16}$$

where each symbol contains $\log_2 M$ bits of information. Hence for M = 4 and from equations (2.15 - 2.16)

$$P_b(4) \simeq \frac{1}{2} \operatorname{erfc}\left[\frac{\rho}{\sqrt{2}}\right] \qquad (2.17)$$

But the bit energy for 4-phase PSK is half that of binary PSK. Hence for equal bit energy to noise power spectral density ratios, 4-phase CPSK and binary CPSK have identical bit error performance. This result is significant since 4-phase CPSK requires only half the bandwidth of binary CPSK for the same transmitted power. Fig. 2-2 illustrates the symbol error performance for M-ary CPSK as a function of the bit energy to noise ratio defined as

$$\frac{E_b}{N_o} = \frac{\rho}{\log_2 M}$$

2.1 MODELLING OF SATELLITE NONLINEARITY

In order to analyse the nonlinear effects of a TWT on the performance of communication systems or to compensate for this nonlinear distortion, it is first necessary to develop a relatively simple, analytical model of the tube.

In recent years considerable effort has been made to develop analytic expressions that approximate the TWT nonlinearity. In an attempt to investigate the effect of intermodulation noise caused by TWT nonlinearity or the intersymbol interference effect (caused by adjacent symbols),

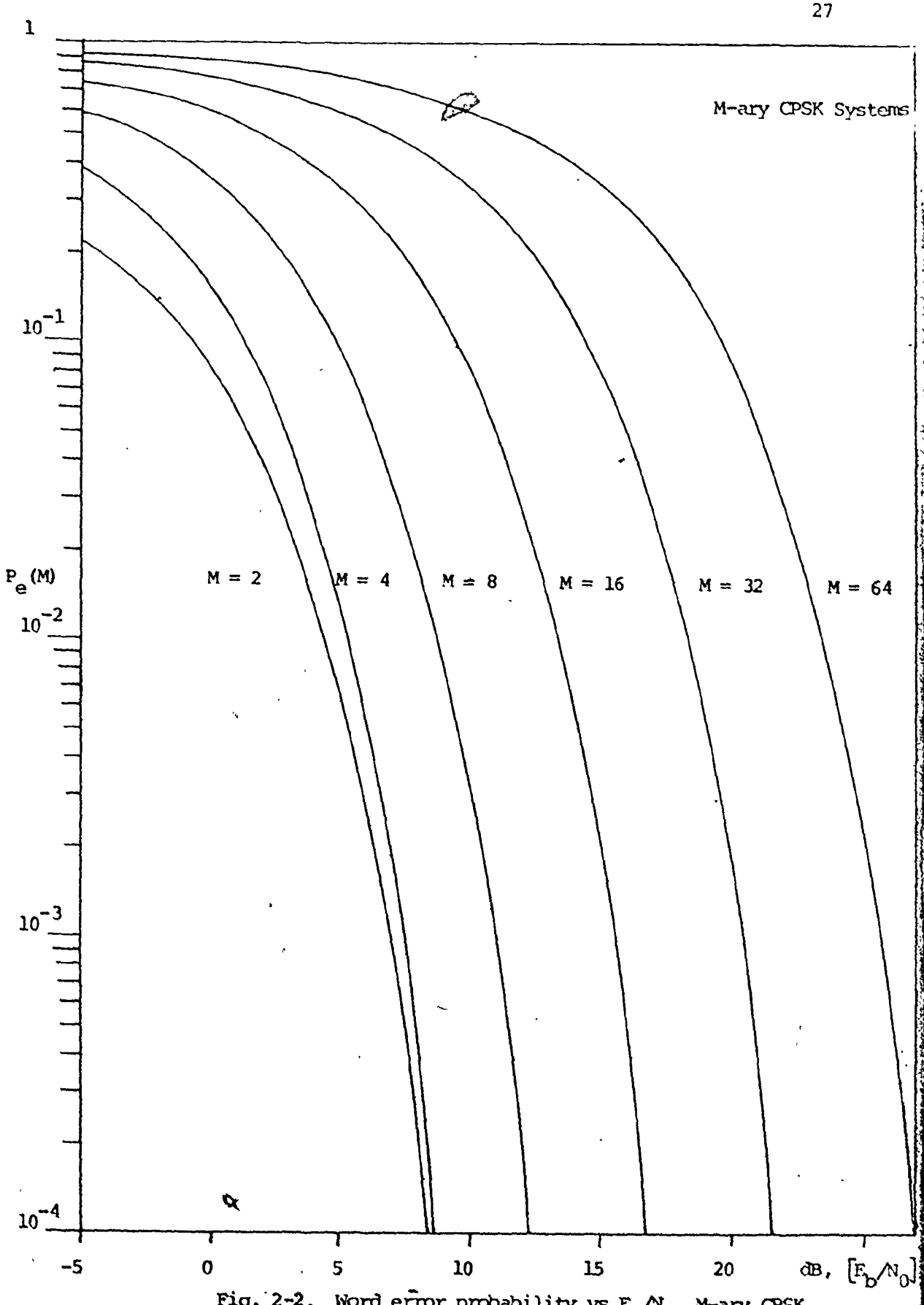

Fig. 2-2. Word error probability vs E_b/N_0, M-ary CPSK.

different models of the tube have been developed [11-13, 25, 31 33-34, 51]. Basically these models are either the cascade combination of phase and amplitude nonlinearities as shown in Figure 2-3 or some form of quadrature envelope nonlinearity model as depicted in Figure 2-4. However, the models developed earlier [11-13, 25, 31, 33-34, 51] only approximate the tube characteristics over certain, restricted regions of tube operation, as dictated by the amount of the peak-power-limited interferences at the input of the tube, and the characteristics of the tube beyond saturation are not critical. However, in the case when up-link noise is present at the input of the tube, these models can lead to an anomalous behaviour of the equivalent noise statistics at the output. This occurs because the noise is not peak-limited or bounded. The cascade model of the tube in the presence of noise at the input has been considered in reference [80].

In this section we introduce another approximation for the envelope nonlinearities in the quadrature model of the TWT as originated in [31, 51] and depicted in Figure 2-4. The two envelope nonlinearities $Z_p(R)$ and $Z_q(R)$ in the in-phase and quadrature paths are assumed here to take the form

$$Z_p(R) = C_1 R e^{-C_2 R^2} \quad I_o[C_2 R^2] \tag{2.18}$$

$$Z_q(R) = S_1 R e^{-S_2 R^2} \quad I_1[S_2 R^2] \tag{2.19}$$

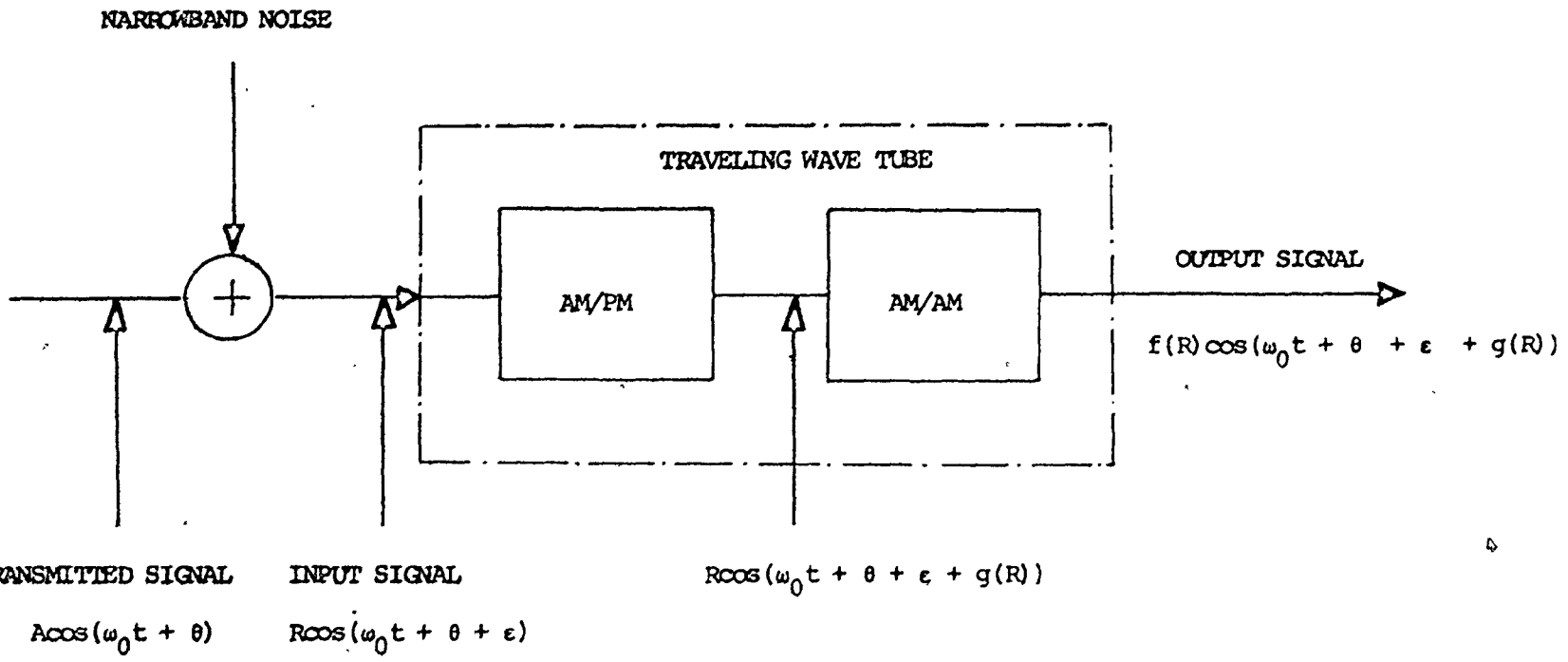

Fig. 2-3. Cascade model of TWT

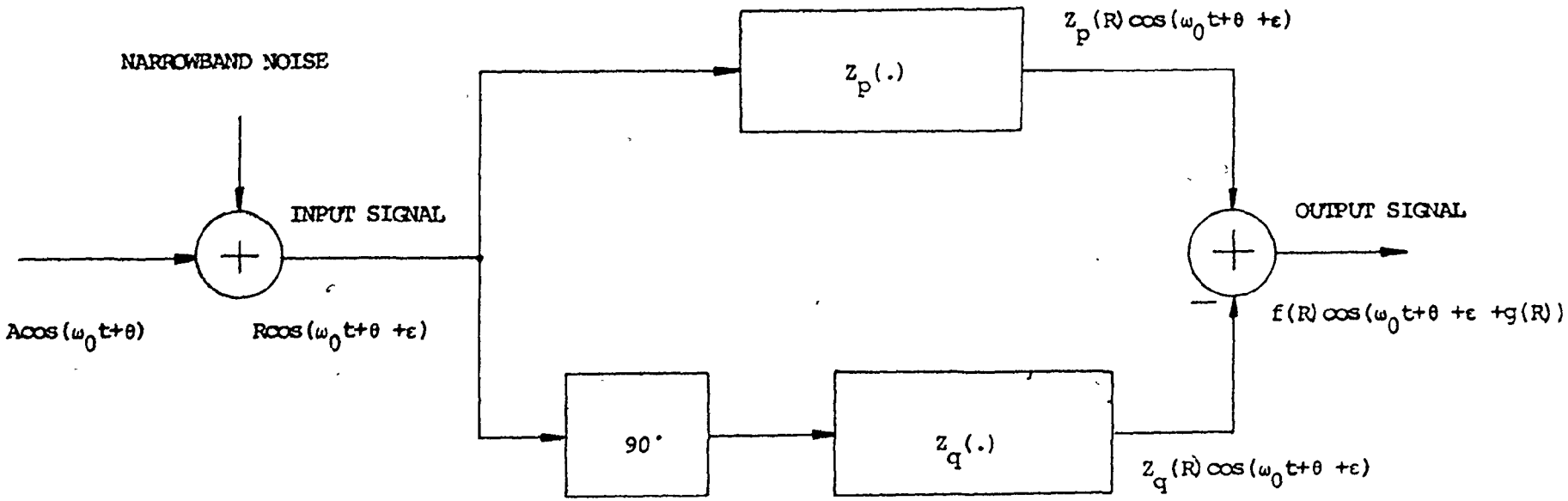

Fig. 2-4. General quadrature model of TWT

where $I_n(.)$ is the modified Bessel function of the first kind of order n and R is the envelope of the TWT input signal.

The coefficients (C_1, C_2, S_1, S_2) are computed from a conventional optimization subroutine as described in Appendix A, so as to yield a least squares curve fit to the actual tube nonlinearities and are found to be

$$C_1 = 1.61245 \quad , \quad C_2 = .053557$$

$$S_1 = 1.71850 \quad , \quad S_2 = .242218$$

for a Hughes 261-H tube as used in the Intelsat IV satellite.

Unlike the other quadrature models [25, 31, 33 - 34, 51], this Bessel function approximation only needs a few coefficients (four as compared with sixteen in [31]) to give a good fit to the TWT nonlinearities up to and beyond saturation. In addition the model is well behaved for all R and permits straightforward evaluation of the TWT output noise statistics. For very large R, equations (2.18) and (2.19) can be expanded asymptotically to give [2].

$$\lim_{R \to \infty} Z_p(R) = \frac{C_1}{\sqrt{2\pi C_2}}$$

and

$$\lim_{R \to \infty} Z_q(R) = \frac{S_1}{\sqrt{2\pi S_2}} \qquad (2.20)$$

Each $Z_p(R)$ and $Z_q(R)$, as shown in equation (2.20),

is asymptotically constant and therefore well behaved for large R. This distinct characteristic of our model circumvents any anomaly that may arise in evaluating the statistics of the interference terms at the output of TWT, subject to the up-link noise at the input.

For small R, $Z_p(R)$ and $Z_q(R)$ can be expressed as a power series in R. Retaining only the first term in such power series expansion, we get [2].

$$Z_p(R) \simeq C_1 R$$

$$Z_q(R) \simeq \frac{S_1 R^2}{2} \qquad (2.21)$$

The nonlinearities in equations (2.18) and (2.19) are plotted and compared with the measured characteristics of the tube (Hughes 261-H) in Fig. 2-5. It is obvious from this figure that the model proposed provides an excellent approximation to the actual tube characteristics in the region of interest for tube operation.

This quadrature model of a TWT as described by equations (2.18 - 2.19) can also be extended to include other types of nonlinear amplifiers exhibiting gain compression and AM/PM conversion effects. Examples of such amplifiers include Klystron power amplifiers and crossed field amplifiers.

Table 2-1 summarizes the existing models of the traveling wave tube (TWT), that have been used so far in the

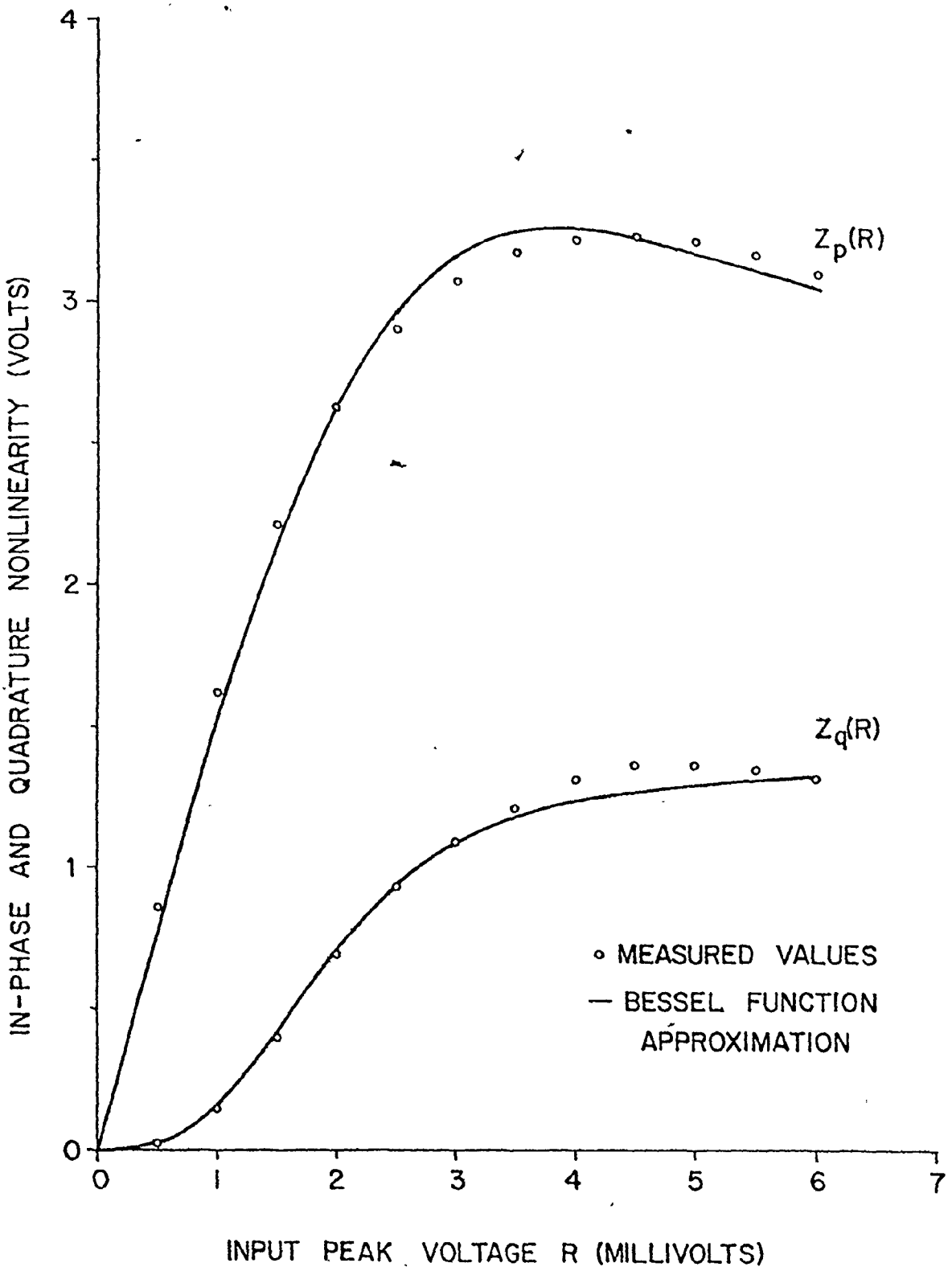

Fig. 2-5. The nonlinear characteristics of TWT (Hughes 261-H) and the Bessel function approximation.

Table 2-1: MODELS OF TWT

Model type (originators)	$Z_p(R)$ or $f(R)$	$Z_q(R)$ or $g(R)$	References
Cascade (Berman & Mahl)	Fourier sine series	Exponential plus quadratic function	[11-13]
Cascade (Thomas et al)	Exponential and linear function	Exponential plus quadratic function	[80]
Cascade (Schwartz et al)	Hard- or soft-limiting envelope nonlinearity	Zero phase shift	[4, 48-50, 59, 70]
Quadrature (Kaye et al)	Series of Bessel functions of the first kind of order one	Series of Bessel functions of the first kind of order one	[34, 51]
Quadrature (Eric)	Odd polynomial of R	Odd polynomial of R	[25, 31, 33]
Quadrature (Hetrakul & Taylor)	Modified Bessel function of the first kind of order zero	Modified Bessel function of the first kind of order one	[42]

analysis of satellite communications systems, and provides some indication of the advantages and disadvantages of the various models.

The specific overall channel model for the communication system considered in the thesis is shown in Fig. 2-6. The input to the satellite repeater consists of a single carrier, M-ary phase-modulated, constant-envelope signal and zero-mean, stationary Gaussian noise. The bandpass filter bandwidth, unless it is stated explicitly otherwise, is assumed to be wide enough to pass the signal with negligible distortion and to limit the up-link noise to a bandwidth that is small compared to the center frequency of the filter. The traveling wave tube amplifier on board the satellite exhibits two kinds of nonlinearity, namely the AM/AM and AM/PM conversion effects as described earlier. The TWT is followed by an ideal zonal bandpass filter that confines the output spectrum to essentially only the fundamental band of the signal. After passing through the satellite repeater, the signal is transmitted to the receiver and independent thermal noise is added to it on the down-link. The receiver processes the composite signal and extracts the information-bearing signal coherently using a locally generated carrier reference signal. It is assumed throughout the thesis that carrier and bit timing recovery at the receiver have been achieved.

The system model depicted in Fig. 2-6 is also valid

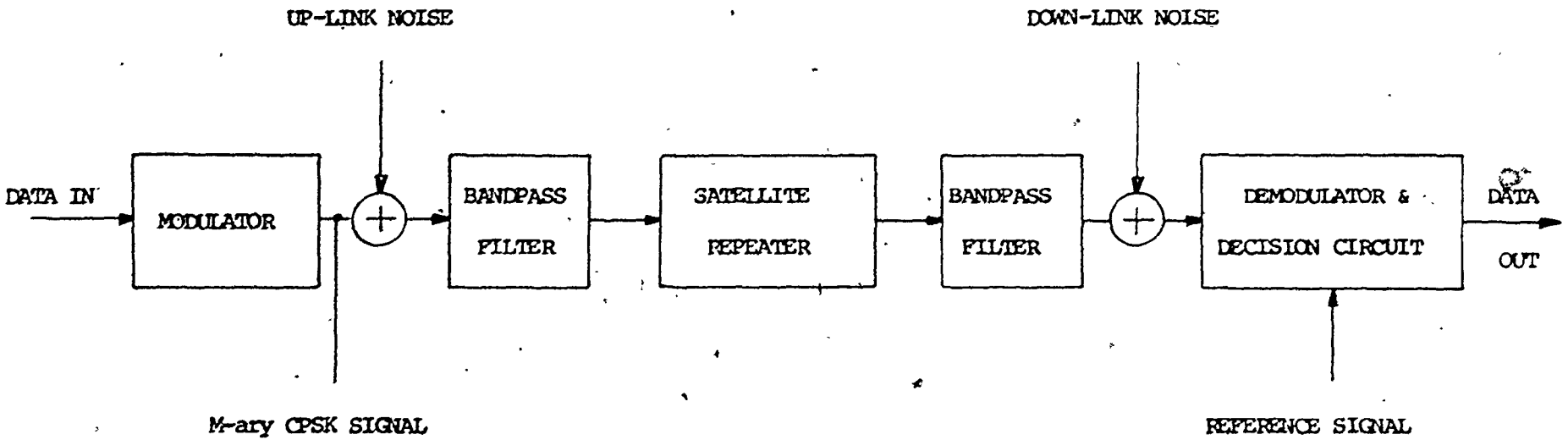

Fig. 2-6. Block diagram of the communication system.

for the analysis of M-ary CPSK signals transmitted through a linear channel with a limiting front end in the receiver. In some practical applications, insertion of a limiter in the receiver front end may be desirable from consideration of dynamic range requirements. In such applications, we only need to disregard the down-link noise component in our model and replace the satellite repeater nonlinearity by a hard-limiter.

CHAPTER 3

COMPENSATION OF SATELLITE NONLINEARITY

The signal distortion resulting from the nonlinearity of the traveling wave tube (TWT) amplifier has presented a number of problems to designers of various multiple access satellite communication systems and has been a significant factor in determining communications system performance. The evolution of multiple access techniques from essentially analog frequency-division multiple access (FDMA) to essentially digital time-division multiple access (TDMA), though in no small measure motivated by the problem of nonlinear distortion caused by the TWT, has not resulted in complete elimination of the problems but merely in a shift in emphasis. For example, the basic characteristics of nonlinear power transfer and amplitude dependent phase modulation (AM/PM) conversion produced by the TWT operating close to maximum power output result in the problems associated with intermodulation and cross-modulation distortion, gain suppression, large signal capture (small signal suppression), and harmonic distortion in systems employing multicarrier FDMA techniques. However, these same nonlinear characteristics of the TWT also cause single carrier waveform distortion, co-channel interference

as a result of spectrum-spreading, additional inter-symbol interference and reduced error rate performance in systems employing single-carrier TDMA techniques.

In this chapter different means of compensating the TWT, in order to alleviate the degradation caused by TWT nonlinearity, are investigated. In section 3.1 an expression for an optimal bandpass nonlinearity that maximizes its output signal to interference power ratio (C/I) for a certain class of input signals is derived. This is followed by a discussion of three main compensation techniques which can be used in conjunction with the TWT so that the overall transfer characteristic of the tube approximates that of the optimal bandpass nonlinearity.

3.1 OPTIMUM BANDPASS NONLINEARITY

To simplify our notation without loss of generality we shall consider the case of an unmodulated sinusoidal signal of amplitude A, plus narrow-band Gaussian noise at the input to the general quadrature model of the TWT (depicted in Fig. 2-2). In terms of the envelope, R , and phase, ε, the input signal can be written as

$$x(t) = R(t) \cos[\omega_0 t + \varepsilon(t)] \qquad (3.1)$$

The joint probability density function (pdf) of the envelope, R, and the phase, ε, of the input signal is

then [67]

$$p(R,\varepsilon) = \frac{R}{2\pi\sigma^2} \exp\left[-\frac{A^2-2A\,R\cos\varepsilon+R^2}{2\sigma^2}\right] \qquad (3.2)$$

for $0 \le R < \infty$ and $0 \le \varepsilon \le 2\pi$

where σ^2 is the input noise variance.

The pdf of the envelope R can be obtained by integrating equation (3.2) with respect to ε and can be shown to be [67]

$$p(R) = \frac{R}{\sigma^2} I_o\left[\frac{AR}{\sigma^2}\right] \exp\left[-\frac{A^2+R^2}{2\sigma^2}\right] \qquad 0 \le R < \infty \qquad (3.3)$$

where $I_0(.)$ is the modified Bessel function of the first kind of order zero.

Similarly, the integration of equation (3.2) over R would yield the pdf of the phase, ε, as [67]

$$p(\varepsilon) = \frac{e^{-\rho}}{2\pi} + \frac{\cos\varepsilon}{2}\sqrt{\frac{\rho}{\pi}}\, e^{-\rho\sin^2\varepsilon}\, \mathrm{erfc}\{-\sqrt{\rho}\cos\varepsilon\}$$

$$0 \le \varepsilon \le 2\pi$$

where $\rho = \frac{A^2}{2\sigma^2}$ = equivalent input CNR and the complementary error function erfc (x) is defined as:

$$\mathrm{erfc}(x) = \frac{2}{\sqrt{\pi}} \int_x^\infty e^{-t^2}\, dt$$

For our purpose, we define the optimum bandpass nonlinearity as the nonlinear device that maximizes the output signal power subject to a constant signal plus noise power at the output. This criterion is equivalent to maximizing the output SNR. The joint pdf of the envelope, R, and phase, ε, and the pdf of the envelope, R, are assumed to take the forms shown in equations (3.2) and (3.3). This criterion of optimality, i.e. maximum output SNR, has been shown by Jain and Blachman [18, 49] to correspond to the minimum probability of error for the case of a binary CPSK signal transmitted through a nonlinear, purely amplitude limiting channel.

In the case of a nonlinear channel with AM/PM conversion as depicted in Fig. 2-2, the signal power and the total signal plus noise power at the output can be defined as [15]

$$S = \frac{1}{2} \{[E_{R,\varepsilon}(Z_p(R) \cos\varepsilon)]^2 + [E_{R,\varepsilon}(Z_q(R) \cos\varepsilon)]^2\} \tag{3.4}$$

and

$$S + N = \frac{1}{2} \{E_R[Z_p^2(R) + Z_q^2(R)]\}$$

where Z_p and Z_q are the in-phase and quadrature envelope nonlinearities in equations (2.18) and (2.19), and $E_{R,\varepsilon}(\cdot)$ denotes the statistical average over R and ε.

The objective is to determine $Z_p^*(\cdot)$ and $Z_q^*(\cdot)$,

the optimum in-phase and quadrature envelope nonlinearities such that S is maximized subject to a prescribed, constant value, C, of S + N. From equations (3.4 - 3.5), we may then define an unconstrained objective function as

$$J = \{\int_0^\infty \int_0^{2\pi} Z_p(R) \cos \varepsilon p(R,\varepsilon)\, dR d\varepsilon\}^2 + \{\int_0^\infty \int_0^{2\pi} Z_q(R) \cos \varepsilon p(R,\varepsilon)\, dR d\varepsilon\}^2 + \hat{\lambda}\{2C - \int_0^\infty [Z_p^2(R) + Z_q^2(R)]\, p(R)\, dR\} \tag{3.6}$$

where $\hat{\lambda}$ is the well known Lagrange multiplier.

By taking the integral in equation (3.6) as the Riemann sum and equating the differentials of J with respect to $Z_p(R)$ and $Z_q(R)$, for fixed R, to zero, we obtain the following necessary conditions defining the optimum envelope nonlinearities, $Z_p^*(R)$, and $Z_q^*(R)$ as

$$2\hat{\lambda} Z_p^*(R)\, p(R) = \left\{\int_0^\infty \int_0^{2\pi} Z_p^*(R) \cos \varepsilon\, p(R,\varepsilon)\, dR.d\varepsilon\right\} \cdot \left\{\int_0^{2\pi} \cos \varepsilon\, p(R,\varepsilon)\, d\varepsilon\right\} \tag{3.7}$$

and

$$2\hat{\lambda} Z_q^*(R)\, p(R) = \left\{\int_0^\infty \int_0^{2\pi} Z_q^*(R) \cos \varepsilon\, p(R,\varepsilon)\, dR\, d\varepsilon\right\} \cdot \left\{\int_0^{2\pi} \cos \varepsilon\, p(R,\varepsilon)\, d\varepsilon\right\} \tag{3.8}$$

where

$$\hat{\lambda} = \frac{S^*}{2C} = \frac{\{E_{R,\varepsilon}[Z_p^*(R)\cos\varepsilon]\}^2 + \{E_{R,\varepsilon}[Z_q^*(R)\cos\varepsilon]\}^2}{4C} \tag{3.9}$$

From equations (3.7) and (3.8) it is readily evident that

$$Z_p^*(R) = \beta Z_q^*(R) \tag{3.10}$$

for any real constant β including zero. The case when $\beta = 0$, however, yields a trivial solution for equation (3.7) and merely indicates that the characteristic of an optimum bandpass nonlinearity is that of $Z_q^*(R)$.

In general it is then necessary for the optimum bandpass nonlinearity to have

(1) an amplitude characteristic satisfying equations (3.7) and (3.8) to within a multiplicative constant, and

(2) a constant output phase shift, independent of the input envelope, R, which may therefore be set to zero.

Substitution of (3.9) and (3.10) into (3.8) yields

$$S^* Z_q^*(R)\, p(R) = C \frac{2S^*}{1+\beta^2}\left\{\int_0^{2\pi} \cos\varepsilon\, p(R,\varepsilon)\, d\varepsilon\right\} \tag{3.11}$$

Equation (3.11) is now identical to [eqn. 31 of [18]], except for a nonzero constant β. Therefore, by using the same argument as in [18], the optimum quadrature amplitude response characteristic, $Z_q^*(R)$, can be expressed as

$$Z_q^*(R) = K\, I_1\left[\frac{AR}{\sigma^2}\right] / I_o\left[\frac{AR}{\sigma^2}\right] \qquad (3.12)$$

where $K = \sqrt{\dfrac{2C^2}{S^*(1+\beta^2)}}$

From equations (3.10) and (3.12), the overall optimum envelope transfer characteristic $Z^*(R)$, is then obtained as

$$Z^*(R) = \sqrt{[Z_p^*(R)]^2 + [Z_q^*(R)]^2}$$

$$= c\, I_1\left[\frac{AR}{\sigma^2}\right] / I_o\left[\frac{AR}{\sigma^2}\right] \qquad (3.13)$$

where $c = K\sqrt{1+\beta^2}$

The function $Z^*(R)$ increases linearly from zero and rises asymptotically toward the value c for large R. This behaviour closely approximates that of a piecewise linear limiter. Also the larger the up-link carrier to noise ratio, $\frac{A^2}{2\sigma^2}$, the more closely this limiter characteristic approaches that of a hard limiter. Fig. 3-1 shows a plot of $Z^*(R)$ as a function of $\frac{R}{A}$ for different values of input carrier to noise ratio defined as

$$(CNR)_I = \frac{A^2}{2\sigma^2} = \rho$$

The results obtained in this section confirm the previous conjectures [44, 51, 82] for the optimum transfer characteristics of bandpass nonlinear saturation devices with AM/PM coversion. To facilitate the compensator design presented in the subsequent analysis, it will be assumed that

(1) amplitude dependent phase shift at the output is

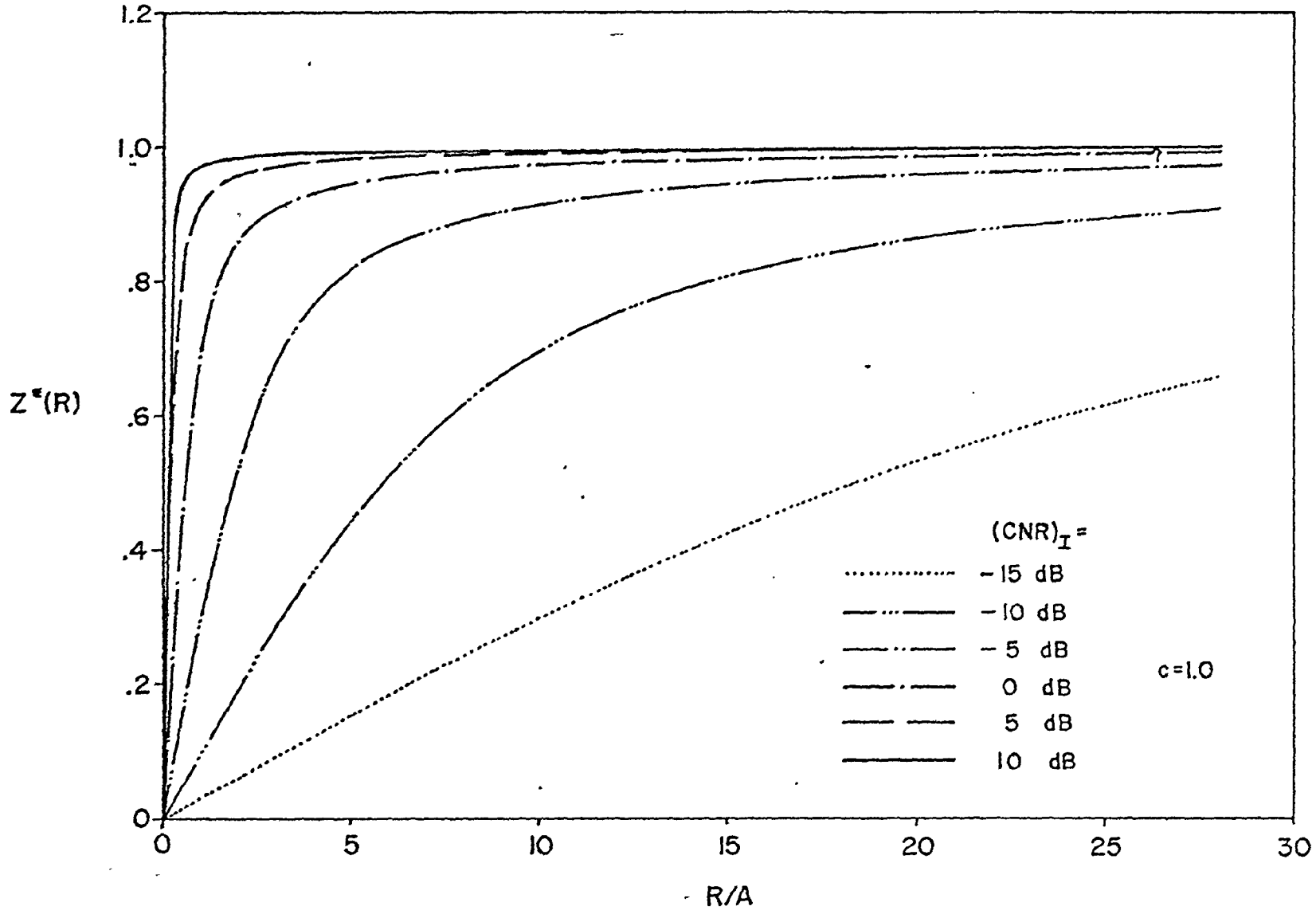

Fig. 3-1. The optimum envelope transfer characteristic

completely eliminated.

(2) the envelope nonlinearity should approximate that of a piecewise linear limiter.

This choice of a design objective avoids the problem of designing a compensator whose characteristic depends on the input CNR, ρ. Although it is only an approximation to the optimum transfer characteristics, it has been shown to yield very good results for the case of multicarrier signals [51, 82].

3.2 TWT LINEARIZATION TECHNIQUES

In order to compensate for the signal distortion caused by TWT nonlinearities, various linearization techniques have been attempted in the past. There exist, fundamentally, two different approaches.

The first approach takes advantage of the fact that the satellite usually contains a number of independent TWT's which together form a multiport transponder of n inputs and n outputs. By the proper design of an n x n Butler matrix phase-shifting network preceding and following these n nonlinear devices, the effect of intermodulation noise generated by each TWT nonlinearity can be substantially reduced [19, 68, 82].

The second approach is to alter the nonlinear characteristics of the overall compensated TWT by means of

input-signal predistortion or feedforward correction of the output signal. Other methods include the equalization of AM/PM conversion effect by controlling the helix voltage modulation [74, 86] and the control of basic frequency and/or spatial characteristics by proper design of the slow wave structure of the TWT [81].

In this section we shall first briefly review the main compensation methods, namely, Butler matrix, feedforward correction and signal predistortion method. A procedure and novel implementation of the signal predistortion circuit is then suggested in section 3.2.3.

3.2.1 Butler matrix transponder (BMT)

The basic configuration of the BMT amplifier network is shown in Fig. 3-2. It consists of two complementary (n x n) Butler matrix networks which precede and follow a set of nonlinear amplifiers. These networks perform a special phase shifting operation on the signal at the input and output of the amplifiers and cause a substantial fraction of the intermodulation products (IMP) appearing at output ports to fall outside the frequency band of the transmitted signal. Consequently a significant portion of the IMP can be reduced by proper filtering at the output ports and the amplifiers can be operated closer to saturation for a specified output C/I ratio. More details on the mathematical description of a Butler matrix transponder (BMT) can be

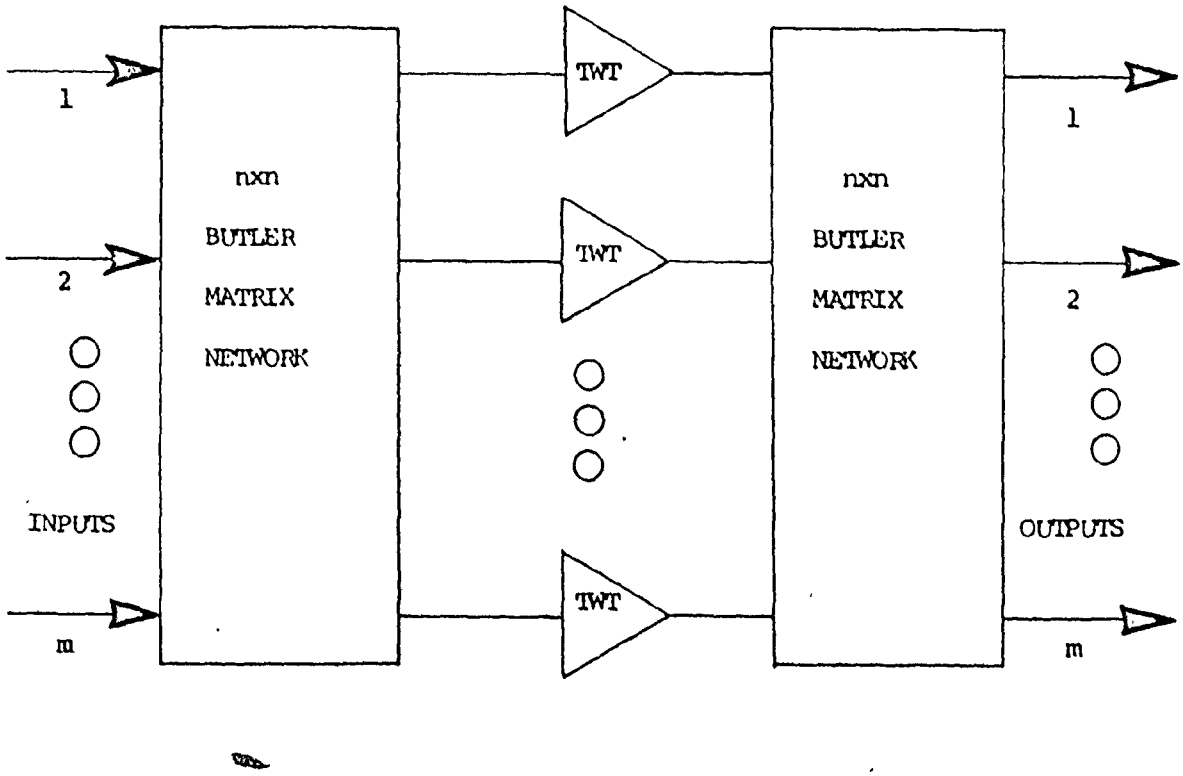

Fig. 3-2. m-Channel Butler Matrix Transponder

found in [68]. In addition to its main feature of rejecting the out of band IMP, the BMT also provides a means of increasing the RF power per channel in the case when the number of inputs to the BMT exceeds the number of existing channels. Furthermore, under non-peak loading condition, the BMT offers a power sharing capability which allows some channels to operate with a greater output power than others without C/I degradation in any channel.

However, in the case of single-carrier operation as in TDMA systems, it has been pointed out in [68] that the BMT loses its power saving qualities and more distortion could occur. The other disadvantages of the BMT include a required increase in the transmission bandwidth as well as the obvious one of requiring multichannel operation.

3.2.2 Feed-forward technique

This method of linearization makes use of a subsidiary TWT to help in the compensation of the operating amplifier tube. A schematic block diagram of the feed-forward linearization technique is shown in Fig. 3-3. The input signal to the transponder is divided into two portions. Part one goes through the main amplifier, TWT_1, and a sampling is taken through a directional coupler with a coupling factor $\frac{1}{G_{ss1}}$ where G_{ss1} approximates the small-signal in-band gain of TWT_1. This sample is compared with

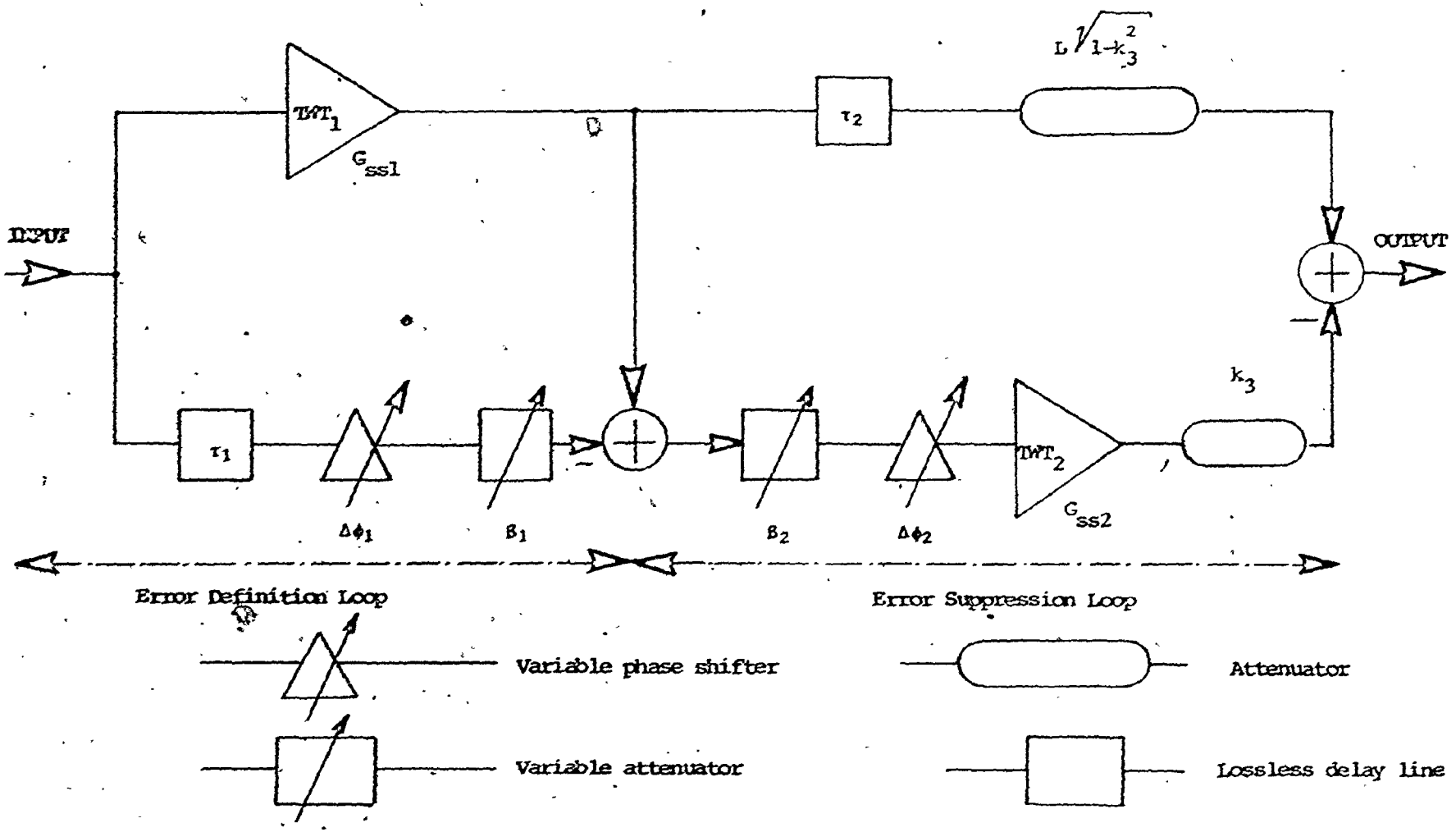

Fig. 3-3. Open-loop feedforward amplifier model.

the reference path signal which has been delayed by a time τ_1, equal to the propagation delay of TWT_1. The phase and amplitude of this delayed reference signal is adjusted by an amount $\Delta\phi_1$ and β_1 by means of a variable phase-shifter and an attenuator. The time-shifted error obtained is then passed through another attenuator, β_2, and a phase-shifter and amplified by a subsidiary tube, TWT_2, whose small signal gain, G_{ss2}, is such that the error is restored to the appropriate level to cancel the error of the main tube. The linearity of the compensated tube is achieved by the proper adjustment of the variable phase shifters and attenuators [71]. An appropriate time delay τ_2 equal to the propagation delay of TWT_2 must also be provided in the main amplifier path in order to achieve synchronization of the two paths. The fixed attenuators in the main and reference paths in the final stage represent the loss in the directional couplers and the delay line. This method allows the output signal and the sample of the input signal to be compared and corrected to any desired degree of accuracy [71-73].

The main advantage of the feed-forward technique is its simplicity. The subsidiary tube, TWT_2 is usually operated at very low level and can be used as a standby amplifier in the satellite. Furthermore, as distinct from feedback techniques the feed-forward TWT amplifier does not contain any closed loops and hence is an inherently

stable system.

The main disadvantage of the feed-forward technique is that of requiring the second TWT and two extra low-loss delay waveguides. This may put a restriction on the weight of the compensated tube. Furthermore, the degree of reliability of this technique depends on the balance of the two loops which may be impaired by several long term effects, such as, aging and temperature effects, temperature difference of the delay lines and shift in TWT helix supply voltages. The latter factor is critical because the TWT characteristics are sensitive to changes in its helix voltage and the feed-forward technique therefore requires a highly regulated power supply [7].

3.2.3. Signal predistortion technique

The technique of signal predistortion has recently been applied to the compensation of traveling wave tube amplifier nonlinearities. The design method requires accurate knowledge of the tube. Kaya et al [51] have initiated the development of two different approaches to the synthesis of a predistortion compensator in cascade with the TWT. The first approach consists of separate envelope and phase predistortion networks connected in cascade. The predistorted envelope of the input signal is first detected and then applied to the input of a phase-correction network. A simple implementation of this

technique has been reported in [75].

An alternative approach is to simultaneously predistort the envelope and phase of the input signal by using two separate envelope nonlinearities, one in the in-phase path and the other in the quadrature path. In the subsequent analysis we shall describe a design procedure and a possible, novel implementation of a quadrature-model compensator and the performance improvement attainable for the case of single carrier, binary PSK transmission.

Fig. 3-4 depicts a predistortion compensator in cascade with the TWT. The quadrature model of the TWT is as described in section 2.1, in which $Z_p(.)$ and $Z_q(.)$ are assumed to take the forms.

$$Z_p(R) = C_1 R\, e^{-C_2 R^2} I_o[C_2 R^2] \qquad (3.14)$$

$$Z_q(R) = S_1 R\, e^{-S_2 R^2} I_1[S_2 R^2] \qquad (3.15)$$

For our purposes we shall seek a set of envelope nonlinearities, $G_p(R)$ and $G_q(R)$, the in-phase and quadrature components of the compensation network, such that the overall transfer characteristics approximate that of a piecewise linear envelope limiter with zero envelope-dependent phase shift as described in section 3.1. In terms of $G_p(R)$ and $G_q(R)$, the desired envelope and phase shift at the output

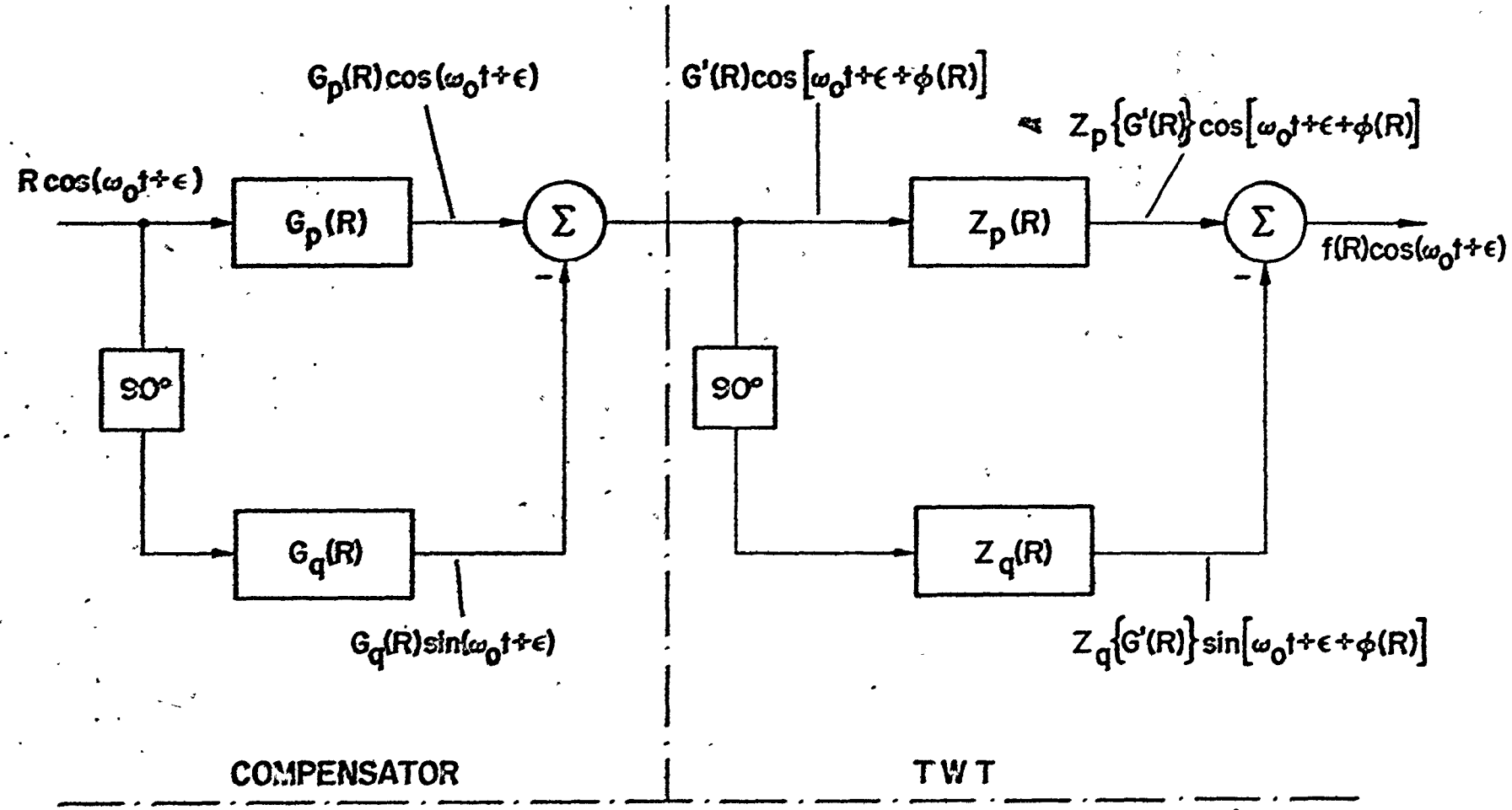

Fig. 3-4. Predistortion compensator for TWT

of the compensated TWT can be written as

$$f(R) = C_1 G_p(R)\, e^{-C_2[G_p^2(R)+G_q^2(R)]}\, I_o[C_2\{G_p^2(R)+G_q^2(R)\}]$$
$$-S_1 G_q(R)\, e^{-S_2[G_p^2(R)+G_q^2(R)]}\, I_1[S_2\{G_p^2(R)+G_q^2(R)\}] \tag{3.16}$$

and

$$0 = C_1 G_q(R)\, e^{-C_2[G_p^2(R)+G_q^2(R)]}\, I_0[C_2\{G_p^2(R)+G_q^2(R)\}]$$
$$+S_1 G_p(R)\, e^{-S_2[G_p^2(R)+G_q^2(R)]}\, I_1[S_2\{G_p^2(R)+G_q^2(R)\}] \tag{3.17}$$

The objective here is to determine $G_p(R)$ and $G_q(R)$ such that equations (3.16) and (3.17) are satisfied where $f(R)$ is a piecewise linear limiter characteristic defined by

$$f(R) = \begin{cases} \dfrac{R_0 R}{R_1} & 0 \le R \le R_1 \\ R_0 & R > R_1 \end{cases} \tag{3.18}$$

where R_0 is the TWT output saturation voltage and R_1 is the minimum voltage corresponding to saturation of the limiter. The exact solution of these equations is a very difficult problem, and in order to obtain a tractable problem from which meaningful results can be obtained, we approximate

$G_p(R)$ and $G_q(R)$ as the polynomials:

$$G_p(R) = \sum_{k=1}^{M} a_k R^{2k-1} \tag{3.19}$$

$$G_q(R) = \sum_{k=1}^{M} b_k R^{2k-1} \tag{3.20}$$

where the coefficients a_k and b_k are to be determined so as to satisfy equations (3.16) and (3.17) in some optimal sense.

The coefficients a_k and b_k can be determined from a conventional optimization subroutine [8] such that equations (3.16) and (3.17) are satisfied in a least squared error sense. The required coefficients a_k and b_k for two different values of M are tabulated in Tables 3-1 and 3-2 for the Intelsat IV tube (Hughes 261-H). Corresponding to these sets of coefficients the resulting optimal compensator characteristics are as shown in Fig. 3-5 and the overall compensated envelope transfer and phase shift characteristics are shown in Fig. 3-6. It is evident from the plot in Fig. 3-6 that the overall envelope transfer characteristic can be made to closely approximate that of a piecewise - linear envelope - limiting device by increasing M, i.e. more complexity in the compensation network. Furthermore, the amount of AM/PM conversion effect is evidently reduced at the expense of increasing phase-slope

TABLE 3-1.

The coefficients a_k and b_k for the compensators $(M=4)$*

k	a_k	b_k
	millivolt/(millivolt)$^{2k-1}$	
1	1.04931	-1.29116 (-1)
2	1.03959 (-1)	-9.40475 (-2)
3	-8.30888 (-3)	5.99492 (-3)
4	1.44447 (-4)	-9.81332 (-5)

*The negative integer in parentheses following each entry in the table represents the power of ten by which the entry should be multiplied.

TABLE 3-2.

The coefficients of a_k and b_k for the compensators (M=6) *

k	a_k	b_k
	millivolt/(millivolt)$^{2k-1}$	
1	1.00184	-1.06837 (-2)
2	1.53746 (-1)	-1.76412 (-1)
3	-1.64945 (-2)	1.88326 (-2)
4	4.53263 (-4)	-7.70929 (-4)
5	1.84654 (-8)	1.31865 (-5)
6	-9.50101 (-8)	-7.35811 (-8)

*The negative integer in parentheses following each entry in the table represents the power of ten by which the entry should be multiplied.

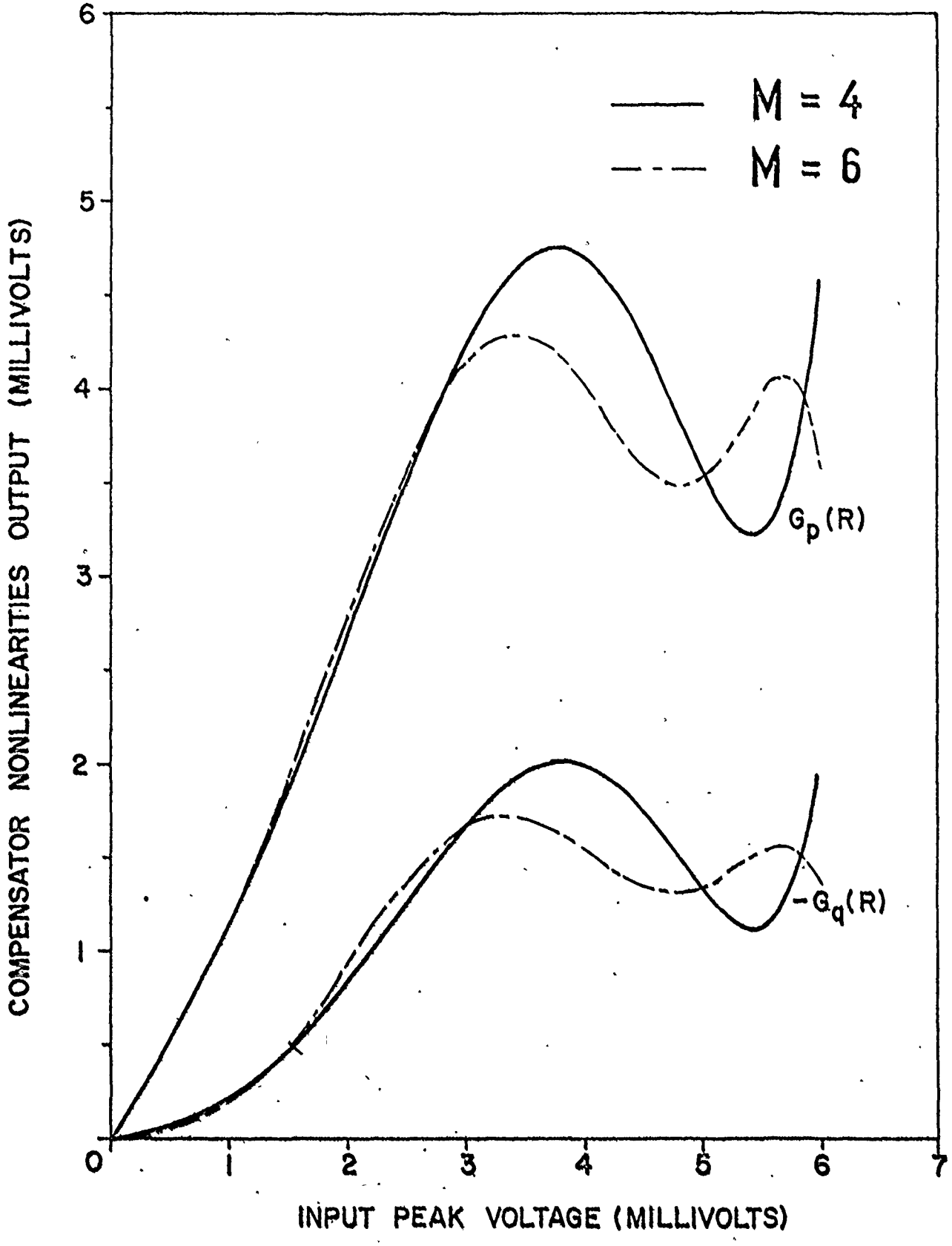

Fig. 3-5. The compensator characteristics

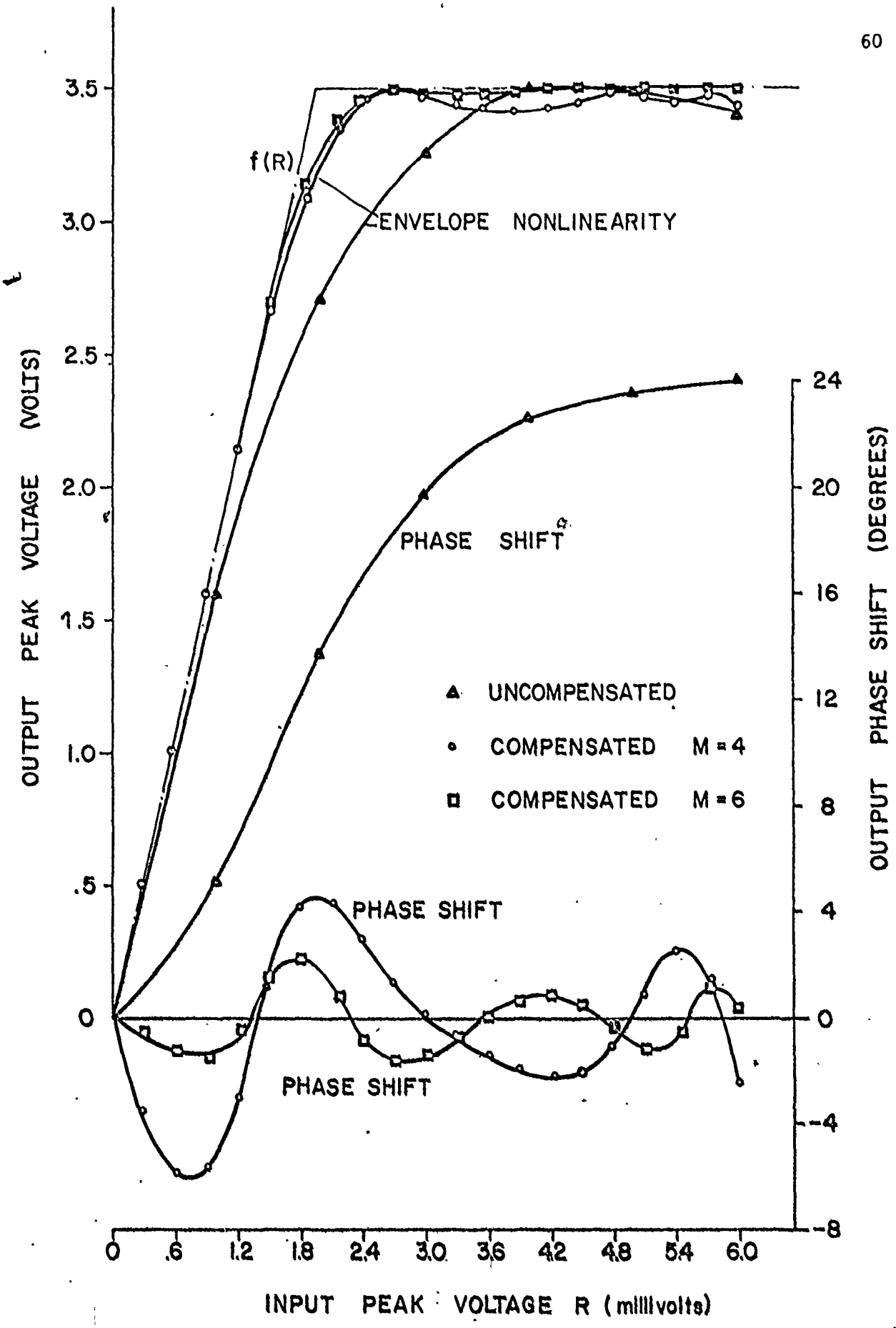

Fig. 3-6. The single carrier characteristics of the compensated and uncompensated tube (hoe 261-H)

variations. These phase-slope effects are undesirable as they tend to spread out the output spectrum. However, they can be mitigated by determining a set of coefficients a_k and b_k such that equation (3.16) is satisfied in the minimax sense subject to appropriate inequality constraints on equation (3.17).

An implementation of the compensation network based on equations (3.19) and (3.20) would require an envelope detector preceding a set of power law devices. An alternative method that does not require the envelope detector is to pass the RF signal directly through nonlinear devices $N_p(.)$ and $N_q(.)$

If $N_p(u)$ and $N_q(u)$ denote the in-phase and quadrature nonlinearities acting on the instantaneous signal u, we can express $N_p(.)$ and $N_q(.)$ as the first order inverse Chebyshev transforms of $G_p(R)$ and $G_q(R)$ [18]. This results in instantaneous signal nonlinearities of the form (Appendix C).

$$N_p(u) = \sum_{k=1}^{M} A_k u^{2k-1} \tag{3.21}$$

$$N_q(u) = \sum_{k=1}^{M} B_k u^{2k-1} \tag{3.22}$$

where

$$A_k = \frac{\sum_{j=0}^{k-1} (-1)^{k-j-1} \binom{2k-1}{j} k a_k}{2^{2(k-1)} [2(k-j)-1]}$$

$$B_k = \frac{\sum_{j=0}^{k-1} (-1)^{k-j-1} \binom{2k-1}{j} kb_k}{2^{2(k-1)} [2(k-j)-1]} .$$

A schematic diagram representing a possible implementaion of the compensator is depicted in Fig. 3-7. This compensator may be implemented with a set of power-law devices or alternatively with RF multipliers together with appropriate gain elements.

The performance of this compensated satellite channel has been investigated by means of computer simulation using a general purpose satellite simulation program, [23]. The results of the simulation are shown in Fig. 3-8 for the case of a binary CPSK system operating in a single carrier per channel mode and in the absence of up-link noise. The transmitting and receiving filters are chosen to be identical 4 pole, ½dB ripple Chebyshev filters with 85 MHz bandwidth. Throughout the simulation, perfect carrier recovery and bit timing are assumed at the receiver. For different values of transmission rate, it is evident from Fig. 3-8 that some marginal gain, about 0.3 - 0.5 dB, in system performance can be obtained as a result of the compensation. This order of improvement compares well with measurements obtained by others [21]. For the case of multicarrier signals it is well known [51, 82] that this overall transfer characteristics of the tube suppresses the intermodulation effect and can provide up to 10 dB

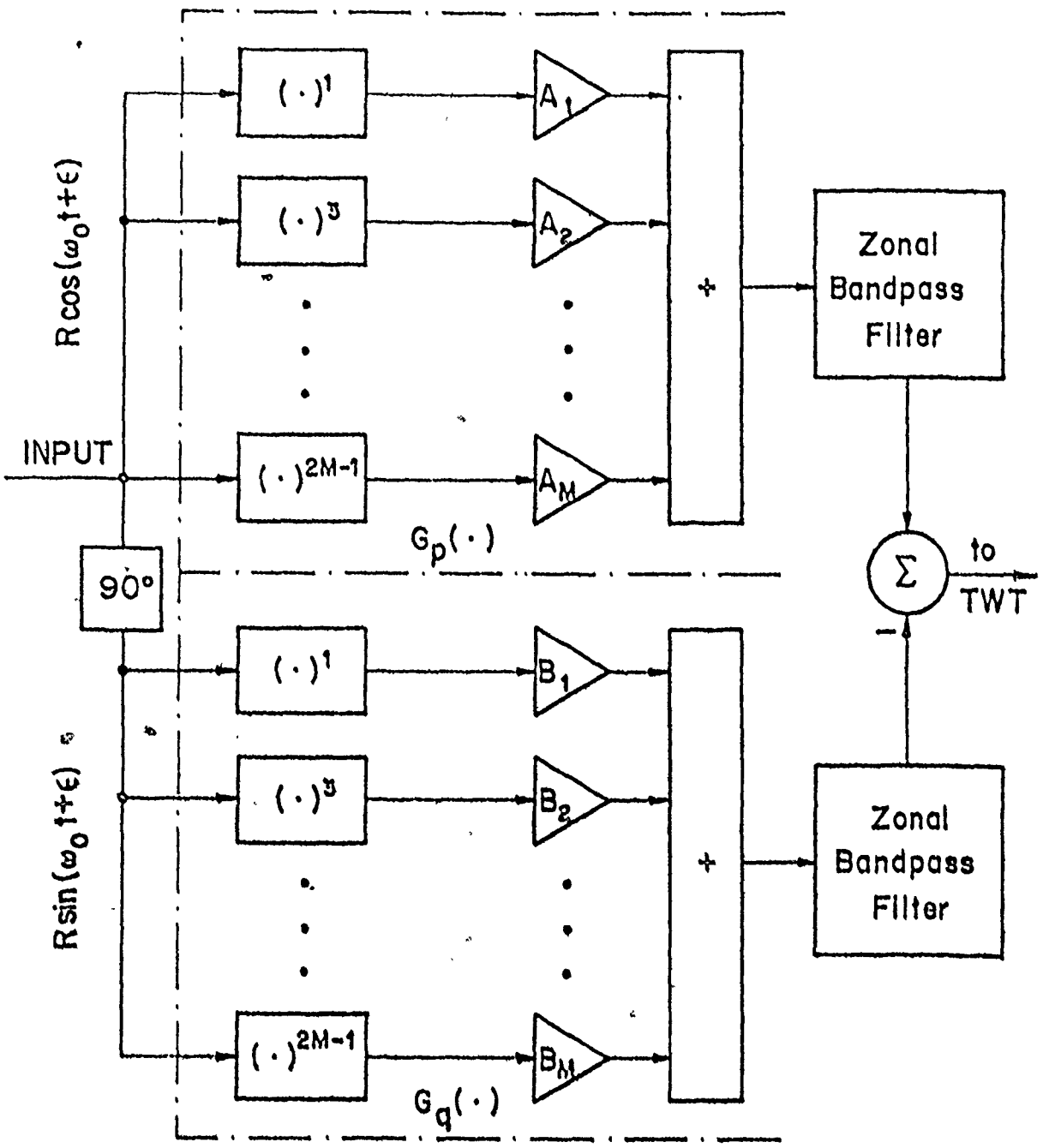

Fig. 3-7. Implementation of the nonlinear compensator.

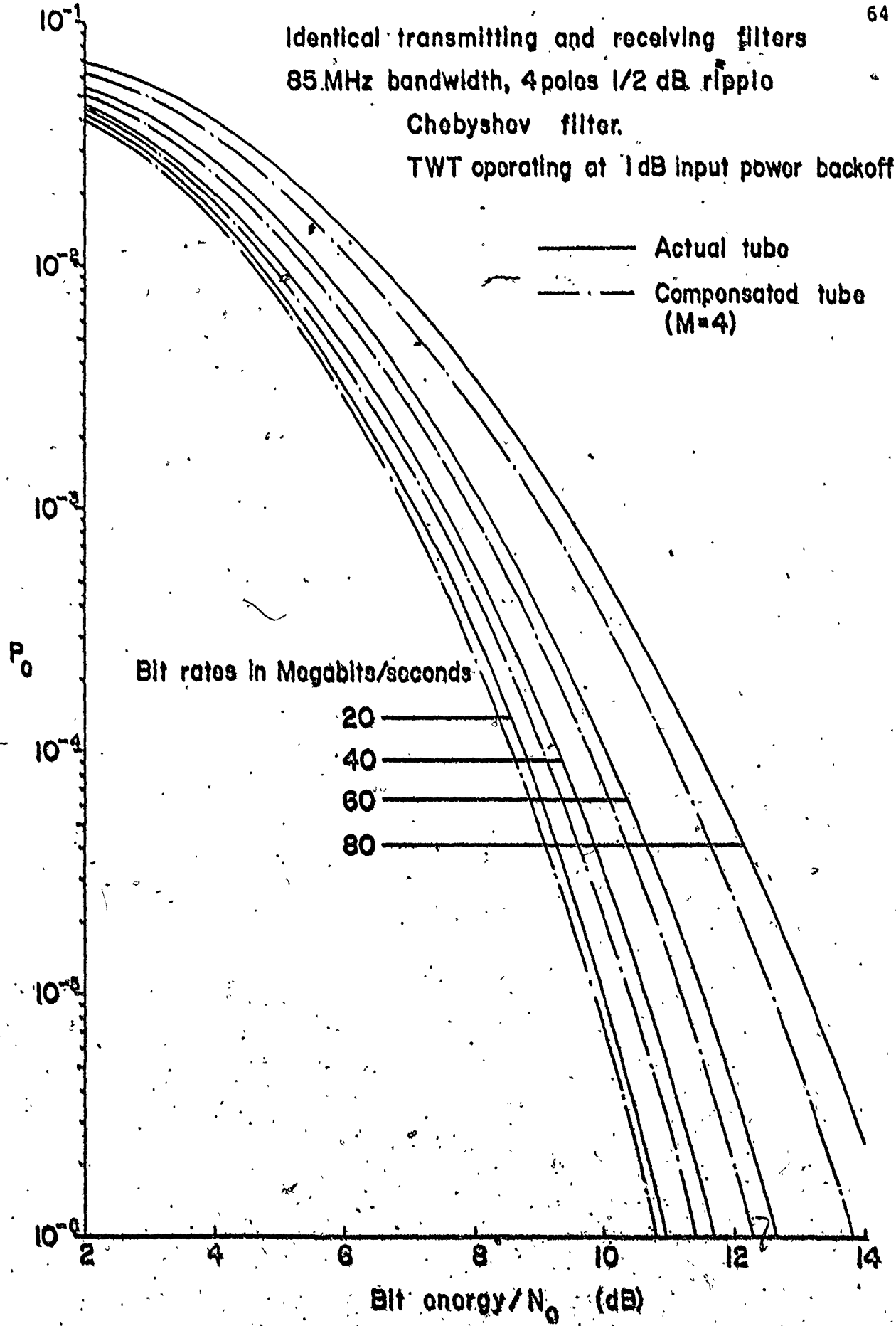
Identical transmitting and receiving filters
85 MHz bandwidth, 4 poles 1/2 dB ripple
Chebyshov filter.
TWT operating at 1 dB input power backoff
Actual tube
Compensated tube (M=4)
Bit rates in Megabits/seconds
20
40
60
80
P_0
10^{-1}
10^{-2}
10^{-3}
10^{-4}
10^{-5}
10^{-6}
2
4
6
8
10
12
14
Bit energy / N_0 (dB)

Fig. 3-8. of

improvement in carrier to interference power ratio (C/I) when the TWT is operating at 6 dB input power backoff.

CHAPTER 4

PERFORMANCE ANALYSIS OF CPSK SYSTEMS THROUGH NONLINEAR CHANNELS

The effect of satellite repeater nonlinearities on the performance of digital communication systems has been the subject of extensive study [4-6, 10, 23, 29-30, 41, 43, 47, 49-50, 59, 63, 70]. As early satellite transponders were power limited, it was necessary to operate the traveling wave tube (TWT) amplifier near saturation so as to obtain maximum transmitted power. Under such conditions a hard-limiter without envelope dependent phase-shift was found to model reasonably accurately the satellite transponder [4-6, 30, 47, 49, 59, 70]. Moreover, in certain applications [70], the TWT was preceded by a bandpass hard limiter in order to keep the envelope of the input signal to the TWT at a constant level and thereby to eliminate the undesired effect of AM/PM conversion. Another factor that favors this hard-limiting model in the analysis of CPSK signals transmitted through the satellite transponder is its mathematical tractability. Furthermore it closely approximates the optimal bandpass nonlinearity for the case of high up-link carrier to noise power ratio (CNR) as discussed in chapter 3.

However, the recent development of higher power satellite TWT's and the increase in user demand to access the satellite leads to a bandwidth rather than a power-limited channel. Other modulation

techniques that utilize bandwidth more effectively than binary CPSK (for example, M-ary CPSK (see section 2.1)) then need to be considered. In this case the hard-limiter no longer accurately models the satellite transponder since the effect of AM/PM conversion as discussed in Chapter 1 becomes more significant [10, 23, 32-33, 41, 46, 63]. Unfortunately, the analysis of bandwidth-limited systems involves evaluating the statistics of the intersymbol interference (ISI). Even for the case of a linear channel it is very difficult to determine the probability density function of the intersymbol interference in closed form except for a very few special cases [46], and this greatly complicates the analysis. The presence of a bandpass nonlinearity in the channel further complicates the analysis and the usual method of analyzing such a complex problem is by means of computer simulation [23, 41, 63] or in some cases the combined use of numerical and analytical methods [10, 32-33].

Our objective in this chapter is to investigate the effect of the nonlinear distortion caused by the TWT on the performance of a coherent phase-shift keying (CPSK) system. Some computer simulation results, obtained by others, on the performance degradation, as a result of bandlimitation (which causes ISI) and TWT nonlinearity, are discussed in section 4.1. This is then followed by the analysis of the performance of CPSK signals transmitted through a power-limited satellite channel including the effect of noise in both the up-link and down-link paths. Our objective in section 4.2 is to develop an analytical methodology to handle the general nonlinear satellite channel which includes both gain

compression and AM/PM conversion.

4.1) SIMULATION STUDIES OF BAND LIMITATION EFFECTS

The satellite communications link of interest in this section is modelled as shown in Fig. 4-1. In satellite communications, the angular carrier frequency ω_0 is much larger than the transmitted symbol rate, $\frac{1}{T}$, and complex baseband envelope functions* [83] can be used to represent both the transmitted and received signal. Let the complex baseband envelope of the transmitted signal be

$$\underline{a}(t) = \sum_{n\epsilon I} f(t-nT)\, e^{j\theta_n g(t-nT)} \qquad (4.1)$$

where

1) $f(t)$ is a rectangular pulse of unity amplitude defined as

$$f(t) = 1 \quad \text{for} \quad 0 \leq t \leq T$$
$$= 0 \quad \text{otherwise}$$

2) $g(t)$ is the waveform of the signaling pulse used in the system to shape the phase variation

---

* A bandpass signal, $a(t)$, with angular center frequency, ω_0, and its complex envelope function, $\underline{a}(t)$, are related by

$$a(t) = Re\{\underline{a}(t)\, e^{j\omega_0 t}\}$$

where Re denotes the real part of the complex quantity.

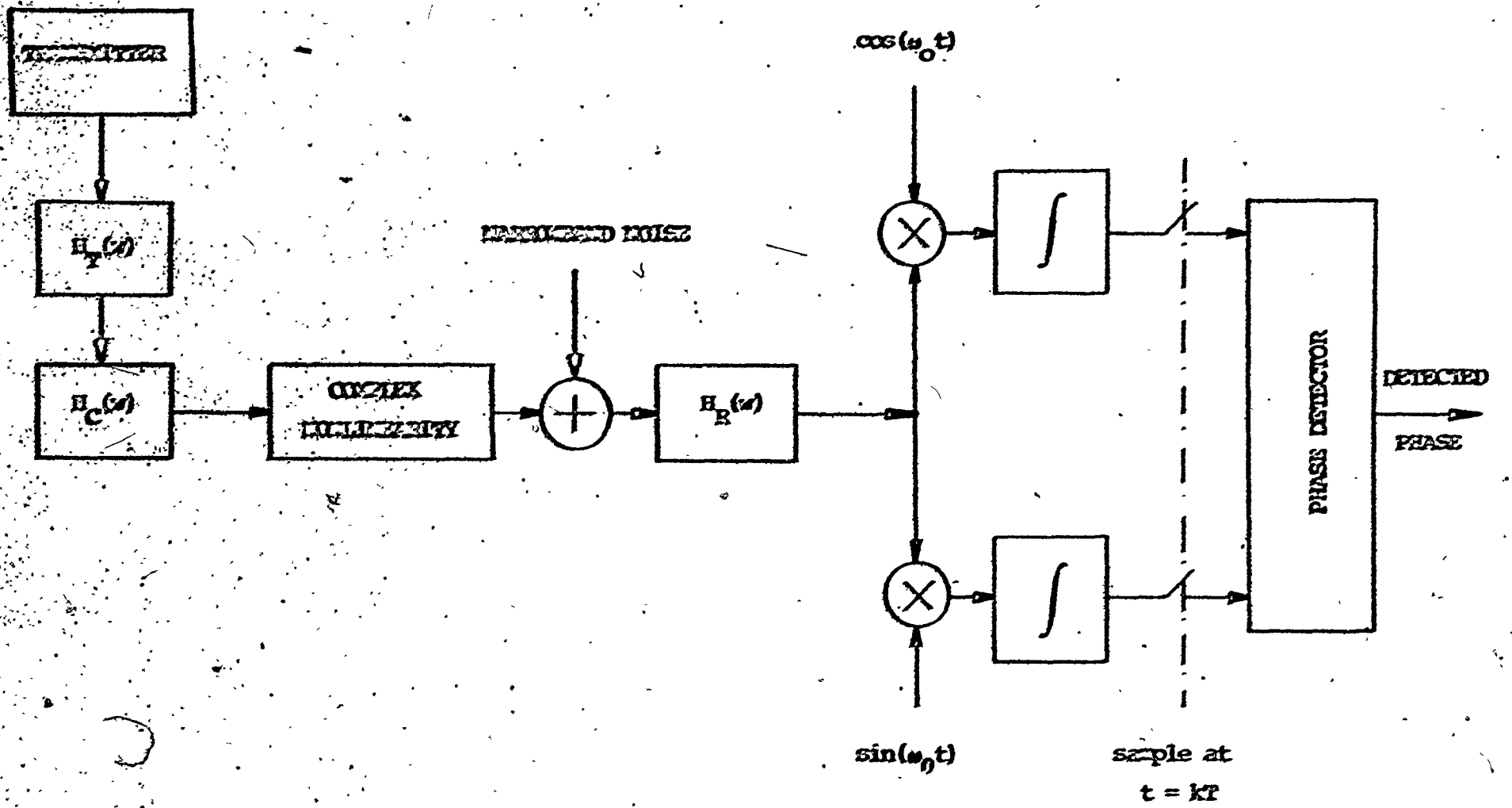

Fig. 4-1. Bandlimited M-ary CPSK system transmission through a nonlinear channel.

3) θ_n is the transmitted phase during the nth symbol interval and is assumed to take the equally likely values

$$\theta_n(i) = [2i - \text{sgn}(i)]\frac{\pi}{M} \qquad (4.2)$$

where

$$i = -\frac{M}{2}, \ldots, -1, 1, \ldots, \frac{M}{2}, \quad \text{for M even}$$

and

$$\text{sgn}(i) = \text{sign of } i$$

4) $I \triangleq \{-\infty, \ldots, -1, 0, 1, \ldots, \infty\}$ is the set of integers.

Let $\underset{\sim}{h}(t)$ denote half the complex baseband envelope of the cascaded transmitting and channel filter impulse response given by

$$\underset{\sim}{h}(t) \triangleq h_c(t) + jh_s(t) \qquad (4.3)$$

where the subscripts c and s denote the in-phase and quadrature components.

$\underset{\sim}{h}(t)$ is usually obtained from the inverse Fourier transform of its corresponding transfer function $H(\omega)$ defined as

$$H(\omega) = \begin{cases} H(\omega+\omega_0) & |\omega| < \bar{\omega} \\ 0 & \text{elsewhere} \end{cases} \qquad (4.4)$$

where $\bar{\omega}$ is the overall system equivalent low-pass bandwidth, and $H(\omega)$ is the bandpass transfer function of the cascaded transmitting and channel filter.

The complex envelope of the signal at the input of the nonlinear

repeater is given by

$$\underset{\sim}{u}(t) = \int_{-\infty}^{\infty} \underset{\sim}{s}(t-\tau)\, \underset{\sim}{h}(\tau)\, d\tau$$

$$= \sum_{n\in I} [a(t;\theta_n) + jb(t;\theta_n)] \qquad (4.5)$$

where

$$a(t;\theta_n) = \int_{-\infty}^{\infty} h_c(\tau)\, f(t-nT-\tau)\, \cos[\theta_n g(t-nT-\tau)]\, d\tau$$

$$- \int_{-\infty}^{\infty} h_s(\tau)\, f(t-nT-\tau)\, \sin[\theta_n g(t-nT-\tau)]\, d\tau$$

$$b(t;\theta_n) = \int_{-\infty}^{\infty} h_c(\tau)\, f(t-nT-\tau)\, \sin[\theta_n g(t-nT-\tau)]\, d\tau$$

$$+ \int_{-\infty}^{\infty} h_s(\tau)\, f(t-nT-\tau)\, \cos[\theta_n g(t-nT-\tau)]\, d\tau \qquad (4.6)$$

If the nonlinear device is represented by the quadrature model discussed in Chapter 2, the complex baseband envelope signal at its output can then be written as

$$\underset{\sim}{v}(t) = [z_p(|u|) + jz_q(|u|)] \exp[j\psi(t)] \qquad (4.7)$$

where

$$\psi(t) = \tan^{-1}\left[\frac{\sum_{n\in I} b(t;\theta_n)}{\sum_{n\in I} a(t;\theta_n)}\right]$$

$$|u(t)| = \sqrt{\left[\sum_{n\in I} a(t;\theta_n)\right]^2 + \left[\sum_{n\in I} b(t;\theta_n)\right]^2} \qquad (4.8)$$

If half the complex baseband envelope of the impulse response of the receiving filter is denoted by

$$\underset{\sim}{p}(t) = p_c(t) + jp_s(t) \tag{4.9}$$

then the complex baseband envelope of signal, $\underset{\sim}{v}(t)$, plus down-link noise, $\underset{\sim}{n}(t)$, after passing through the receiving filter is

$$\begin{aligned} \underset{\sim}{r}(t) &= \int_{-\infty}^{\infty} [\underset{\sim}{v}(\tau) + \underset{\sim}{n}(\tau)]\, \underset{\sim}{p}(t-\tau)\, d\tau \\ &= A(t;\theta_{n_c I}) + jB(t;\theta_{n_c I}) + n_c(t) + jn_s(t) \end{aligned} \tag{4.10}$$

where

$$\begin{aligned} A(t;\theta_{n_c I}) &= \mathrm{Re}\left(\int_{-\infty}^{\infty} \underset{\sim}{v}(\tau)\, \underset{\sim}{p}(t-\tau)\, d\tau \right) \\ B(t;\theta_{n_c I}) &= \mathrm{Im}\left(\int_{-\infty}^{\infty} \underset{\sim}{v}(\tau)\, \underset{\sim}{p}(t-\tau)\, d\tau \right) \end{aligned}$$

and

$$\begin{aligned} n_c(t) &= \mathrm{Re}\left(\int_{-\infty}^{\infty} \underset{\sim}{n}(\tau)\, \underset{\sim}{p}(t-\tau)\, d\tau \right) \\ n_s(t) &= \mathrm{Im}\left(\int_{-\infty}^{\infty} \underset{\sim}{n}(\tau)\, \underset{\sim}{p}(t-\tau)\, d\tau \right) \end{aligned} \tag{4.11}$$

where Re and Im denote the real and imaginary part of the complex quantities, and $\underset{\sim}{n}(t)$ is the complex baseband envelope of the down-link noise.

During the interval $0 < t \leq T$, we assume at the receiver that the transmitted phase is θ_0, and that it is detected by sampling the received signal at time t_0, $0 < t_0 \leq T$ and comparing the received signal phase at this instant with a suitable threshold. From equation (4.10)

we can write

$$\underset{\sim}{r}(t_0) = A(t_0, \theta_{n\epsilon I}) + n_c(t_0) + j[B(t_0, \theta_{n\epsilon I}) + n_s(t_0)] \tag{4.12}$$

Then the phase angle at time t_0 as determined at the receiver is given by

$$\phi(t_0) = \tan^{-1}\left[\frac{B(t_0, \theta_0, \theta_{n\epsilon I'}) + n_s(t_0)}{A(t_0, \theta_0, \theta_{n\epsilon I'}) + n_c(t_0)}\right] \tag{4.13}$$

where $I' \triangleq \{-\infty, \ldots, -1, 1, \ldots, \infty\}$

As the signal is passed through the filters in the system it becomes delayed in time and distorted in amplitude and as it passes through the traveling wave tube it undergoes an amplitude amplification and simultaneously an envelope dependent rotation of the output phase with respect to the input phase. Geometrically, the received signal at sampling time t_0 may be represented as shown in Fig. 4-2. In Fig. 4-2 the received phase $\phi(t_0)$ is assumed to fall into the correct decision region given that $\theta_0 = \frac{\pi}{8}$ is transmitted (for the case of eight-phase PSK (M=8)).

Since the θ_n's are assumed to be random variables uniformly distributed over M values as shown above then the probability of correct detection is given by the probability that $\phi(t_0)$ lies between the decision thresholds of the transmitted phase θ_0, for all possible θ_0's. Mathematically this can be expressed as

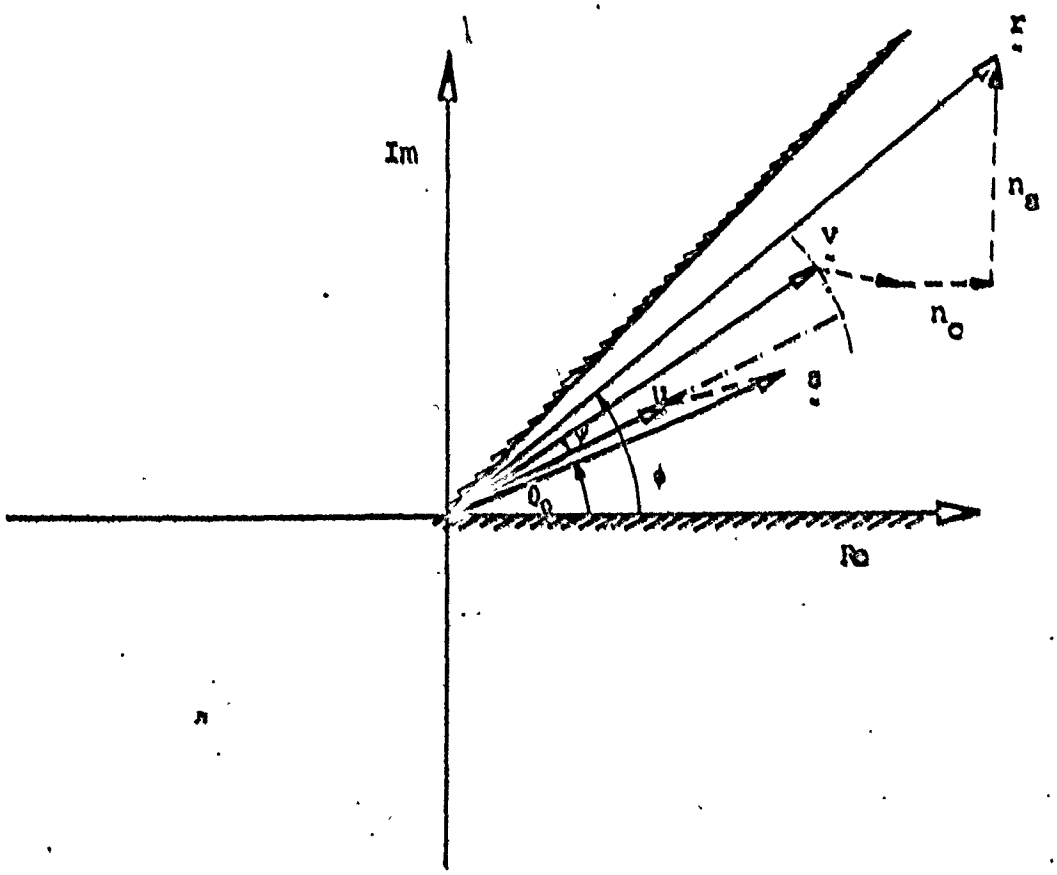

DECISION THRESHOLD

DUE TO THE NONLINEAR EFFECT

DUE TO BANDLIMITATION & NOISE DISTURBANCES.

Fig. 4-2. Complex plane representation of the received signal at t_0 , (M=0).

$$P_c(M) = \frac{1}{M} \sum_{i=-M/2}^{M/2} \Pr\{\theta_0(i) - \frac{\Pi}{M} < \phi(t_0) < \theta_0(i) + \frac{\Pi}{M} \mid \theta_0(i)\} \tag{4.14}$$

under the hypothesis that the threshold levels $\phi_T(i)$ are

$$\phi_T(i) = \theta_0(i) \pm \frac{\Pi}{M} \tag{4.15}$$

and the probability of error is then given as

$$P_e(M) = 1 - P_c(M) \tag{4.16}$$

The difficulty in the analytical evaluation of the probability of error in equation (4.16) is largely due to the fact that the probability distribution function of the intersymbol interference is very hard to obtain except for a very few special cases [46], and even if it is known one has to determine the probability distribution function after the complex nonlinear transformation. In principle, if the exact number of random variables causing the intersymbol interference is known and is finite, equation (4.14) can be evaluated by an exhaustive, direct enumeration over these random variables. However, the computational effort is formidable since the number of possible combinations of these random variables grows exponentially with their numbers. In an attempt to reduce the amount of necessary computation, Forcina [32] has suggested the combination of direct enumeration and simulation methods. This method was applied to the case of four-phase CPSK without the receiving filter

and with no AM/PM conversion. However, the results are obtained with unknown accuracy and the amount of computation necessary in the direct enumeration part is still substantial especially for the case of severe interferences in which the effect of intersymbol interference extends over many bit periods. Benedetto et al [10] have suggested the use of the Gauss-quadrature formula [9] in order to reduce the necessary computation. The method, however, still requires the calculation of various moments of the random variables arising from the nonlinear transformation of the intersymbol interference as shown in equation (4.7). This moment calculation, as it is nonrecursive, is laborious, especially when high accuracy is required. The last resort is to evaluate the performance of a band-limited CPSK system through a nonlinear satellite channel by means of computer simulations [23, 63]. The main features of these simulation programs are similar to each other. However, the modular form of the simulation program in [23] offers more flexibility in comparing different types of modulation that are applicable to satellite communications. The results obtained from the computer simulation for CPSK systems (described in more detail in [23]) are as shown in figures 4-3 to 4-8 for M=2, 4 and 8 respectively. Both the transmitting and receiving filters are assumed to be identical 4 pole, ½ dB ripple Chebyshev filters with 85 MHz, 3 dB bandwidth and symmetrical response with respect to the midband angular carrier frequency ω_0. Two operating conditions of the TWT are examined, one with the tube operating at saturation (1 dB input power backoff*)

*Input power backoff is defined as the difference (in dB) between the actual mean input power of the modulated signal and that required to saturate the tube.

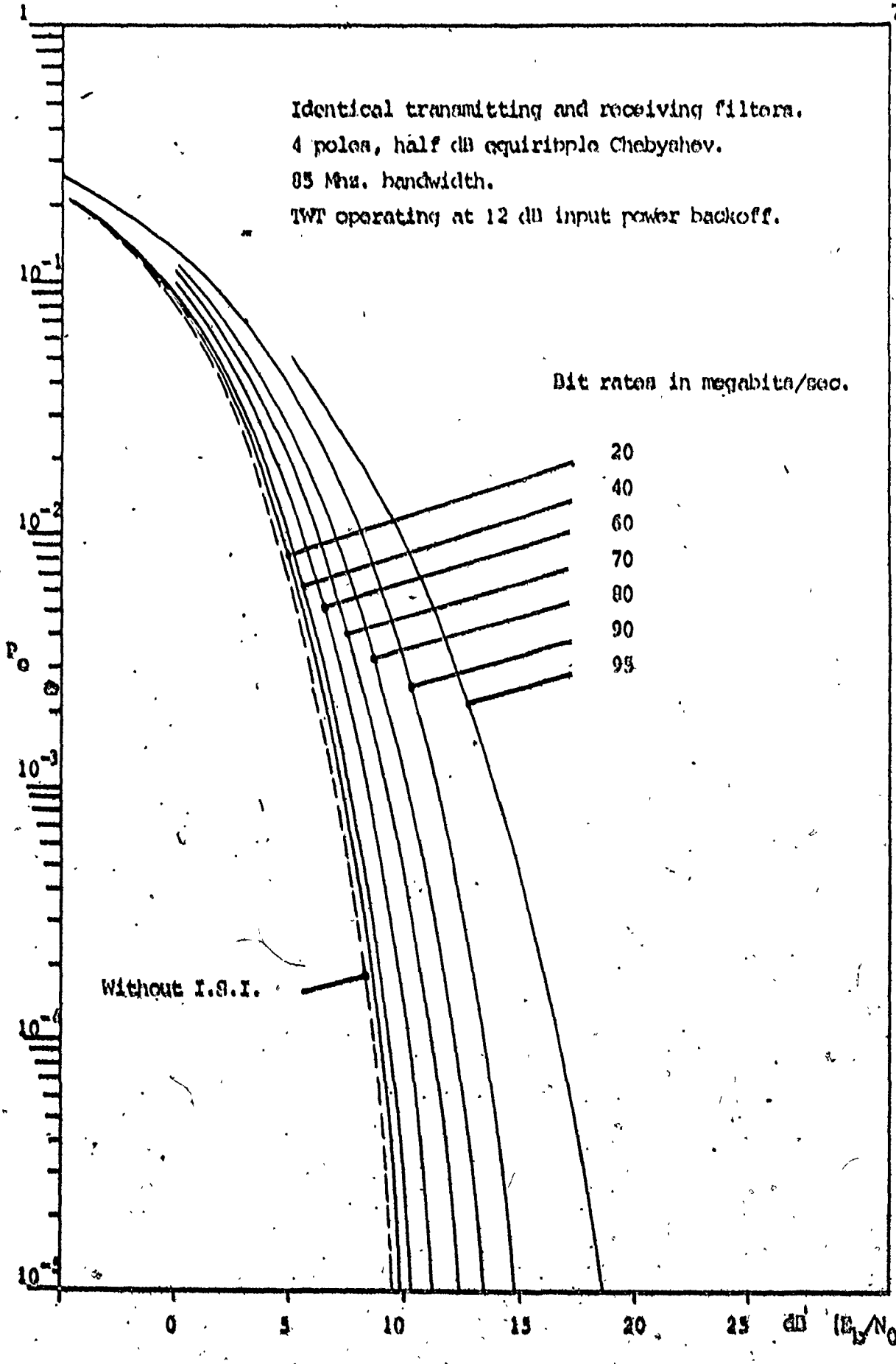

Fig. 4-3. ... vs E_b/N_0

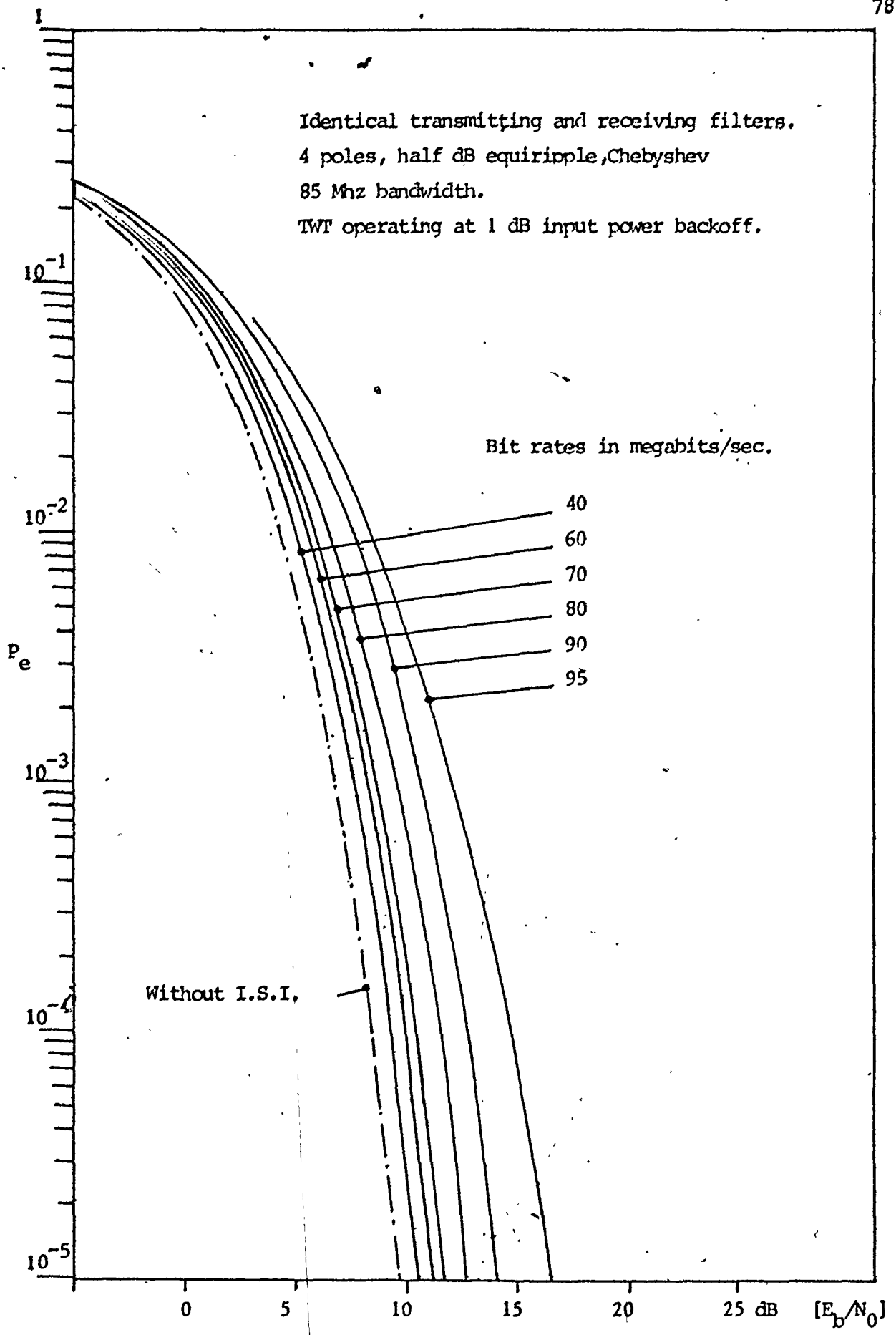

Fig. 4-4. Probability of error vs E_b/N_0, 2-phase CPSK

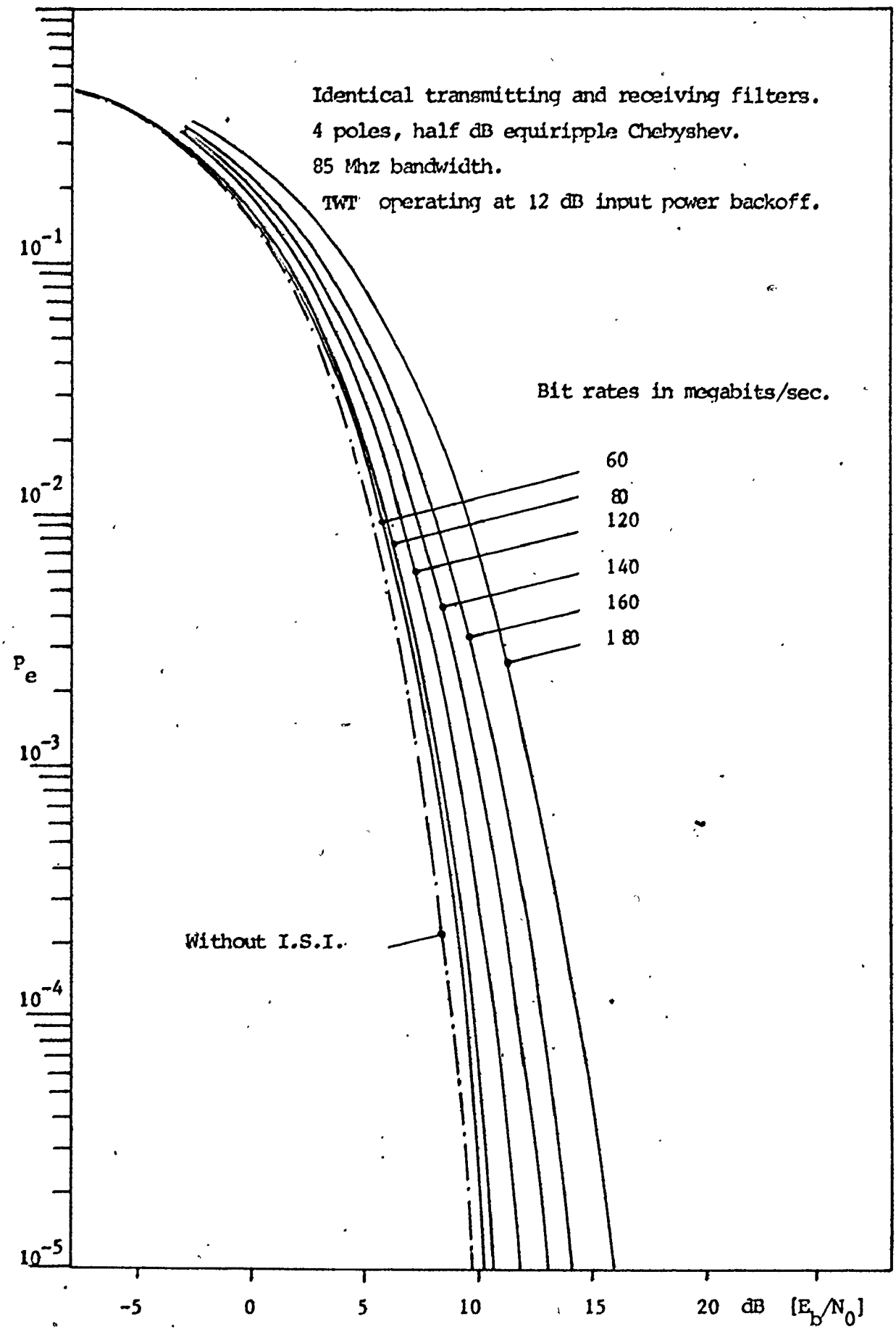

Fig. 4-5. Probability of error vs E_b/N_0, 4-phase CPSK

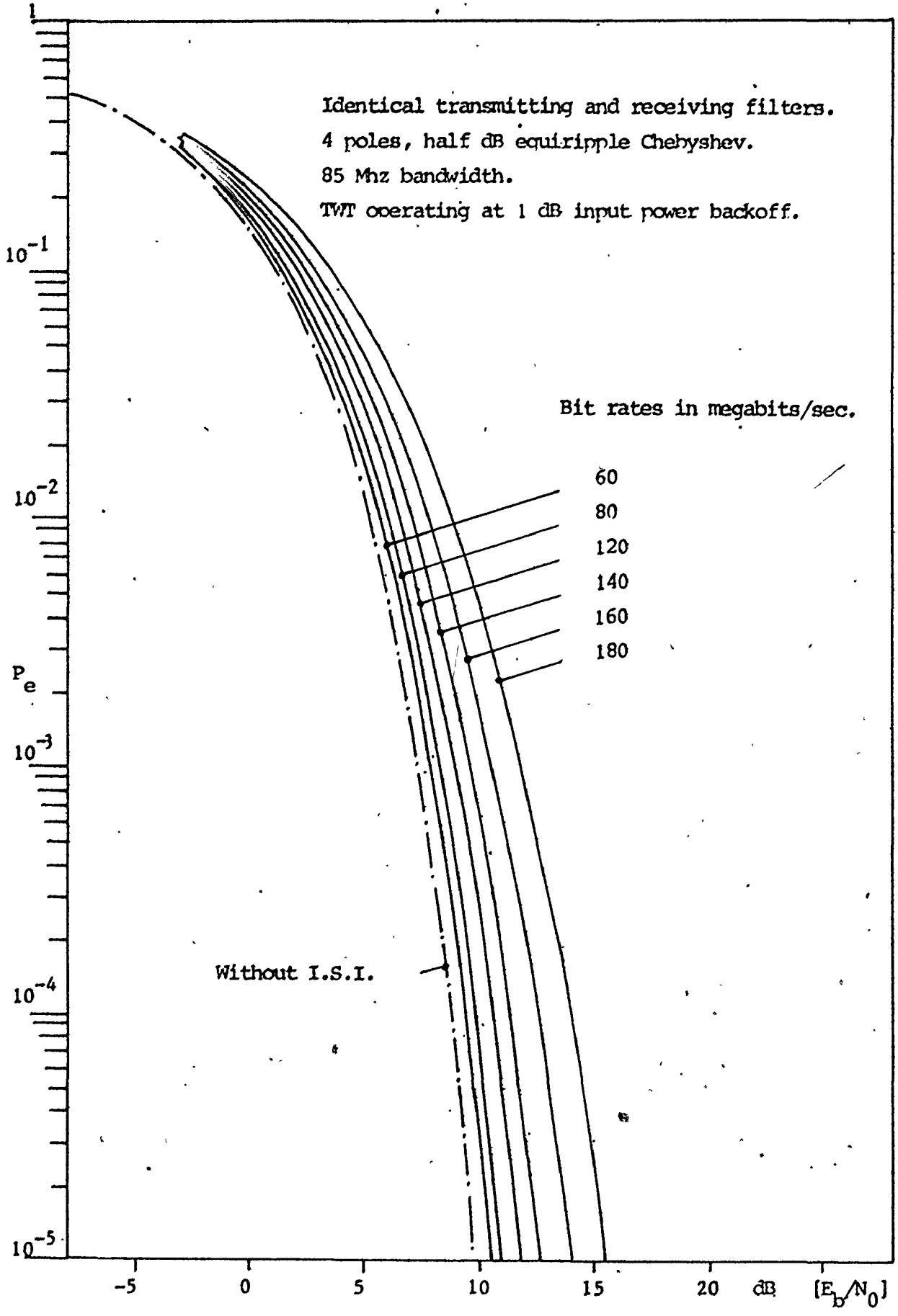

Fig. 4-6. Probability of error vs E_b/N_0, 4-phase CPSK

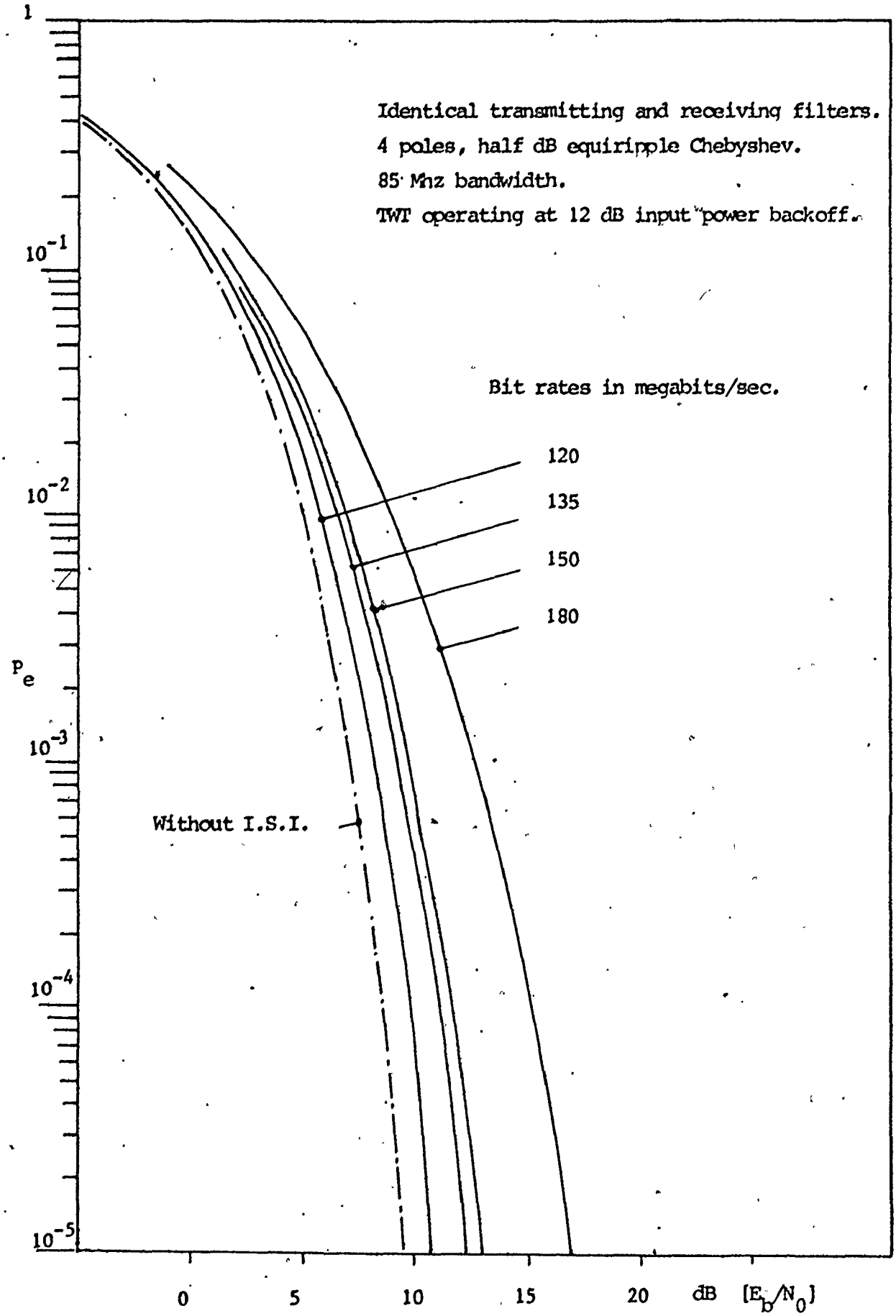

Fig. 4-7. Probability of error vs E_b/N_0, 8-phase CPSK

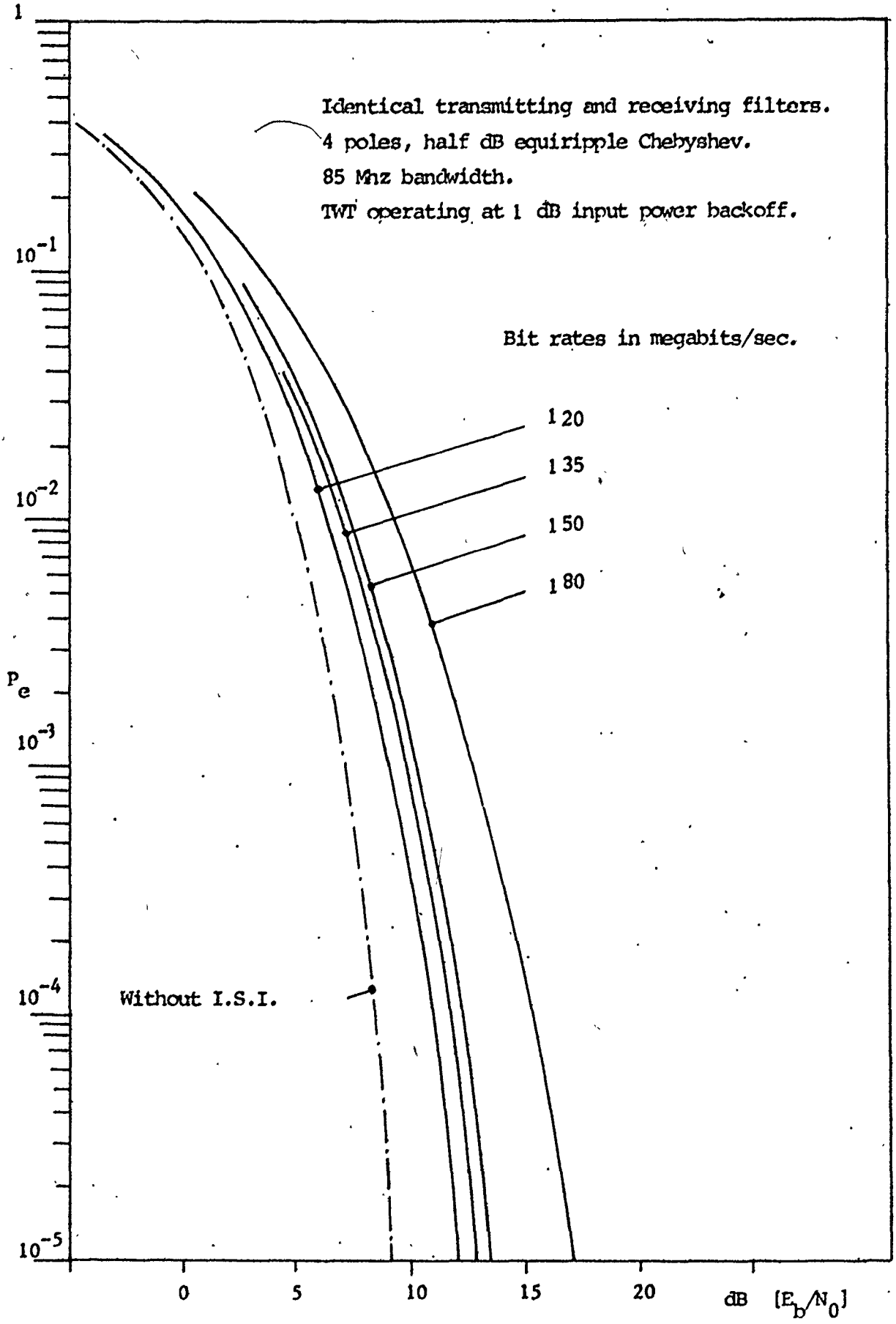

Fig. 4-8. Probability of error vs E_b/N_0, 8-phase CPSK

and the other with the tube operating in the linear region (12 dB input power backoff) of the power transfer characteristic. Figures 4-3 to 4-4 show the probability of error of a binary CPSK system (M=2) as a function of bit energy to noise power spectral density ratio, $[E_b/N_0]$, and for various transmission rates. The performance degradation increases as the transmission rates approach the filter bandwidth. However, at high transmission rates and high $[E_b/N_0]$, the performance of the system with the TWT operating at saturation is slightly superior to that when TWT is operating in the linear region. This is due to the fact that, at saturation, the phase shift at the output of the tube due to input envelope fluctuation is relatively constant and can be compensated for by a coherent receiver. On the other hand, the phase shift at the output of the TWT, operating in the linear region, is more dependent on the input signal envelope fluctuations. It then becomes more difficult to track this phase variation with a coherent receiver. Similar results can be obtained for the case of four- and eight-phase CPSK. In all the cases considered it is evident that the performance degradation increases as the transmission rates increase (as the bit rate approaches the filter bandwidth).

It is well known that the transmission rate (measured in bits/sec) of M-ary CPSK is $\log_2 M$ times that of binary CPSK. However, the transmitted power required to attain the same symbol error probability does not vary linearly with the transmission rate. For example, if we require a symbol error probability of 10^{-3} and a fixed symbol rate of 60 Megasymbols/second with the TWT operating at 1 dB input power backoff,

comparison of figures 4-4, 4-6 and 4-8 indicates that the four-phase CPSK system requires an extra 2 dB in the transmitted power over that of the binary CPSK case. However, the eight-phase CPSK requires an extra transmitted power of approximately 12.5 dB.

To conclude this section we point out that, to date, the analysis of bandlimited CPSK signals transmitted through a bandpass nonlinearity is still very incomplete and quite inconclusive. Although computer simulation methods may be used to assess the performance of such systems, the accuracy of the results obtained is generally unknown. Furthermore, in actual satellite communications systems, the effect of up-link thermal noise disturbance must be included in the analysis. This effect can not be readily investigated by means of computer simulation without the use of very large amounts of computer time.

In the following sections we shall disregard the effects of intersymbol interferences and shall confine our attention to the nonlinear analysis in the presence of only up- and down-link thermal noises. Such a simplified model not only yields a mathematically tractable problem but also the solution leads to significant further insight into the effect of bandpass nonlinearities on the performance of M-ary CPSK systems.

4.2) EFFECT OF THERMAL NOISE DISTURBANCES

Our objective in this section is to investigate the effect of up-link and down-link thermal noise disturbances on the performance of a coherent phase shift keying (CPSK) system. A block diagram of the communication system considered in this section is shown in Fig. 4-9. On

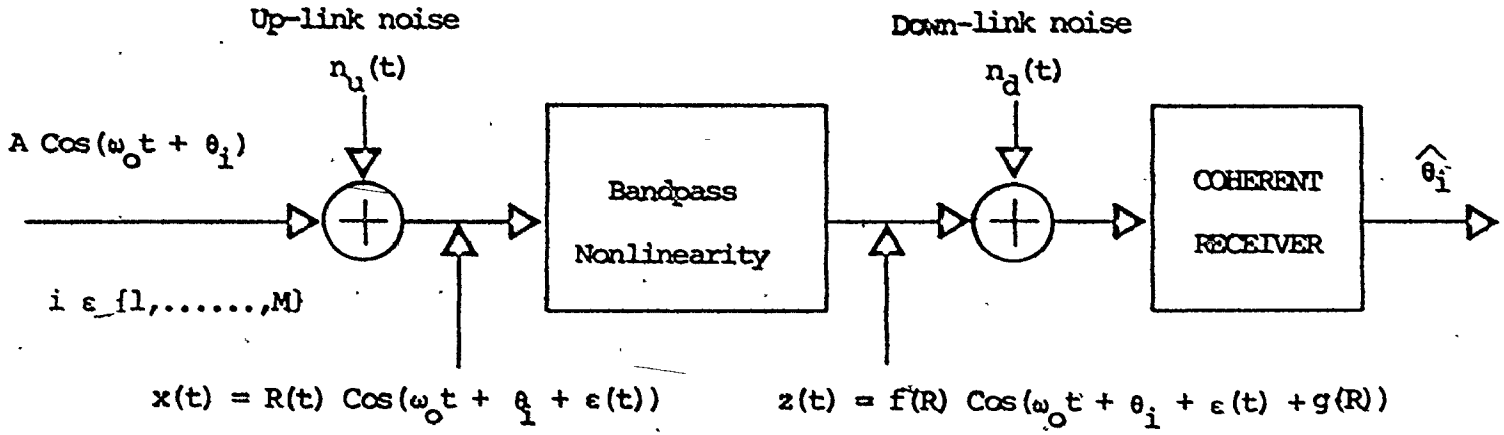

Fig. 4-9. CPSK transmission through a nonlinear channel

the up-link path the transmitted CPSK signal and the thermal noise are added to form the input signal to the satellite repeater. The bandpass filter preceding the TWT is assumed to pass the signal without distortion but to restrict the up-link noise to a finite bandwidth, W. The signal after passage through the filter is amplified by the TWT and retransmitted to a ground station.

On the down-link the retransmitted signal is further corrupted by independent additive thermal noise to form the receiver input signal. An ideal coherent receiver with an appropriate CPSK decision circuit is assumed. One possible implementation of such a receiver is shown in Fig. 4.10. At the receiver the RF signal is down-converted to baseband, where β is the average of the AM/PM effect introduced by the TWT. The baseband signal in each branch is then integrated and sampled every bit duration. This is the well-known integrate and dump (I&D) filter. This receiver structure is a specific form of a correlation receiver. It will be assumed throughout our discussion that phase coherence and bit timing recovery have been achieved at the receiver.

In an attempt to determine an upper bound on the probability of error for binary CPSK spread spectrum signals transmitted through a hard-limited satellite repeater, Aein [4-6] approximated the integrate and dump filter by a sample and sum detector. It was pointed out in [4] that for the case of an up-link noise limited channel with small down-link noise disturbances the error probability could be computed by the use of the complementary error function as if the correlator output statistics obeyed the normal distribution law. By approximating the integrate and dump filter by a sample and sum detector, Davisson et al [29-30] have

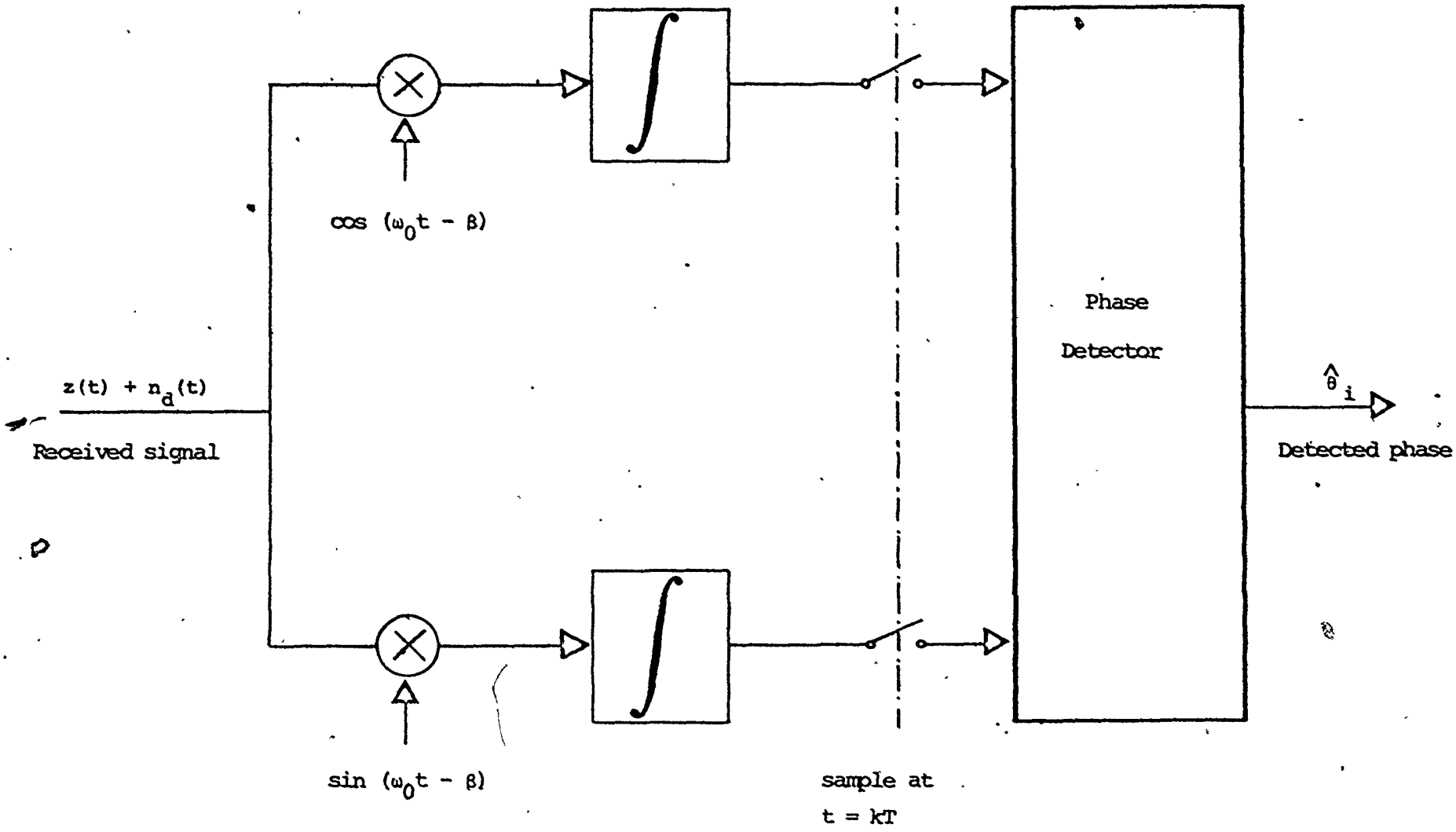

Fig. 4-10. A coherent receiver for CPSK system

calculated the probability of error for binary CPSK signals transmitted through a piecewise-linear envelope-limiting repeater. However, their method requires the direct numerical convolution of the probability density functions of the sample and sum detection outputs and is very tedious because a large number of samples must be used in order to give a good approximation to the integrate and dump filters.

In view of the difficulties associated with the integrate and dump filter or its approximation by a sample and sum detection, Jacobs [47] originated the substitution of this pre-detection integration by a single sample and majority logic decision device. The probability of error is then related to the single sample detection error which is considerably simpler to evaluate. Lyons [57,59] put forward a method of characterizing the noise statistics at the output of the general bandpass nonlinearity. Essentially, in his method the equivalent (desired) signal component at the output of the nonlinearity is defined as the statistical average of the output signal conditioned on the knowledge of the transmitted information. Once the equivalent signal component is defined the effective noise component is simply the signal at the output of TWT less the equivalent signal component. Jain and Blachman [49] have expressed the probability of error in terms of infinite series of modified Bessel functions of the first kind for the case of binary CPSK signals transmitted through a hard-limited repeater with a single sample and majority logic receiver.

In section 4.2.1 we make use of Lyons's approach [57, 59] to

characterize the in-phase and quadrature noise and their statistics at the output of a piecewise-linear soft-limiter. Based on these statistics the probability of error for a receiver with a single sample and majority logic detector is computed. A similar approach is applied in section 4.2.2 for the case of an actual TWT channel [45]. However, due to the complexity of the TWT nonlinearities, the analytical expressions for the equivalent noise statistics are very difficult to obtain. In this case we expand the probability density functions in terms of Gram-Charlier series as used by Cramer [28]. Our emphasis in this section will be on binary CPSK systems although the method in general can be extended to the M-ary CPSK case.

4.2.1) Piecewise-linear envelope limiting repeater

Let us assume the transmitted M-ary CPSK signal, within each symbol duration, to be of the form

$$y(t) = A \cos[\omega_0 t + \theta_i] \qquad 0 \leq t \leq T \qquad (4.17)$$

where

A = signal amplitude

ω_0 = angular carrier frequency

T = symbol duration

$\theta_i = (2i-1)\frac{\pi}{M}$; $i = 0, 1, 2, \ldots, M-1$

each value of θ_i having equal probability of being transmitted.

Then the total signal at the input of the nonlinear device may be written as

$$x(t) = [A + n_1(t)] \cos(\omega_0 t + \theta_i) - n_2(t) \sin(\omega_0 t + \theta_i) \quad (4.18)$$

where $n_1(t)$ and $n_2(t)$, representing the in-phase and quadrature noise components, are zero mean Gaussian random variables with variance N_u watts.

In terms of envelope and phase relationships, (4.18) can be written as

$$x(t) = R(t) \cos[\omega_0 t + \theta_i + \varepsilon(t)] \quad (4.19)$$

where

$$R(t) = \sqrt{[A + n_1(t)]^2 + [n_2(t)]^2}$$

and

$$\varepsilon(t) = \tan^{-1}\left[\frac{n_2(t)}{A + n_1(t)}\right] \quad (4.20)$$

The signal at the output of the piecewise-linear envelope-limiting repeater then becomes [43]

$$z(t) = f(R) \cos[\omega_0 t + \theta_i + \varepsilon(t)] \quad (4.21)$$

where the limiter nonlinearity is described by

$$f(R) = \begin{cases} \frac{R}{\lambda} & 0 \le R \le \lambda \\ 1 & R > \lambda \end{cases} \quad (4.22)$$

The constant λ is known as the limiter softness factor. When λ is equal to zero a hard-limiting envelope nonlinearity as discussed in [59] is obtained.

Following the work of Lyons [57] the effective signal component, $s'(t)$ at the output of the nonlinear device is defined as the conditional average of equation (4.21). The averaging of $z(t)$, conditioned on the knowledge of the transmitted phase θ_i, is made over all the random fluctuations due to the up-link noise components. We can then write

$$s'(t) = A' \cos[\omega_0 t + \theta_i] \tag{4.23}$$

where A' is the effective signal amplitude defined by

$$A' = E_{R,\varepsilon}[f(R) \cos \varepsilon]$$

As shown in Appendix C.2, this value of A' for the piecewise-linear envelope limiting repeater can be written as

$$A' = \frac{\sqrt{\pi\rho}}{2} e^{-\rho/2} \{I_0[\rho/2] + I_1[\rho/2]\} - 2\gamma e^{-\rho} \int_0^1 (1-x)x\, e^{-\gamma x^2} I_1[A\lambda x/N_u]\, dx \tag{4.24}$$

where $E_{R,\varepsilon}[\cdot]$ denotes the statistical averaging over R and ε.

$\rho = A^2/2N_u$ is the up-link carrier to noise power ratio

$I_n(\cdot)$ = modified Bessel function of the first kind of order n

$\gamma = \lambda^2/2N_u$

The first term on the right hand side of equation (4.24) corresponds to A' for the case of a hard-limited channel ($\lambda = 0$) and was originally derived by Blachman [17], the second term represents the correction term due to the limiter softness factor, λ.

The effective noise component at the output of the nonlinear device is then obtained by subtracting (4.23) from (4.21) and is given by

$$n'(t) = n_1'(t) \cos[\omega_0 t+\theta_i] - n_2'(t) \sin[\omega_0 t+\theta_i]$$

where

$$n_1'(t) = f(R) \cos \varepsilon - A' \tag{4.25}$$

$$n_2'(t) = f(R) \sin \varepsilon \tag{4.26}$$

Now define

$$x = \frac{A + n_1}{\lambda} \tag{4.27}$$

$$y = \frac{n_2}{\lambda} \tag{4.28}$$

The variables x and y, as defined are Gaussian random variables with means A/λ and zero respectively, and both with the same variance N_u/λ^2.

In terms of x and y we can write

$$n_1' = \begin{cases} x - A' & 0 \le x^2+y^2 \le 1 \\ \dfrac{x}{\sqrt{x^2+y^2}} - A' & x^2+y^2 > 1 \end{cases} \tag{4.29}$$

and

$$n_2' = \begin{cases} y & 0 \le x^2+y^2 \le 1 \\ \dfrac{y}{\sqrt{x^2+y^2}} & x^2+y^2 > 1 \end{cases} \tag{4.30}$$

The probability distribution function of n_1' can be obtained by integrating these Gaussian random variables, x and y, over the appropriate regions in the x-y plane (see Appendix C.1). Once the probability distribution function is obtained the corresponding probability density function can be evaluated from

$$p_{n_1'}(\alpha) = \frac{d}{d\alpha}\left[\Pr\{n_1' < \alpha\}\right] \tag{4.31}$$

Performing the indicated differentiation in equation (4.31) yields (Appendix C.1)

$$p_{n_1'}(\alpha) = \begin{cases} 0 & |\alpha+A'| > 1 \\ \dfrac{2\lambda}{\sqrt{N_u}}\,\phi\left[\dfrac{\lambda(\alpha+A')-A}{\sqrt{N_u}}\right]\left\{\Phi\left[\dfrac{\lambda\sqrt{1-(\alpha+A')^2}}{\sqrt{N_u}}\right]-\dfrac{1}{2}\right\}+ & \\ \dfrac{\sqrt{\frac{2}{\pi}}\exp\left[-\dfrac{A^2}{2N_u}\left[1-(\alpha+A')^2\right]\right]}{\sqrt{1-(\alpha+A')^2}}\left\{\Phi\left[\dfrac{\lambda-A(\alpha+A')}{\sqrt{N_u}}\right]+\right. & \\ \left.\dfrac{A(\alpha+A')}{\sqrt{N_u}}\,\phi\left[\dfrac{A(\alpha+A')-\lambda}{\sqrt{N_u}}\right]\right\} & |\alpha+A'| \le 1 \end{cases} \tag{4.32}$$

where

$$\phi(x) = \frac{1}{\sqrt{2\pi}}\exp[-x^2/2]$$

and

$$\Phi(x) = \frac{1}{\sqrt{2\pi}} \int_{-\infty}^{x} \exp[-\alpha^2/2]\, d\alpha = \frac{1}{2}\,\mathrm{erfc}[-x/\sqrt{2}]$$

where erfc(·) denotes the complementary error function.

Using the same procedure the following expression can be derived for the probability density function of the quadrature noise component n_2'

$$p_{n_2'}(\beta) = \begin{cases} 0 & |\beta| > 1 \\ \dfrac{\lambda}{\sqrt{N_u}}\,\Phi\left[\dfrac{\lambda\beta}{\sqrt{N_u}}\right]\left\{\Phi\left[\dfrac{\lambda\sqrt{1-\beta^2}-A}{\sqrt{N_u}}\right] - \Phi\left[\dfrac{-\lambda\sqrt{1-\beta^2}-A}{\sqrt{N_u}}\right]\right\} & \\ + \dfrac{\exp[-A^2\beta^2/2N_u]}{\sqrt{2\pi(1-\beta^2)}}\left\{\Phi\left[\dfrac{\lambda-A\sqrt{1-\beta^2}}{\sqrt{N_u}}\right] + \Phi\left[\dfrac{\lambda+A\sqrt{1-\beta^2}}{\sqrt{N_u}}\right]\right. & \\ \left. + \dfrac{A\sqrt{1-\beta^2}}{\sqrt{N_u}}\left\{\Phi\left[\dfrac{\lambda+A\sqrt{1-\beta^2}}{\sqrt{N_u}}\right] - \Phi\left[\dfrac{\lambda-A\sqrt{1-\beta^2}}{\sqrt{N_u}}\right]\right\}\right\} & \\ & |\beta| \le 1 \end{cases} \qquad (4.33)$$

Figures 4-11 to 4-22 illustrate the behavior of $p_{n_1'}(\alpha - A')$ and $p_{n_2'}(\beta)$ for different values of a normalized limiter softness factor, $\lambda^* = \lambda/A$, and different up-link bit energy to noise power spectral density ratios. The plots indicate that for $\lambda^* = 0$, corresponding to the hard-limited channel, the equivalent quadrature noise component

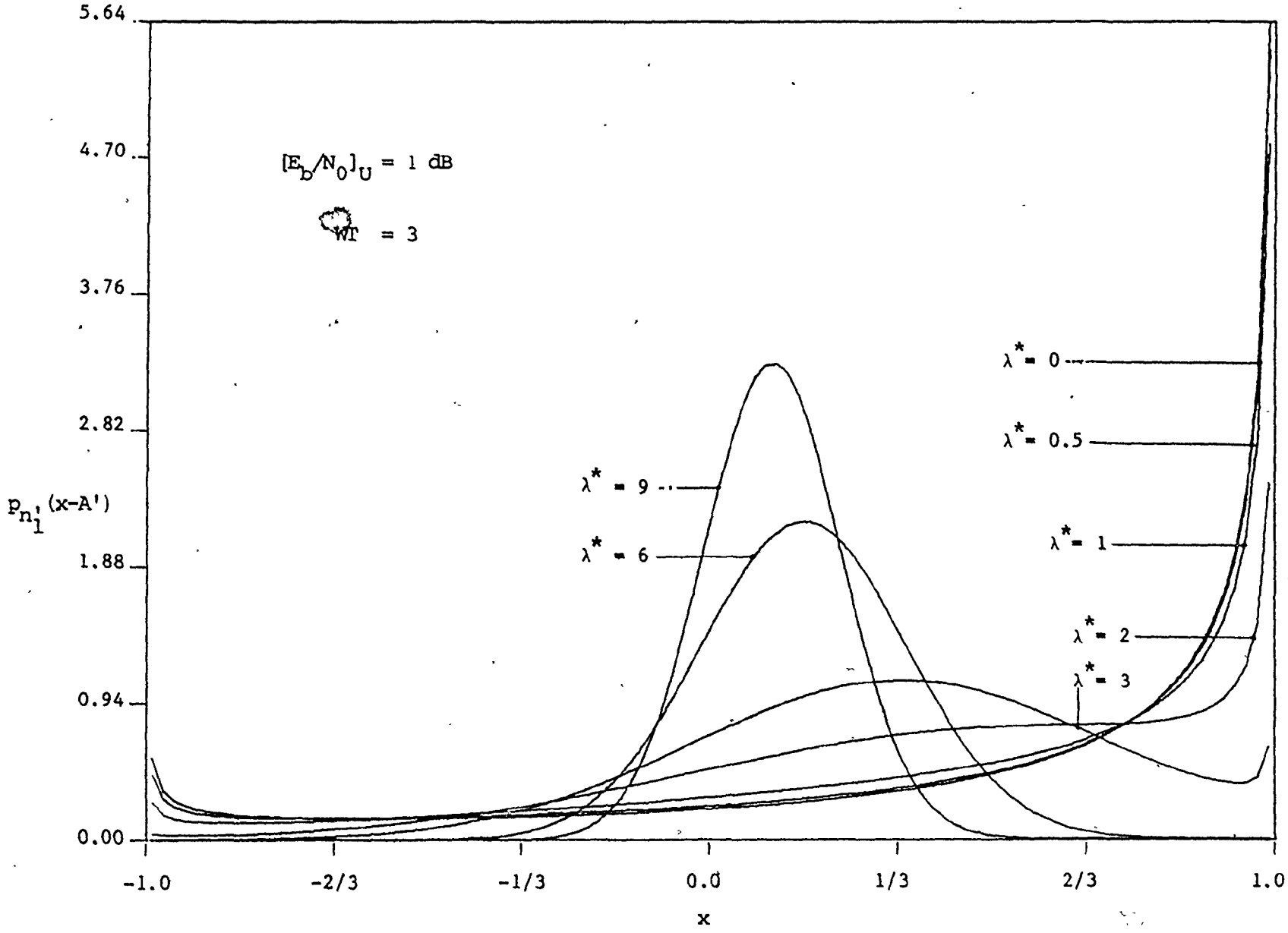

Fig. 4-11. Shifted pdf of in-phase noise from limiter, $p_{n_1'}(x-A')$

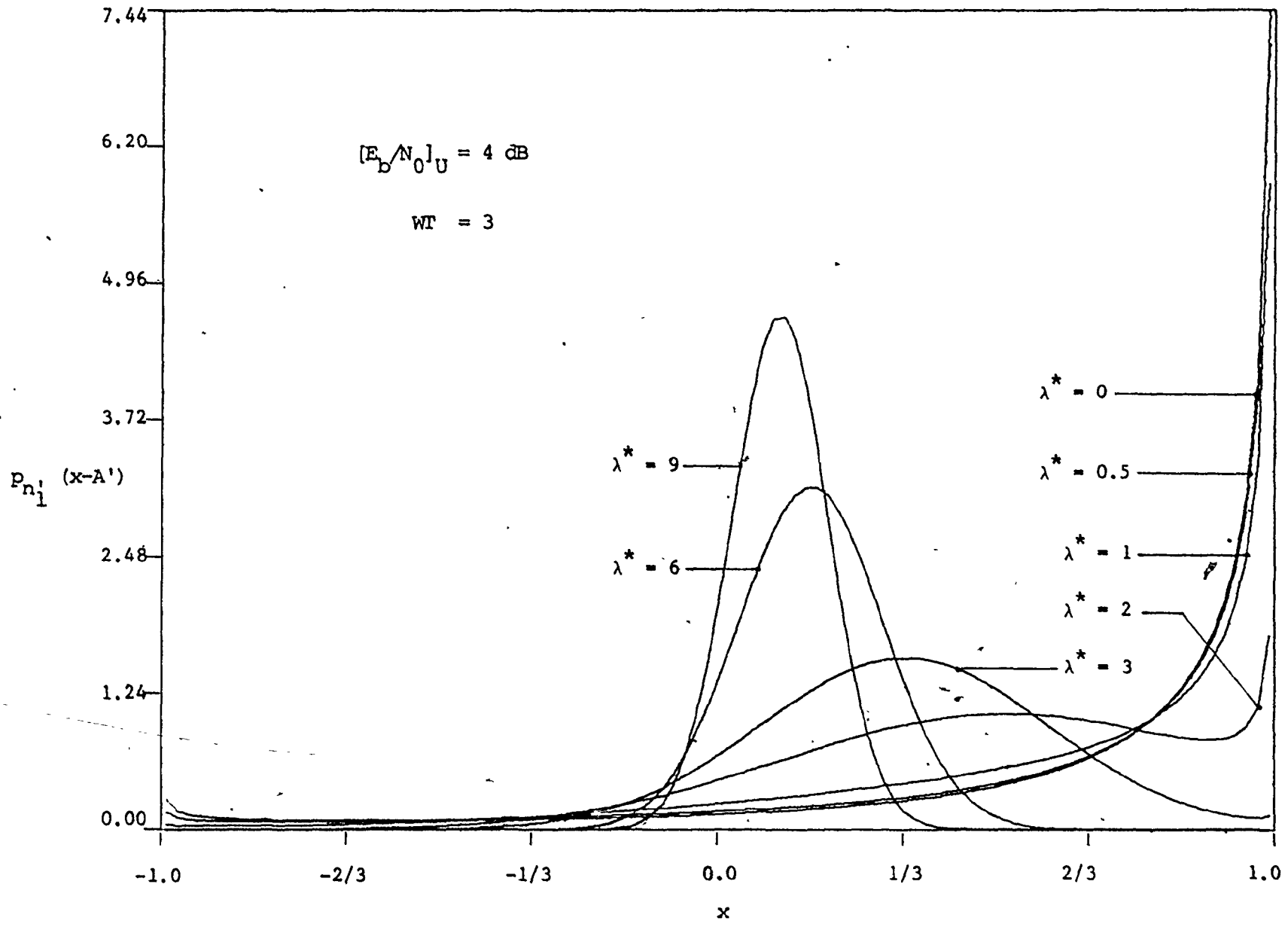

Fig. 4-12. Shifted pdf of in-phase noise from limiter, $p_{n_1'}(x-A')$

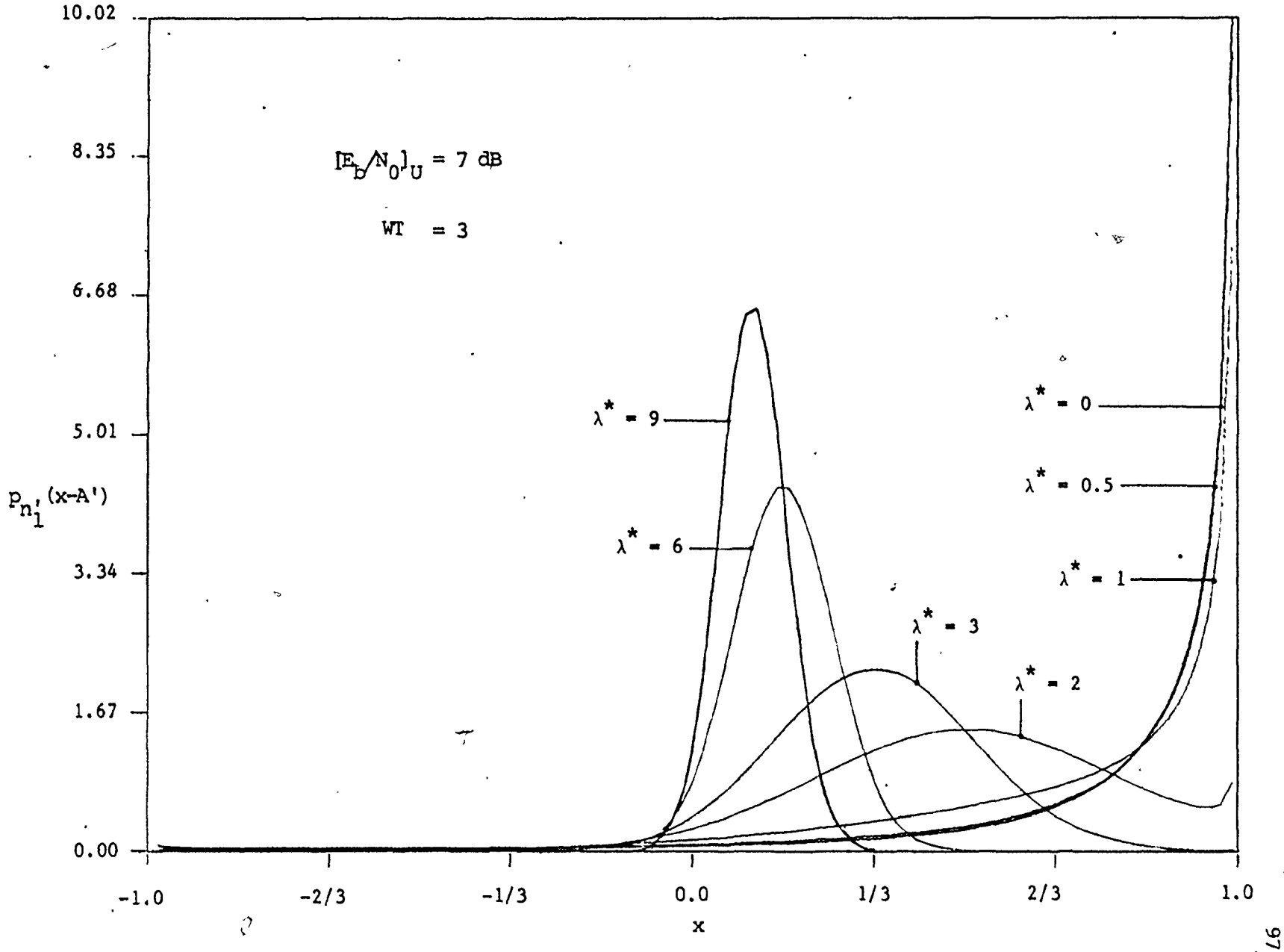

Fig. 4.13. Shifted pdf of in-phase noise from limiter, $p_{n_1'}(x-A')$

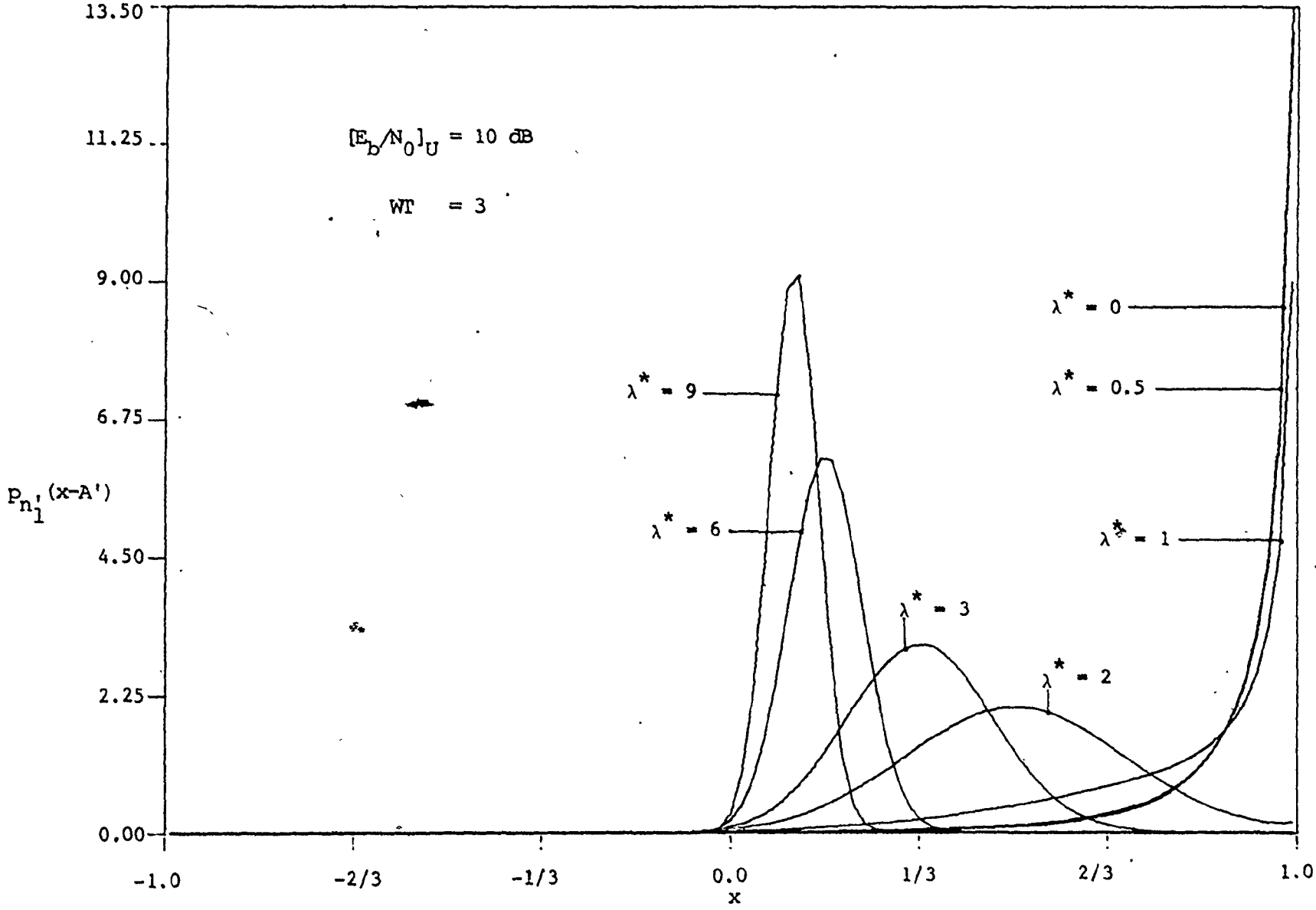

Fig. 4.14. Shifted pdf of in-phase noise from limiter, $p_{n_1'}(x-A')$

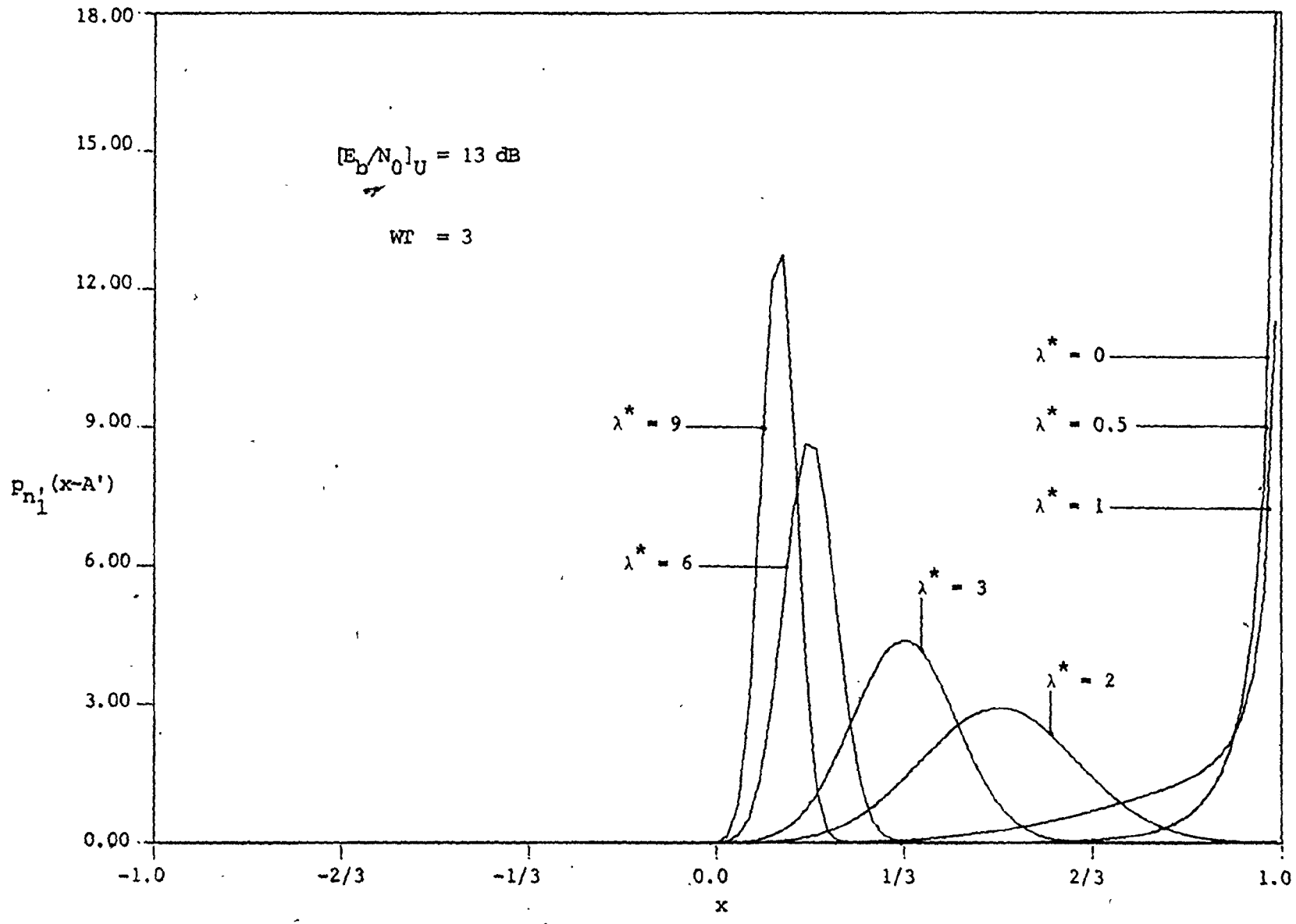

Fig. 4.15. Shifted pdf of in-phase noise from limiter, $p_{n_1'}(x-A')$

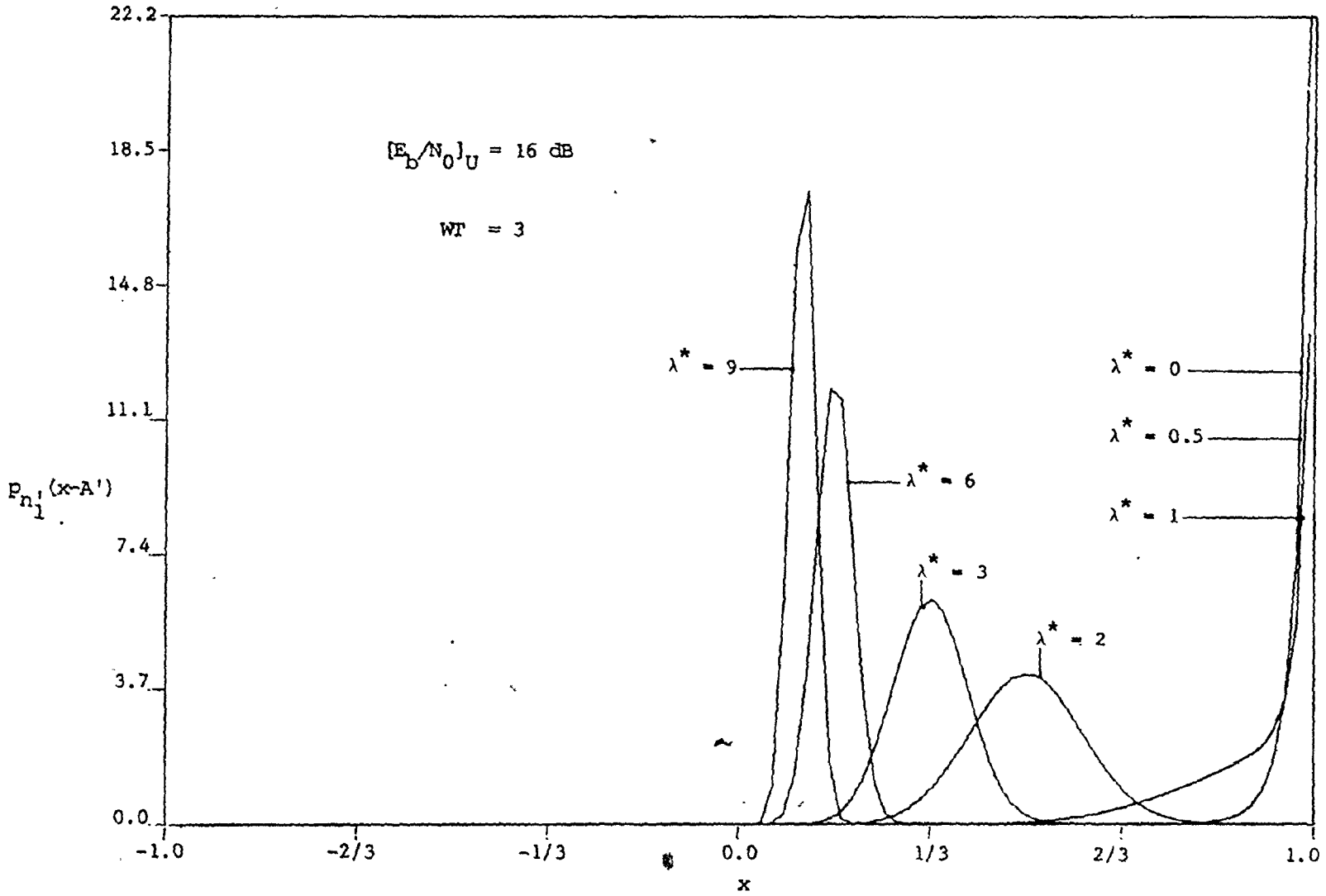

Fig. 4.16. Shifted pdf of in-phase noise from limiter, $p_{n_1'}(x-A')$

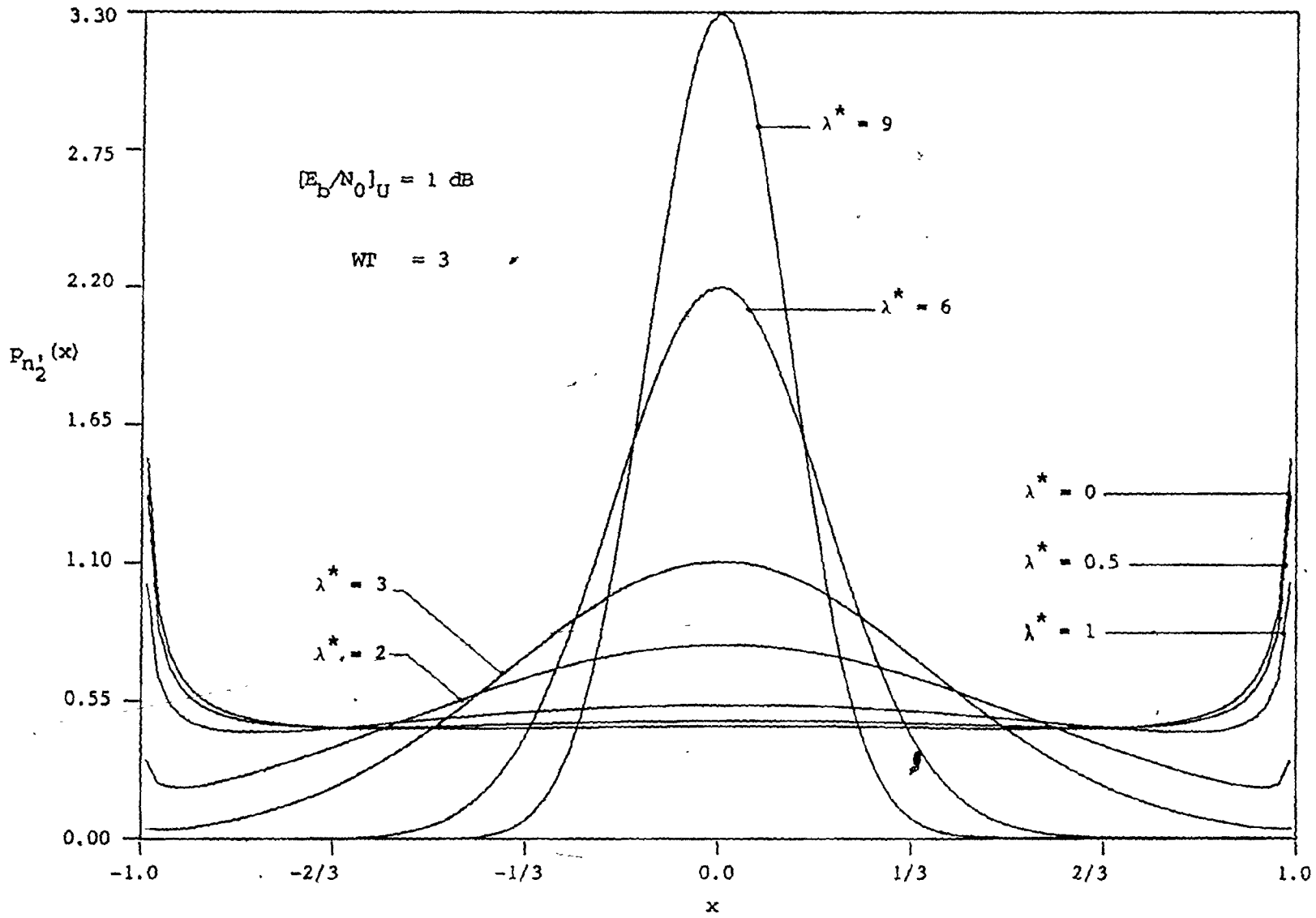

Fig. 4-17. Pdf of quadrature noise from limiter, $p_{n_2'}(x)$

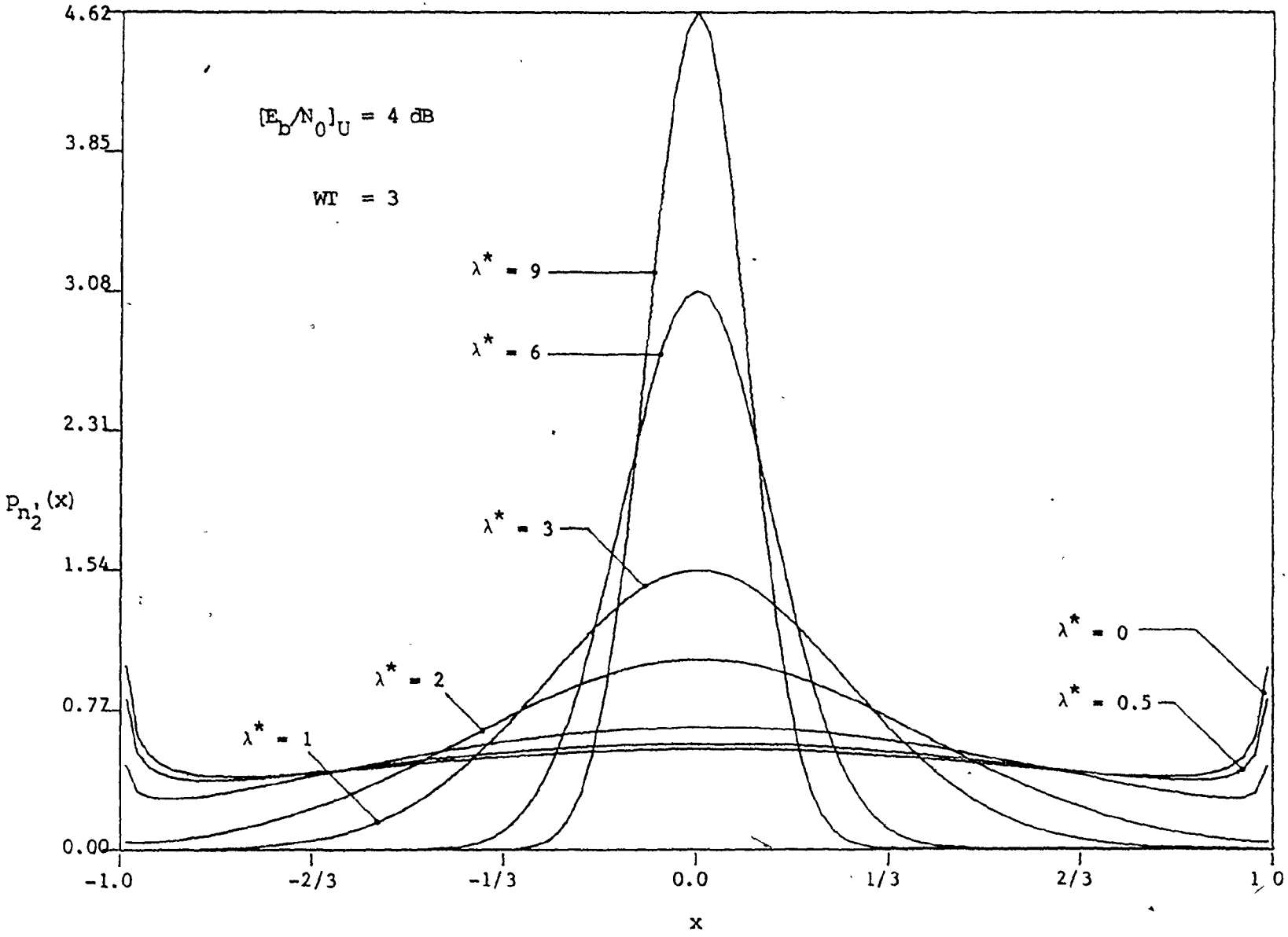

Fig. 4-18. Pdf of quadrature noise from limiter, $p_{n_2'}(x)$

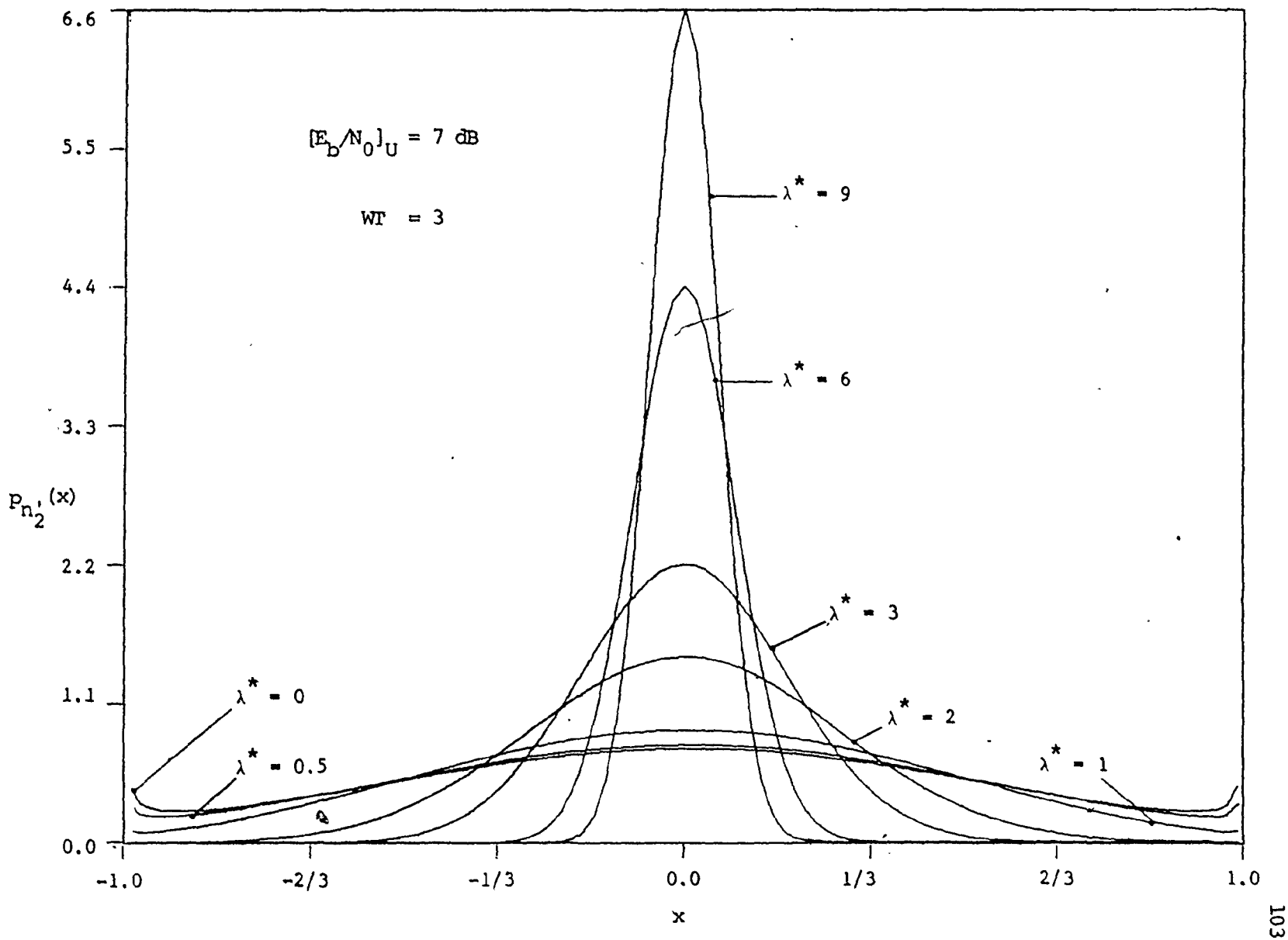

Fig. 4-19. Pdf of quadrature noise from limiter, $p_{n_2'}(x)$

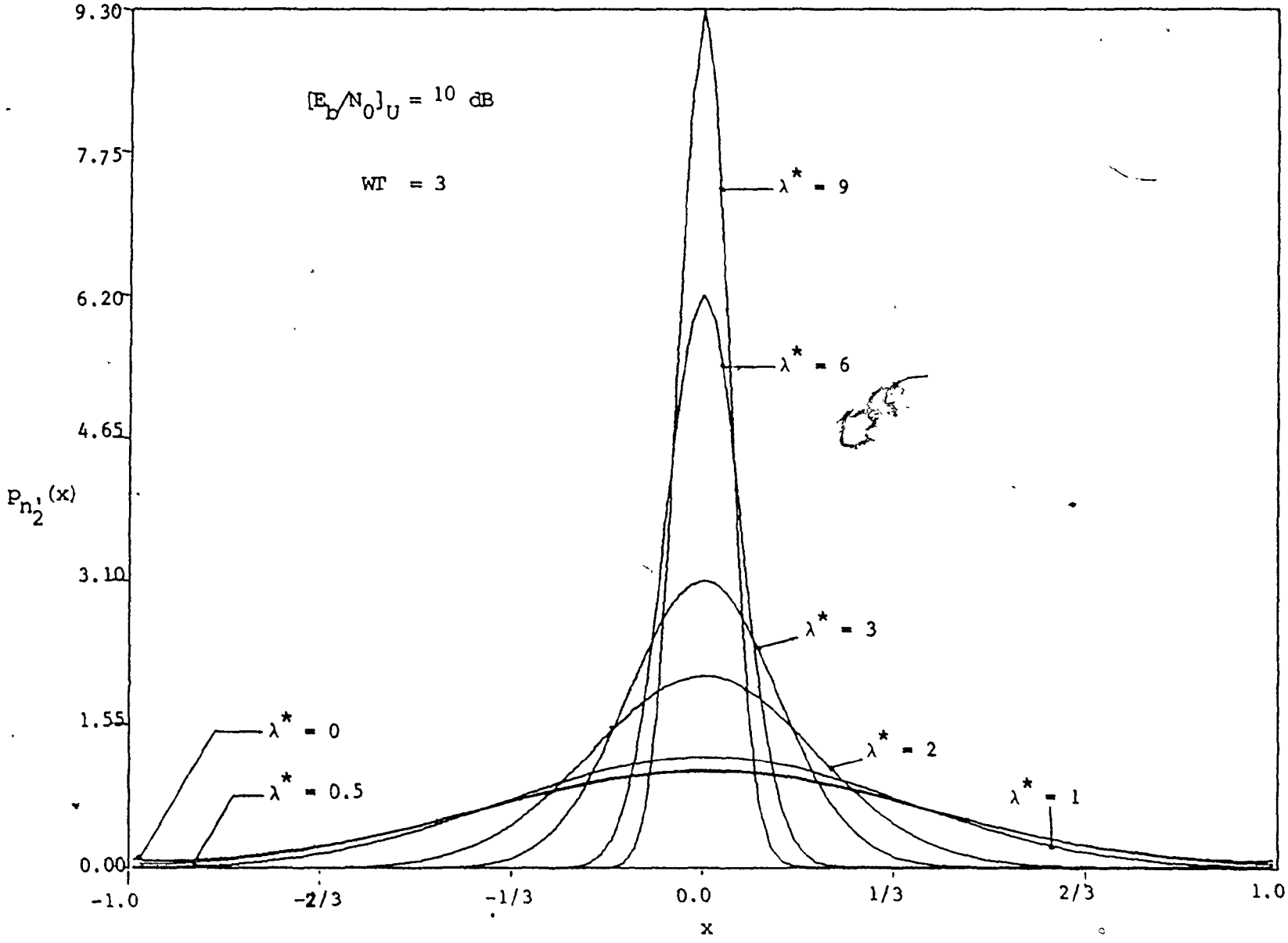

Fig. 4-20. Pdf of quadrature noise from limiter, $p_{n_2'}(x)$

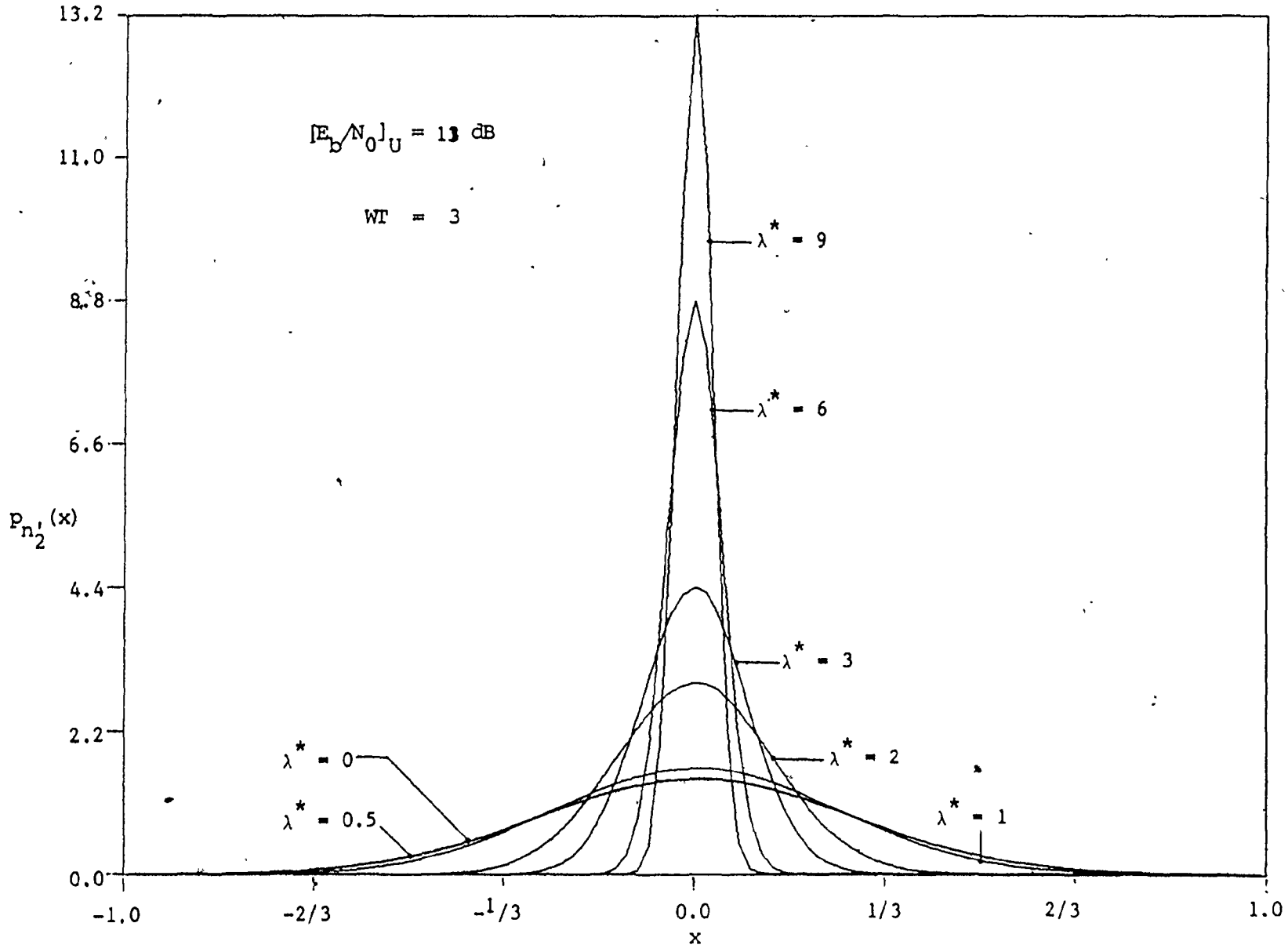

Fig. 4-21. Pdf of quadrature noise from limiter, $p_{n_2'}(x)$

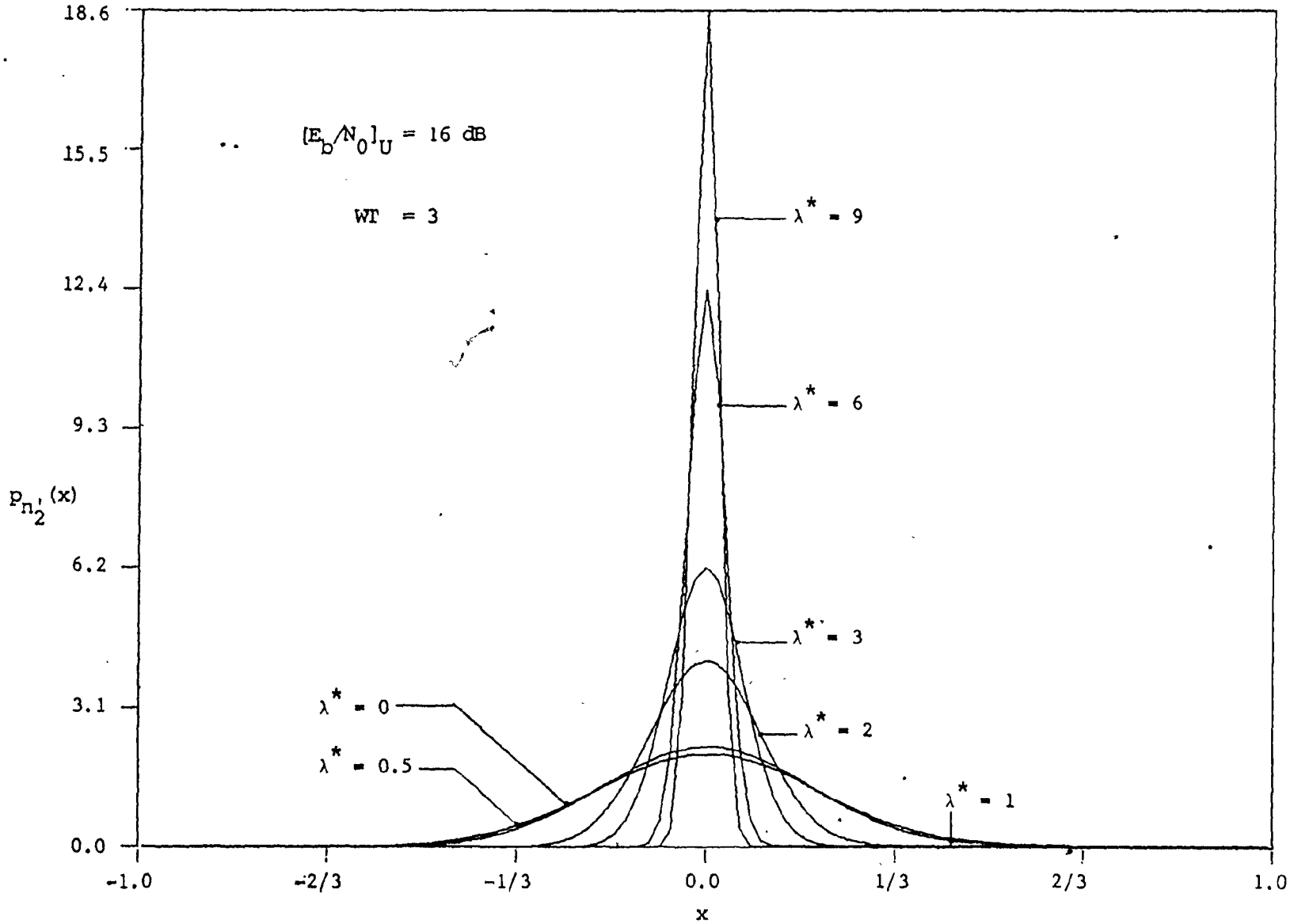

Fig. 4-22. Pdf of quadrature noise from limiter, $p_{n_2'}(x)$

behaves in a similar manner to Gaussian noise at large up-link $[E_b/N_0]$, however, at small up-link $[E_b/N_0]$, both $p_{n_1'}(x-A')$ and $p_{n_2'}(x)$ behave like $\frac{1}{\pi\sqrt{1-x^2}}$.

As λ^* increases, implying that the channel becomes more and more linear, both $p_{n_1'}(x-A')$ and $p_{n_2'}(x)$ tend toward Gaussian density functions for all values of up-link bit energy to noise power spectral density ratio.

In order to obtain P_e, the receiver error rate, we must take into account both the noise component of the limiter output due to the up-link Gaussian noise and additive down-link Gaussian noise. Let us assume that ξ_1 and ξ_2, representing the in-phase and quadrature components of the down-link noise component, are zero mean Gaussian random variables with variance N_d watts. We may then define the total in-phase and quadrature components of the noise at the receiver input as

$$u = n_1' + \xi_1 \tag{4.34}$$

$$v = n_2' + \xi_2 \tag{4.35}$$

The probability density functions $p_u(x)$ and $p_v(x)$ of the in-phase and quadrature noise components may then be obtained by convolving the corresponding density functions of n_1' and ξ_1 or n_2' and ξ_2 respectively. For example the in-phase probability density function $p_u(x)$ is given by

$$p_u(x) = \int_{-1-A'}^{1-A'} p_{n_1'}(z)\, p_{\xi_1}(x-z)\, dz \tag{4.36}$$

where

$$p_{\xi_1}(x) = p_{\xi_2}(x) = \frac{1}{\sqrt{2\pi N_d}} \exp[-x^2/2N_d] \tag{4.37}$$

are the probability density functions of the in-phase and quadrature noise components, ξ_1 and ξ_2, in the down-link. The probability density function of the quadrature noise, v, may be similarly obtained.

Since each sample of the signal at the input of the TWT is statistically independent and the TWT itself is assumed to be memoryless, it then follows that the samples at the output of the TWT are statistically independent. Using this assumption the conventional integrate and dump detector will be replaced by a single sample detector and majority logic decision device. The error probability is then given by the probability that more than half the, WT = 2ℓ+1, baseband samples are detected in error [47], where W is the system bandwidth.

Using the binomial distribution, the error probability can then be computed from

$$P_e = \sum_{j=0}^{\ell} \frac{(2\ell+1)!}{(2\ell+1-j)!\; j!} p^{2\ell+1-j}(1-p)^j \tag{4.38}$$

In this expression, p, the probability of one sample being in error is given by the probability that u and/or v, as defined in equations (4.34-4.35), fall outside the correct decision region. It can be shown

that [59]

$$p = p_1 + p_2(1-p_1)$$

where $$p_1 = Pr[u+A' < 0] = \int_{-\infty}^{-A'} p_u(x)\, dx \qquad (4.39)$$

$$p_2 = Pr[\,|v| - u \tan\tfrac{\pi}{M} > A'\tan\tfrac{\pi}{M} \,|u+A' > 0] \qquad (4.40)$$

To determine p_1, we first define

$$y = x + A' \qquad (4.41)$$

Then substituting equations (4.36) and (4.41) into (4.39) yields

$$p_1 = \int_{-\infty}^{0} \int_{-1-A'}^{1-A'} p_{n_1'}(z)\, p_{\xi_1}(y-A'-z)\, dzdy \qquad (4.42)$$

Now define the new random variables α and β as

$$y = \frac{\beta-1}{\beta+1} \qquad (4.43)$$

$$z = \sin\alpha \qquad (4.44)$$

Substituting equations (4.43-4.44) into (4.42) and integrating over β, yields after some manipulation

$$p_1 = \int_{-1}^{1} \left\{ \frac{2\lambda}{\sqrt{N_u}}\, \phi\left[\frac{\lambda\alpha-A}{\sqrt{N_u}}\right] \Phi\left[\frac{-\alpha}{\sqrt{N_d}}\right] \left\{ \phi\left[\frac{\lambda\sqrt{1-\alpha^2}}{\sqrt{N_u}}\right] - \frac{1}{2} \right\} +$$

$$+\sqrt{\frac{\pi}{2}}\exp\left[\frac{-A^2}{2N_u}\cos^2\left(\frac{\alpha\pi}{2}\right)\right]\phi\left[-\frac{\sin\left(\frac{\alpha\pi}{2}\right)}{\sqrt{N_d}}\right]\left\{\phi\left[\frac{\lambda-A\sin\left(\frac{\alpha\pi}{2}\right)}{\sqrt{N_u}}\right]+\right.$$

$$\left.\frac{A\sin\left(\frac{\alpha\pi}{2}\right)}{\sqrt{N_u}}-\phi\left[\frac{A\sin\left(\frac{\alpha\pi}{2}\right)-\lambda}{\sqrt{N_u}}\right]\right\}\Bigg\}\,d\alpha \qquad (4.45)$$

Similarly, substitution of equations (4.34-4.35) into equation (4.40) yields after some manipulation*

$$P_2 \simeq \frac{\pi^2}{2}\int_0^1\int_{-1}^1 p_{n_1'}[-A'-\sin\left(\frac{\alpha\pi}{2}\right)]\,p_{n_2'}[\sin\left(\frac{\beta\pi}{2}\right)]\cdot$$

$$\phi\left[\frac{\sin\left(\frac{\alpha\pi}{2}\right)\sin\left(\frac{\pi}{M}\right)+\sin\left(\frac{\beta\pi}{2}\right)\cos\left(\frac{\pi}{M}\right)}{\sqrt{N_d}}\right]\cos\left(\frac{\alpha\pi}{2}\right)\cos\left(\frac{\beta\pi}{2}\right)\,d\alpha d\beta \qquad (4.46)$$

Equations (4.38, 4.45-4.46) allow us to calculate the probability of error for an M-ary CPSK system operating over a soft-limited channel, where the integrals in (4.45) and (4.46) must be evaluated numerically.

In figures 4-23 to 4-25, the probability of error, P_e, is plotted as a function of down-link bit energy to noise power spectral density ratio $[(A')^2WT/2N_d]$, for different values of normalized limiter softness factor, λ^*, and different up-link bit energy to noise power spectral density ratios $[A^2WT/2N_u]$. Also shown in these figures is the plot of the corresponding probability of error for the linear channel using a matched filter receiver, the optimal receiver for linear channel. The results in figures 4-23 to 4-25 indicate that for a majority logic receiver the

---

* This is an approximation based on the assumed independence of n_1' and n_2'.

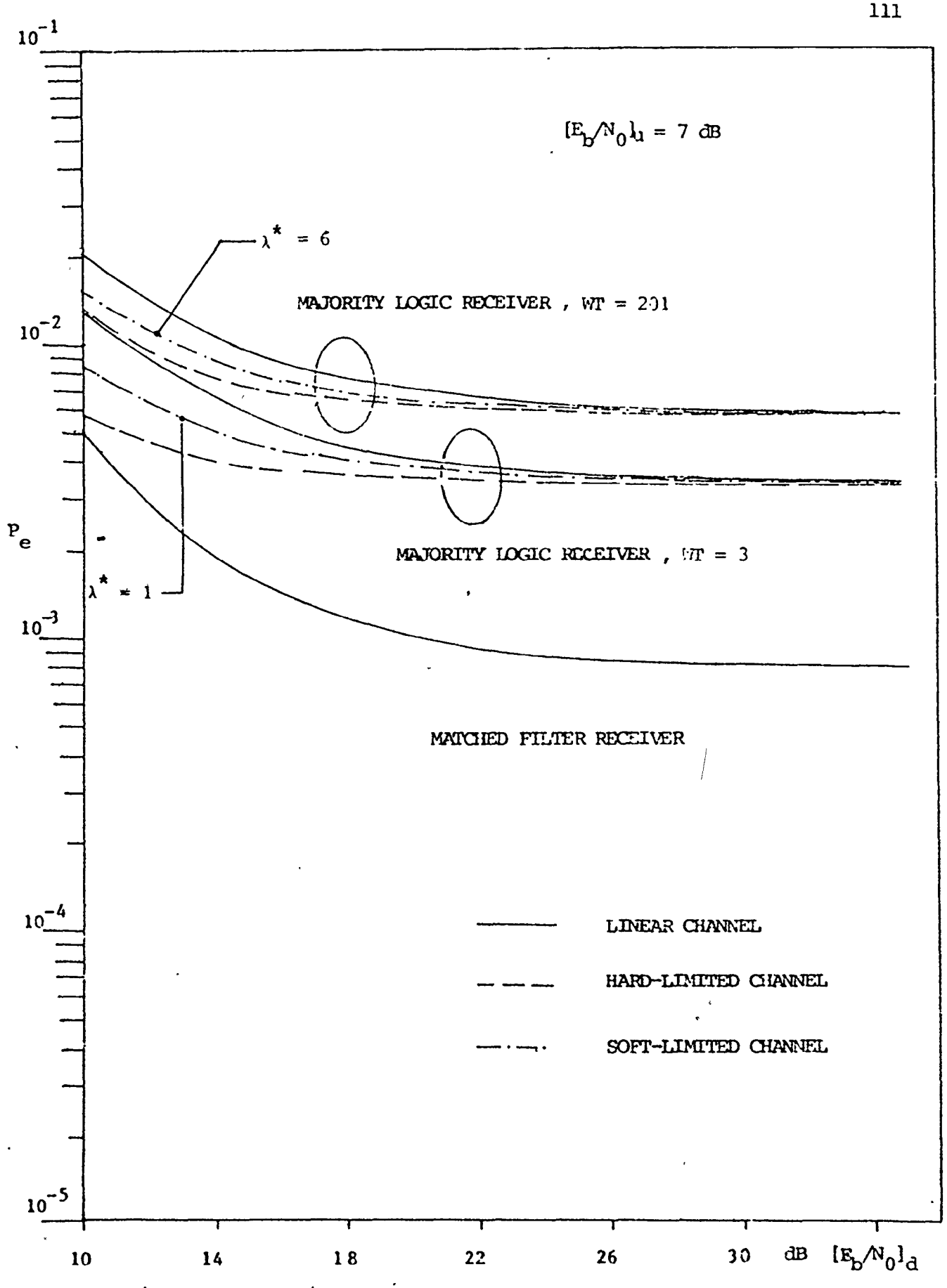

Fig. 4-23. Probability of error vs E_b/N_0, 2-phase CPSK

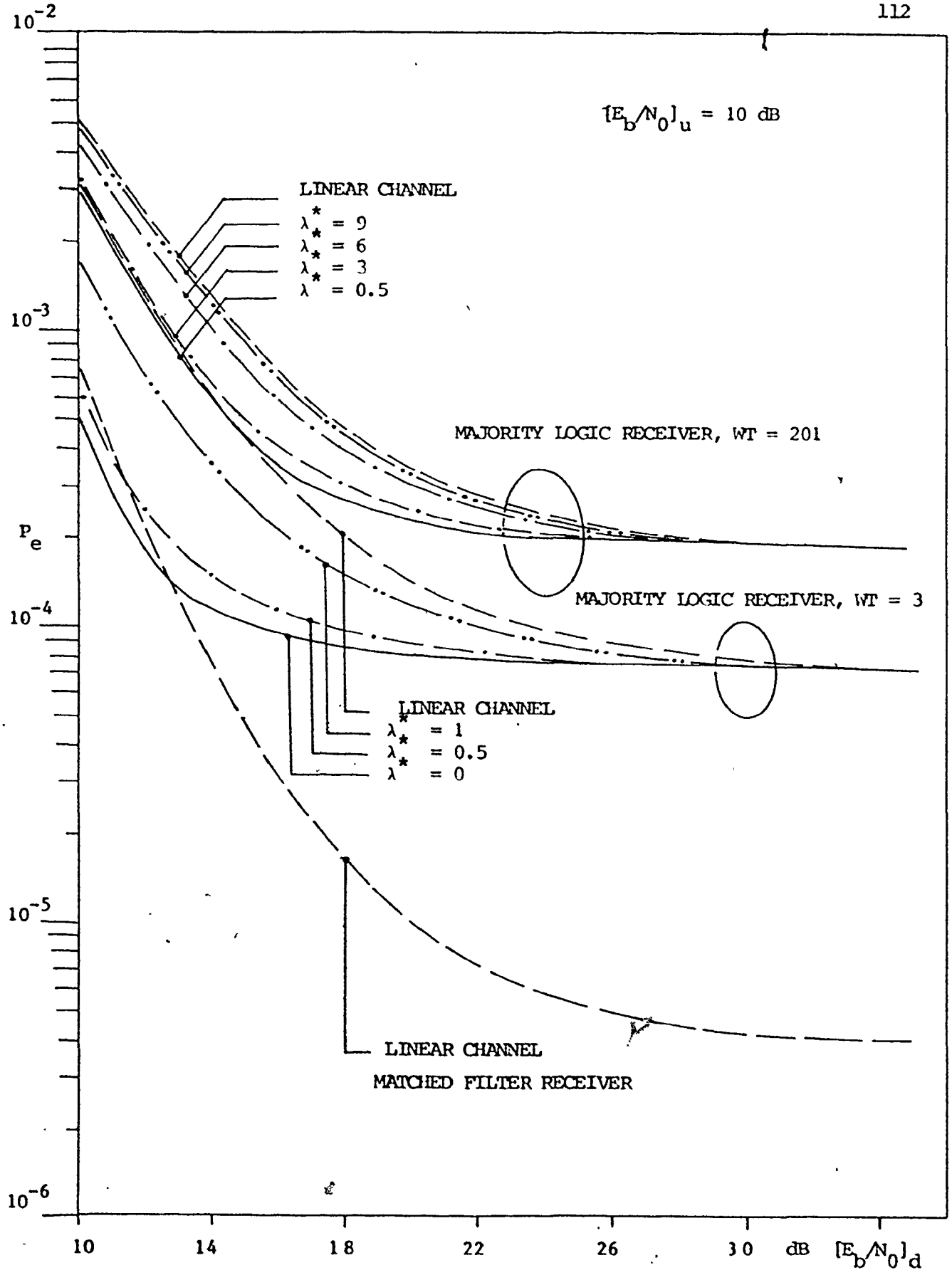

Fig. 4-24. Probability of error vs E_b/N_0, 2-phase CPSK

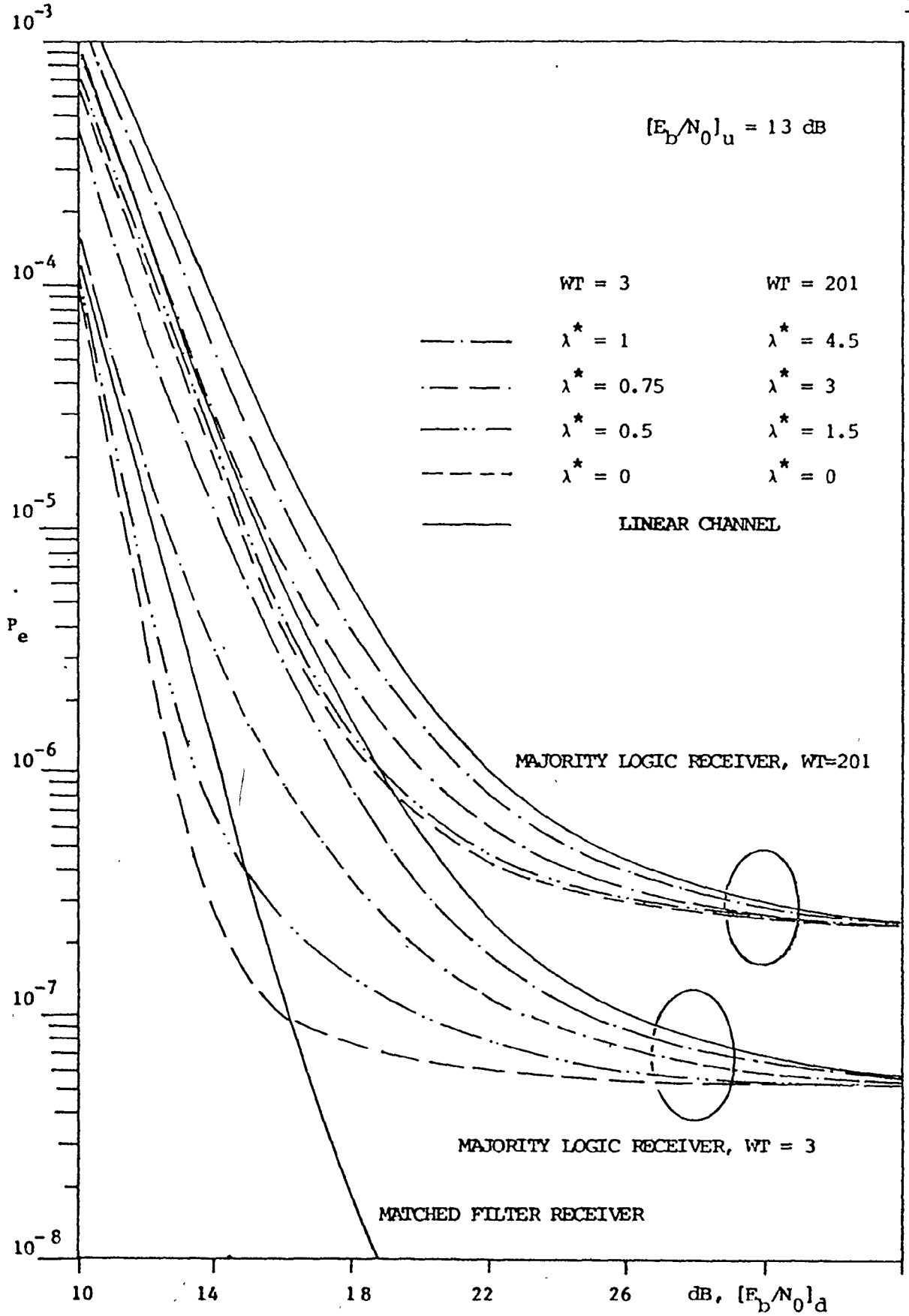

Fig. 4-25. Probability of error vs E_b/N_0, 2-phase CPSK

presence of hard-limiter or any form of soft-limiter can improve the performance of the system. Ostensibly, this superiority in the performance of the limited channel may strike some communication theorists as anomalous. However, we point out that our claim of this improvement in the performance of the amplitude-limited channel can only apply to the case of the single sample detection, majority logic receiver. This same conclusion has also been made by others [49, 59] for the case of a hard-limited channel. The generalization to the piecewise-linear limiter is, however, new. Heuristically one can justify the afore-mentioned performance improvement by considering the amplitude-limited channel as a form of regenerative repeater. The "soft-averaging" in the piecewise-linear envelope limited channel tends to recover the signal phase from the up-link in-phase noise, the only source of impairment for the binary case, and thereby reduces the degrading effect of the total noise. However, without down-link thermal disturbance, such improvement is only marginal because in this case the limiter in the repeater will now be cascaded directly to the hard-decision device in the receiver and the combined effect is the same as if we were to consider the linear channel.

Figures 4-26 and 4-27 depict similar results for the case of 4- and 8-phase CPSK where the up-link and down-link carrier to noise power ratios are defined as

$$(CNR)_u = A^2/2N_u$$

$$(CNR)_d = (A')^2/2N_d \qquad (4.47)$$

To conclude this section we restress the fact that a majo-

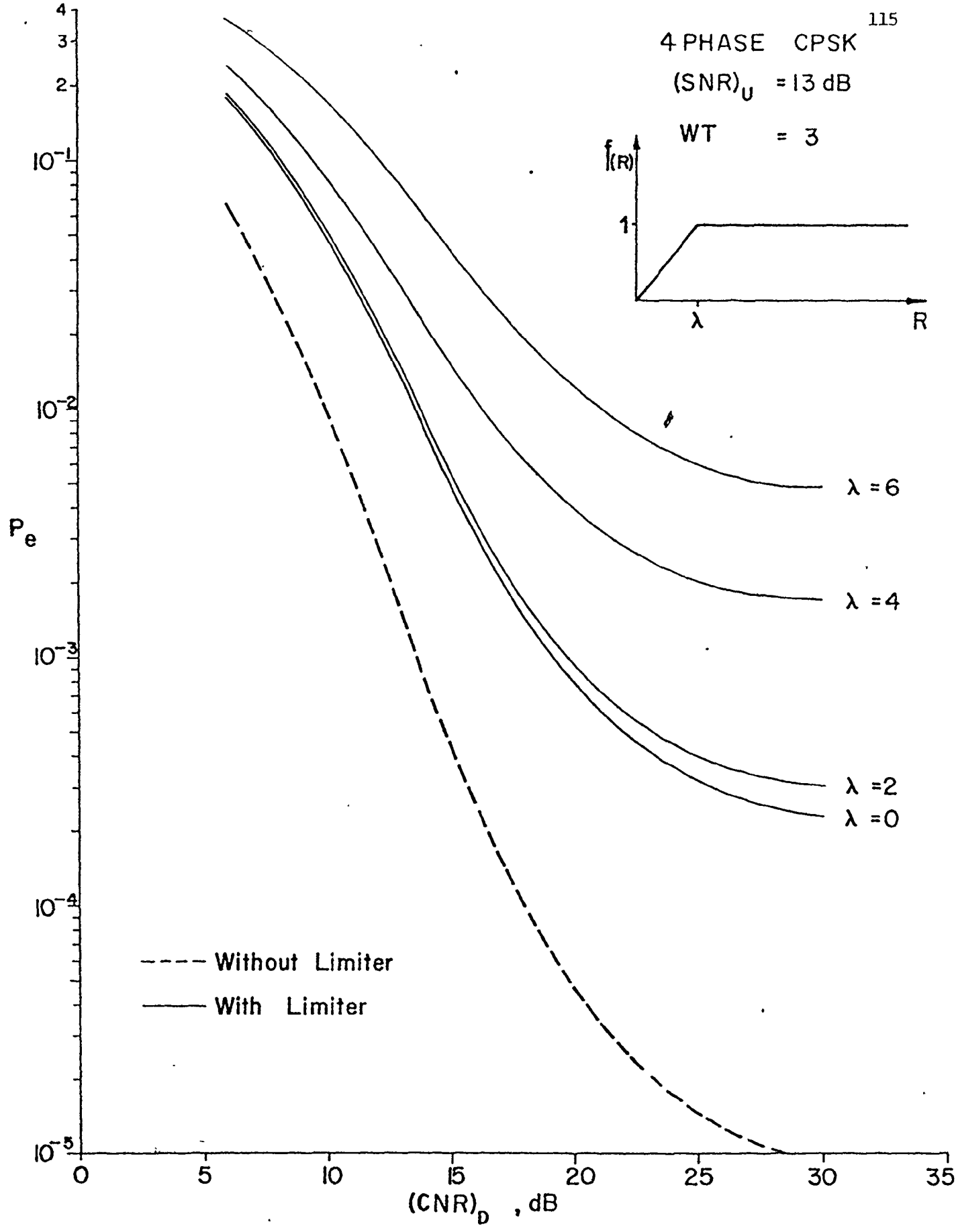

Fig. 4-26. Probability of error vs E_b/N_0, 4-phase CPSK

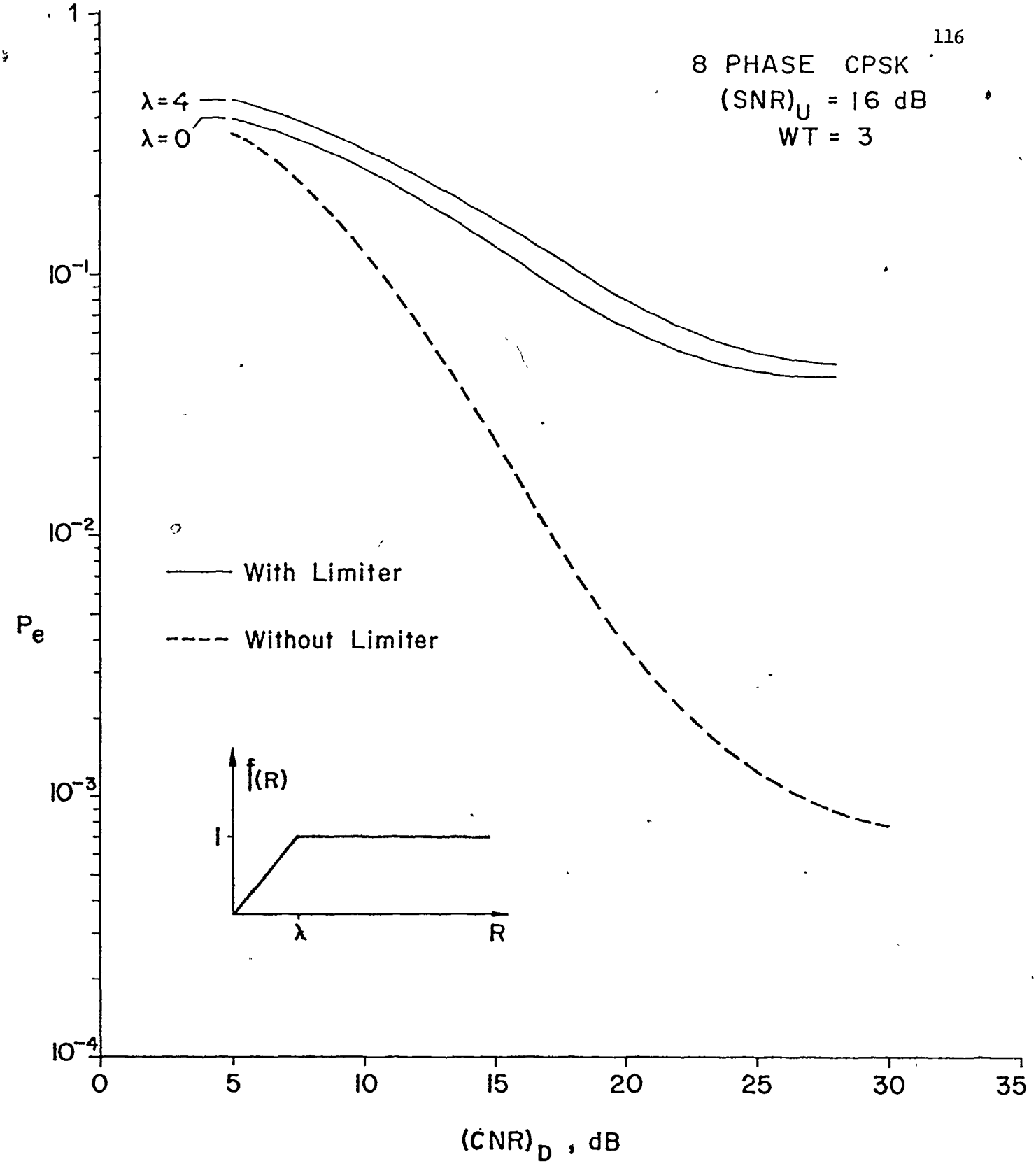

Fig. 4-27. Probability of error vs E_b/N_0, 8-phase CPSK

rity logic receiver is not a good approximation to a matched filter receiver for a linear channel [47]. The performance of the majority logic receiver is generally poorer on the linear channel than that of the matched filter which is the optimal receiver for the linear channel. The main reason for using the majority logic receiver in the present work is to avoid the difficulties associated with evaluating the stochastic integral arising in the analysis of the matched filter receiver. Any conclusions reached in the case of a majority logic receiver should not be assumed to translate to the situation when a matched filter is used. Further investigations on the performance of an optimal receiver (in the maximum likelihood sense) will be deferred until Chapter 5.

4.2.2) Actual TWT channel

In this section we shall apply the same method to analyze the performance of a CPSK system through a nonlinear channel containing an actual TWT amplifier. A typical model of such a communications system is as shown in Fig. 4-28. The nonlinear quadrature model of the TWT developed in Chapter 2 will be assumed throughout the analysis. Similar to the argument leading to equation (4.21), the signal at the output of the TWT amplifier then becomes

$$z(t) = Z_p(R)\cos(\omega_0 t + \theta_i + \varepsilon) - Z_q(R)\sin(\omega_0 t + \theta_i + \varepsilon) \tag{4.48}$$

where $Z_p(\cdot)$ and $Z_q(\cdot)$ are as defined in equations (2.18-2.19).

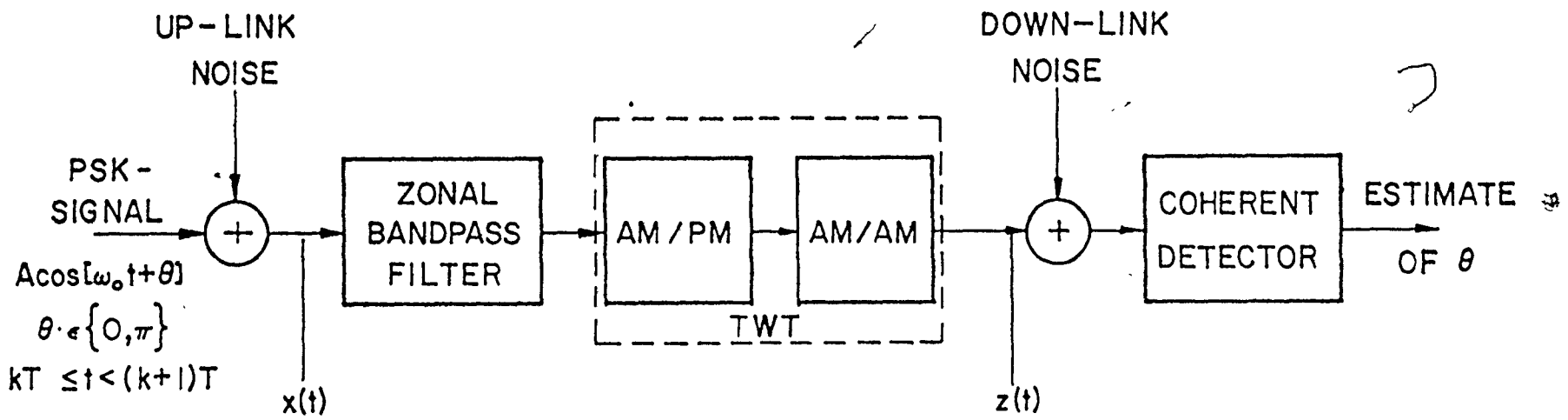

Fig. 4-28. Model for binary CPSK transmission through a satellite type channel

The effective signal component, $s'(t)$, at the output of the nonlinear device is defined as the conditional average of (4.48) over all R and ε. Hence

$$s'(t) = A' \cos(\omega_0 t + \theta_i - \beta) \tag{4.49}$$

where A' and β are the effective signal amplitude and phase shift defined by

$$A' = \sqrt{\{E_{R,\varepsilon}[Z_p(R) \cos \varepsilon]\}^2 + \{E_{R,\varepsilon}[Z_q(R) \cos \varepsilon]\}^2}$$

and

$$\beta = - \tan^{-1} \left[\frac{E_{R,\varepsilon}\{Z_q(R) \cos \varepsilon\}}{E_{R,\varepsilon}\{Z_p(R) \cos \varepsilon\}} \right] \tag{4.50}$$

where $E_{R,\varepsilon}[\cdot]$ denotes the expectation over R and ε.

The following equality is used in deriving the expressions for A' and β.

$$E_{R,\varepsilon}[Z_p(R) \sin \varepsilon] = E_{R,\varepsilon}[Z_q(R) \sin \varepsilon] = 0 \tag{4.51}$$

Based on the specific quadrature model of TWT as described in equations (2.18-2.19), the values of A' and β as defined in equation (4.50) can actually be evaluated in closed form as shown in Appendix D.1.

The effective noise at the output of the TWT is then obtained by subtracting (4.49) from (4.48) and is given by

$$n'(t) = n_1'(t)\cos(\omega_0 t + \theta_i - \beta) - n_2'(t)\sin(\omega_0 t + \theta_i - \beta)$$

where

$$n_1'(t) = Z_p(R)\cos(\varepsilon + \beta) - Z_q(R)\sin(\varepsilon + \beta) - A' \qquad (4.52)$$

$$n_2'(t) = Z_p(R)\sin(\varepsilon + \beta) - Z_q(R)\cos(\varepsilon + \beta) \qquad (4.53)$$

Due to the complexity of $Z_p(\cdot)$ and $Z_q(\cdot)$ it is very difficult to find the probability density function, $p_{n_1'}(x)$, in closed form. However n_1' as defined in (4.52) is a bounded random variable and $Z_p(R)$, $Z_q(R)$ are smoothly continuous nonlinearities. Consequently the probability density function of n_1' must be of bounded variation and can be expressed in terms of a Gram-Charlier series expansion as [28]

$$p_{n_1'}(x) = \frac{1}{\sqrt{2\pi N_u'}} e^{-\frac{x^2}{2N_u'}} \sum_{k=0}^{\infty} \frac{h_k}{k!} H_k\left[x/\sqrt{N_u'}\right] \qquad (4.54)$$

where N_u' is the variance of n_1' and $H_k(x)$ is the Hermite polynomial of degree k satisfying

$$H_{k+1}(x) = x\,H_k(x) - k\,H_{k-1}(x) \qquad (4.55)$$

with

$$H_0(x) = 1$$

$$H_1(x) = x$$

The Hermite polynomials up to the twelfth degree are as shown in Table 4-1.

Table 4-1: HERMITE POLYNOMIALS

$H_0(x)$	1
$H_1(x)$	x
$H_2(x)$	$x^2 - 1$
$H_3(x)$	$x^3 - 3x$
$H_4(x)$	$x^4 - 6x^2 + 3$
$H_5(x)$	$x^5 - 10x^3 + 15x$
$H_6(x)$	$x^6 - 15x^4 + 45x^2 - 15$
$H_7(x)$	$x^7 - 21x^5 + 105x^3 - 105x$
$H_8(x)$	$x^8 - 28x^6 + 210x^4 - 420x^2 + 105$
$H_9(x)$	$x^9 - 36x^7 + 378x^5 - 1260x^3 + 945x$
$H_{10}(x)$	$x^{10} - 45x^8 + 630x^6 - 3150x^4 + 4725x^2 - 945$
$H_{11}(x)$	$x^{11} - 55x^9 + 990x^7 - 6930x^5 + 17325x^3 - 10395x$
$H_{12}(x)$	$x^{12} - 66x^{10} + 1485x^8 - 13860x^6 + 51975x^4 - 62370x^2 + 10395$

The coefficient h_k in equation (4.54) is calculated as the integral

$$h_k = \int_{\Omega} H_k[x/\sqrt{N_u'}]\, p_{n_1'}(x)\, dx \tag{4.56}$$

where Ω is the range of x and corresponds to $0 \leq R < \infty$ and $-\pi \leq \varepsilon \leq \pi$. Substituting (4.55) in (4.56) we obtain a recursive form for h_k as

$$h_k = \int_{\Omega} \frac{x}{\sqrt{N_u'}}\, H_{k-1}[x/\sqrt{N_u'}]\, p_{n_1'}(x)\, dx - (k-1) \int_{\Omega} H_{k-2}[x/\sqrt{N_u'}]\, p_{n_1'}(x)\, dx \tag{4.57}$$

from which it is readily seen that the evaluation of each successive h_k requires only the evaluation of the kth moment of the random variable n_1' as given in (4.52) since all other terms have been previously calculated. It should be noted that the first three coefficients may be evaluated by inspection as

$$h_0 = 1$$

$$h_1 = 0$$

$$h_2 = 0$$

For the remaining coefficients h_k, $k \geq 3$, numerical integration techniques (for details, see Appendix D.2) are used to evaluate the required moments of n_1' and hence the coefficients h_k. An identical procedure is followed to obtain the statistics of the quadrature noise component n_2'.

The results obtained from the evaluation of the variances of n_1' and n_2' indicate that at large values of the input carrier to noise power ratio $(CNR)_I$, defined as

$$(CNR)_I = \frac{A^2}{2N_u}$$

the equivalent in-phase noise is suppressed by the limiting action of the TWT, and hence there is an increase in the in-phase CNR at the TWT output. This is shown in Fig. 4-29 which depicts the equivalent in-phase and quadrature noise variances as a function of the input carrier to noise power ratio $(CNR)_I$. Also shown in Fig. 4-29 is a plot of the ratio of the in-phase TWT output CNR to the input CNR where the output CNR is given by

$$(CNR)_O = \frac{(A')^2}{2N_u'}$$

This curve is comparable to results obtained by Lesh [52] for the case of an error function type of limiter. This improvement in in-phase CNR at the TWT output suggests that somewhat improved error-rate performance, compared to the linear channel, may be obtained for signals which contained no quadrature energy, as in the case of binary CPSK signals.

In principle, the performance of any M-ary CPSK system can be evaluated, similarly to that in section 4.2.1, once the probability density function of n_1' and the joint probability density function of n_1' and n_2'

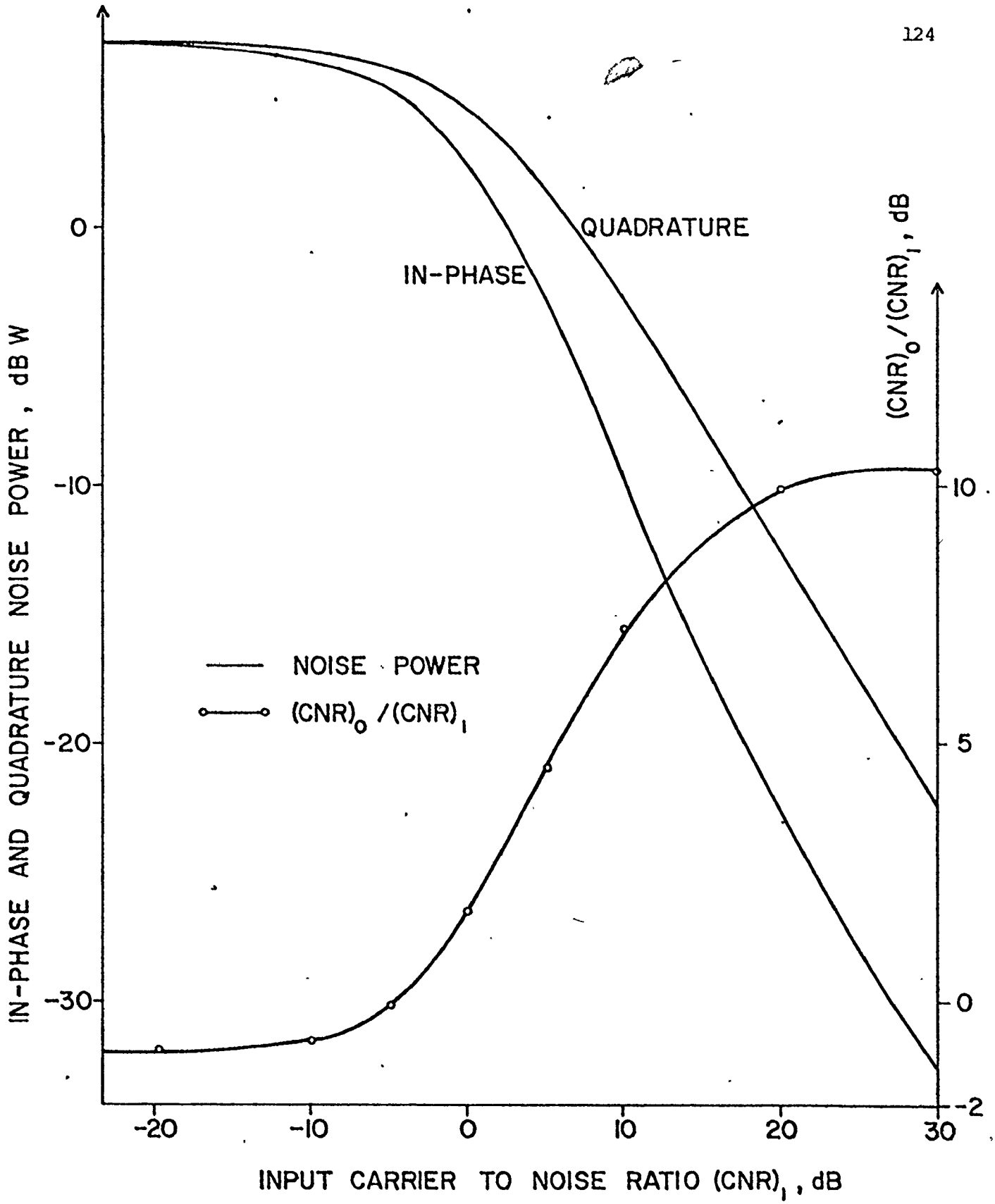

Fig. 4-29. Variance of equivalent in-phase and quadrature noise and ratio of output to input CNR (2.5 dB input power backoff).

are known, albeit in an infinite series expansion form as in (4.54). However, the computation becomes rather complicated, for the case of M greater than two, unless some form of bounding technique is used [85]. In the subsequent analysis we shall consider only the performance of a binary CPSK system transmitted through the actual TWT channel. Following the method described in section 4.2.1, the probability density function of the total interference, n_T, is then obtained by convolving the equivalent in-phase noise density function in (4.54) with the Gaussian density function of the down-link noise ξ_1 (having variance N_d watts) to get

$$p_{n_T}(x) = \frac{1}{\sqrt{2\pi N_d}} \int_{-\infty}^{\infty} p_{n_1'}(x-z) \exp[-z^2/2N_d]\, dz \qquad (4.58)$$

Substitution of (4.54) into (4.58) yields after some manipulation [38, pp. 837]

$$p_{n_T}(x) = \frac{\exp[-x^2/2N_T]}{\sqrt{2\pi N_T}} + \sum_{n=3}^{\infty} \frac{h_n [N_u'/N_T]^{\frac{n}{2}}}{n!\sqrt{2\pi N_T}} \exp[-x^2/2N_T]\, H_n[x/\sqrt{N_T}] \qquad (4.59)$$

where $N_T = N_u' + N_d$ is the total noise variance and $h_1 = h_2 = 0$ from equation (4.57).

The first term in equation (4.59) is the Gaussian term which would be obtained in the case of a linear channel and the remaining terms represent correction factors which account for the nonlinear effects of the channel.

The probability of one sample being in error, p, is then given by

$$p = \int_{-\infty}^{-A'} p_{n_T}(x)\, dx \tag{4.60}$$

Substitution of (4.59) into (4.60) yields after some manipulation [38, pp. 837]

$$p = \frac{1}{2}\operatorname{erfc}(\sqrt{\rho}) + \frac{e^{-\rho}}{\sqrt{2\pi}} \sum_{n=3}^{\infty} \frac{(-1)^n}{n!}\, h_n[N_u' / N_T]^{\frac{n}{2}}\, H_{n-1}[\sqrt{2\rho}] \tag{4.61}$$

where ρ is the effective received carrier to noise power ratio, defined as

$$\rho = \frac{(A')^2}{2N_T}$$

The absolute convergence property of the series in (4.61) is discussed in some detail in Appendix E. Suffice it to say at this point that the error which arises as a result of truncating the series expansion of equation (4.61) at the (L-1)st term can be made as small as desired, provided that L is sufficiently large and satisfies

$$L > 2 + \frac{1}{2}\left[\frac{2\sqrt{\rho}}{\ln[N_T / N_u']} - \frac{\ln[N_T / N_u']}{2\sqrt{\rho}}\right]^2 \tag{4.62}$$

A computer program has been written to compute the bit error rate of a coherent binary CPSK system from equations (4.38) and (4.61) for the case of $WT = 3$ and for different values of up-link and down-link carrier to noise power ratios, $(CNR)_u$, $(CNR)_d$ defined as

$$(CNR)_u = \frac{A^2}{2N_u}$$

$$(CNR)_d = \frac{(A')^2}{2N_d}$$

In this program the contributions in the nonlinear correction term in equation (4.61) up to and including the eighth moment are included in the computation. This was found experimentally to yield quite precise results in the range of up-link CNR considered. For example the percentage contribution of the eighth term in equation (4.61) to the bit error rate in (4.38) was found to be less than 2% for all up-link CNR below 5 dB. This contribution is still within 1% for the case of 10 dB up-link CNR provided that the down-link CNR is kept small (less than or equal to 10 dB). However, at higher values of up-link and down-link CNR's, more terms are needed due to the increasingly non-Gaussian nature of n_1'. Typical numerical values of the noise moments are listed in Table 4-2 for different values of up-link CNR.

In Fig. 4-30, the computed bit error rates are plotted and compared with the corresponding results for the linear channel using a single sample detection and majority logic receiver. The bit error rate

Table 4-2: NUMERICAL CALCULATION OF MOMENTS OF IN-PHASE NOISE

A', β mth MOMENT $(\text{VOLTS})^m$	UP-LINK CARRIER TO NOISE RATIO $(\text{CNR})_{U'}$ (dB)				
	-10	-5	0	5	10
A' (volt)	$8.7105\text{x}10^{-1}$	1.50309	2.29829	2.89994	3.18779
β (radian)	-.43658	-.40186	-.36057	-.33576	-.33155
m = 1	$3.32421\text{x}10^{-4}$	$1.49927\text{x}10^{-5}$	$-4.44881\text{x}10^{-7}$	$5.67843\text{x}10^{-8}$	$8.73919\text{x}10^{-6}$
m = 2	4.58953	3.62611	1.76501	$4.71406\text{x}10^{-1}$	$9.64520\text{x}10^{-2}$
m = 3	-5.91645	-7.30001	-3.99085	$-6.99811\text{x}10^{-1}$	$-6.10510\text{x}10^{-2}$
m = 4	4.16007x10	3.93109x10	1.75641x10	1.98796	$8.41965\text{x}10^{-2}$
m = 5	$-1.09157\text{x}10^{2}$	$-1.46993\text{x}10^{2}$	-7.19095x10	-5.93829	$-1.24416\text{x}10^{-1}$
m = 6	$5.10399\text{x}10^{2}$	$6.63206\text{x}10^{2}$	$3.24335\text{x}10^{2}$	2.01804x10	$2.20425\text{x}10^{-1}$
m = 7	$-1.73932\text{x}10^{3}$	$-2.86816\text{x}10^{3}$	$-1.51070\text{x}10^{3}$	-7.43842x10	$-4.40788\text{x}10^{-1}$
m = 8	$7.24872\text{x}10^{3}$	$1.29189\text{x}10^{4}$	$7.27251\text{x}10^{3}$	$2.93126\text{x}10^{2}$	$9.77318\text{x}10^{-1}$

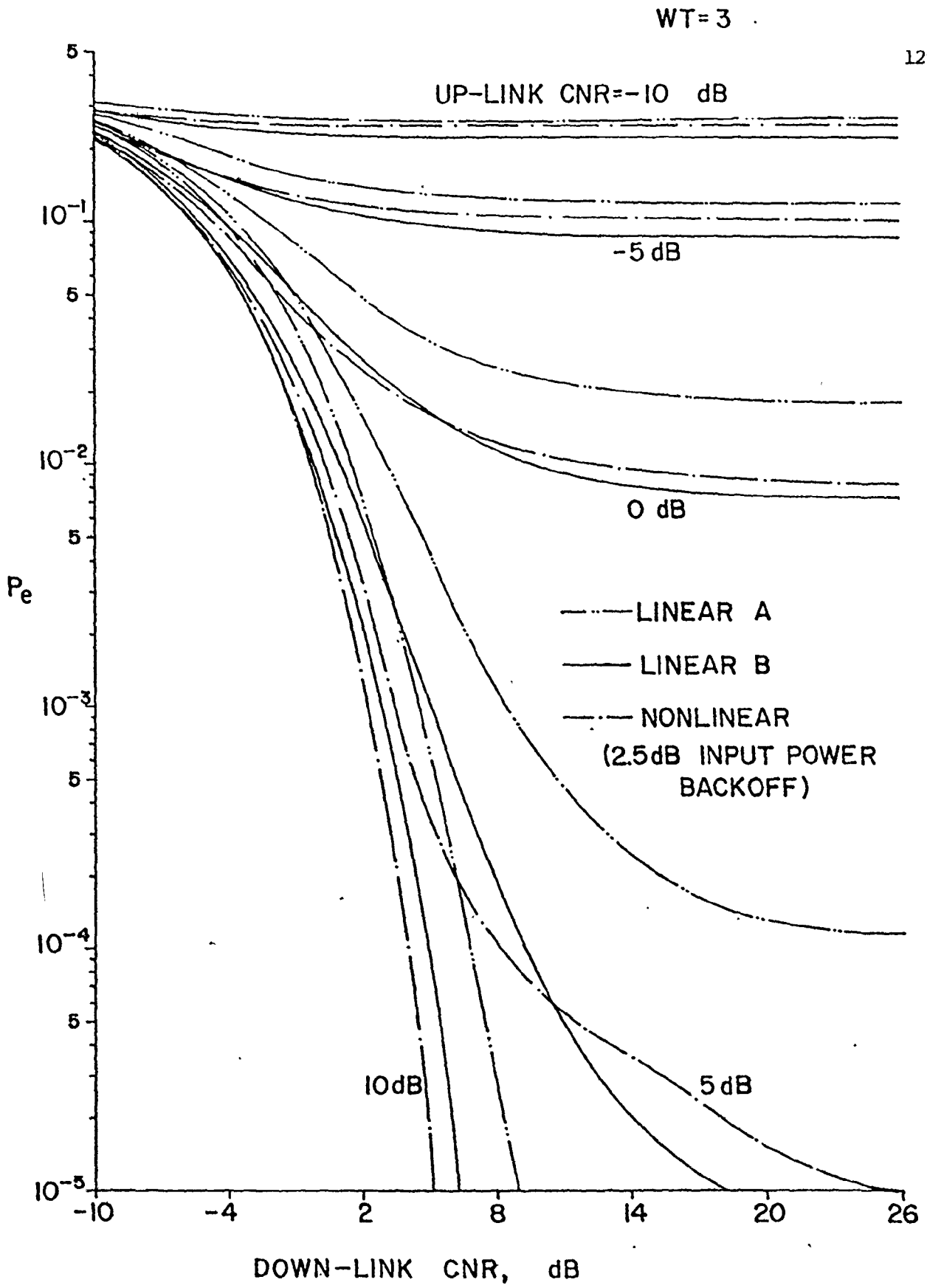

Fig. 4-30. Bit error rate for a binary CPSK system as a function of received CNR (A; majority logic receiver, B; matched filter receiver).

for this case is given in (4.38) with

$$p = \frac{1}{2}\,\mathrm{erfc}\left[\sqrt{\frac{\gamma_u\gamma_d}{\gamma_u+\gamma_d}}\right] \tag{4.63}$$

where erfc(x) denotes the complementary error function as defined earlier, and

$$\gamma_u = \frac{A^2}{2N_u} \quad \text{is the up-link CNR}$$

$$\gamma_d = \frac{A^2}{2N_d} \quad \text{is the down-link CNR.}$$

Also shown in Fig. 4.30 are plots of the bit error rate for the case of a linear channel using a matched filter receiver. The bit error rate for this case is given by

$$P_e = \frac{1}{2}\,\mathrm{erfc}(\sqrt{\gamma_T}) \tag{4.64}$$

where

$$\gamma_T = \frac{\gamma_u\gamma_d}{\gamma_u+\gamma_d}\,\frac{WT}{}$$

The plots in Fig. 4-30 exhibit an irreducible error rate for large down-link carrier to noise power ratio due to the presence of the up-link noise component. It is clear from the plots that in the case of a majority logic receiver, the performance over a nonlinear channel is superior to that over the linear channel. This same conclusion was reached by Jain [49] and Lyons [59] for the case of a hard-limited channel.

CHAPTER 5

RECEIVER STRUCTURES FOR NONLINEAR WIDEBAND BINARY CPSK CHANNELS

The discussion of the effect of thermal noise disturbances on the performance of binary CPSK systems in section 4.2 has been confined to the case of single sample detection followed by a majority logic decision. In this chapter we shall extend this analysis to cover two other receiver structures, namely, the correlation receiver and the maximum likelihood (ML) receiver. The analysis of the correlation receiver is of interest because it is the optimal receiver for the linear channel. This receiver structure has been analyzed in the context of a bandpass nonlinear channel by Davisson et al [29], Jain [48] and Jones et al [50]. However, the method of analysis yields results only for the case of pure amplitude limiting and is not readily extendible to the case of a bandpass nonlinearity exhibiting AM/PM conversion. Our method of analysis will be somewhat similar to that of Jain [48] with the notion of equivalent signal and noise at the output of the nonlinearity as discussed in Chapter 4.

In section 5.2 we discuss the maximum likelihood receiver for the nonlinear channel. This receiver structure

yields an estimate of the transmitted phase that most likely caused a given received signal at the receiver over one symbol duration. It is well known that for the case of equally likely transmitted symbols and a binary CPSK system, as of interest here, the maximum likelihood criterion, as used in section 5.2, yields the receiver with minimum average risk per decision. Furthermore, for the case of linear channel with only additive Gaussian noise disturbances the maximum likelihood receiver can be shown to be equivalent to the correlation receiver which is optimum in a decision theoretic sense. However, it is usually difficult to calculate the performance of this maximum likelihood receiver and we resort to approximation techniques in order to assess its performance.

5.1. CORRELATION RECEIVER

A block diagram representing a conventional correlation receiver for a binary CPSK system is shown in Fig. 5-1.a. The receiver cross-correlates the received signal with the reference carrier. The output of the cross-correlator, assuming that all the harmonics higher than the first are suppressed, is then passed through an integrator. The output of the integrator is then sampled at the end of each symbol duration and fed into a threshold detector which yields the detected phase $\hat{\theta}_i$.

To simplify the analysis, we approximate the integration operation by sampling and weighted summation as shown in Fig. 5-1.b. The choice of scaling factor, $\frac{1}{\sqrt{WT}}$,

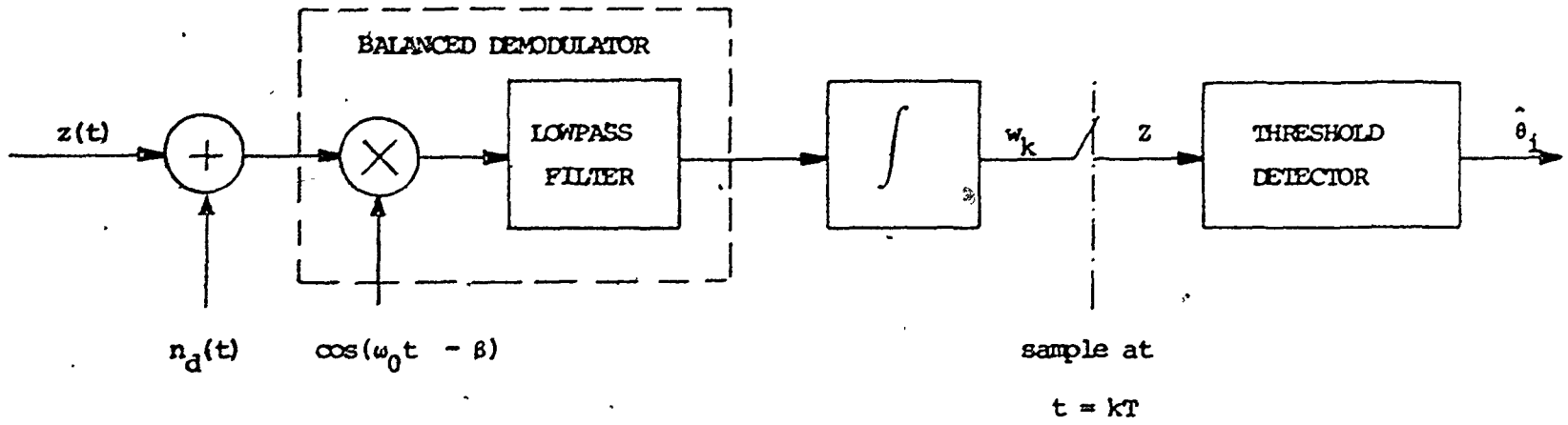

Fig. 5-1 a. Actual correlation receiver, $(k-1)T \leq t \leq kT$

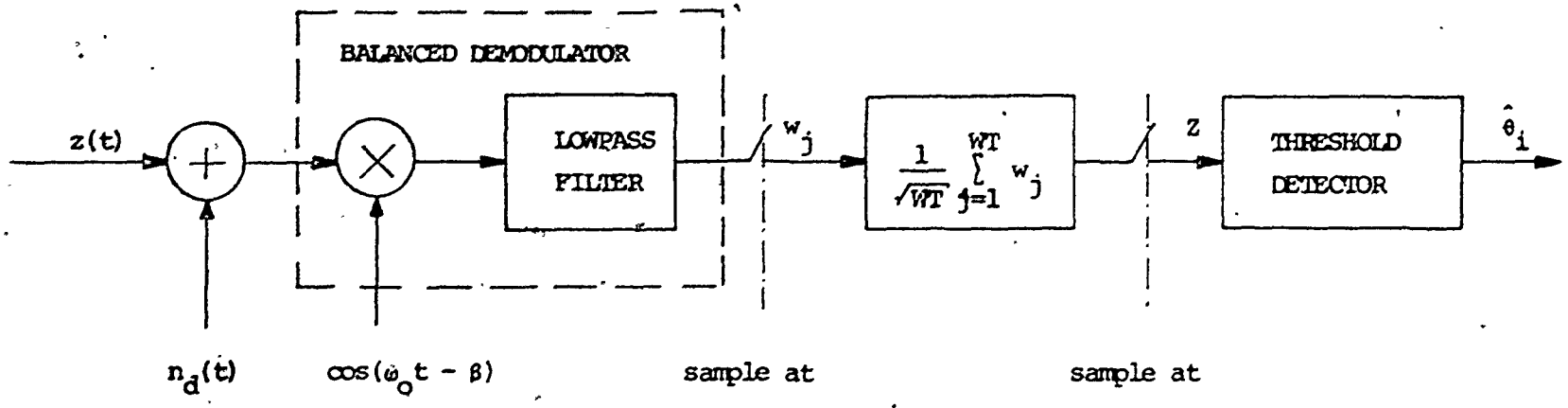

Fig. 5-1 b. Approximate correlation receiver, $(k-1)T \leq t \leq kT$

is optional and is used here only for notational conveniences in the subsequent analysis. In Fig. 5-1.b, the output of the cross correlator, after the lowpass filter, is sampled every $\Delta T = \frac{1}{W}$ seconds over the whole bit duration. All WT samples are then fed to the threshold detector. The transmitted phase, θ, can take values of 0 or π, each with equal probability, and the probability of making an incorrect decision does not depend on whether 0 or π is being transmitted within any particular bit duration. Hence we shall assume throughout our discussion in this section that $\theta = 0$ is being transmitted. The output signal, Z, to the threshold detector then becomes

$$Z = \frac{1}{\sqrt{WT}} \sum_{j=1}^{WT} w(j\Delta T) \tag{5.1}$$

$$= \sqrt{WT}\, A' + \frac{1}{\sqrt{WT}} \sum_{j=1}^{WT} [n_1'(j\Delta T) + \xi_1(j\Delta T)] \tag{5.2}$$

where A' and n_1' are the effective signal amplitude and the equivalent in-phase noise component at the output of the bandpass nonlinearity. The term ξ_1 represents the additive down-link Gaussian noise component as defined in section 4.2.

We now define

$$N_1 = \frac{1}{\sqrt{WT}} \sum_{j=1}^{WT} n_1'(j\Delta T) \tag{5.3}$$

$$N_2 = \frac{1}{\sqrt{WT}} \sum_{j=1}^{WT} \xi_1(j\Delta T) \tag{5.4}$$

It is clear that N_2 is still a zero-mean Gaussian random variable of variance N_d watts. The characteristic function, $C_{N_2}(v)$ of N_2 can be written as

$$C_{N_2}(v) = \exp\left[-\frac{N_d v^2}{2}\right] \tag{5.5}$$

Since the bandpass nonlinearity of interest is assumed to be memoryless and each input sample is statistically independent of all other samples, it then follows that the output samples n_1' must also be statistically independent. If $C(v)$ and $C_{N_1}(v)$ represent the characteristic functions of the samples $\frac{n_1'}{\sqrt{WT}}$ and N_1 respectively, then based on the statistical independence of n_1' and equation (5.3) we can write

$$C_{N_1}(v) = [C(v)]^{WT} \tag{5.6}$$

From the Fourier transform relationship between the characteristic function and the corresponding probability density function [27], we can expand the characteristic function $C(v)$ in terms of the central moments of n_1' as

$$C(v) = \sum_{p=o}^{\infty} \frac{m_p}{p!}\left[\frac{iv}{\sqrt{WT}}\right]^p \tag{5.7}$$

where $m_p = E[(n_1')^p]$

and $E[n_1'] = 0$

Taking the logarithm in equation (5.6)

$$\ell n\,[C_{N_1}(v)] = WT\,\ell n\,[C(v)] = WT\,\ell n\left[1 + \sum_{p=1}^{\infty} \frac{m_p}{p!}\left[\frac{iv}{\sqrt{WT}}\right]^p\right] \qquad (5.8)$$

Expanding $\ell n\,(1 + x)$ into a power series in x as [1,pp. 68]

$$\ell n\,(1 + x) = \sum_{i=1}^{\infty} (-1)^{i-1}\frac{x^i}{i}, \quad -1 \le x \le 1 \qquad (5.9)$$

equation (5.8) becomes

$$\ell n\,[C_{N_1}(v)] = WT \sum_{r=1}^{\infty} \frac{\mu_r}{r!}\left[\frac{iv}{\sqrt{WT}}\right]^r \qquad (5.10)$$

where μ_r is the rth cumulant of n_1' and is related to the moment m_r by the following recursive relationship [14]

$$\mu_{r+1} = m_{r+1} - \sum_{i=1}^{r} \frac{r!}{i!(r-i)!}\,\mu_{r+i-1}\,m_i \qquad (5.11)$$

Exponentiating (5.10) and expanding the exponential term as an infinite series we obtain

$$C_{N_1}(v) = \exp\left[i\sqrt{WT}\,\mu_1 - \mu_2 v^2/2\right].\left\{\sum_{m=0}^{\infty} \frac{(WT)^m}{m!}\left[\sum_{r=3}^{\infty} \frac{\mu_r}{r!}\left[\frac{iv}{\sqrt{WT}}\right]^r\right]^m\right\} \qquad (5.12)$$

The exponential factor is the contribution of a Gaussian random variable with mean μ_1 and variance μ_2. By expanding equation (5.12) and collecting terms of the same power of WT, we obtain

$$C_{N_1}(v) = \exp\left[i\sqrt{WT}\,\mu_1 - \mu_2 v^2/2\right].\left\{1 - \frac{i}{\sqrt{WT}}\frac{\mu_3}{6}v^3\right.$$

$$+ \frac{1}{WT}\left[\frac{\mu_4}{24}v^4 - \frac{\mu_3^2}{72}v^6\right]$$

$$+ \frac{i}{(\sqrt{WT})^3}\left[\frac{\mu_5}{120}v^5 - \frac{\mu_3\mu_4}{144}v^7 + \frac{\mu_3^3}{1296}v^9\right]$$

$$+ \frac{1}{(WT)^2}\left[-\frac{\mu_6}{720}v^6 + \frac{\mu_4^2}{1152}v^8 + \frac{\mu_3\mu_5}{720}v^8 - \frac{\mu_3^2\mu_4}{1728}v^{10} + \right.$$

$$\left.\left.\frac{\mu_3^4}{31104}v^{12}\right] + \cdots\cdots\right\} \qquad (5.13)$$

The probability of error can now be calculated from equations (5.2, 5.6) and (5.13) as follows

$$P_e = \Pr[Z<0]$$

$$= \Pr[N_1+N_2 < -\sqrt{WT}\,A']$$

$$= \frac{1}{2} - \frac{1}{\pi}\int_0^\infty \mathrm{Im}\left[C_{N_1}(v)C_{N_2}(v)e^{iA'\sqrt{WT}}\right]\frac{dv}{v} \qquad (5.14)$$

where Im(.) denotes that the imaginary part must be taken.

Equation (5.14) follows from the statistical independence between N_1 and N_2 and from the Fourier inversion relationship between the cumulative distribution function and the characteristic function of a random variable [27].

Substitution of equations (5.6) and (5.13) into (5.14) yields an explicit expression for P_e with the use of the following integration formulae [61]

$$\int_0^\infty v^{2p} \cos\left[\sqrt{WT}\, A'v\right] \exp\left[-\gamma^2 v^2/2\right] dv = (-1)^{WT} \sqrt{\frac{\pi}{2}}\, \frac{e^{-\rho}}{\gamma^{2p+1}} \cdot H_{2p}(\sqrt{2\rho}) \qquad (5.15)$$

$$\int_0^\infty v^{2p+1} \sin\left[\sqrt{WT}\, A'v\right] \exp\left[-\gamma^2 v^2/2\right] dv = (-1)^{WT} \sqrt{\frac{\pi}{2}}\, \frac{e^{-\rho}}{\gamma^{2p+2}} \cdot H_{2p+1}(\sqrt{2\rho}) \qquad (5.16)$$

where $H_p(.)$ is the Hermite polynomial as defined in Chapter 4 and $\rho = (A')^2 WT/2\gamma^2$.

After some manipulations the bit error rate can be expressed as follows

$$P_e = \frac{1}{2}\,\mathrm{erfc}[\sqrt{\rho}\,] - \frac{\exp[-\rho]}{\sqrt{WT}\,\gamma^3\sqrt{2\pi}}\left[\frac{\mu_3}{6} H_2(\sqrt{2\rho})\right]$$

$$+ \frac{\exp[-\rho]}{WT\,\gamma^4\sqrt{2\pi}}\left[\frac{\mu_4}{24} H_3(\sqrt{2\rho}) + \frac{\mu_3^2}{72\gamma^2} H_5(\sqrt{2\rho})\right]$$

$$- \frac{\exp[-\rho]}{(\sqrt{WT})^3\gamma^5\sqrt{2\pi}}\left[\frac{\mu_5}{120} H_4(\sqrt{2\rho}) + \frac{\mu_3\mu_4}{144\gamma^2} H_6(\sqrt{2\rho}) + \frac{\mu_3^3}{1296\gamma^4} H_8(\sqrt{2\rho})\right]$$

$$+ \frac{\exp[-\rho]}{(WT)^2\gamma^6\sqrt{2\pi}}\left[\frac{\mu_6}{720} H_5(\sqrt{2\rho}) + \left\{\frac{\mu_4^2}{1152\gamma^2} + \frac{\mu_3\mu_5}{720\gamma^2}\right\}\right.$$

$$\cdot H_7(\sqrt{2\rho})$$

$$+ \frac{\mu_3^2\mu_4}{1728\gamma^4} H_9(\sqrt{2\rho}) + \frac{\mu_3^4}{31104\gamma^6} H_{11}(\sqrt{2\rho}) \Bigg] - \ldots\ldots\ldots \quad (5.17)$$

where

$\gamma^2 = \mu_2 + N_d$ denotes the total received noise power and $\rho = \frac{WT(A')^2}{\gamma^2}$ is the total received bit energy to total noise power spectral density ratio.

The first term in equation (5.17) is similar to the bit error rate expression for a linear additive Gaussian noise channel. The other terms represent correction terms due to the channel nonlinearity. Equation (5.17) and the knowledge of the moments of n_1' are sufficient to calculate the bit error performance of any nonlinear channel with a correlation receiver. Of computational significance is the presence of the WT factors in the denominator. For large values of WT, our approximate correlation receiver approaches the conventional correlation receiver and the computational effort required in the computation of P_e as shown in equation (5.17) is greatly reduced. Equation (5.17) resembles equation (4.63), so the absolute convergence property can be readily established as in Appendix E. For WT = 1 the correlation receiver is nothing but a single sample detection as discussed in Chapter 4, and equation (5.17) reduces to exactly the same expression as equation (4.63).

The probability of error for the case of a hard-

limited repeater was computed from equation (5.17) for different values of up-link, $(CNR)_u = A^2/2N_u$, and down-link carrier to noise power ratio, $(CNR)_d = (A')^2/2N_d$, as defined in section 4.2, and results of the computation are depicted in Fig. 5-2 for the case of WT = 100. In the case of the hard-limiter, different moments of n_1' can be directly evaluated in closed form as follows

$$E[(n_1')^k] = E[(\cos\varepsilon - A')^k]$$

$$= \sum_{j=1}^{k} \frac{k!(-A')^{k-j}}{j!(k-j)!} E[\widehat{\cos}^j\varepsilon] \qquad (5.18)$$

But

$$\cos^j \varepsilon = \begin{cases} \sum_{i=o}^{\frac{1}{2}(j-2)} \frac{j!}{(j-i)!\, i\, !2^{j-1}} \cos[(j-2i)\varepsilon] + \frac{j!}{2^j[(j/2)!]^2} & j \text{ even} \\ \sum_{i=o}^{\frac{1}{2}(j-1)} \frac{j!}{(j-i)!\, i\, !2^{j-1}} \cos[(j-2i)\varepsilon] & j \text{ odd} \end{cases} \qquad (5.19)$$

and [16]

$$E[\cos j\varepsilon] = \left(\frac{j}{2}\right) ! \; \frac{\rho_1^j}{j!} \; {}_1F_1[j/2;\, j+1;\, -\rho_1^2] \qquad (5.20)$$

where $\rho_1^2 = \frac{A^2}{2N_u}$ the up-link carrier to noise power ratio

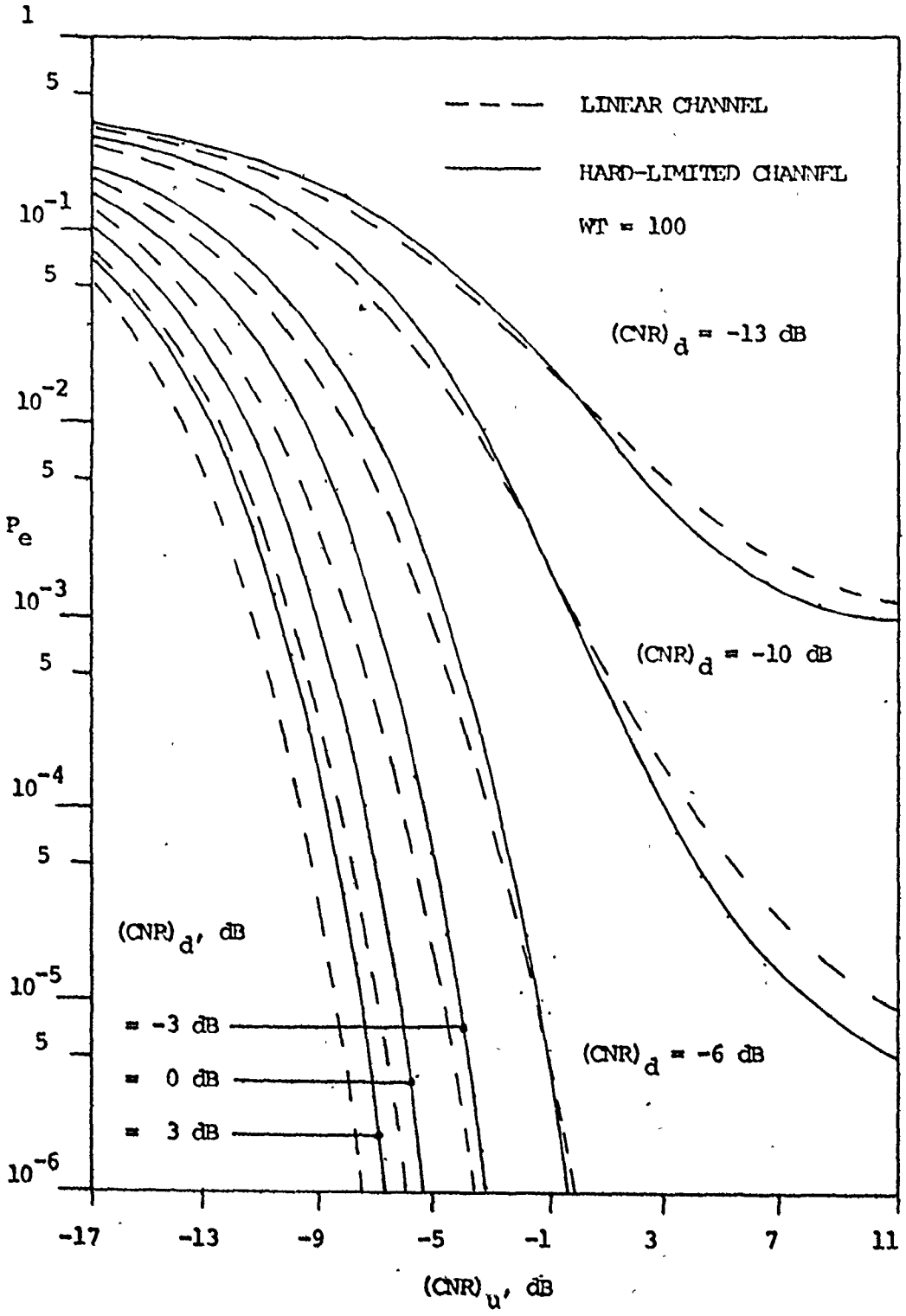

Fig. 5-2. Probability of error vs up-link CNR, 2-phase CPSK where $[E_b/N_0]_d = (CNR)_d + 10 \log_{10} WT$, and $[E_b/N_0]_u = (CNR)_u + 10 \log_{10} WT$.

and ${}_1F_1(a;b; -x)$ is the confluent hypergeometric function [3].

It is evident from Fig. 5-2 that the error rate for a hard-limited channel is higher than for the linear channel at low values of $(CNR)_u$ but that it gets smaller as $(CNR)_u$ increases. If up-link carrier to noise power ratio becomes very large the error rate of a hard-limited channel and that of a linear channel will approach the same value which is dictated by the down-link carrier to noise ratio, $(CNR)_d$. The improvement in the error rate for large $(CNR)_u$ is mainly due to the improvement in the output CNR compared to that at the output of the linear channel (see Fig. 4-29). Furthermore, in this region of high $(CNR)_u$, the major contribution to the error rate is provided by the leading Gaussian term in equation (5.17). The successive higher order terms tend to increase the error rate, but their contribution is so small that P_e still remains lower than that of the linear channel.

5.2. MAXIMUM LIKELIHOOD RECEIVER

In the case of wideband binary CPSK signal transmission through a linear additive white Gaussian noise channel, it is well-known that the combination of a cross-correlator followed by an integrate and dump circuit and a threshold detector as described in Fig. 5-1.a., provides optimal performance. In fact, it is the maximum likelihood receiver

for the linear channel. However, this is not so for the case of a bandpass nonlinear channel with Gaussian noise being added to the signal both before and after the nonlinearity . This particular nonlinear channel may be regarded (as shown in section 4.2) as a linear channel with additive non-Gaussian disturbances. For this type of channel, the maximum likelihood receiver must be redefined, and should offer an improvement in system performance. Such a receiver is well-known to yield the minimum probability of error when the transmitted information digits are equally likely.

Following the same analysis as detailed in section 4.2, the output of the balanced demodulator, as shown in Fig. 5-1.b may be expressed as

$$w(t) = \alpha A' + \alpha n'(t) + \xi(t) \quad , \quad (k-1)T \leq t \leq kT \tag{5.21}$$

where $\alpha = \pm 1$ depending on whether $\theta = 0$ or π is transmitted and $n'(t)$ represents the equivalent in-phase noise at the output of the nonlinear device as defined by equation (4.54).

$\xi(t)$ is the in-phase component of the Gaussian, down-link noise which is zero mean with variance N_d watts.

If we consider WT samples of w(t) within one bit duration, we can rewrite equation (5.21) at sampling instant $t = k\,\Delta T$ as

$$w_k \triangleq w(k\Delta T) = \alpha A' + \alpha n'_k + \xi_k \tag{5.22}$$

where $\Delta T = \frac{1}{W}$

We shall assume in the subsequent analysis that the probability density function of n_k' and ξ_k are known either in closed form as in section 4.2.1 or in a series expansion form as in section 4.2.2.

Define the new random variables

$$z_k^+ = n_k' + \xi_k \tag{5.23}$$

and

$$z_k^- = -n_k' + \xi_k \tag{5.24}$$

with the following probability density functions

$$p_{z_k^+}(z) = p_{n_k'}(z) * p_{\xi_k}(z) \tag{5.25}$$

and

$$p_{z_k^-}(z) = p_{n_k'}(-z) * p_{\xi_k}(z) \tag{5.26}$$

where * denotes the convolutional integral.

The following conditional probability density function of w_k, conditioned on α, can be obtained from the equations (5.22), (5.25 - 5.26) as

$$p(w_k|\alpha=1) = p_{z_k^+}(w_k - A') \tag{5.27}$$

and

$$p(w_k|\alpha=-1) = p_{z_k^-}(w_k + A') \tag{5.28}$$

Based on the statistical independence of all WT samples of w_k, within one bit duration, the conditional likelihood ratio expression can then be written as

$$L[w_k : k=1,.....,WT] = \prod_{k=1}^{WT} \frac{p_{z_k^+}[w_k - A']}{p_{z_k^-}[w_k + A']} \tag{5.29}$$

Taking the logarithm in equation (5.29)

$$\ell[w_k : k=1,...,WT] \triangleq \ell n\{L[w_k : k=1,....,WT]\}$$

$$= \sum_{k=1}^{WT} \Lambda(w_k) \tag{5.30}$$

where $$\Lambda(w_k) = \ell n \left[\frac{p_{z_k^+}(w_k - A')}{p_{z_k^-}(w_k + A')}\right] \tag{5.31}$$

The nonlinear function $\Lambda(w_k)$ depends on the statistics of n' and ξ as shown in equations (5.25 - 5.26) and (5.31). The decision statistics $\ell[w_k : k=1,...,WT]$ must now be fed into the threshold logic and the decision on the transmitted α is based on

$$\text{Accept} \begin{cases} \alpha = 1(\theta=0) \text{ if } \ell[w_k : k=1,...WT] > 0 \\ \alpha = -1(\theta=\pi) \text{ if } \ell[w_k : k=1,....WT] < 0 \end{cases} \tag{5.32}$$

For the case of a purely amplitude limiting channel as discussed in section 4.2, it can be shown that

$$p_{z_k^+}(w_k - A') = \frac{1}{\sqrt{2\pi N_d}} \int_{-1}^{1} \exp\left[-\frac{(w_k - u)^2}{2N_d}\right] p_{n_k'}(u - A')\, du \tag{5.33}$$

and

$$p_{z_k^-}(w_k + A') = \frac{1}{\sqrt{2\pi N_d}} \int_{-1}^{1} \exp\left[-\frac{(w_k + u)^2}{2N_d}\right] p_{n_k'}(u - A')\, du \tag{5.34}$$

where N_d = down-link noise power.

A' = equivalent in-phase signal amplitude and $p_{n_k'}(.)$ is the probability density function of the equivalent in-phase noise component at the output of the limiter.

From equations (4.25), (4.28) and (5.33 - 5.34) we can determine $\Lambda(w_k)$, the desired nonlinear device that is needed at the receiver. Figures 5-3 to 5-10 describe the characteristics of $\Lambda(w_k)$ for different values of normalized limiter softness factor, $\lambda^* = \lambda/A$, and for various values of up-link and down-link bit energy to noise power spectral density ratio. It is evident in Figures 5-3 to 5-6 that $\Lambda(w_k)$ is a bounded nonlinear function of w_k which becomes more and more linear as λ^* or up-link bit energy to noise spectral density ratio, $[E_b/N_o]_u$, increases. Heuristically, the increase in $[E_b/N_o]_u$ essentially reduces the effect of the limiter and in the asymptotic case when no up-link noise is present this maximum likelihood receiver should be the same as the correlation receiver in Fig. 5-1.b. However, for fixed channel and $\left[\frac{E_b}{N_o}\right]_u$, an increase in $\left[\frac{E_b}{N_o}\right]_d$ implies that the contribution due to down-link Gaussian noise becomes less significant than that due to the equivalent, up-link, non-Gaussian noise component. In such a case the large component of the signal that appears at the input of the receiver would likely be due to the up-link noise component and should be severely compressed, as shown in Figures 5-7 to 5-10, in order to reduce this up-link noise effect. On the other hand, if the down-link noise component is large, the receiver characteristics should again approximate the correlation receiver as shown in Figure 5-1 a.

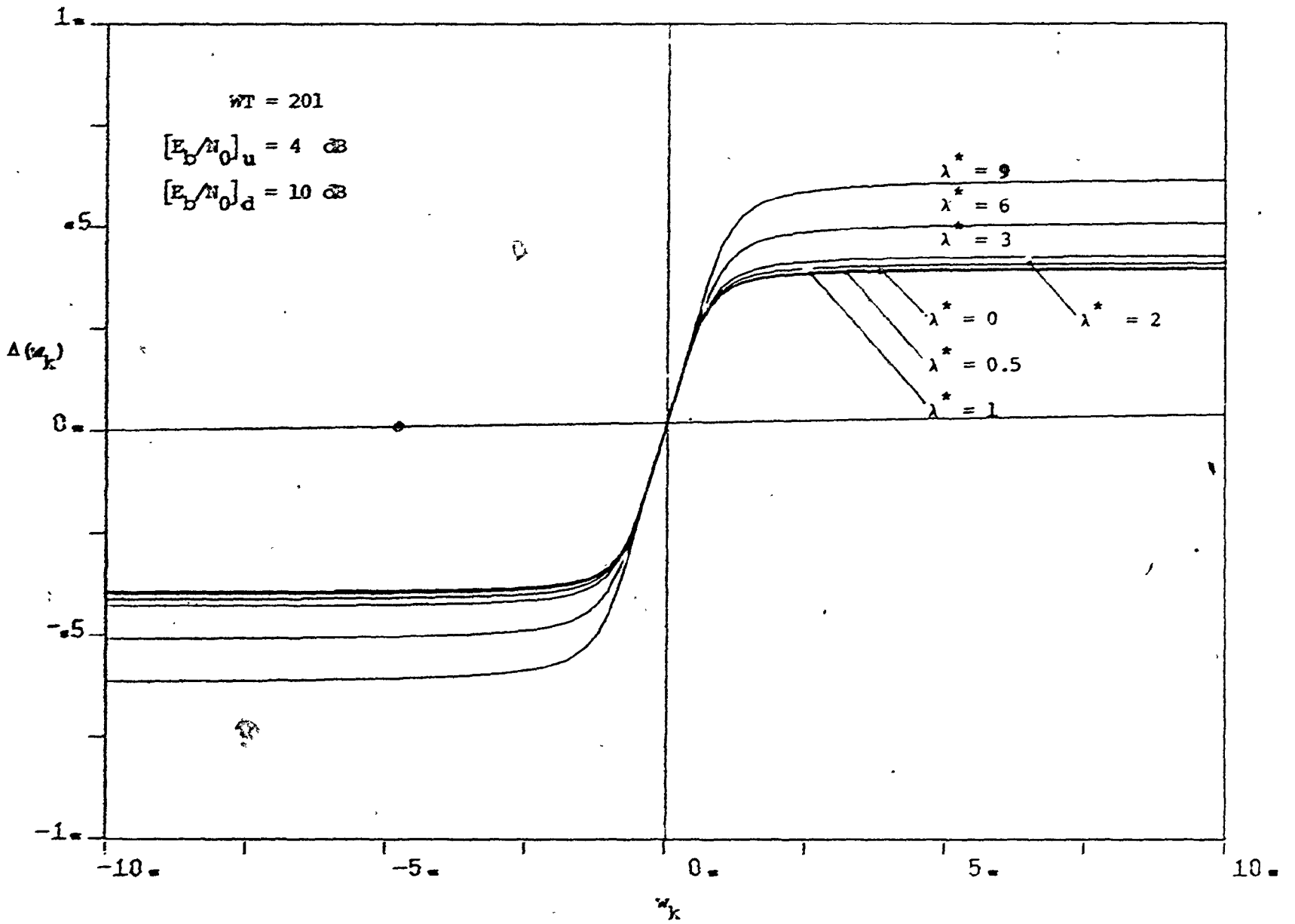

Fig. 5-3. Maximum-likelihood nonlinearity for soft-limited channel

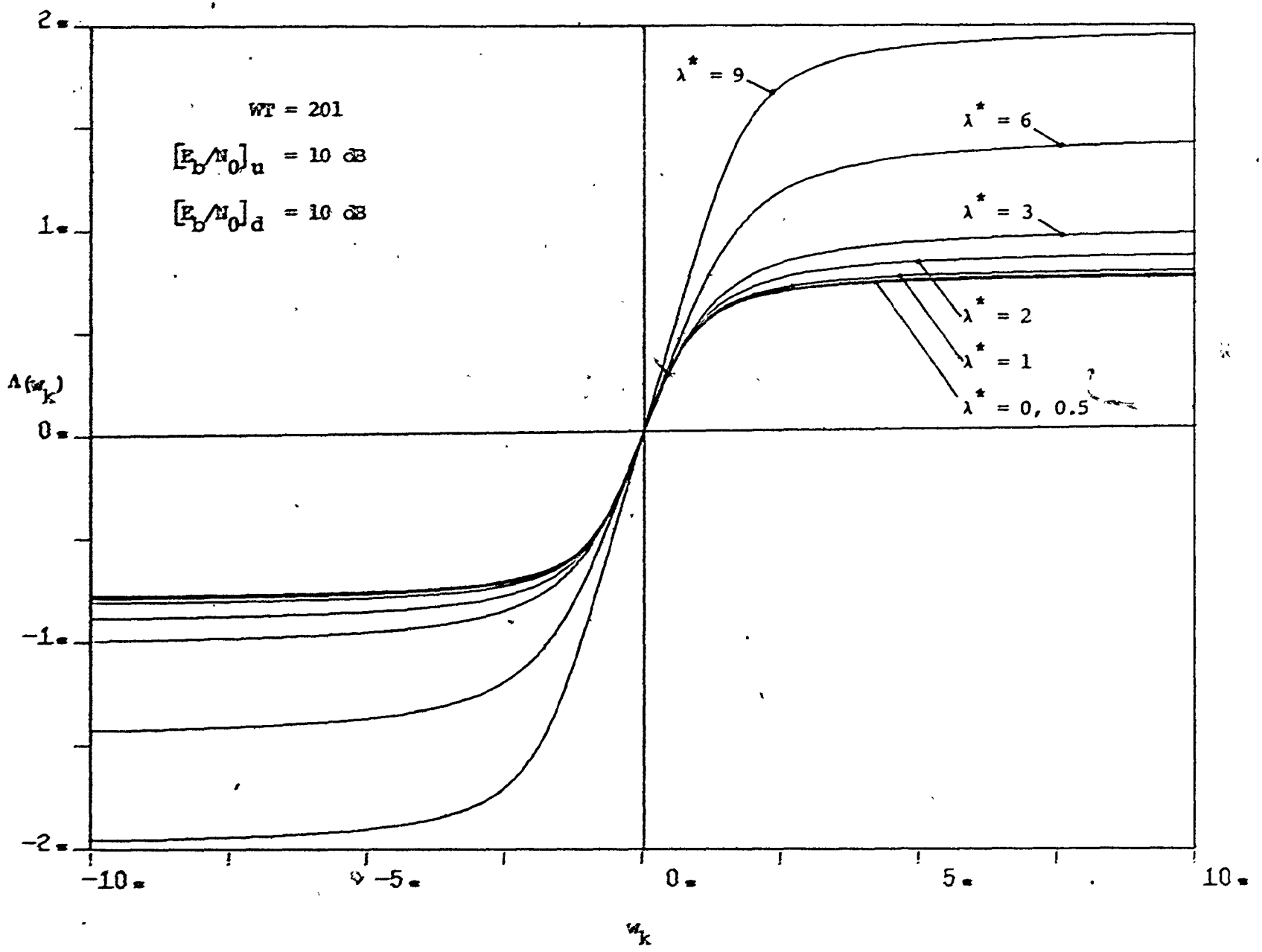

Fig. 5-4. Maximum-likelihood nonlinearity for soft-limited channel

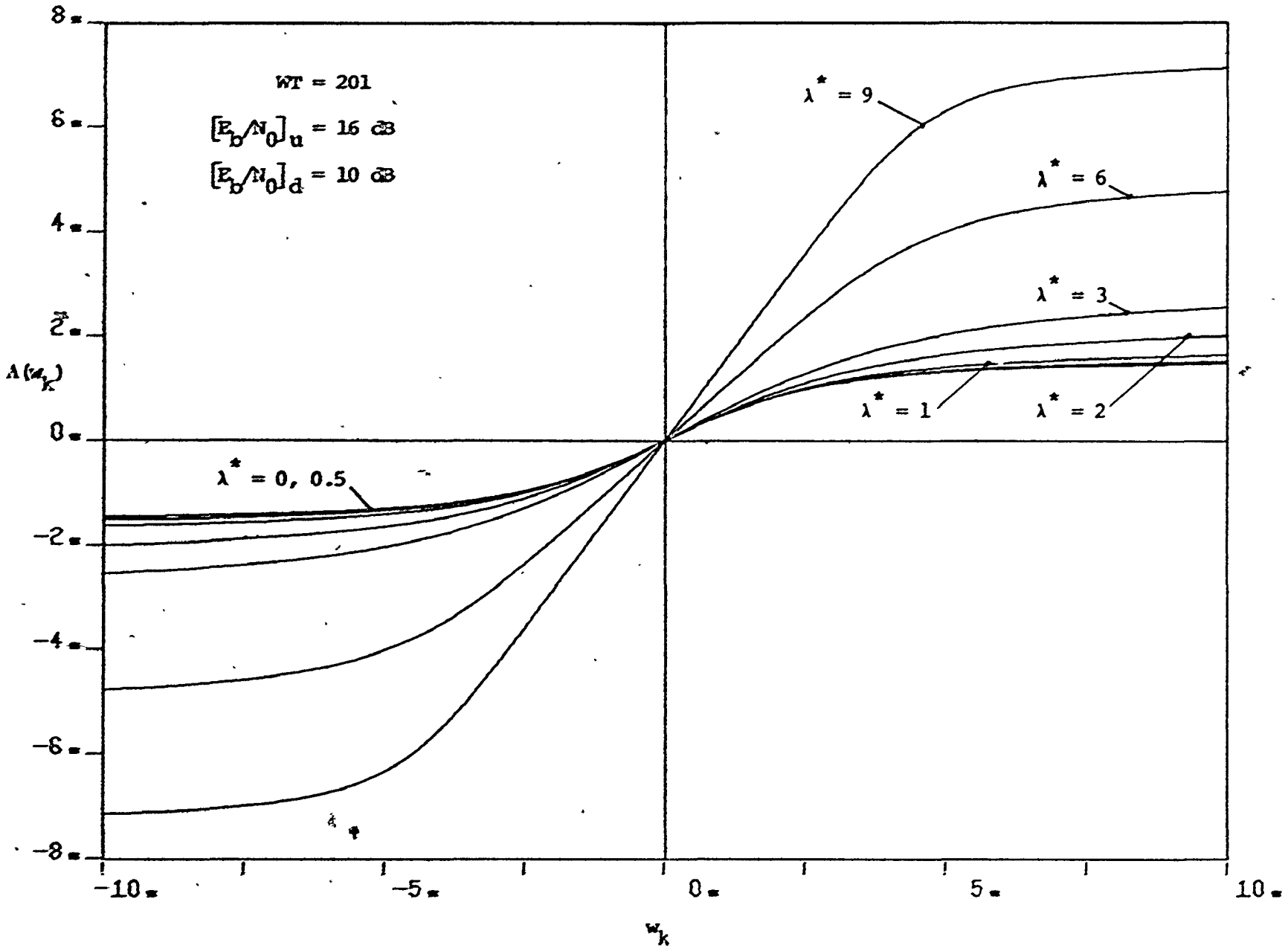

Fig. 5-5. Maximum-likelihood nonlinearity for soft-limited channel

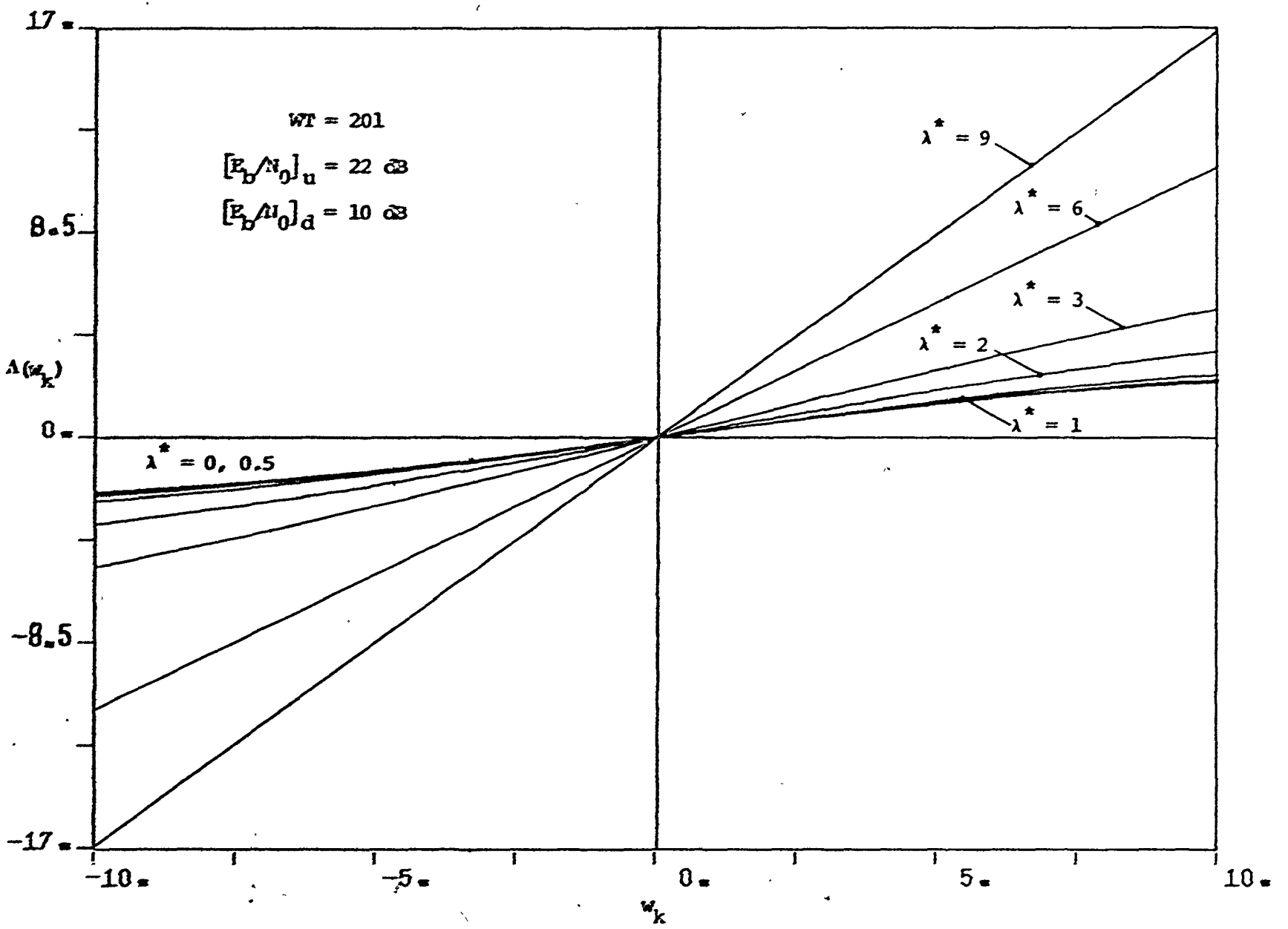

Fig. 5-6. Maximum-likelihood nonlinearity for soft-limited channel

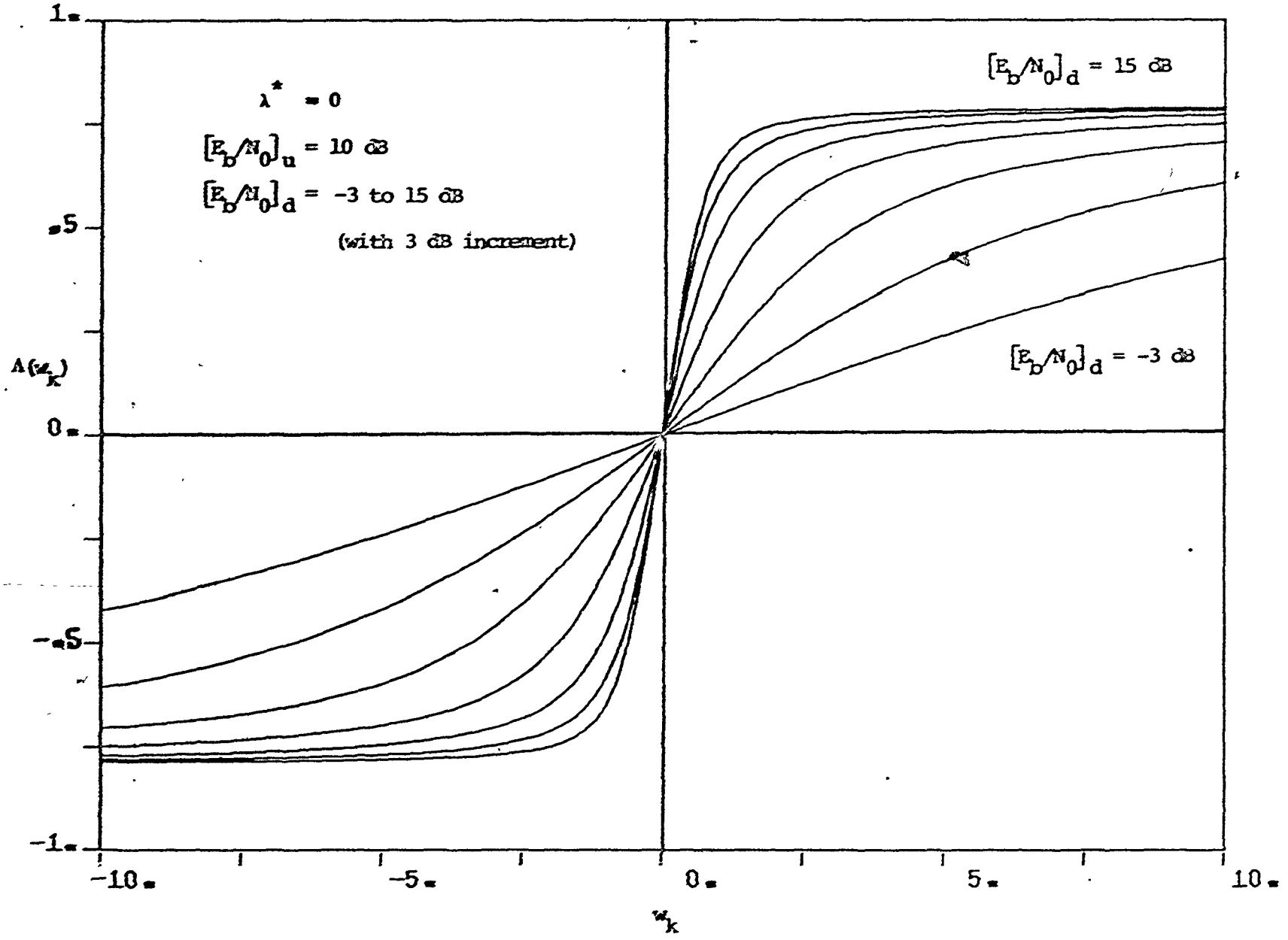

Fig. 5-7. Maximum-likelihood nonlinearity for soft-limited channel

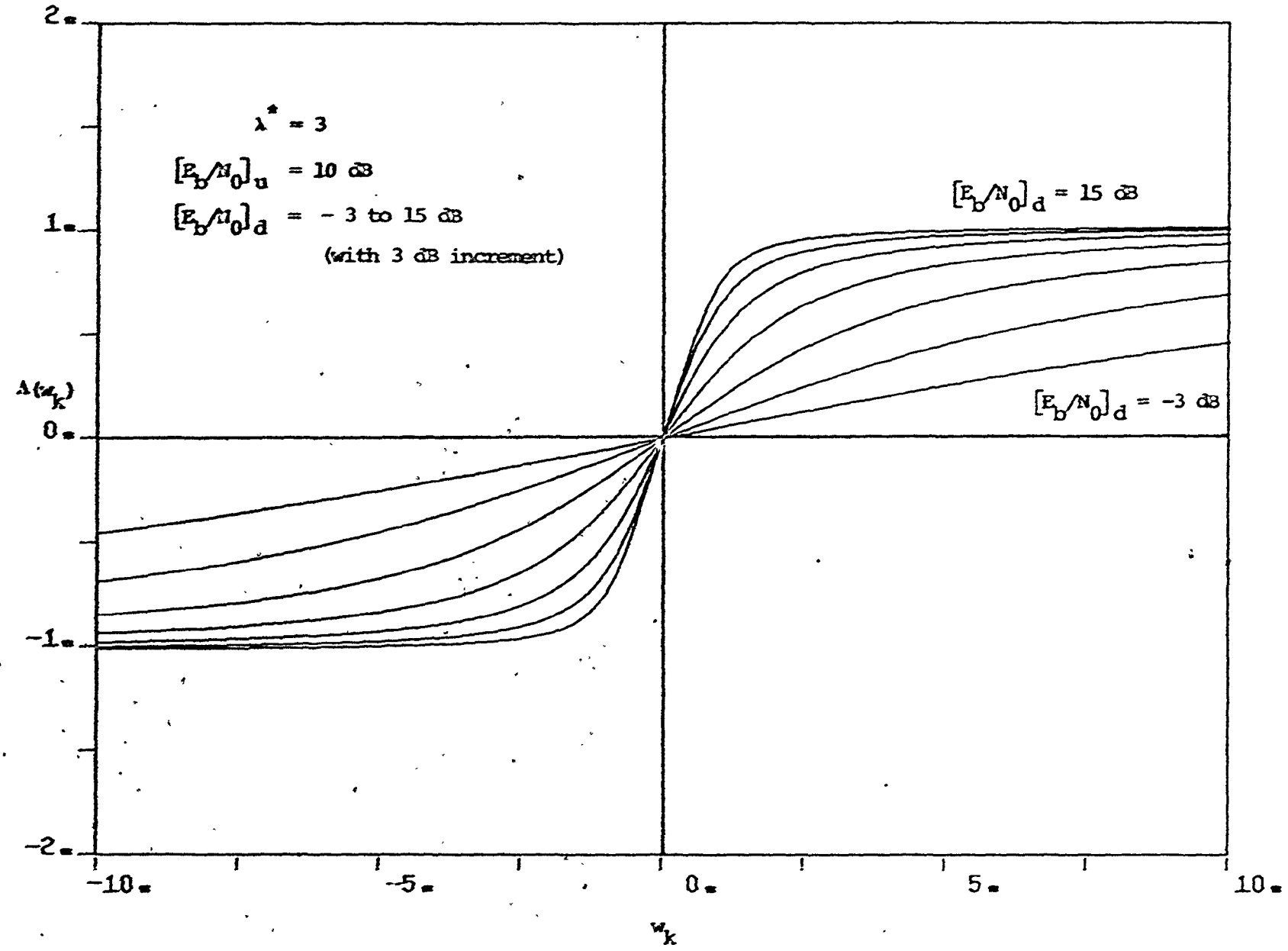

Fig. 5-8. Maximum-likelihood nonlinearity for soft-limited channel

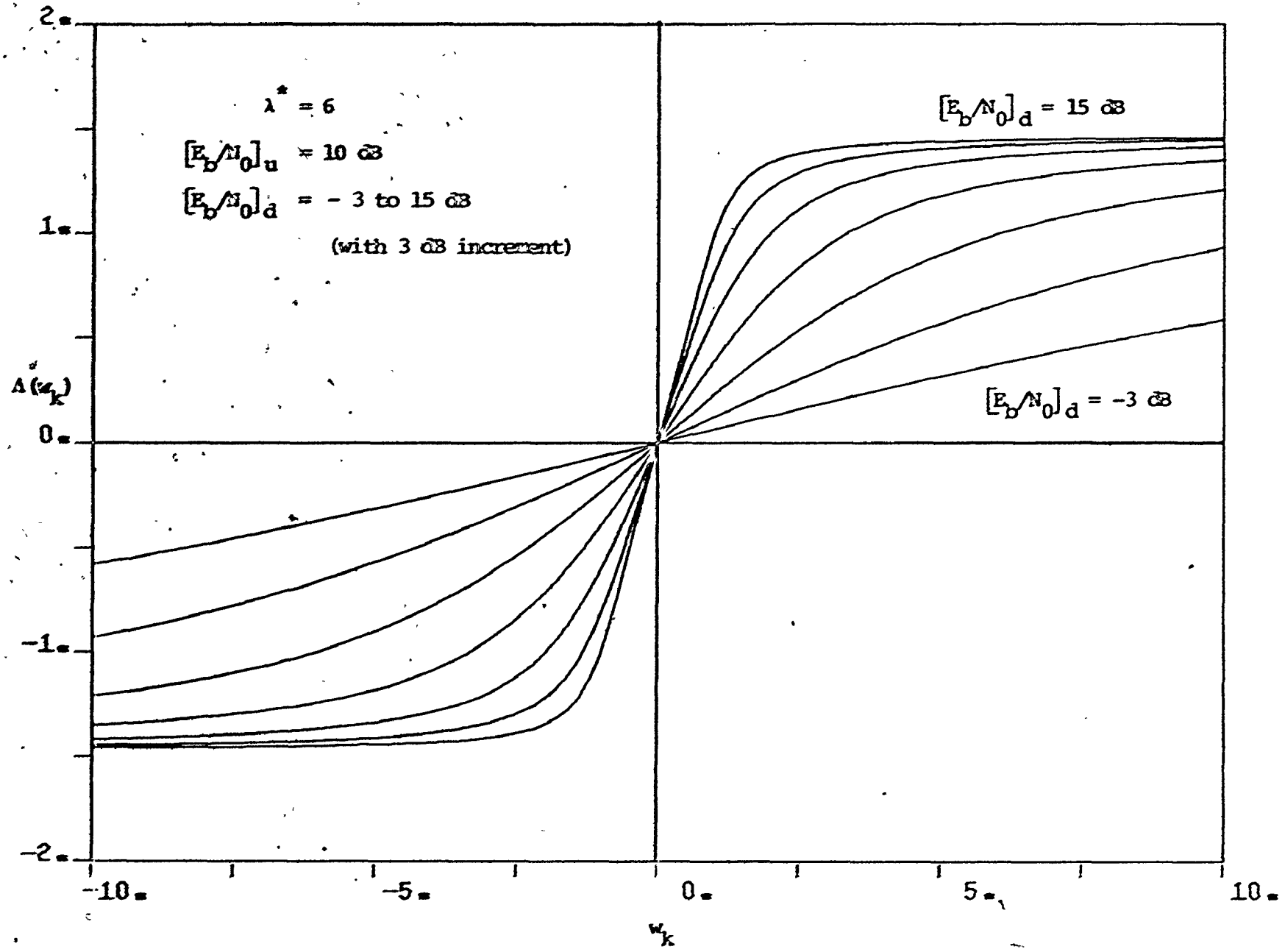

Fig. 5-9. Maximum-likelihood nonlinearity for soft-limited channel

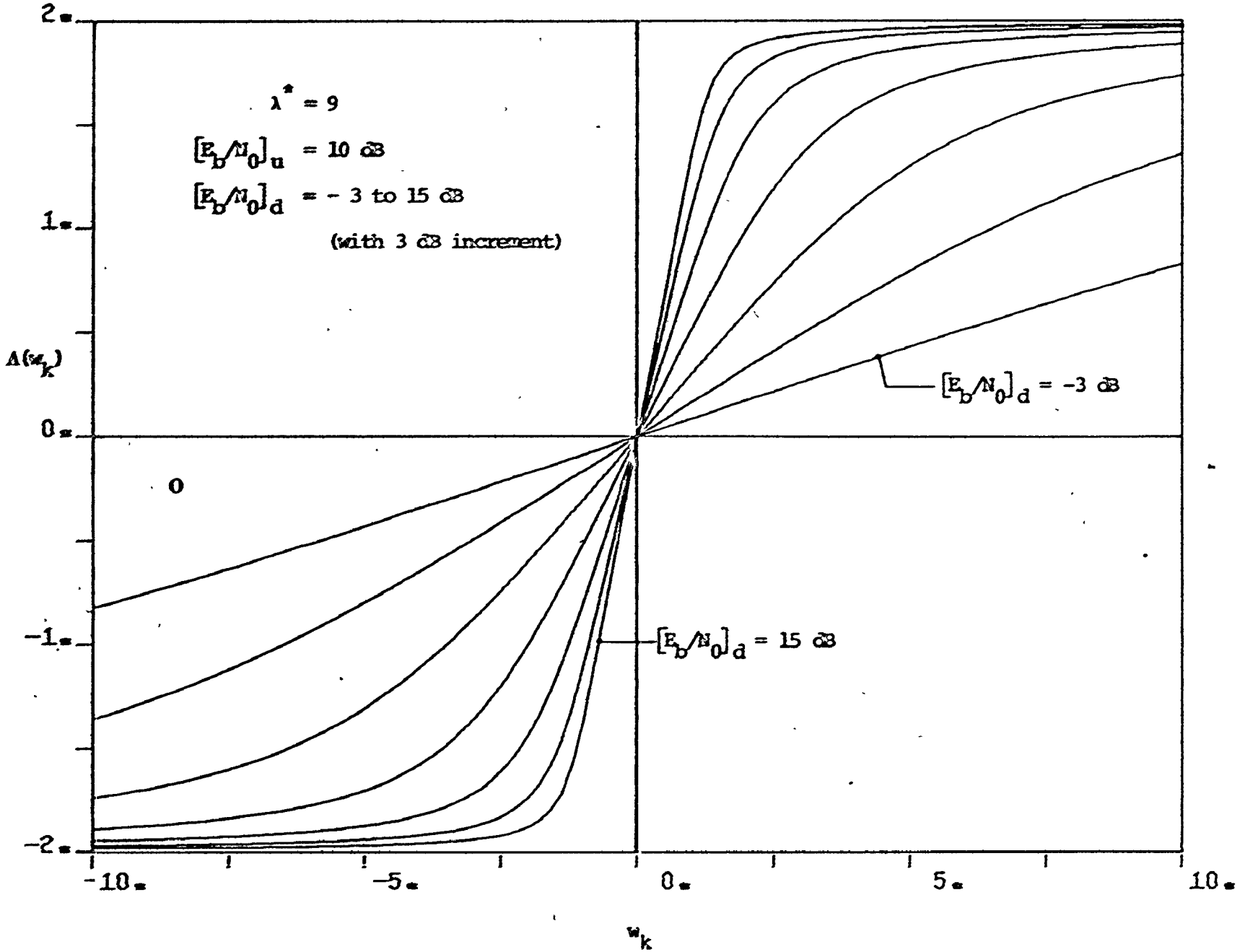

Fig. 5-10. Maximum-likelihood nonlinearity for soft-limited channel

Figure 5-11 depicts a block diagram representing the proposed maximum likelihood receiver.

Having selected the test statistics, $\ell[w_k : k=1,\ldots,WT]$, the error performance of this maximum likelihood receiver is determined by its distribution function, which is generally difficult to find without resorting to extensive numerical computation. However, for sufficiently large WT, ℓ as defined in equation (5.30) is a sum of a large number of statistically independent, bounded variates. Furthermore, since the received signal w_k is a sampled version of the received signal that is continuous within the bit duration, then ℓ can be shown to have an unbounded variance for asymptotically large WT [66]. Consequently, we can invoke the Central Limit Theorem [37] to ensure that the random variable ℓ is asymptotically normal for large WT. It is then reasonable to speak of the ratio of statistical mean of ℓ to its standard deviation as a measure of system performance.

If $a=1$, was actually transmitted, then from the asymptotically normal distribution of ℓ it can be shown that $\frac{\ell}{W}$ is also asymptotically normally distributed with mean

$$\mu = \frac{1}{W} \sum_{k=1}^{WT} \int_{-\infty}^{\infty} p_{Z_k^+}(w_k - A') \, \Lambda(w_k) \, dw_k \qquad (5.35)$$

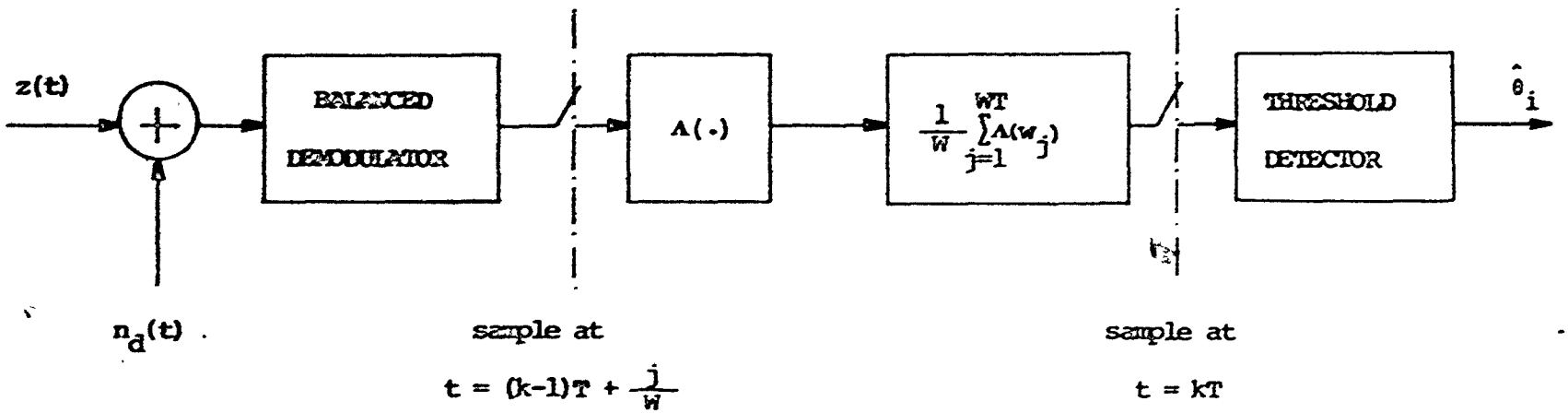

Fig. 5-11. Maximum-likelihood receiver, $(k-1)T \leq t \leq kT$

and variance

$$\sigma^2 = \frac{1}{W^2} \sum_{k=1}^{WT} \int_{-\infty}^{\infty} p_{Z_k^+}(w_k - A') \, \Lambda^2(w_k) \, dw_k - \mu^2 \qquad (5.36)$$

We now define γ as the ratio of the statistical mean of ℓ to its standard deviation as

$$\gamma = \frac{\mu}{\sigma} \qquad (5.37)$$

and since $\frac{\ell}{W}$ is asymptotically normal distributed, the asymptotic performance of the system is completely determined by this parameter. Since the transmitted phase θ can take the value of 0 or π with equal probability and the cost of making an incorrect decision is the same whether 0 or π is being transmitted, then the single threshold to which the log-likelihood ratio, $\frac{\ell}{W}$, must be compared can be shown to be zero. Based on the binary decision that is made at the receiver according to equation (5.32), the asymptotic error probability is then given by

$$P_0 = Pr(\ell \leq 0 \mid a=1)$$

$$= \frac{1}{2} \operatorname{erfc}(\gamma/\sqrt{2}) \qquad (5.38)$$

where erfc(.) denotes the complementary error function. Figure 5-12 illustrates the asymptotic error performance of the maximum likelihood receiver for a hard-limited channel with different values of up-link and down-link bit energy to noise spectral density ratio. For small $\left[\frac{E_b}{N_o}\right]_d$ the performance

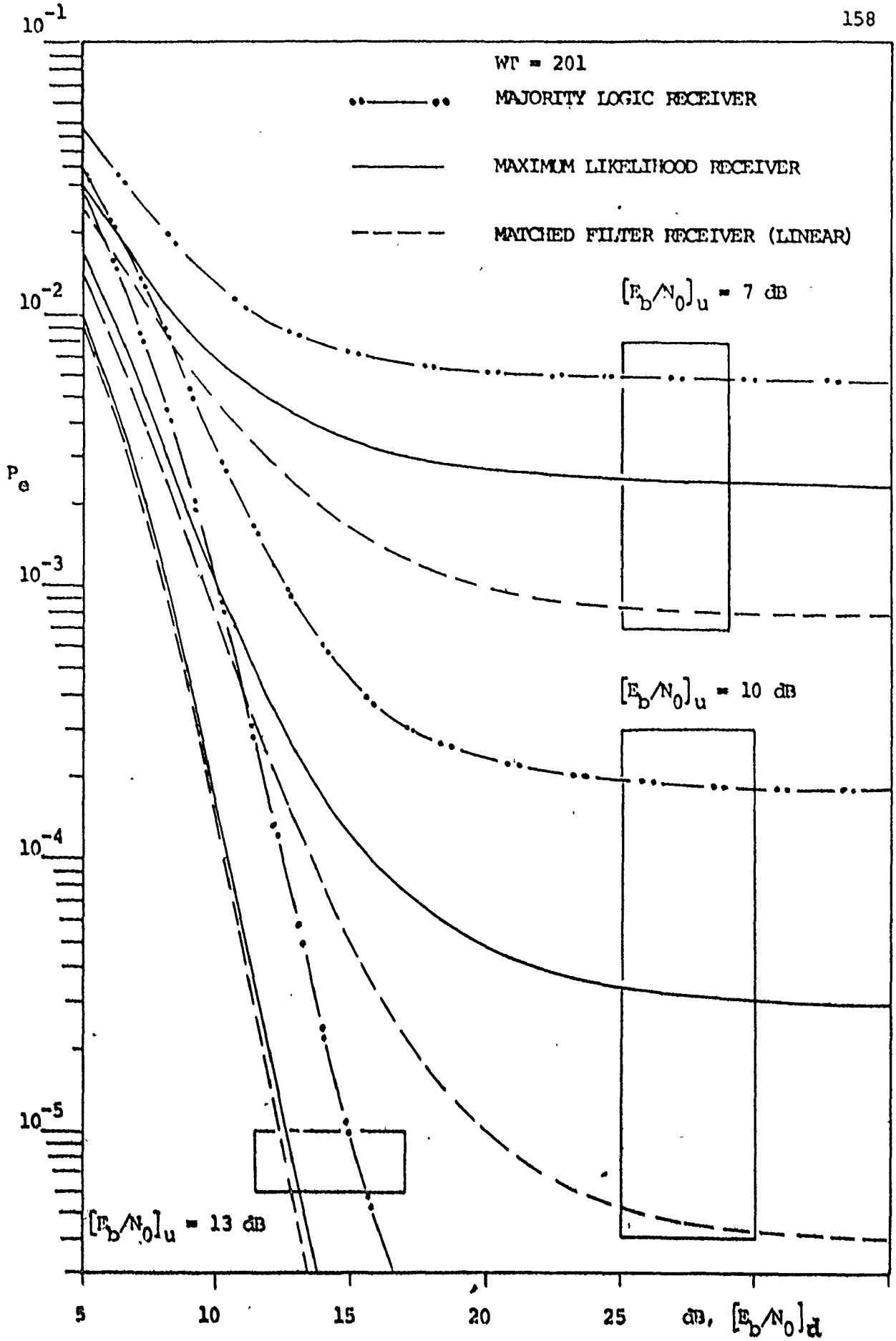

Fig. 5-12. Performance of binary CPSK transmission through hard-limited channel

of the maximum likelihood receiver is slightly inferior to that of the matched filter receiver for the linear channel. The explanation for this is evident in Figure 5-7 which indicates that the maximum likelihood receiver characteristic is more linear for small $\left[\frac{E_b}{N_0}\right]_d$ and the statistics of the received noise approach the Gaussian normal distribution as assumed earlier. For large $\left[\frac{E_b}{N_o}\right]_d$ the performance of the maximum likelihood receiver yields an improvement over that of the majority logic receiver, however, it is poorer than that of the matched filter receiver for the case of the linear channel. Figures 5-13 to 5-15 illustrate the performance of the maximum likelihood receiver for the piecewise-linear limiting channel. Of importance is the fact that the performance of the maximum likelihood receiver approaches that of the linear matched filter case as λ^* increases. Intuitively this should be so as the matched filter is nothing but the maximum likelihood receiver for the linear channel and the sampled output of the matched filter is a normally distributed random variable.

To conclude this section we emphasize the point that our analysis of maximum likelihood receiver is not restricted to the case of a purely amplitude limiting channel but also is extendible to cover the case of an actual TWT channel. In such a case the Gram-Charlier series expansion must again be used, as in section 4.2.2, in order to characterize the proba-

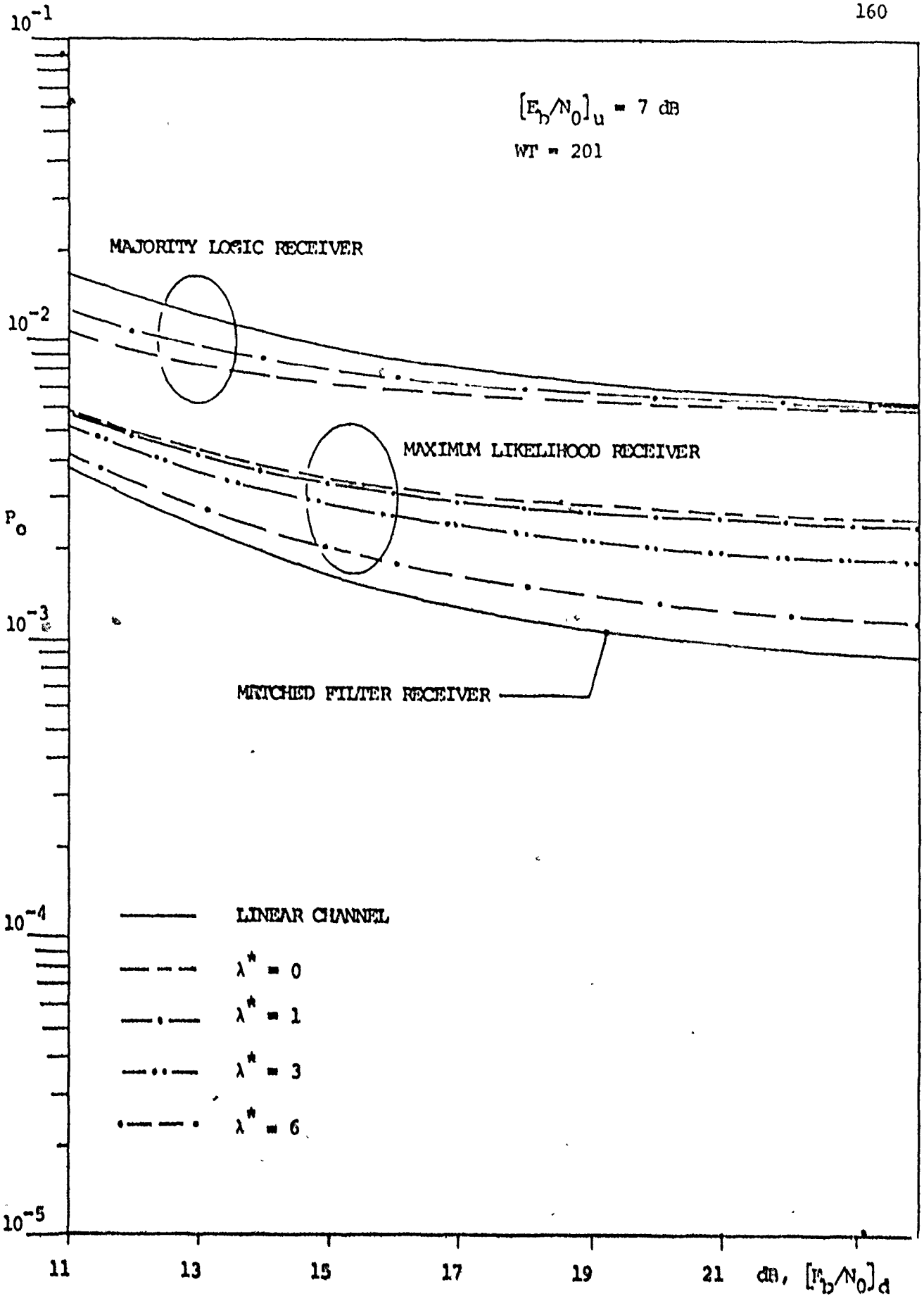

Fig. 5-13. Performance of binary CPSK transmission through soft-limited channels

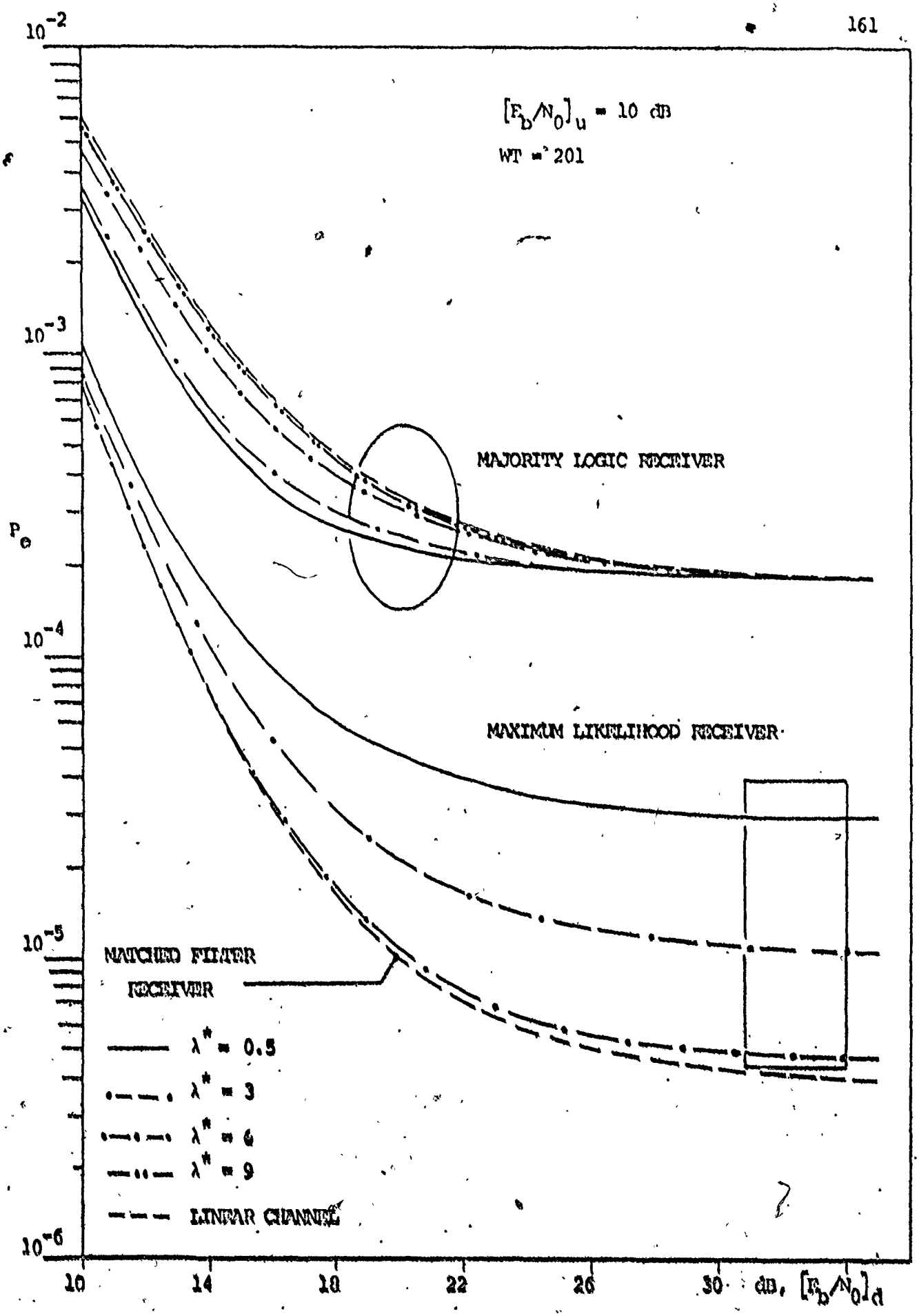

Fig. 5-14. Performance of binary CPSK transmission through soft-limited ch

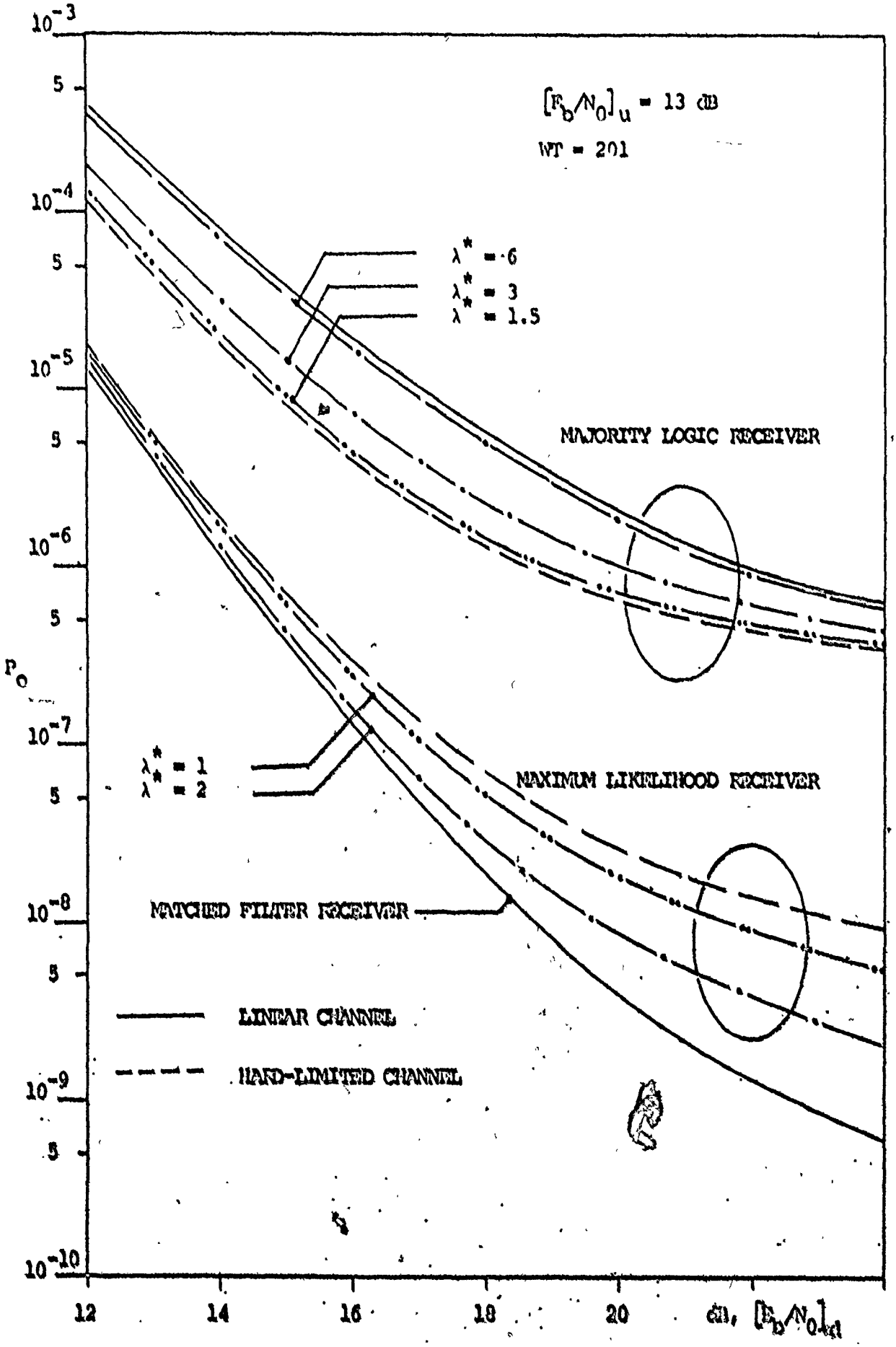
$[E_b/N_0]_u$ = 13 dB
WT = 201
λ^* = 6
λ^* = 3
λ^* = 1.5
MAJORITY LOGIC RECEIVER
MAXIMUM LIKELIHOOD RECEIVER
λ^* = 1
λ^* = 2
MATCHED FILTER RECEIVER
LINEAR CHANNEL
HARD-LIMITED CHANNEL
P_e
10^{-3}
5
10^{-4}
5
10^{-5}
5
10^{-6}
5
10^{-7}
5
10^{-8}
5
10^{-9}
5
10^{-10}
12
14
16
18
20
dB, $[E_b/N_0]_d$

bility density function of n_1'. Once this is known, a procedure, similar to that developed in this section, may be used to derive the maximum likelihood receiver and to assess the performance of such a receiver. However, because closed form expressions are not available for the probability density function of n_1' the assessment of the performance of this receiver is a very difficult task.

CHAPTER 6

CONCLUSIONS AND SUGGESTIONS FOR FUTURE STUDY

6.1) CONTRIBUTIONS OF THE THESIS

In this thesis an attempt has been made to investigate the effect of bandpass nonlinearities on the performance of coherent phase shift keying systems. A need for such investigation arises in the case of satellite communications where the transmitted signal (CPSK) and up-link noise are passed through a TWT on board the satellite prior to retransmission to a receiving earth station. The major contributions of the thesis may be summarized as follows:

(1) A novel quadrature model of TWT has been developed. As compared to the other existing models our proposed nonlinear quadrature model offers the following advantages:

(a) it only needs the choice of four parameters to give a good fit to the actual tube nonlinearity up to and beyond saturation,

(b) it is well behaved for all input levels and permits straightforward evaluation of the noise statistics at the output of the tube.

(2) For nonlinear devices with AM/PM conversion, the characteristics of the optimal bandpass nonlinearity that yield maximum signal to interference power ratio have been derived,

(3) Based on (1) and (2), a possible implementation of a

signal predistortion compensator in cascade with the actual TWT has been suggested. The compensator, consisting of a simple arrangement of appropriate attenuators and power law devices, has been shown, by computer simulation, to yield about 1 dB improvement in system performance for the case of a single carrier per channel mode of operation.

(4) Analytical expressions for the probability density functions of the equivalent in-phase and quadrature noise components at the output of a piecewise-linear envelope limiting device have been derived. These expressions allow straightforward evaluation of the probability of error for M-ary CPSK signals transmitted through such a limiter with both up- and down-link noise present.

(5) In the case of an actual TWT, the Gram-Charlier series expansion has been applied to approximate the pdf of the equivalent in-phase noise component at the output of TWT. This pdf has been used to evaluate the performance of binary CPSK signals transmitted through the actual TWT channel with a single sample detection and majority logic decision device at the receiver as in case (4). This analysis is readily extendible to the general case of M-ary CPSK system provided a similar expansion is also used to approximate the pdf of the equivalent quadrature noise component at the output of TWT.

(6) Further exploratory results have also been obtained for the case of binary CPSK signals transmitted through a purely amplitude limiting nonlinear channel with the correlation receiver or the maximum-likelihood receiver. In the case of a correlation receiver the bit error rate expression has been derived as an infinite series expansion

somewhat similar to the case of a majority logic receiver. The exact expression for the performance of a maximum likelihood receiver is generally difficult to derive. However, an approximate expression has been derived based on the assumption that the statistics of the output of the maximum likelihood receiver, prior to the threshold detector, obey the normal distribution law.

6.2) SUGGESTIONS FOR FUTURE STUDY

There are numerous directions in which the present study could be extended. A few of these are listed below:

(1) The error rate analysis of M-ary CPSK signals transmitted through a nonlinear satellite channel with combined effects of intersymbol interferences and additive, thermal, up- and down-link noises should be investigated. In order to solve such a complex problem, the desired signal and interference terms at the output of the nonlinear device must be specifically defined in such a way that an evaluation of the statistics of the interference terms can be readily accomplished.

(2) The overall transfer characteristics of a bandpass nonlinearity that maximizes its output carrier to interference power ratio for the case of multicarrier input signal have been conjectured [51, 82] to be that of a piecewise-linear envelope limiter with zero envelope dependent phase shift at the output. However, there is no existing analysis that justifies this conjecture for the case of multicarrier

input. Of equal importance in the compensator analysis is the hardware implementation of the resulting compensation network and the sensitivity in the performance of the overall compensated TWT as each component in the compensation network varies.

(3) The hardware implementation and the performance analysis of the maximum likelihood (ML) receiver should be considered. The exact expression for the performance of such a receiver may not be possible and one may have to resort to a computer simulation technique in order to assess the improvement in detectability of such a receiver over more conventional, existing receivers.

(4) The performance analysis of the correlation receiver and the ML receiver in Chapter 5 should be extended to the case of M-ary CPSK signal transmission.

(5) The evaluation of the power spectrum spread of CPSK signals caused by TWT amplifier nonlinearities is also an important problem. Excessive spread produces adjacent transponder (or adjacent channel) interference which may be unacceptable. Sharper filters at the satellite repeater output and/or at the earth station input could be used to keep this undesired interference within acceptable levels. However, it is well known that sharper filters will introduce additional intersymbol interference. Thus, a compromise is necessary, and in order to provide an optimal tradeoff between intersymbol interference and adjacent channel interference, an accurate evaluation of the power spectrum spread of CPSK signal is just as important as an assessment of the system's performance in the presence of intersymbol interference

and additive up- and down-link Gaussian noises.

(6) The entire analysis presented in this thesis is based on the assumption of perfect synchronization in both carrier and bit timing recovery. Such an assumption , though greatly simplifying our analysis, is not readily justified without sacrifice in hardware complexity at the receiver. Carrier phase error and bit timing error are well known to result in further degradation in the performance of CPSK transmission system through a linear channel. The investigation of such synchronization problems for the nonlinear channel should also be carried out.

APPENDIX A

CURVE FITTING THE QUADRATURE MODEL OF TWT

The basic input-output relationship of the TWT is normally obtained from output power (dBW) and output phase (degrees) measurements for various values of input power (dBm) [13,31]. The output data are then transformed into instantaneous envelope for the case of single carrier measurement by using the well-known relationship

$$P = \frac{A^2}{2}$$

where P is the instantaneous signal power

and A is the signal amplitude.

The instantaneous envelope transfer function $g(x)$ and phase shift, $\phi(x)$ are then combined to yield the measured quadrature model of the tube to which a suitably chosen set of $g_p(x)$ and $g_q(x)$ can be determined. Using equations (2.18) and (2.19) we may now form an unconstrained objective function

$$J = \sum_{i=1}^{M} \left[(g(x_i) \cos[\phi(x_i)] - g_p(x_i))^2 + (g(x_i) \sin[\phi(x_i)] - g_q(x_i))^2 \right] \qquad (A.1)$$

where M is the total number of subdivisions of the range of the input envelope.

Since the right hand side of equation (A.1) is a continuous, differentiable function of C_1, C_2, S_1, S_2, the coefficients in $Z_p(\cdot)$ and $Z_q(\cdot)$, a conventional optimization subroutine can then be used to minimize J by proper selection of these coefficients [8].

APPENDIX B

THE CHEBYSHEV TRANSFORM

If a narrowband signal,

$$u(t) = R(t) \cos[2\pi f_0 t + \epsilon(t)] \tag{B.1}$$

with center frequency f_0, is fed to a memoryless nonlinear device whose output v is a function of its input u at the same instant, then this output can in general be written as

$$v(u) = v(R \cos \theta) \tag{B.2}$$

where $\theta = 2\pi f_0 t + \epsilon(t)$

Since (B.2) is an even periodic function of θ, it is represented exactly, for all θ, by the Fourier series

$$v(R \cos \theta) = \tfrac{1}{2} v_0(R) + \sum_{m=1}^{\infty} v_m(R) \cos m\theta \tag{B.3}$$

where

$$v_m(R) = \frac{2}{\pi} \int_0^{\pi} v(R \cos \theta) \cos m\theta \, d\theta \tag{B.4}$$

Setting $\theta = \cos^{-1}(u/R)$, equations (B.3) and (B.4) can be written as

$$v(u) = \tfrac{1}{2} v_0(R) + \sum_{m=1}^{\infty} v_m(R) \, T_m(u/R) \tag{B.5}$$

and

$$v_m(R) = \frac{2}{\pi} \int_{-R}^{R} v(u)\ T_m(u/R)\ [R^2-u^2]^{-1/2}\ du \qquad (B.6)$$

where $T_m(x) \triangleq \cos(m\cos^{-1}x)$, is the Chebyshev polynomial of order m [1]. Equations (B.5) and (B.6) are generally known as the Chebyshev transform pair. Equation (B.6) relates the mth zone envelope nonlinearity to the instantaneous voltage transfer characteristics of the bandpass nonlinear device.

In many cases, however, the problem is not to find $v_m(R)$ for a given v(u) but rather to find what v(u) will yield some desired $v_m(R)$. It is therefore necessary to know how to invert the transformation in (B.6) for v(u). Blachman [18] has pointed out that the inverse Chebyshev transform for any arbitrary m can be expressed as

$$v(u) = \frac{1}{2} \int_0^{\pi/2} [v_m(u\cos\phi)\ B_m(\csc\phi) + uv_m'(u\cos\phi)\cos^{\frac{1}{2}-\frac{1}{2}(-1)^m}\phi]\ d\phi \qquad (B.6)$$

where $v_m'(x) = \frac{d}{dx}[v_m(x)]$

$$B_0(x) = 0$$

$$B_1(x) = 1$$

and $$B_{m+1}(x) = B_{m-1}(x) + 2m\,T_m(x) \qquad (B.7)$$

with $$T_m(\csc\phi) = \tfrac{1}{2}(\csc\phi + \tan\phi)^m + \tfrac{1}{2}(\csc\phi - \tan\phi)^m \qquad (B.8)$$

Equation (B.6) holds true to within an arbitrary odd (when m is even) or even (when m is odd) function of u and/or any polynomial in u of degree less than m. For the case when $m = 1$, equation (B.6) can be simplified to

$$v(u) = \frac{1}{2}\int_0^{\pi/2} [v_1(u\cos\phi) + uv_1'(u\cos\phi)\cos\phi]\, d\phi \qquad (B.9)$$

plus an arbitrary even function of u.

To conclude this appendix we shall work out the expression for the in-phase instantaneous voltage nonlinearity $N_p(u)$ that will yield the desired first-zone envelope nonlinearity $G_p(R)$ expressed in terms of a polynomial in R as

$$G_p(R) = \sum_{k=1}^{M} a_k R^{2k-1} \qquad (B.10)$$

From equations (B.9) and (B.10) we can express $N_p(u)$ to within an additive constant as

$$N_p(u) = \sum_{k=1}^{M} k a_k u^{2k-1} \int_0^{\pi/2} \cos^{2k-1}\phi\, d\phi \qquad (B.11)$$

Using the following integration formula [39]

$$\int \cos^{2k-1}\phi\, d\phi = \frac{1}{2^{2(k-1)}} \sum_{j=0}^{k-1} \binom{2k-1}{j} \frac{\sin(2k-1-2j)\phi}{(2k-1-2j)}$$

equation (B.11) can be written as

$$N_p(u) = \sum_{k=1}^{M} A_k u^{2k-1}$$

where

$$A_k = \sum_{j=0}^{k-1} \left[\frac{(-1)^{k-j-1} \binom{2k-1}{j}_k}{2^{2(k-1)} [2(k-j)-1]} a_k \right]$$

APPENDIX C

THE NOISE STATISTICS AND CALCULATION OF A' FOR PIECEWISE LINEAR AMPLITUDE LIMITING (SOFT-LIMITING) CHANNELS.

C.1) Derivation of the noise statistics

The equivalent in-phase and quadrature noise components at the output of an envelope soft-limiting repeater can be expressed as;

$$n_1' = \begin{cases} x - A' & 0 \leq x^2+y^2 \leq 1 \\ \dfrac{x}{\sqrt{x^2+y^2}} - A' & x^2+y^2 > 1 \end{cases} \qquad \text{(C.1)}$$

and

$$n_2' = \begin{cases} y & 0 \leq x^2+y^2 \leq 1 \\ \dfrac{y}{\sqrt{x^2+y^2}} & x^2+y^2 > 1 \end{cases} \qquad \text{(C.2)}$$

where $$x = \frac{A + n_1}{\lambda}$$

$$y = \frac{n_2}{\lambda} \qquad \text{(C.3)}$$

Since n_1 and n_2 are assumed to be zero mean, normal random variables with variance N_u, then the probability density functions of x and y, as defined in (C.3) can be written as

$$p_X(x) = N\left[\frac{A}{\lambda}, \frac{N_u}{\lambda^2}\right] \tag{C.4}$$

$$p_Y(y) = N\left[0, \frac{N_u}{\lambda^2}\right] \tag{C.5}$$

where $N[\mu,\sigma^2]$ denotes the pdf of normal random variable with mean μ, and variance σ^2.

Consider first the in-phase noise component. The probability density function (pdf) of n_1' is defined as the derivative of its corresponding probability distribution function (PDF).

$$p_{n_1'}(\alpha) \triangleq \frac{d}{d\alpha}\{Pr[n_1' < \alpha]\} \tag{C.6}$$

From equation (C.1), the probability distribution function of n_1' can be obtained by integrating the pdf's of x and y in equations (C.4-C.5) over the appropriate regions in x-y plane. To facilitate the analysis we shall subdivide the range of α into different regions.

For $\alpha+A' < -1$, it follows that

$$Pr[n_1' < \alpha] = Pr[x < \alpha+A' < -1 \; ; \; 0 \leq x^2+y^2 \leq 1] + Pr\left[\frac{x}{\sqrt{x^2+y^2}} < \alpha+A' < -1 \; ; \; 1 < x^2+y^2\right]$$

$$= 0 \tag{C.7}$$

Similarly for $\alpha+A' > 1$,

$$\Pr[n_1' < \alpha] = \Pr[x < \alpha+A' \; ; \; 0 \leq x^2+y^2 \leq 1] + \Pr\left[\frac{x}{\sqrt{x^2+y^2}} < \alpha+A' \; ; \; 1 < x^2+y^2\right]$$

$$= 1 \tag{C.8}$$

In the range $0 \leq \alpha+A' \leq 1$, the region of integration, $\mathcal{A}'$, is given by

$$\mathcal{A}' = \begin{cases} x \leq \alpha+A' & 0 \leq x^2+y^2 \leq 1 \\ \dfrac{|y|}{x} > \sqrt{\dfrac{1-(\alpha+A')^2}{(\alpha+A')^2}} & 0 \geq x, \quad x^2+y^2 > 1 \end{cases} \tag{C.9}$$

It can be shown that for $-1 \leq \alpha+A' \leq 0$, the region of integration, $\mathcal{A}$, is the complement of $\mathcal{A}'$, and is given by

$$\mathcal{A} = \begin{cases} x < \alpha+A' & 0 \leq x^2+y^2 \leq 1 \\ \dfrac{-|y|}{x} > \sqrt{\dfrac{1-(\alpha+A')^2}{(\alpha+A')^2}} & 0 \geq x, \quad x^2+y^2 > 1 \end{cases} \tag{C.10}$$

The regions $\mathcal{A}$ and $\mathcal{A}'$ are as shown in Fig. C-1.

The probability distribution function of n_1' is then given by

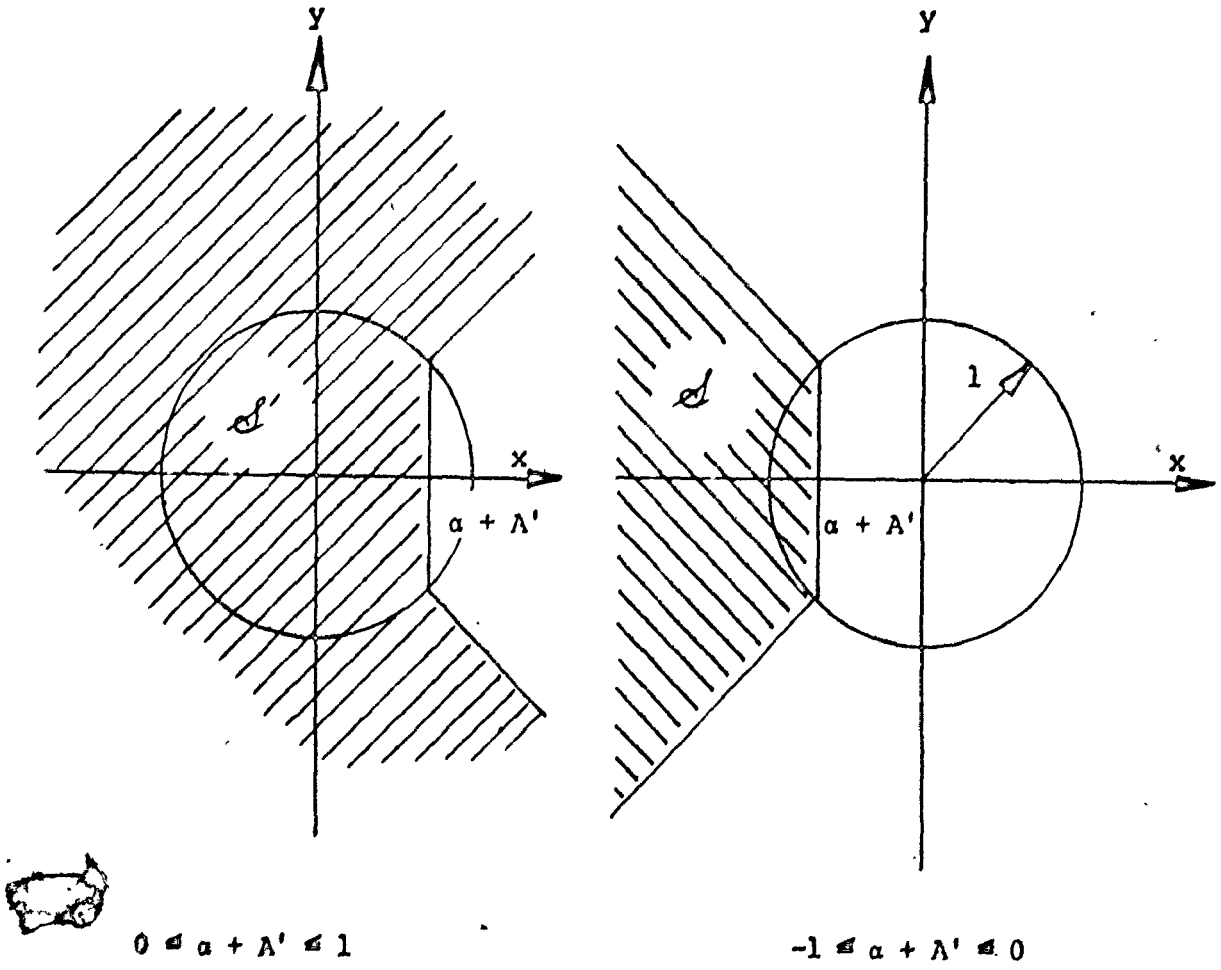

Fig. C-1. Integration regions used in the determination of the in-phase noise statistics.

$$\Pr[n_1' < \alpha] = \begin{cases} 0 & \alpha < -1-A' \\ 1 & \alpha > 1-A' \\ 1 - \int\int_{\mathcal{A}} p_X(x)p_Y(y)\,dxdy & 0 \le (\alpha+A') \le 1 \\ \int\int_{\mathcal{A}} p_X(x)p_Y(y)\,dxdy & -1 \le (\alpha+A') \le 0 \end{cases} \tag{C.11}$$

Substitution of equations (C.4-C.10) into (C.11) yields

$$\Pr[n_1' < \alpha] = \begin{cases} 0 & \alpha < -1-A' \\ 1 & \alpha < 1-A' \\ 1 - \dfrac{2\lambda}{\sqrt{N_u}} \displaystyle\int_{\alpha+A'}^{\infty} \phi\left[\frac{\lambda x - A}{\sqrt{N_u}}\right] \left\{ \phi\left[\frac{\lambda x\sqrt{1-(\alpha+A')^2}}{\sqrt{(\alpha+A')^2 N_u}}\right] - \frac{1}{2} \right\} dx & 0 \le \alpha+A' \le 1 \\ \dfrac{2\lambda}{\sqrt{N_u}} \displaystyle\int_{-\infty}^{\alpha+A'} \phi\left[\frac{\lambda x - A}{\sqrt{N_u}}\right] \left\{ \phi\left[\frac{-\lambda x\sqrt{1-(\alpha+A')^2}}{\sqrt{(\alpha+A')^2 N_u}}\right] - \frac{1}{2} \right\} dx & -1 \le \alpha+A' \le 0 \end{cases} \tag{C.12}$$

where

$$\phi(x) = \frac{1}{\sqrt{2\pi}} \exp(-x^2/2)$$

$$\Phi(x) = \frac{1}{\sqrt{2\pi}} \int_{-\infty}^{x} \exp(-\alpha^2/2)\,d\alpha = \frac{1}{2}\operatorname{erfc}(-x/\sqrt{2})$$

The probability density function of the in-phase noise, n_1', is obtained by differentiating the distribution function in (C.12) with respect to α to get

$$p_{n_1'}(\alpha) = \begin{cases} 0 & |\alpha+A'| > 1 \\ \frac{2\lambda}{\sqrt{N_u}}\,\phi\left[\frac{\lambda(\alpha+A') - A}{\sqrt{N_u}}\right]\left\{\phi\left[\frac{\lambda\sqrt{1-(\alpha+A')^2}}{\sqrt{N_u}}\right] - \frac{1}{2}\right\} + & \\ \frac{\sqrt{2/\pi}\,\exp\left[\frac{-A^2}{2N_u}(1-(\alpha+A')^2)\right]}{\sqrt{1-(\alpha+A')^2}}\left\{\phi\left[\frac{\lambda - A(\alpha+A')}{\sqrt{N_u}}\right] + \right. & \\ \left. \frac{A(\alpha+A')}{\sqrt{N_u}}\,\phi\left[\frac{A(\alpha+A') - \lambda}{\sqrt{N_u}}\right]\right\} & |\alpha+A'| \le 1 \end{cases} \tag{C.13}$$

In the case of a hard-limited channel substitution of $\lambda=0$ into (C.13) yields

$$[p_{n_1'}(\alpha)]_{\lambda=0} = \begin{cases} 0 & |\alpha+A'| > 1 \\ \sqrt{2/\pi}\,\exp[-A^2(1-(\alpha+A')^2)/2N_u]\{\phi[A(\alpha+A')/\sqrt{N_u}] + & \\ \frac{A(\alpha+A')}{\sqrt{N_u}}\,\phi[A(\alpha+A')/\sqrt{N_u}]\} & |\alpha+A'| \le 1 \end{cases} \tag{C.14}$$

The in-phase noise pdf as expressed in (C.14) is identical to that derived by Lyons [58, eqn 20].

Similarly it can be shown that the probability distribution

function of n_2' is given by

$$\Pr[n_2' < \beta] = \begin{cases} 0 & \beta < -1 \\ 1 & \beta > 1 \\ 1 - \int\int_{\mathcal{A}'} p_X(x)p_Y(y)\,dxdx & 0 \le \beta \le 1 \\ \int\int_{\mathcal{A}''} p_X(x)p_Y(y)\,dxdy & -1 \le \beta \le 0 \end{cases} \tag{C.15}$$

The integration regions $\mathcal{A}'''$ and $\mathcal{A}''$ corresponding to the cases where $0 \le \beta \le 1$ and $-1 \le \beta \le 0$ are as shown in Fig. C-2. After some manipulations, equation (C.15) can be expressed as

$$\Pr[n_2' < \beta] = \begin{cases} 0 & \beta < -1 \\ 1 & \beta > 1 \\ 1 - \dfrac{\lambda}{\sqrt{N_u}} \displaystyle\int_{\beta}^{\infty} \phi\left[\frac{\lambda y}{\sqrt{N_u}}\right] \left\{ \phi\left[\frac{\lambda y\sqrt{1-\beta^2}}{\beta\sqrt{N_u}} - \frac{A}{\sqrt{N_u}}\right] - \right. \\ \left. \phi\left[\frac{-\lambda y\sqrt{1-\beta^2}}{\beta\sqrt{N_u}} - \frac{A}{\sqrt{N_u}}\right] \right\} dy & 0 \le \beta \le 1 \\ \dfrac{\lambda}{\sqrt{N_u}} \displaystyle\int_{-\infty}^{\beta} \phi\left[\frac{\lambda y}{\sqrt{N_u}}\right] \left\{ \phi\left[\frac{\lambda y\sqrt{1-\beta^2}}{\beta\sqrt{N_u}} - \frac{A}{\sqrt{N_u}}\right] - \right. \\ \left. \phi\left[\frac{-\lambda y\sqrt{1-\beta^2}}{\beta\sqrt{N_u}} - \frac{A}{\sqrt{N_u}}\right] \right\} dy & -1 \le \beta \le 0 \end{cases} \tag{C.16}$$

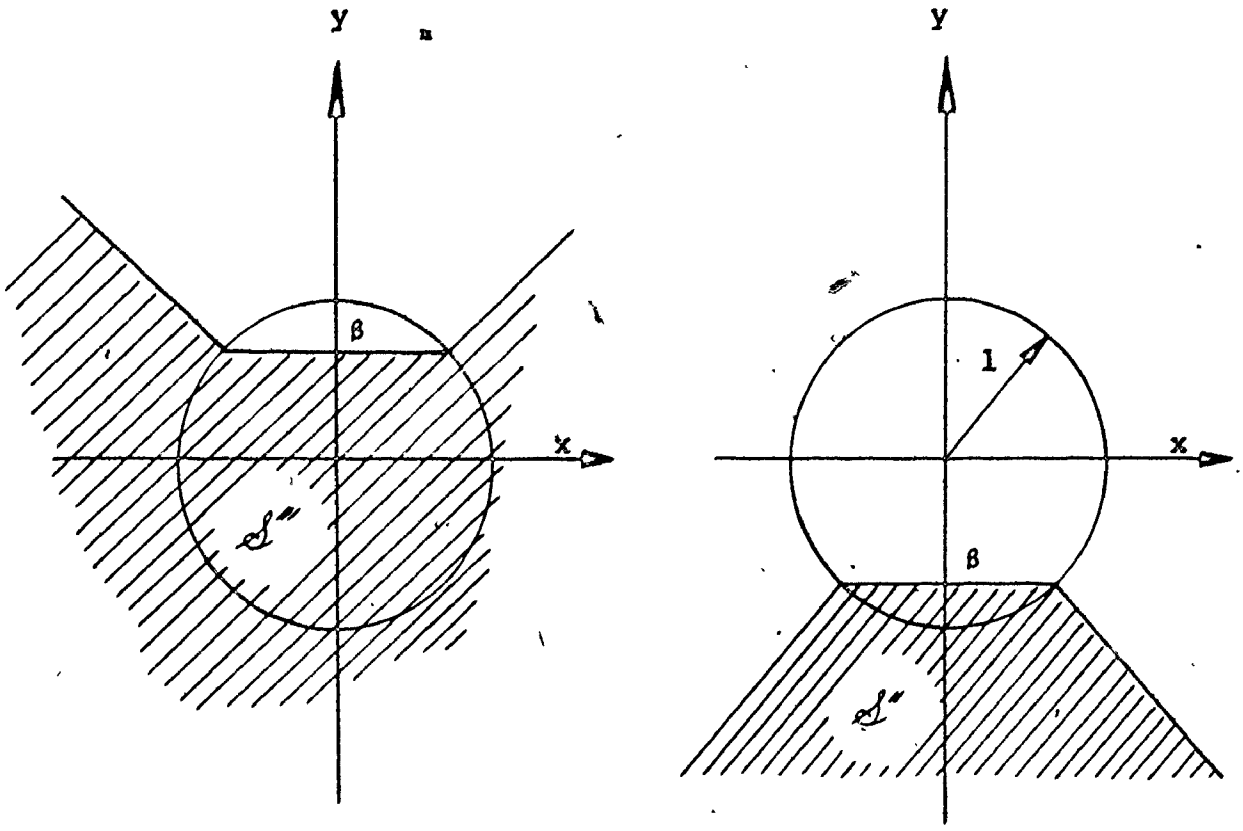

$0 \leq \beta \leq 1$ $\qquad$ $-1 \leq \beta \leq 0$

Fig. C-2. Integration regions used in the determination of the quadrature noise statistics.

Differentiation of (C.16) with respect to β yields the pdf of quadrature noise component, n_2', as

$$p_{n_2'}(\beta) \triangleq \frac{d}{d\beta}\{Pr[n_2' < \beta]\}$$

$$\begin{cases} 0 & |\beta| > 1 \\ \frac{\lambda}{\sqrt{N_u}}\,\phi\left[\frac{\lambda\beta}{\sqrt{N_u}}\right]\left\{\phi\left[\frac{\lambda\sqrt{1-\beta^2}-A}{\sqrt{N_u}}\right]-\phi\left[\frac{-\lambda\sqrt{1-\beta^2}-A}{\sqrt{N_u}}\right]\right\} \\ \quad + \frac{\exp(-A^2\beta^2/2N_u)}{\sqrt{2\pi(1-\beta^2)}}\left\{\phi\left[\frac{\lambda-A\sqrt{1-\beta^2}}{\sqrt{N_u}}\right]+\phi\left[\frac{\lambda+A\sqrt{1-\beta^2}}{\sqrt{N_u}}\right]\right. \\ \quad \left. + \frac{A\sqrt{1-\beta^2}}{\sqrt{N_u}}\left\{\phi\left[\frac{\lambda+A\sqrt{1-\beta^2}}{\sqrt{N_u}}\right]-\phi\left[\frac{\lambda-A\sqrt{1-\beta^2}}{\sqrt{N_u}}\right]\right\}\right\} \\ & |\beta| \le 1 \end{cases} \quad (C.17)$$

Substitution of $\lambda = 0$ into (C.17) yields the pdf of n_2' for the case of hard-limiting channel as

$$[p_{n_2'}(\beta)]_{\lambda=0} = \begin{cases} 0 & |\beta| > 1 \\ \frac{\exp[-A^2\beta^2/2N_u]}{\sqrt{2\pi(1-\beta^2)}}\left\{2\phi[A\sqrt{1-\beta^2}/\sqrt{N_u}] + \frac{A\sqrt{1-\beta^2}}{\sqrt{N_u}}\right. & \\ \left.\phi[A\sqrt{1-\beta^2}/\sqrt{N_u}] - \phi[-A\sqrt{1-\beta^2}/\sqrt{N_u}]\right\} & |\beta| \le 1 \end{cases} \quad (C.18)$$

C.2) Calculation of A'

For a piecewise-linear envelope limiting channel the effective signal amplitude A' is defined in section 4.2.1 as

$$A' = E_{R,\varepsilon}[f(R)\cos\varepsilon] \tag{C.19}$$

From the definition of f(R) and the well-known joint probability density function of R and ε, equation (C.19) can be written as

$$A' = E_{\varepsilon}[\cos\varepsilon] - \int_0^{\lambda}\int_0^{2\pi}[1-(R/\lambda)]\,\frac{R\cos\varepsilon}{2\pi N_u}\exp\left[-\frac{R^2+A^2-2AR\cos\varepsilon}{2N_u}\right]d\varepsilon dR \tag{C.20}$$

Integration of equation (C.20) with respect to ε yields

$$A' = E_{\varepsilon}[\cos\varepsilon] - \int_0^{\lambda}[1-(R/\lambda)]\,\frac{R}{N_u}e^{-\rho}\exp[-R^2/2N_u]\,I_1[AR/N_u]\,dR \tag{C.21}$$

Defining $x = R/\lambda$ and substituting the well-known identity [17]

$$E_{\varepsilon}[\cos\varepsilon] = \tfrac{1}{2}\sqrt{\pi\rho}\,e^{-\rho/2}\{I_0(\rho/2) + I_1(\rho/2)\}$$

into equation (C.21) yields the desired result in equation (4.25).

APPENDIX D

CALCULATIONS OF A', β AND VARIOUS NOISE MOMENTS FOR SATELLITE CHANNELS

D.1) Calculation of A' and β

The effective signal amplitude, A', and phase shift, β, at the output of TWT are defined as

$$A' = \sqrt{\{E_{R,\varepsilon}[Z_p(R)\ \cos\varepsilon]\}^2 + \{E_{R,\varepsilon}[Z_q(R)\ \cos\varepsilon]\}^2}$$

and

$$\beta = -\tan^{-1}\left[\frac{E_{R,\varepsilon}[Z_q(R)\ \cos\varepsilon]}{E_{R,\varepsilon}[Z_p(R)\ \cos\varepsilon]}\right] \qquad (D.1)$$

where $E_{R,\varepsilon}[\cdot]$ denotes the expectation over R and ε .

For the case when the input signal to TWT is the sum of sine wave plus narrowband Gaussian noise, the joint probability density function of the envelope, R, and phase, ε , is

$$p(R,\varepsilon) = \frac{R}{2\pi\sigma^2}\ \exp\left[-\frac{A^2 - 2AR\cos\varepsilon + R^2}{2\sigma^2}\right] \qquad (D.2)$$

$$\text{for } 0 \leq R < \infty \quad \text{and} \quad 0 \leq \varepsilon \leq 2\pi$$

where σ^2 is the input noise variance

A is the amplitude of the transmitted sinusoidal signal.

Define

$$x = R \cos \epsilon$$

$$y = R \sin \epsilon \tag{D.3}$$

and $$P_0 = E_{R,\epsilon}\{Z_p(R) \cos \epsilon\} \tag{D.4}$$

$$P_1 = E_{R,\epsilon}\{Z_q(R) \cos \epsilon\} \tag{D.5}$$

Substitution of equations (D.2-D.3) into (D.4) and (D.5) yields

$$P_0 = C_1 \int_{-\infty}^{\infty}\int_{-\infty}^{\infty} \frac{x}{2\pi\sigma^2} \exp\{-C_2(x^2+y^2)\}\, I_0\{C_2(x^2+y^2)\} \cdot \exp\left\{-\frac{(x-A)^2+y^2}{2\sigma^2}\right\} dxdy \tag{D.6}$$

$$P_1 = S_1 \int_{-\infty}^{\infty}\int_{-\infty}^{\infty} \frac{x}{2\pi\sigma^2} \exp\{-S_2(x^2+y^2)\}\, I_1\{S_2(x^2+y^2)\} \cdot \exp\left\{-\frac{(x-A)^2+y^2}{2\sigma^2}\right\} dxdy \tag{D.7}$$

Since

$$I_0\{C_2(x^2+y^2)\} \triangleq \frac{1}{\pi} \int_0^{\pi} \exp\{C_2(x^2+y^2)\cos \phi\} d\phi$$

then

$$P_0 = \frac{C_1 e^{-\rho}}{2\pi^2\sigma^2} \int_0^{\pi} d\phi \int_{-\infty}^{\infty}\int_{-\infty}^{\infty} x \exp\{Ax\sigma^{-2} - (x^2+y^2)(C_2 + \frac{1}{2\sigma^2} - C_2 \cos \phi)\} dxdy \tag{D.8}$$

where $\rho = \frac{A^2}{2\sigma^2}$ is the input CNR

Defining $\alpha = C_2(1-\cos\phi) + \frac{1}{2\sigma^2}$ and completing the square, we obtain

$$P_0 = \frac{AC_1 \int_0^{\pi} \exp\{-\rho(1-\frac{1}{2\alpha\sigma^2})\}d\phi}{4\pi\sigma^4\alpha^2} \qquad (D.9)$$

Defining $\psi = \frac{\pi-\phi}{2}$

$$\alpha = 2C_2(\Omega+\cos^2\psi) \qquad (D.10)$$

where $\Omega = \frac{1}{4C_2\sigma^2}$

and integrating over ϕ we obtain

$$P_0 = \frac{AC_1 \exp\left[\frac{\rho(1+\frac{1}{2\Omega})}{4C_2\sigma^2(1+\Omega)} - \rho\right]}{16C_2^2\sigma^4\{[\Omega(1+\Omega)]^{\frac{1}{2}}\}^3}\{(\Omega+\tfrac{1}{2})\, I_0[\rho/8C_2\sigma^2\Omega(1+\Omega)]$$

$$+ \tfrac{1}{2}I_1[\rho/8C_2\sigma^2\Omega(1+\Omega)]\} \qquad (D.11)$$

In order to determine P_1, we start by substituting

$$I_1\{S_2(x^2+y^2)\} \triangleq \frac{1}{\pi}\int_0^{\pi} \exp\{S_2(x^2+y^2)\cos\phi\}\cos\phi \; d\phi$$

into equation (D.7), and after some manipulations similar to the previous steps, we obtain

$$P_1 = \frac{-AS_1 \exp\left[\frac{\rho\left(1+\frac{1}{2\Omega'}\right)}{4S_2\sigma^2(1+\Omega')} - \rho\right]}{16S_2^2\sigma^4\{[\Omega'(1+\Omega')]^{1/2}\}^3}\{\tfrac{1}{2} I_0[\rho/8S_2\sigma^2\Omega'(1+\Omega')]$$

$$+ (\Omega'+\tfrac{1}{2})\ I_1[\rho/8S_2\sigma^2\Omega'(1+\Omega')]\} \qquad (D.12)$$

where $\Omega' = \frac{1}{4S_2\sigma^2}$

In terms of P_0 and P_1 we can write

$$A' = \sqrt{(P_0)^2 + (P_1)^2}$$

and $$\beta = -\tan^{-1}(P_1/P_0)$$

D.2) Numerical evaluation of moments of in-phase noise components.

The output in-phase noise component, n_1', is expressed in terms of the input envelope and phase, R and ϵ, as

$$n_1' = C_1 R\, e^{-C_2R^2}\, I_0(C_2R^2)\, \cos(\epsilon+\beta) -$$

$$S_1 R\, e^{-S_2R^2}\, I_1(S_2R^2)\, \sin(\epsilon+\beta) - A' \qquad (D.13)$$

The kth moment of the in-phase noise is obtained by averaging the kth power of n_1' with respect to R and ϵ.

$$E\{(n_1')^k\} = \int_0^{\infty}\int_{-\pi}^{\pi} \frac{(n_1')^k R}{2\pi N_u} \exp\left[-\frac{R^2 + A^2 - 2AR\cos\varepsilon}{2N_u}\right] dR d\varepsilon \tag{D.14}$$

In order to use numerical integration to evaluate (D.14), the infinite limit of integration must be replaced by a finite limit. Using the transformation of variables

$$R = \tan\left[\frac{\pi+x}{4}\right] = \tan z$$

$$\varepsilon = y$$

and substituting (D.13) into (D.14), the kth moment of the in-phase noise n_1' can be expressed as

$$E\{(n_1')^k\} = \frac{1}{8\pi N_u}\int_{-\pi}^{\pi}\int_{-\pi}^{\pi} \{C_1 \tan z\, e^{-C_2\tan^2 z} I_0(C_2\tan^2 z)\cdot$$

$$\cos(y+\beta) - S_1 \tan z\, e^{-S_2\tan^2 z} I_1(S_2\tan^2 z)\sin(y+\beta) - A'\}^k \cdot \{$$

$$\tan z \sec^2 z \exp\left[-\frac{\tan^2 z + A^2 - 2A\tan z\cos y}{2N_u}\right]\} dx dy \tag{D.15}$$

Equation (D.15) is computed numerically using the modified Gauss product formula [45]. First, the integration region in equation (D.15) is subdivided into 2^{2M} identical squares. To each square, the 15th degree, 64-point Gauss product formula [78] is applied to evaluate the double integration. These 2^{2M} values are then summed to yield the kth moment of the in-phase noise. In all the cases considered it was

found empirically that the value M = 5 is sufficient to give results accurate to 6 significant digits. The value for h_k can then be computed from equation (4.49) once the first k moments of the in-phase noise are known.

The convergence rates of the final value for different noise moments as a function of M are shown in figures D-1 to D-7, for different values of up-link carrier to noise power ratio.

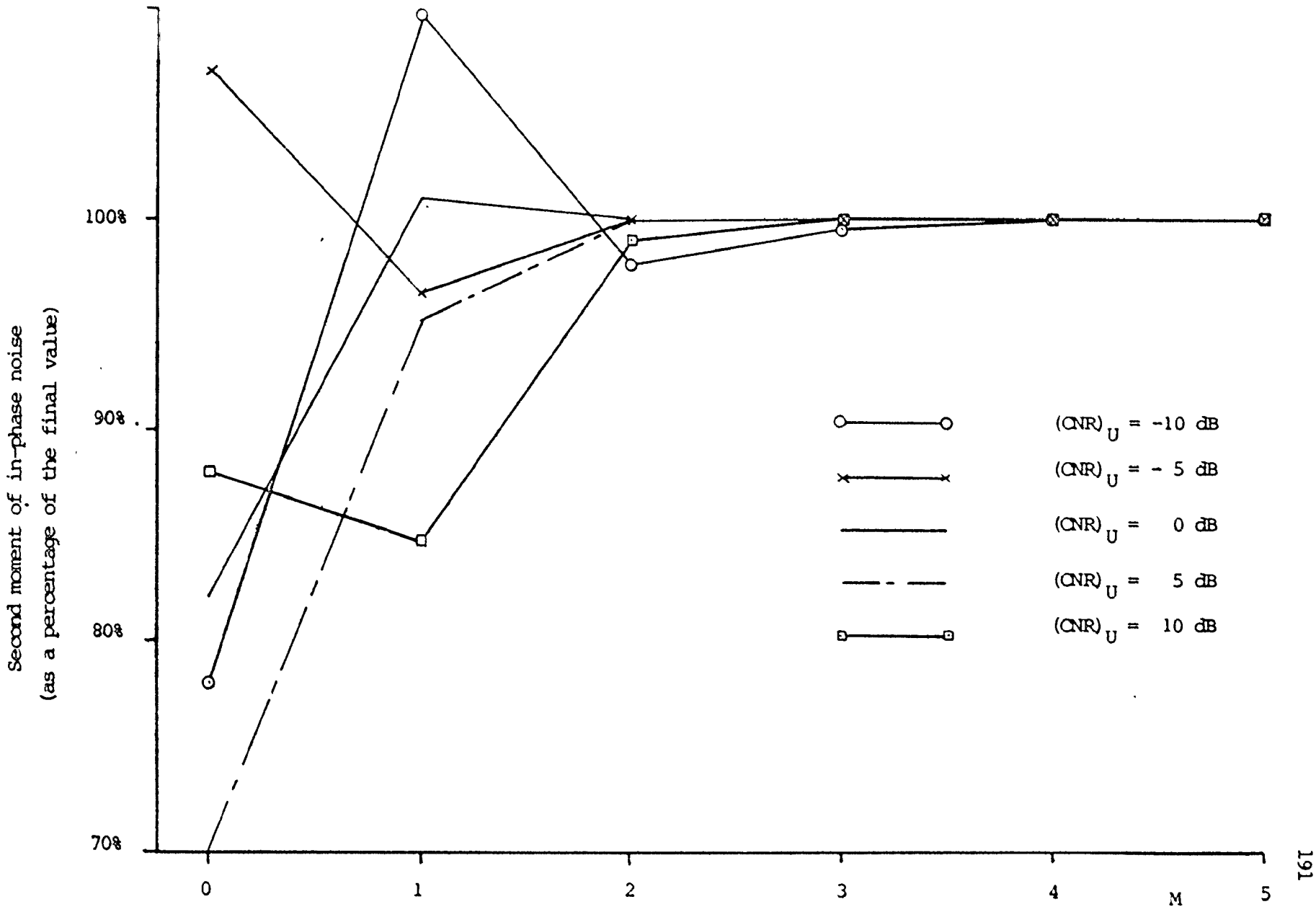

Fig. D-1. Convergence of the second moment of in-phase noise to the final value as a function of M.

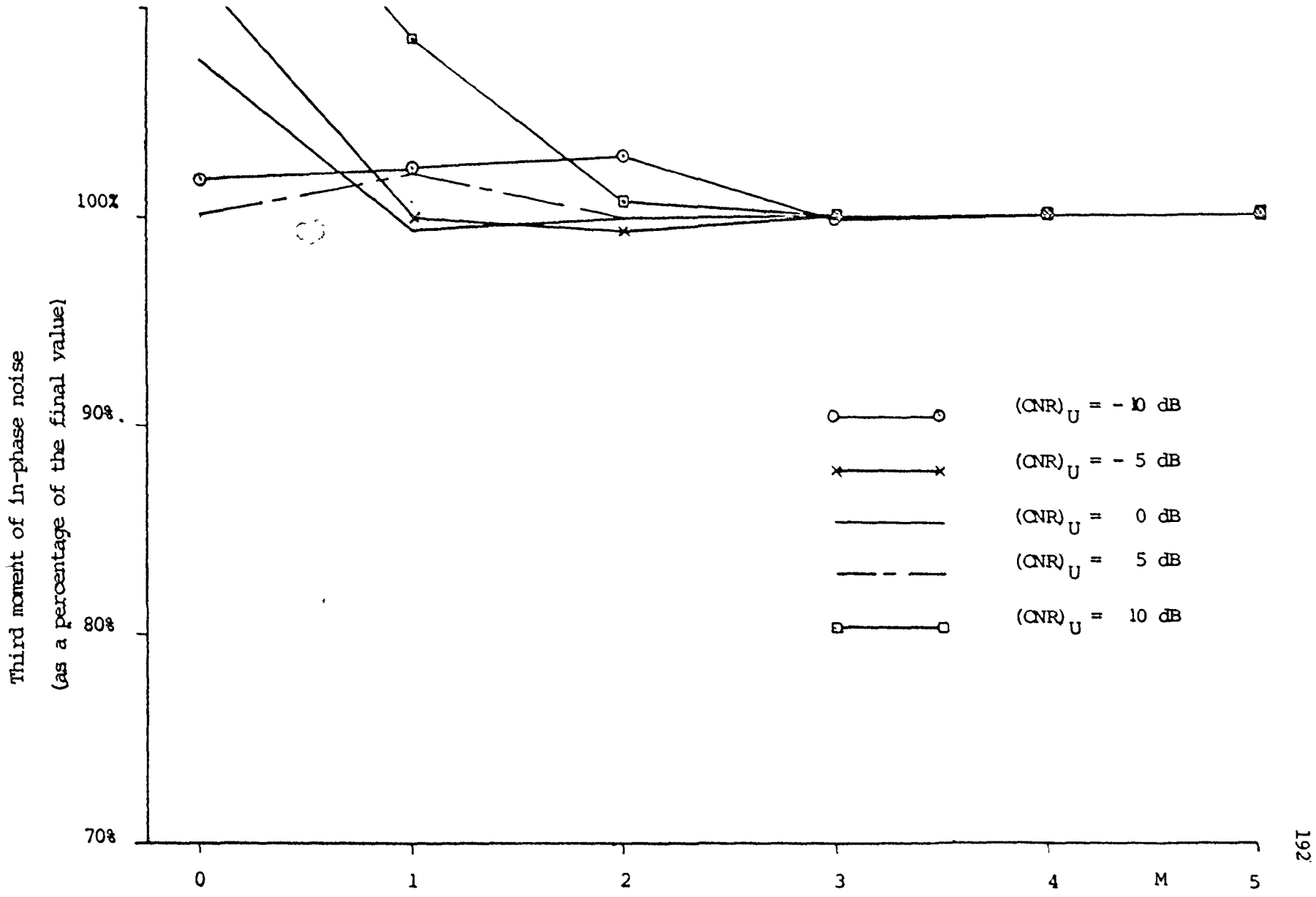

Fig. D-2. Convergence of the third moment of in-phase noise to the final value as a function of M.

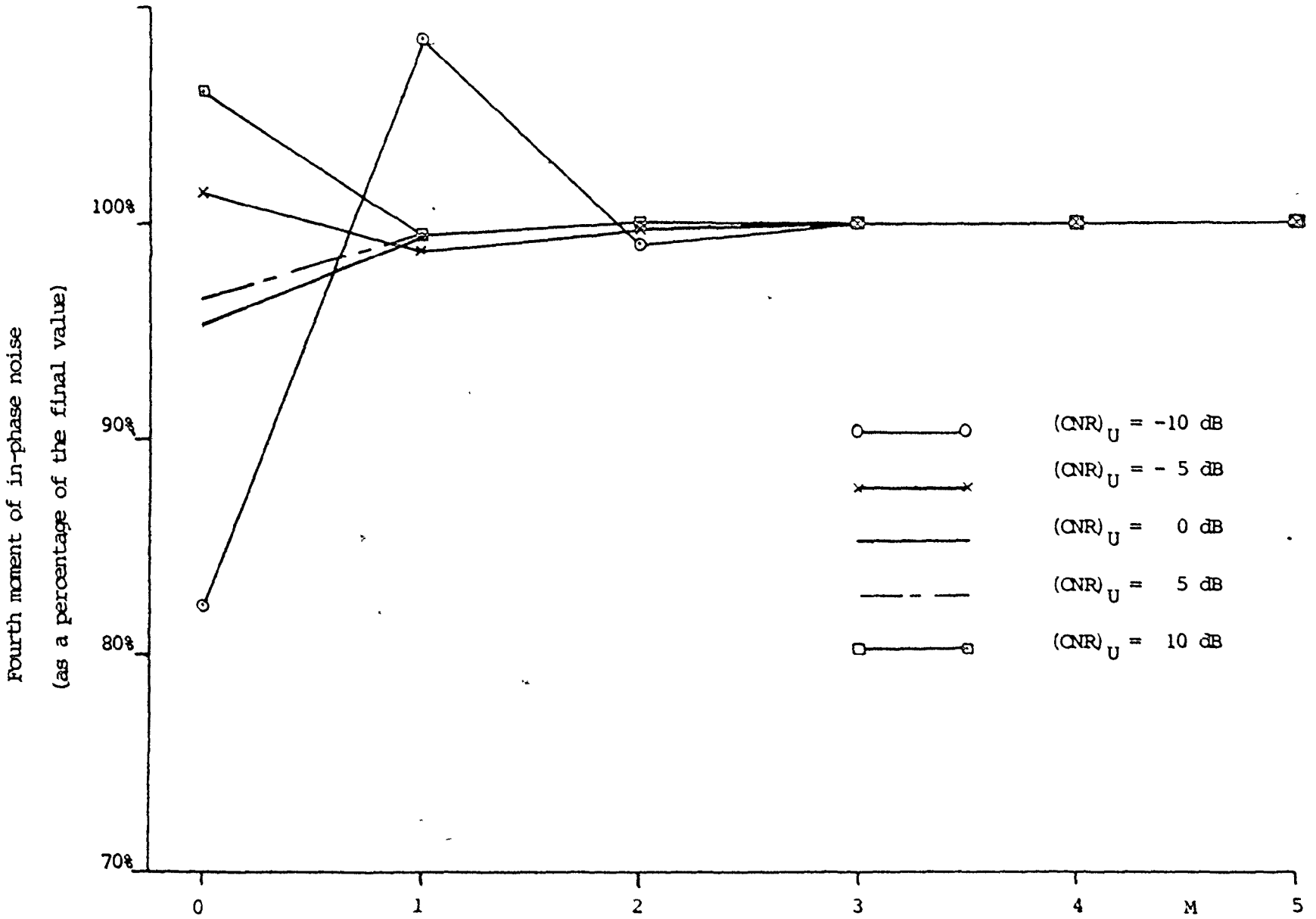

Fig. D-3. Convergence of the fourth moment of in-phase noise to the final value as a function of M.

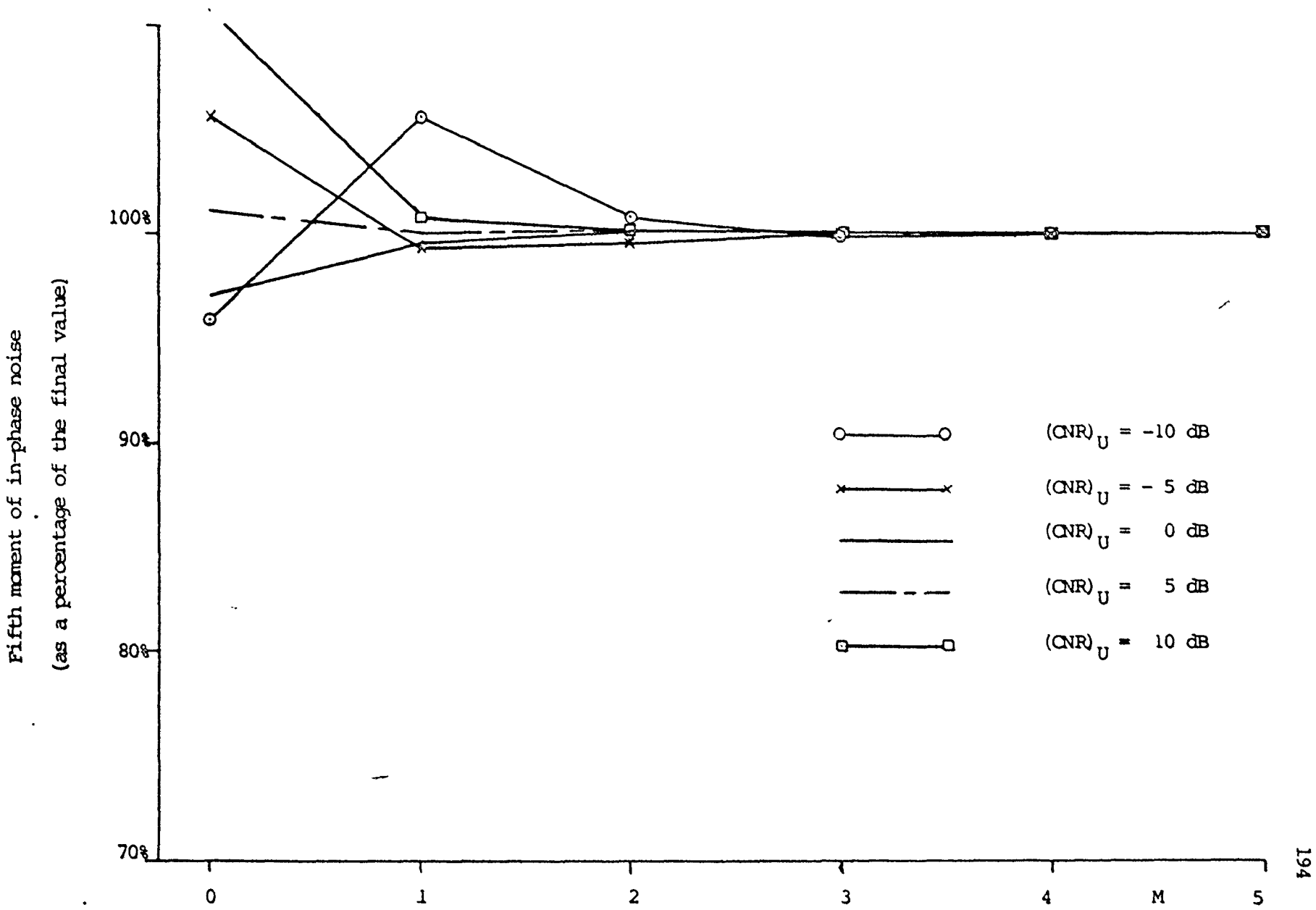

Fig. D-4. Convergence of the fifth moment of in-phase noise to the final value as a function of M.

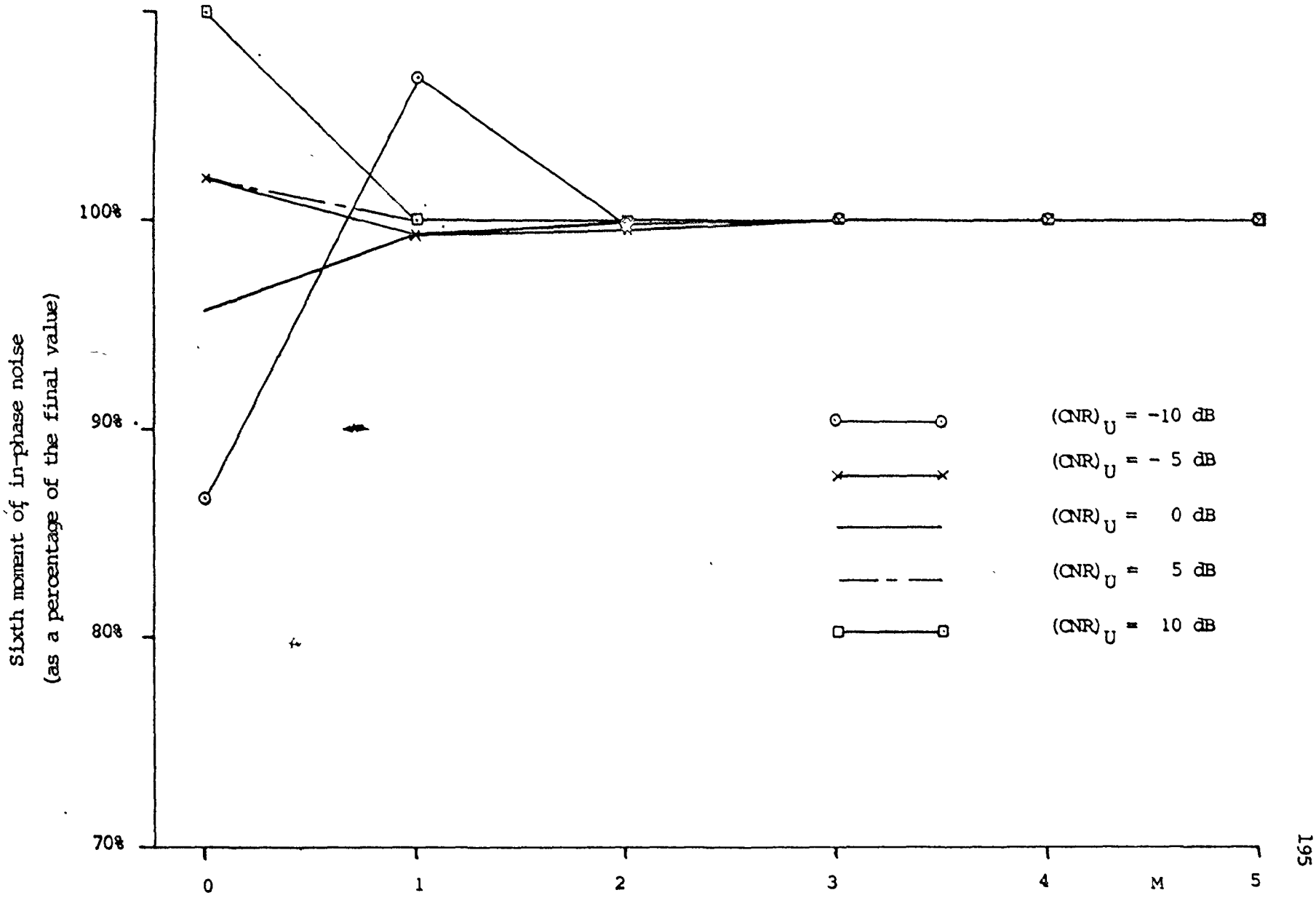

Fig. D-5. Convergence of the sixth moment of in-phase noise to the final value as a function of M.

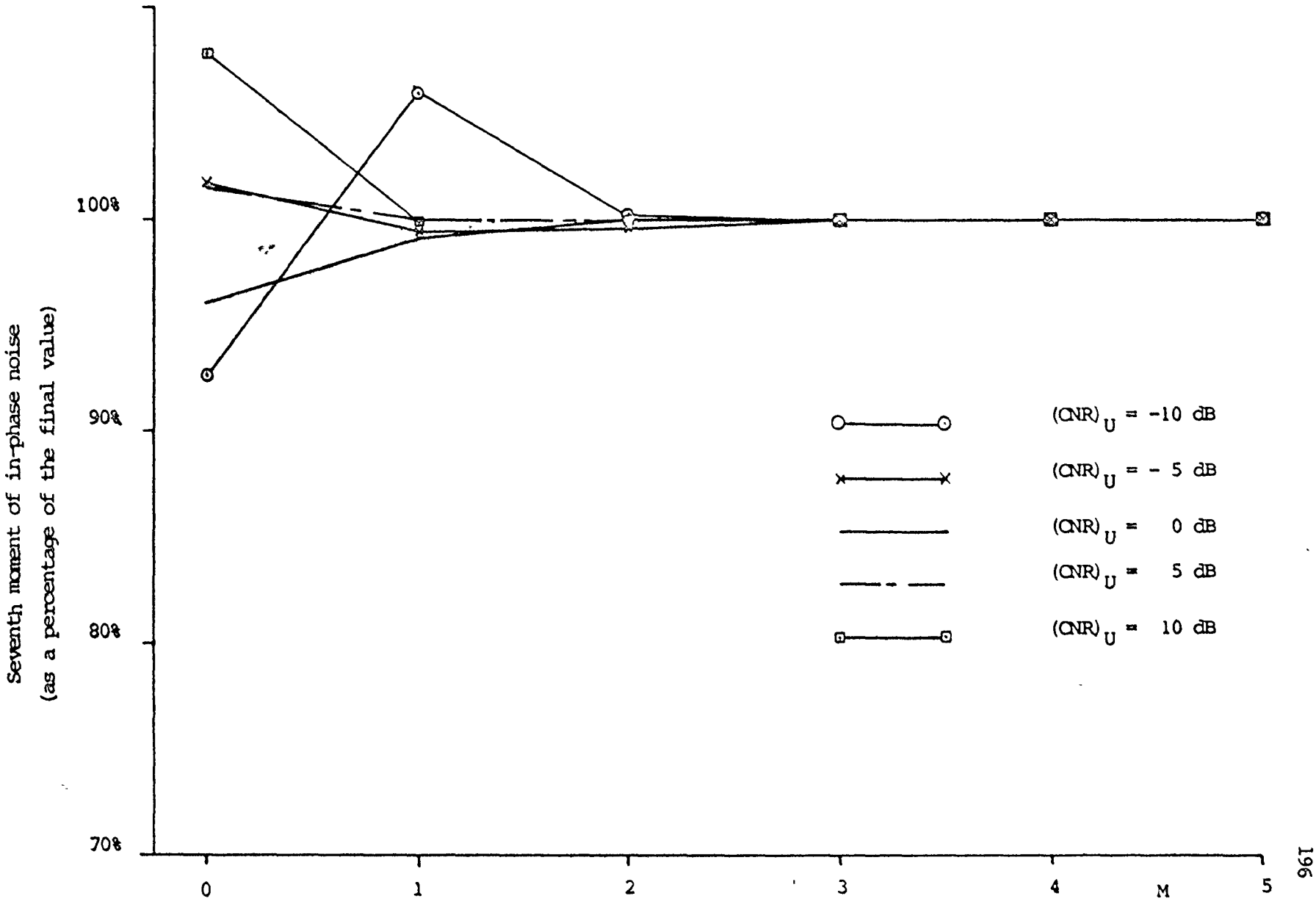

Fig. D-6. Convergence of the seventh moment of in-phase noise to the final value as a function of M.

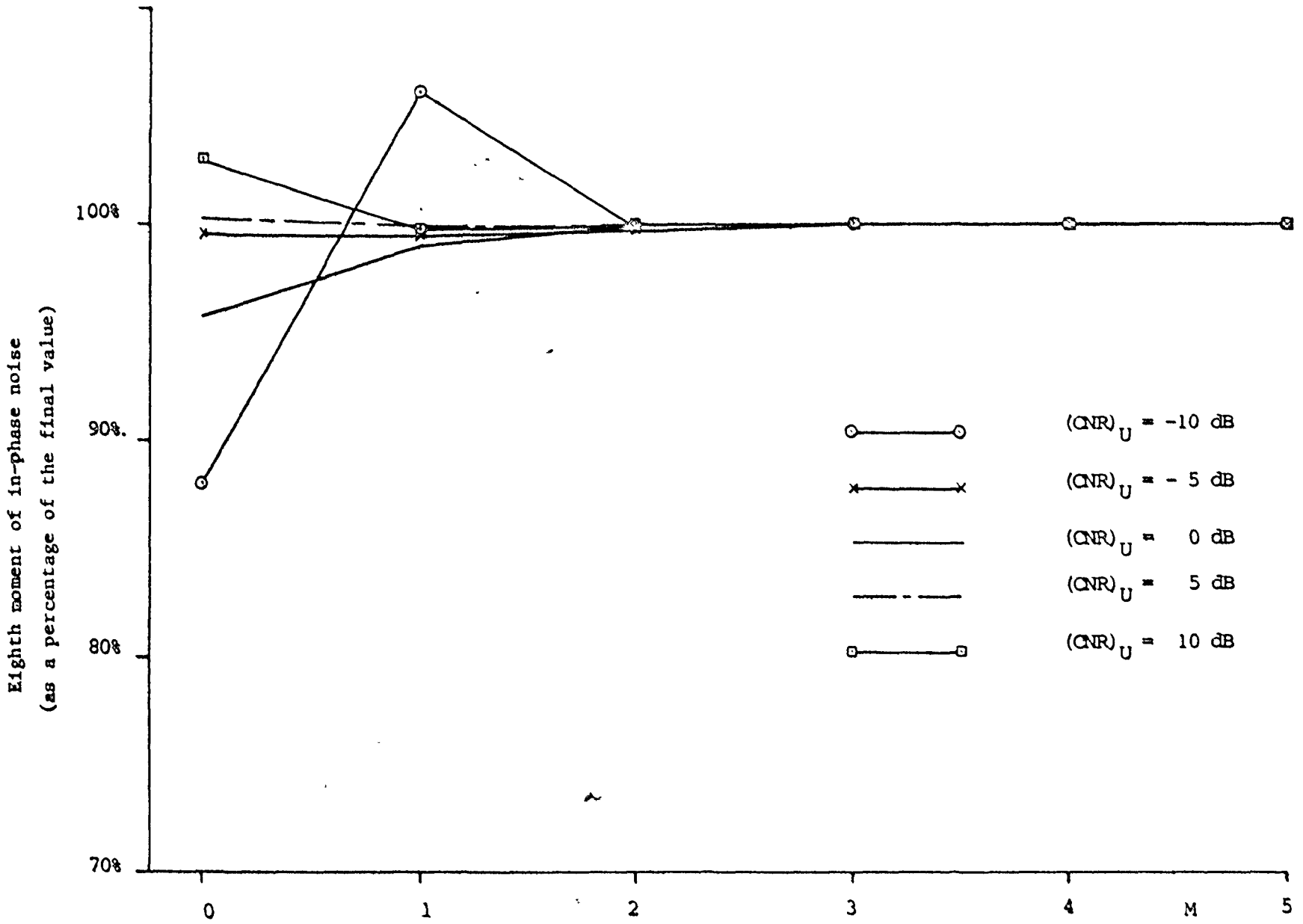

Fig. D-7. Convergence of the eighth moment of in-phase noise to the final value as a function of M.

APPENDIX E

ABSOLUTE CONVERGENCE PROPERTY OF THE BIT ERROR RATE EXPRESSION

Consider the infinite series expansion for p, the probability of one sample being in error, as given by

$$p = \frac{1}{2}\operatorname{erfc}(\sqrt{\rho}) + \frac{e^{-\rho}}{\sqrt{2\pi}} \sum_{n=3}^{\infty} \frac{(-1)^n}{n!} h_n \left[\frac{N_u'}{N_T}\right]^{n/2} H_{n-1}(\sqrt{2\rho}) \qquad \text{(E.1)}$$

where $\rho = (A')^2/2N_T$

and

$$h_n = \int_{\Omega} H_n\left[\frac{x}{\sqrt{N_u'}}\right] p_{n_1'}(x)\, dx$$

The random variable n_1' is upperbounded by a finite positive number K, such that

$$\sup(x) = K > 0 \qquad \text{for all } x \in \Omega$$

Using the well-known inequality for Hermite polynomials [40] one can show that

$$|h_n| \leq (n-1)!!\, e^{\frac{K^2}{4N_u'}} \qquad \text{for n even} \qquad \text{(E.2)}$$

and

$$|h_n| \leq (n-2)!!\sqrt{n}\, e^{\frac{K^2}{4N_u'}} \qquad \text{for n odd} \qquad \text{(E.3)}$$

where $(2n-1)!! = 1\cdot3\cdot5\cdot7\cdot9\cdots\cdots(2n-3)\cdot(2n-1)$

and K is as defined above.

Furthermore the Hermite polynomial is upperbounded by [38]

$$|H_{n-1}(\sqrt{2\rho})| \leq \frac{2^{-\langle \frac{n-1}{2} \rangle} (n-1)!\, e^{2\sqrt{\rho \langle \frac{n-1}{2} \rangle}}}{\langle \frac{n-1}{2} \rangle!} \qquad (E.3)$$

where $\langle x \rangle$ denotes the integer part of the real number x.

The error which arises as a result of truncating the series expansion of equation (E.1) at the (L-1)st term can be written as

$$R_L = \sum_{n=L}^{\infty} \frac{e^{-\rho}}{\sqrt{2\pi}} \frac{(-1)^n}{n!} h_n \left[\frac{N_u'}{N_T}\right]^{n/2} H_{n-1}(\sqrt{2\rho}) \qquad (E.4)$$

$$\leq \frac{e^{-\rho}}{\sqrt{2\pi}} \sum_{n=L}^{\infty} \frac{|h_n|}{n} \left[\frac{N_u'}{N_T}\right]^{n/2} \frac{2^{-\langle \frac{n-1}{2} \rangle} e^{2\sqrt{\rho \langle \frac{n-1}{2} \rangle}}}{\langle \frac{n-1}{2} \rangle!} \qquad (E.5)$$

Without loss of generality we may assume that L is even in the subsequent analysis.

Substitution of (E.2) into (E.5) and rearranging as sums of even and odd terms we obtain

$$R_L \leq \frac{e^{-\rho}}{\sqrt{2\pi}} e^{\frac{K^2}{4N_u'}} \sum_{k=\frac{L}{2}}^{\infty} [S_{2k} + S_{2k+1}] \qquad (E.6)$$

where the sequences S_{2k} and S_{2k+1} are defined as follows

$$S_{2k} = \frac{(2k-1)!!}{2k} \left[\frac{N_u'}{N_T}\right]^k \frac{2^{-(k-1)} e^{2\sqrt{\rho(k-1)}}}{(k-1)!} \qquad (E.7)$$

$$S_{2k+1} = \frac{(2k-1)!!}{(2k+1)} \left[\frac{N'_u}{N_T} \right]^{\frac{2k+1}{2}} \frac{\sqrt{2k+1}\, 2^{-k}\, e^{2\sqrt{\rho k}}}{k!} \qquad (E.8)$$

It is then easy to show for the even and odd terms

$$\left| \frac{S_{2k+2}}{S_{2k}} \right| = \frac{(2k+1)}{(2k+2)} \left[\frac{N'_u}{N_T} \right] e^{2\sqrt{\rho}\{\sqrt{k} - \sqrt{k-1}\}} \qquad (E.9)$$

and

$$\left| \frac{S_{2k+3}}{S_{2k+1}} \right| = \sqrt{\frac{(2k+1)}{(2k+3)}} \cdot \frac{(2k+1)}{(2k+2)} \left[\frac{N'_u}{N_T} \right] e^{2\sqrt{\rho}\{\sqrt{k+1} - \sqrt{k}\}} \qquad (E.10)$$

From D'Alembert's ratio test of absolute convergence and equations (E.9) and (E.10) it then follows that the series of S_{2k} and S_{2k+1} are jointly absolutely convergent for any $k \geq \frac{L}{2}$ such that

$$L > 2 + \frac{1}{2} \left[\frac{2\sqrt{\rho}}{\ln [N_T/N'_u]} - \frac{\ln [N_T/N'_u]}{2\sqrt{\rho}} \right]^2 \qquad (E.11)$$

The value for L, as indicated in (E.11), depends on the ratio of total noise power at the receiver, N_T, to the equivalent up-link noise power, N'_u and tends to diverge as N'_u approaches zero. However, for the trivial case of no up-link noise, $N'_u = 0$, the series terms in (E.1) are reduced to zero and the system performance, p, is affected only by the down-link Gaussian noise.

For any values of $k \geq \frac{L}{2}$ and L satisfying (E.11), equations (E.9) and (E.10) become

$$\left|\frac{S_{2k+2}}{S_{2k}}\right| < \left[\frac{N'_u}{N_T}\right] e^{2\sqrt{\rho}\,\{\sqrt{L/2} - \sqrt{(L-2)/2}\}} \triangleq Q_e(L) < 1 \tag{E.12}$$

and similarly

$$\left|\frac{S_{2k+3}}{S_{2k+1}}\right| < \left[\frac{N'_u}{N_T}\right] e^{2\sqrt{\rho}\,\{\sqrt{(L+2)/2} - \sqrt{(L/2)}\}} \triangleq Q_0(L) < 1 \tag{E.13}$$

Using the results for the sum of infinite geometric series, we obtain

$$\sum_{k=\frac{L}{2}}^{\infty} S_{2k} < \frac{(L-1)!!}{L}\left[\frac{N'_u}{N_T}\right]^{\frac{L}{2}} \frac{2^{-\frac{(L-2)}{2}}\, e^{2\sqrt{\rho(L-2)/2}}}{[(L-2)/2]!\;[1-Q_e(L)]} \tag{E.14}$$

and

$$\sum_{k=\frac{L}{2}}^{\infty} S_{2k+1} < \frac{(L-1)!!}{\sqrt{(L+1)}}\left[\frac{N'_u}{N_T}\right]^{\frac{L+1}{2}} \frac{2^{-\frac{L}{2}}\, e^{2\sqrt{\rho L/2}}}{(L/2)!\;[1-Q_0(L)]} \tag{E.15}$$

Combining (E.14) and (E.15) and substituting into (E.6) we get

$$R_L < \frac{e^{-\rho} e^{[K^2/4N'_u]}}{\sqrt{2\pi}}(L-1)!!\left[\frac{N'_u}{N_T}\right]^{\frac{L}{2}} \left\{ \frac{2^{-\frac{(L-2)}{2}}\, e^{2\sqrt{\rho(L-2)/2}}}{L[(L-2)/2]!\;[1-Q_e(L)]} + \sqrt{[N'_u/N_T]}\,\frac{2^{-\frac{L}{2}}\, e^{2\sqrt{\rho L/2}}}{\sqrt{(L+1)}\;[L/2]!\;[1-Q_0(L)]} \right\} \tag{E.16}$$

and since the series S_{2k}, S_{2k+1} are shown to be absolutely convergent, then for a small truncation error bound, δ, it is always possible to find a sufficiently large L satisfying equation (E.11) such that

$$R_L \leq \delta .$$

REFERENCES

[1] ABRAMOWITZ, M. and SEGUN, I.A.: Handbook of mathematical functions, (Dover, 1965).

[2] ibid pp. 377.

[3] ibid pp. 503-537.

[4] AEIN, J.M.: "Normal approximations to the error rate for hard-limited correlators", IEEE Trans. Commun. Technol., vol. COM-15, pp. 44-51, Feb. 1967.

[5] AEIN, J.M.: "Error rate for peak limited coherent binary channels", IEEE Trans. Commun. Technol., vol. COM-16, pp. 35-44, Feb. 1968.

[6] AEIN, J.M.: "SNR and error rate calculations for coherent nonlinear satellite channels", Intelsat/IEE International Conference on Digital Satellite Communications, pp. 25-27, Nov. 1969.

[7] BAKKEN, P.M.: "Feedforward linearizer with two TWT's", Proceedings of the National Telecommunications Conference (NTC'74), pp. 953-958, Dec. 1974.

[8] BANDLER, J.W. and CHU, W.Y.: "Function optimization package version FLOPT1", SOC Internal Report Series, no. SOC-17, McMaster University, August, 1973.

[9] BENEDETTO, S. and BIGLIERI, E.: "Performance of M-ary PSK systems in the presence of intersymbol interference and additive noise", Alta Frequenza, vol. XLI, pp. 55E-69E, April 1972.

[10] BENEDETTO, S., BIGLIERI, E. and CASTELLANI, V.: "Performance evaluation in digital transmission with nonlinearities", Proceedings of Int. Commun. Conf., ICC'74, paper 30E, June 1974.

[11] BERMAN, A.L. and PODRACZKY, E.: "Experimental determination of intermodulation distortion produced in a wide-band communication repeater", IEEE International Convention Record, vol. 15, pt. 2, pp. 69-88, 1967.

[12] BERMAN, A.L. and MAHL, C.E.: "Nonlinear phase shift in traveling-wave tube as applied to multiple access communications satellites", IEEE Trans. Commun. Technol., vol. COM-18, pp. 37-47, Feb. 1970.

[13] BERMAN, A.L., MAHL, C.E. and WACHS, M.R.: "Transmission modeling", COMSAT Technical Review, vol. 2, pp. 489-527, Fall 1972.

[14] BIGLIERI, E.: "A recursive method for computing the coefficients of the Gram-Charlier series", Proceedings of the IEEE, vol. 61, pp. 251-252, Feb. 1973.

[15] BLACHMAN, N.M.: "Bandpass nonlinearities", IEEE Trans. Inform. Theory, vol. IT-10, pp. 162-164, April 1964.

[16] BLACHMAN, N.M.: Noise and its effect on communication, (McGraw-Hill, 1966), pp. 59.

[17] ibid pp. 60, problem 4.6.

[18] BLACHMAN, N.M.: "Detectors, bandpass nonlinearities, and their optimization: Inversion of the Chebyshev transform", IEEE Trans. Inform. Theory, vol. IT-17, pp. 398-404, July 1971.

[19] BUTLER, J.L.: "Digital matrix and intermediate frequency scanning", chapter 3, Scanning antenna, vol. 3, edited by HANSEN R.C., (Academic Press, 1966).

[20] CAHN, C.R.: "Performance of digital phase-modulation communication systems", IRE Trans. Commun. Systems, vol. CS-7, pp. 3-6, May 1969.

[21] CHARAS, Ph. and ROGERS, J.D.: "Improvements in on-board TWTA performance using amplitude and phase predistortion", Proceedings of the International Conference on Satellite Communication System Technology, pp. 270-280, April 1975.

[22] CARTER, C.R.: Synchronization of earth stations to a communications switching satellite, Ph.D dissertation, Department of Electrical Engineering, McMaster University, Canada, August 1974.

[23] CHAN, H.C., TAYLOR, D.P. and HAYKIN, S.S.: "Comparative evaluation of digital modulation techniques: Simulation study", CRL Internal Report Series, no. CRL-18, part 3, Communications Research Laboratory, McMaster University, April 1974.

[24] CHANG, J.C.: "The response of hard-limiting bandpass limiters to PM signals", IEEE Trans. Aerospace and Electronics Systems, vol. AES-6, pp. 398-400, May 1970.

[25] CLAASEN, T.: "Spectral analysis of PSK for digital satellite channels using a third order nonlinear model", Technical Report, no. 68, Royal Institute of Technology, Sweden, Dec. 1973.

[26] CLARKE, A.C.: "Extraterrestrial relays", Wireless World, vol. 5, pp. 303-308, Oct. 1945.

[27] CRAMER, H.: Mathematical method of statistics, (Princeton University Press, 1946), pp. 100.

[28] ibid pp. 223-232.

[29] DAVISSON, L.D. and MILSTEIN, L.B.: "On the performance of digital communication systems with bandpass limiters-Part I: One-link systems", IEEE Trans. Commun. Technol., vol. COM-20, pp. 972-975, Oct. 1972.

[30] DAVISSON, L.D. and MILSTEIN, L.B.: "On the performance of digital communication systems with bandpass limiters-Part II: Two-link systems", IEEE Trans. Commun. Technol., vol. COM-20, pp. 975-980, Oct. 1972.

[31] ERIC, M.J.: "Intermodulation analysis of nonlinear devices for multicarrier inputs", Communications Research Center, Report no. 1234, Ottawa, Canada, Nov. 1972.

[32] FORCINA, G.P.: "Effect of nonlinear channel characteristics on QPSK system performance", Proceedings of Int. Commun. Conf., ICC'73, pp. 31.13-31.18, June 1973.

[33] FREDRICSSON, S.: "Analysis of bandlimited nonlinear QPSK-channels", Technical Report, no. 78, Royal Institute of Technology, Sweden, April 1974.

[34] FUENZALIDA, J.C., SHIMBO, O. and COOK, W.L.: "Time domain analysis of intermodulation effects caused by nonlinear amplifiers", COMSAT Technical Review, vol. 3, pp. 89-143, Spring 1973.

[35] GALLAGER, R.: "Lower bounds on the tail of probability distributions", Quarterly Progress Report, no. 77, MIT Research Laboratory of Electronics, Cambridge, Mass., pp. 277-291, April 1965.

[36] GARDNER, F.M.: "Carrier and clock synchronization for TDMA digital communication", European Space Research Organization, ESTEC Report no. 744976, Noordwijk, Netherlands, June 1974.

[37] GNEDENKO, B.V. and KOLMOGOROV, A.N.: Limit distributions for sums of independent random variables, Translated by CHUNG, K.L., (Addison-Wesley, 1968), pp. 103.

[38] GRADSHTEYN, I.S. and RYZHIK, I.M.: Table of integrals, series and products, Translated by JEFFREY, A., (Academic Press, 1965).

[39] ibid pp. 132, equation 4.

[40] ibid pp. 1034.

[41] HEDDERLY, D.L. and LUNDQUIST, L.: "Computer simulation of a digital satellite communication link", Proceedings of Int. Commun. Conf., ICC'72, paper 2C, pp. 2.15-2.20, June 1972.

[42] HETRAKUL, P. and TAYLOR, D.P.: "Nonlinear quadrature model for a travelling-wave-tube-type amplifier", Electronics Letters, vol. 11, no. 2, pp. 50, Jan. 1975.

[43] HETRAKUL, P., TAYLOR, D.P. and HAYKIN, S.S.: "Effect of a soft-limiter on the error rate of an M-ary CPSK system", Proceedings of Int. Commun. Conf., ICC'74, paper 44B, pp. 44B-1-44B-5, June 1974.

[44] HETRAKUL, P. and TAYLOR, D.P.: "Compensation of bandpass nonlinearities for satellite communications", Proceedings of Int. Commun. Conf., ICC'75, paper 36F, pp. 36F-1-36F-5, June 1975.

[45] HETRAKUL, P. and TAYLOR, D.P.: "Effect of satellite transponder nonlinearity on the performance of binary PSK system", Proceedings of the Third International Conference on Digital Satellite Communications, paper B-1, Kyoto, Japan, Nov. 1975 (also accepted for publication in the IEEE Trans. Commun. Technol.).

[46] HILL, F.S. Jr. and BLANCO, M.A.: "Random geometric series and intersymbol interference", IEEE Trans. Inform. Theory, vol. IT-19, pp. 326-335, May 1973.

[47] JACOBS, I.: "The effects of video clipping on the performance of an active satellite PSK communication system", IEEE Trans. Commun. Technol., vol. COM-13, pp. 195-201, June 1965.

[48] JAIN, P.C.: "Performance of hard-limited spread spectrum transmission systems", Final Report, SRI Project 1328, Stanford Research Institute, March 1972.

[49] JAIN, P.C. and BLACHMAN, N.M.: "Detection of a PSK signal transmitted through a hard-limited channel", IEEE Trans. Inform. Theory, vol. IT-19, pp. 623-630, Sept. 1973.

[50] JONES, J.J., HUANG, J.Y. and LEONG, W.K.S.: "Performance of soft-limiting PSK and DPSK spread spectrum systems", Final Report, AD-777 -897, Philco-Ford Corporation, Feb. 1974.

[51] KAYE, A.R., GEORGE, D.A. and ERIC, M.J.: "Analysis and compensation of bandpass nonlinearities for communications", IEEE Trans. Commun. Technol., vol. COM-20, no. 5, pp. 965-972, Oct. 1972.

[52] LESH, J.R.: "Signal to noise ratios in coherent soft limiters", IEEE Trans. Commun. Technol., vol. COM-22, pp. 803-811, June 1974.

[53] LINDSEY, W.C. and SIMON, M.K.: Telecommunication systems engineering, (Prentice Hall, 1973), pp. 228-234.

[54] ibid pp. 279-280.

[55] LOPRIORE, M. and LUNDQUIST, L.: "Choice of optimum TDMA transmission system", Proceedings of the Second International Conference on Digital Satellite Communications, Paris, France, pp. 175-182, Nov. 1972.

[56] LUCKY, R.W., SALZ, J. and WELDON, E.J.: Principles of data communications, (McGraw-Hill, 1968).

[57] LYONS, R.G.: Methods of nonlinear analysis with applications to multiple access satellite communications, Ph.D dissertation, Department of Electrical Engineering, Carleton University, Canada, July 1971.

[58] LYONS, R.G.: "Multiple access techniques for the Canadian domestic satellite communications systems", Intercon International Convention and Exposition, New York, March 1973.

[59] LYONS, R.G.: "The effect of a bandpass nonlinearity on signal detectability", IEEE Trans. Commun. Technol., vol. COM-22, pp. 51-60, Jan. 1973.

[60] MAGILL, D.J.: "Multiple-access method techniques", in Communications satellite systems technology, (Academic Press, 1966), pp. 667-680.

[61] MAGNUS, W., OBERHETINGER, F. and SONI, R.P.: Formulas and theorems for the special functions of mathematical physics, (Springer-Verlag, 1966), pp. 418.

[62] MORGAN, W.L.: "Communications satellite and new technology", Microwave System News, vol. 4, pp. 64-68, April/May 1974.

[63] MURATANI, T., MATUSHITA, I., TSUJI, Y. and HARA, T.: "Simulation of a PSK transmission system including the nonlinear satellite channel", Proceedings of the Second International Conference on Digital Satellite Communications, Paris, France, pp. 183-192, Nov. 1972.

[64] PIERCE, J.R.: Traveling wave tubes, (D. Van Nostrand, 1950).

[65] PUENTE, J.G., SCHMIDT, W.G. and WERTH, A.M.: "Multiple access techniques for commercial satellites", Proceedings of the IEEE, vol. 59, pp. 219-229, Feb. 1971.

[66] RAPPAPORT, S.S. and KURZ, L.: "An optimal nonlinear detector for digital data transmission through non-Gaussian channels", IEEE Trans. Commun. Technol., vol. COM-14, pp. 266-274, June 1966.

[67] RICE, S.O.: "Statistical properties of a sine wave plus random noise", Bell System Technical Journal, vol. 24, pp. 46-156, 1945.

[68] SANDRIN, W.A.: "The Butler matrix transponder", COMSAT Technical Review, vol. 4, no. 2, pp. 319-345, Fall 1974.

[69] SCHMIDT, W.G., GABBARD, O.G., CACCIAMANI, E.R., MAILLET, W.G. and WU, W.W.: "MAT-1: Intelsat's experimental 700-channel TDMA/DA", Proceedings of the First International Conference on Digital Satellite Communications, London, England, pp. 428-440, Nov. 1969.

[70] SCHWARTZ, J.W., AEIN, J.M. and KAISER, J.: "Modulation techniques for multiple access to a hard-limiting satellite repeater", Proceedings of the IEEE, vol. 54, pp. 763-777, May 1966.

[71] SEIDEL, H., BURRIER, H.R. and FRIEDMAN, A.N.: "Error-controlled high power linear amplifiers at VHF", Bell System Technical Journal, vol. 47, pp. 651-722, May-June, 1968.

[72] SEIDEL, H.: "A microwave feed-forward experiment", Bell System Technical Journal, vol. 50, no. 9, pp. 2879-2916, Nov. 1971.

[73] SEIDEL, H.: "A feedforward experiment applied to an L-4 carrier system amplifier", IEEE Trans. Commun. Technol., vol. COM-19, no. 3, pp. 320-325, June 1971.

[74] SHIMBO, O.: "Effects of intermodulation, AM-PM conversion and additive noise in multicarrier TWT systems", Proceedings of the IEEE, vol. 59, no. 2, pp. 230-238, Feb. 1971.

[75] STANDING, A.F.: "An active-phase and amplitude-correction device for reducing the intermodulation produced by TWT's and Klystrons", Proceedings of the International Conference on Earth Station Technology, pp. 274-279, Oct. 1970.

[76] STIFFLER, J.J.: Theory of synchronous communications, (Prentice-Hall, 1971), pp. 96-99.

[77] ibid pp. 104-108.

[78] STROUD, A.H.: Approximate calculation of multiple integrals, (Prentice-Hall, 1971), pp. 350.

[79] TAYLOR, D.P., HAYKIN, S.S. and CHAN, H.C.: "Comparative evaluation of digital modulation techniques: Literature survey", CRL Internal Report Series, no. CRL-18, part 2, Communications Research Laboratory, McMaster University, Canada, April 1974.

[80] THOMAS, C.M., WEINER, M.Y. and DURRANI, S.H.: "Digital amplitude-phase keying with M-ary alphabets", IEEE Trans. Commun. Technol., vol. COM-22, pp. 168-180, Feb. 1974.

[81] WALSH, D.W.: Theoretical solutions to problems introduced by the TWA in multiple access communication system, Sc.D dissertation, Department of Electrical Engineering, The George Washington University, Washington, D.C., 1974.

[82] WELTI, G.R.: "Nonlinear channel for multicarrier transmission", paper presented at NATO Advanced Studies Institute, Darlington, England, August, 1974.

[83] WOODWARD, P.M.: Probability and information theory, with applications to radar, (Pergamon Press, 1960).

[84] WOZENCRAFT, J.M. and JACOBS, I.M.: Principles of communication engineering, (John Wiley & Sons, 1965), pp. 214.

[85] ibid pp. 264-266.

[86] YAMAGUCHI, K.: "Equalization of intermodulation due to TWT amplification", Trans. Joint Conv. of the Four Elec. Inst. of Japan, no. 1599, 1965.